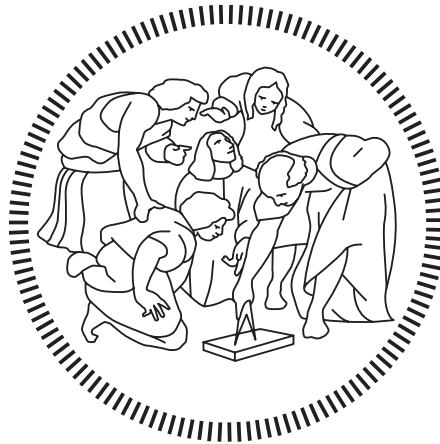


Politecnico di Milano

SCHOOL OF INDUSTRIAL AND INFORMATION ENGINEERING

Master of Science – Energy Engineering



Outdoor thermal comfort and mean radiant
temperature:
comparison of measurement techniques

Supervisor

Prof. Francesco CAUSONE

Co-Supervisor

Eng. Anita TATTI

Eng. Martina FERRANDO

Candidate


Alessandro BONIOLO – 905843

Academic Year 2019 – 2020

Declaration of originality

I hereby declare that I am the sole author of the present thesis. All information in this document has been obtained and presented in accordance with academic rules and ethical conduct. I also declare that, as required by these rules and conduct, I have fully cited and referenced all material and results that are not original to this work.

The content of the thesis is the result of work which has been carried out since the official commencement date of the approved master thesis program.



Alessandro Boniolo

Milano, 31/03/2021

Abstract

The constant urban overheating, influenced by climate change and urbanization, is already decreasing the outdoor thermal comfort and the wellbeing of the urban population. Heat-related problems are a major issue in many cities and the uncontrolled increase in temperature and the climate change projections are worrying researchers and urban planners, who are looking for efficient solutions to assess the thermal characteristics of open environments and their relation with human comfort.

To evaluate the complexity of the outdoor comfort condition, the concept of the Mean Radiant Temperature (MRT) has been adopted: this parameter is aimed at describing the complex radiative exchanges reaching a human body in an outdoor environment. However, the outdoor thermal comfort is a relatively new field of study and there is a lack of standardization of the methodology to assess the MRT in outdoors. Different researchers have therefore adopted in their studies different instruments, methods and standards in the evaluation of this parameter.

This thesis work, therefore, made an attempt to cover the wide range of instruments and techniques adopted in literature, making easier the comparison between them. Taking as reference the results obtained using the most expensive, but also the most accurate, measurement technique (i.e. the one that foresees the use of three net radiometers simultaneously), criticalities, weaknesses and strengths are identified and compared with cheaper alternatives. Along with three net radiometers we used two globe thermometers of different colours (black and grey) and size. Several experimental campaigns were carried out in nine different urban settings, to evaluate the outdoor thermal comfort and how it is influenced by the radiative properties of the materials characterizing each measurement site.

The evaluation of the MRT allowed then to calculate the so-called Universal Thermal Climate Index (UTCI) and, through a set of thermal stress categories, to translate the calculated UTCI in the thermal stress perception that people experience in a given environment.

A first analysis is focused on the difference in MRT and UTCI results obtained with the different instruments adopted. Further data analysis and elaborations were then performed, addressing the use of alternative approaches of the commonly adopted methods. Among these, we considered different view factors in the calculation of the MRT with the net radiometers method, as well as a correction applied to the commonly used convective coefficients describing the heat exchange between the globe thermometers and the surrounding environment.

Keywords: outdoor thermal comfort, mean radiant temperature, net radiometer, globe thermometer

Sommario

I cambiamenti climatici e l'urbanizzazione sono alla base del crescente surriscaldamento nelle aree urbane, fenomeno che sta progressivamente diminuendo il comfort termico esterno e quindi il benessere della popolazione. Ricercatori e urbanisti sono perciò chiamati a trovare efficienti soluzioni per la valutazione ed il miglioramento delle condizioni termiche negli ambienti esterni.

Per studiare la complessità del comfort termico esterno, è stato adottato il concetto di Temperatura Media Radiante (MRT): tale parametro ha lo scopo di descrivere i complessi scambi radiativi che interessano il corpo umano in un ambiente esterno. Il comfort termico esterno è però un campo di studio relativamente nuovo, che soffre la mancanza di una standardizzazione della metodologia per valutare la MRT in ambienti aperti. Ciò spiega il motivo per cui diversi ricercatori si sono avvalsi di differenti strumenti e differenti metodologie nei loro studi in questo ambito.

Questo lavoro di tesi cerca di ripercorrere l'ampia gamma di tecniche e strumenti utilizzati nei più recenti studi, al fine di facilitare il confronto tra di essi. Prendendo come riferimento i risultati ottenuti grazie alla tecnica di misurazione più accurata ma anche più costosa (ovvero quella che prevede l'utilizzo di tre radiometri netti contemporaneamente), si vogliono individuare criticità, debolezze e punti di forza rispetto alle alternative più economiche. Insieme ai tre radiometri netti si è scelto di utilizzare due globotermometri di diverso colore (nero e grigio) e diversa dimensione.

Sono state condotte campagne sperimentali in nove differenti contesti urbani, al fine di studiare il comfort termico esterno e come esso venga influenzato dalle proprietà radiative dei materiali che caratterizzano i differenti ambienti. La valutazione della MRT ha inoltre permesso di calcolare il cosiddetto Universal Thermal Climate Index (UTCI), il quale, attraverso un sistema di categorizzazione, consente di indicare la percezione di stress termico che le persone provano in un determinato ambiente.

In questa tesi, una prima analisi sarà focalizzata sulla differenza riscontrata nei risultati ottenuti con i diversi strumenti a nostra disposizione; ad essa seguono ulteriori analisi ed elaborazioni dei dati raccolti, volte a prendere in considerazione approcci alternativi ai metodi comunemente adottati. Tra questi vengono presi in esame l'utilizzo di differenti fattori di vista nel calcolo della MRT con radiometri netti e diverse alternative ai coefficienti convettivi più frequentemente utilizzati per descrivere lo scambio termico tra i globotermometri e l'ambiente esterno circostante.

Parole chiave: comfort termico esterno, temperatura media radiante, radiometro netto, globotermometro

Extended Abstract

Chapter 1: outdoor thermal comfort assessment

Life of people is strongly influenced by the climate conditions of the environment in which they live. The more comfortable an environment is for the people, the more they will be willing to spend time in it. This turns out to be particularly important in urban areas, where around 55% of the world population lives, a percentage that is expected to grow to 68% by 2050. Furthermore, the increase in urban air temperature due to urbanization has a huge impact on the buildings energy performance and demand and, in the long run, can affect the people health too (Georgatou and Kolokotsa 2016; Kleerekoper, Van Esch, and Salcedo 2012; Kleerekoper, Van Esch, and Salcedo 2012).

This leads to an increasingly interest in the outdoor thermal comfort, especially in urban areas, since they are the most affected environments by the Urban Heat Island (UHI) effect, for which the urban air temperature is higher than the one of the surrounding rural areas (Sangiorgio, Fiorito, and Santamouris 2020). Researchers in this field of study have identified the air temperature, the relative humidity, the air velocity and the radiant fluxes as the most influencing parameters on the outdoor thermal comfort. In particular, the radiant fluxes are subjected to rapid changes in both space and time, due to the variation in the meteorological conditions and the properties of the surrounding environments, increasing the complexity of outdoor thermal comfort evaluation (Lai, Maing, and Ng 2017; Thorsson et al. 2007).

To assess the outdoor thermal comfort, the concept of the Mean Radiant Temperature (MRT) has been introduced. The MRT is “the uniform temperature of an imaginary enclosure made of black surfaces in which the radiant heat transfer from the human body (with emissivity $\epsilon=1$) equals the radiant heat transfer in the actual non-uniform enclosure” (ASHRAE 55 2017). This parameter, abridging all the radiative fluxes reaching a human body in an outdoor environment, has become the focus of the majority of the assessment regarding outdoor thermal comfort.

To describe the heat exchange between the human body and the surrounding environments, several thermal comfort indices have been developed over the years. For this purpose, in this thesis the so-called Universal Thermal Climate Index (UTCI), developed by Jendritzky et al. in 2001 (G. Jendritzky, A. Maarouf 2001), was adopted. This index allows to cover the whole range of heat exchanges between the human body and the outdoor environment, using as input parameters the air temperature, the wind speed, the relative humidity and the MRT.

In order to evaluate the MRT in outdoor environments, different techniques have been developed and described in literature. The most commonly adopted ones are:

- Integral radiation measurements. It is the most accurate method to estimate outdoor MRT as it requires simultaneous measurements of short-wave and long-wave radiation from six directions (east, west, north, south, upward and downward) using three net radiometers.
- Globe thermometer measurements. This method is less expensive than the integral radiation one and it only requires a globe thermometer, which determines the MRT according to a heat balance equation between the globe and the surrounding environment. The colour and the size of the globe affect the accuracy and the response time of the instrument.
- Simulating software. This technique involves numerical microclimate models capable to represent the complex interactions between urban fabric and local weather parameters.

As evidenced, there is not a standardized approach and methodology for outdoor thermal comfort assessments. In particular, Johansson et al.'s study in 2014 (Johansson et al. 2014), comparing several studies reported in the literature in the last decade, identified the presence of a great variety of instruments and methods adopted in outdoor thermal comfort surveys, both as regards micrometeorological instruments and thermal indices. It was also noted that measurement equipment, accuracy and response time were not stated in the majority of the existing studies. Furthermore, the subjective judgment scales to determine thermal perception were different from study to study, along with a poor description of the measurement sites. Finally, many researchers use parts of many different standards since there is no single complete standard for outdoor thermal comfort surveys.

In this work, therefore, an attempt was made to cover the wide range of instruments and techniques adopted in recent studies, with the aim of making a comparison, which would otherwise be difficult to make between different studies following different methodologies and standards. The analysis compares the most accurate method, the one which uses three net radiometers, with the results provided by two globe thermometers of different colour and size, in order to understand if it is possible -and how accurate it is- to use cheaper instruments for the evaluation of the outdoor thermal comfort.

Chapter 2: instruments and methodology

Chapter 2. *Instruments and Methodology* describes the characteristics and specifications of the individual measuring instruments adopted in the thesis, the equations applied in the calculation of MRT and UTCI and the methodology followed in the measurement campaigns carried out.

As discussed above, integral radiation measurement is the most accurate method for assessing MRT in outdoor environments. It consists in using 3 net radiometers that simultaneously measure the radiative fluxes coming from six directions. In this thesis, each radiometer used is a 4-component net radiometer, consisting of 2 pyranometers, 2 pyrgeometers, a heater, a levelling assembly for x- and y-axis, and a Pt100 instrument body temperature sensor. Pyranometers and pyrgeometers measure the short-wave and long-wave radiation received by a plane surface, in W/m^2 .

The simultaneous measurements of short-wave and long-wave radiation fluxes, with the corresponding weight F_i between the body and the surrounding elements, coming from the six directions, provided by the three net radiometers, are taken into account to evaluate the MRT, according to *Equation (0. 1)*:

$$MRT = \left(\frac{\sum_{i=1}^3 \left[F_i \left(\alpha_k (SW_{UP,i} + SW_{DOWN,i}) + \varepsilon_p (LW_{UP,i} + LW_{DOWN,i}) \right) \right]}{\sigma * \varepsilon_p} \right)^{0.25} - 273.15 \quad [^{\circ}C] \quad (0. 1)$$

Where:

- F_i is the view factor for the i-th direction between the human body and the surrounding surfaces, determined by both the position and the orientation of the person.
- $SW_{UP,i}$ is the short-wave radiant fluxes recorded by the i-th radiometer, measured by the correspondent up-facing pyranometer.
- $SW_{DOWN,i}$ is the short-wave radiant fluxes recorded by the i-th radiometer, measured by the correspondent down-facing pyranometer.
- $LW_{UP,i}$ is the long-wave radiant fluxes recorded by the i-th radiometer, measured by the correspondent up-facing pyrgeometer.
- $LW_{DOWN,i}$ is the long-wave radiant fluxes recorded by the i-th radiometer, measured by the correspondent down-facing pyrgeometer.
- α_k is the absorption coefficient for short-wave radiant fluxes (assuming 0.7 as standard value) (VDI 2008).
- ε_p is the emissivity of the human body. According to the Kirchoff's laws, ε_p is equal to the absorption coefficient for short-wave radiant fluxes (assuming 0.97 as standard value)(VDI 2008)
- σ is the Stefan-Boltzmann constant and it is equal to $5.67 \times 10^{-8} Wm^{-2}K^{-4}$.

The F_i factors allow considering different reference shapes, e.g. a standing man and a sphere. In the latter case, all fluxes are weighted identically with a value of 0.167, while in the "standing man" case, the role of the lateral fluxes become relatively greater than the vertical ones, according to F_i values of 0.22 and 0.06 respectively, as suggested by Hoppe's analysis (P Höppe 1992; Peter Höppe 1999).

In this work both the approaches have been adopted, making a comparison between the two different solutions, depending on the tested environment (in particular, in the open field, the vertical radiative fluxes gain importance, which can be better described by the use of the "spherical" view factors).

Along with the integral radiation measurement method, a simpler approach adopting only one net radiometer, measuring the upward and downward direction, is also applied as suggested by Spagnolo and de Dear in their work in 2003 (Spagnolo and de Dear 2003). This approach, evaluating only the vertical radiative fluxes, is expected to be more suitable for approximating the MRT in free field environments. Although the equation proposed by Spagnolo and de Dear was somehow similar to that proposed in the German guideline VDI 3787 (VDI 3787 2008), in this thesis work it was decided to use an equation more similar to (0. 1), but focusing only on vertical radiative fluxes. This made it possible to evaluate their relevance in different environments and meteorological conditions, leading to further discussions on the importance attributed to the view factors adopted in the calculation. The MRT is therefore obtained as follows:

$$MRT = \left(\frac{F_1 \left(\alpha_k (SW_{UP,1} + SW_{DOWN,1}) + \varepsilon_p (LW_{UP,1} + LW_{DOWN,1}) \right)}{\sigma * \varepsilon_p} \right)^{0.25} - 273.15 \quad [^{\circ}C] \quad (0. 2)$$

Where:

- F_1 is the view factor for the single net radiometer measuring the upward/downward direction. It is assumed equal to 0.5 for both upward and downward directions.
- $SW_{UP,1}$ is the short-wave radiant fluxes measured by up-facing pyranometer of the net radiometer measuring the upward/downward direction.
- $SW_{DOWN,1}$ is the short-wave radiant fluxes measured by down-facing pyranometer of the net radiometer measuring the upward/downward direction.
- $LW_{UP,1}$ is the long-wave radiant fluxes measured by up-facing pyrgeometer of the net radiometer measuring the upward/downward direction.
- $LW_{DOWN,1}$ is the long-wave radiant fluxes measured by down-facing pyrgeometer of the net radiometer measuring the upward/downward direction.
- α_k is the absorption coefficient for short-wave radiant fluxes (assuming 0.7 as standard value) (VDI 2008).
- ε_p is the emissivity of the human body. According to the Kirchoff's laws, ε_p is equal to the absorption coefficient for short-wave radiant fluxes (assuming 0.97 as standard value)(VDI 2008).
- σ is the Stefan-Boltzmann constant and it is equal to $5.67 \times 10^{-8} \text{ Wm}^{-2}\text{K}^{-4}$.

The three net radiometers technique was also used in the experimental campaigns to evaluate the radiative properties of the surfaces characterizing the measurement environment. We considered in fact this calculation relevant in order to better define the measurement site and, at the same time, evaluate how different materials could impact differently on outdoor thermal comfort. In particular, one of the three radiometers was always placed parallel to the ground, while another was always parallel to the vertical surface to be tested. In this way the two radiometers in question received the global radiation on the sensor denominated "UP" and the radiation reflected by the vertical/horizontal surface under examination on the sensor denominated "DOWN". The "DOWN" sensors were always located at a distance of about 1 m from the surfaces to be tested, a distance that we considered sufficiently small to approximate the radiation received by these sensors exclusively as radiation reflected by the examined surface, without other contributions. The radiative properties of the surfaces (reflectivity and absorptivity) were thus evaluated according to Equation (0. 3) and Equation (0. 4):

$$\rho = \frac{SW_{DOWN}}{SW_{UP}} \quad (0.3)$$

$$\alpha = 1 - \rho \quad (0.4)$$

Where:

- ρ is the reflectivity of the surface examined
- α is the absorptivity of the surface examined
- SW_{DOWN} is the short-wave radiant flux measured by the pyranometer facing the examined vertical or horizontal surface.
- SW_{UP} is the short-wave radiant flux measured by the pyranometer facing the rest of the environment.

This method only provides a rough estimation of the radiative properties of surfaces tested, but it can be used to evaluate, as a first approximation, the influence that the measured properties have on a given environment.

Along with net radiometers, two different globe thermometers, one black and one grey, were adopted in this thesis work. The black globe thermometer used in the analysis is the standard globe thermometer for indoors, which is black painted with a diameter of 150 mm and a wall thickness of 0.4 mm, made of copper (I. Standard 1998). The emissivity of the globe is $\varepsilon_g = 0.963$. The most important issues regard the response time (ca. 15 min for the standard black globe), the shape (not suitable for representing the radiation load on a standing man) and the black colour of the globe (which absorbs too much short-wave radiation if compared to the clothed human body) (ASHRAE 55 2017; Spagnolo and de Dear 2003; Kántor, Kovács, and Lin 2015).

The grey globe thermometer used in this work has a diameter of 50 mm and an emissivity $\varepsilon_g = 0.93$, similar to the one adopted in Thorsson et al.' study in 2007 (Thorsson et al. 2007). In outdoor thermal comfort assessment, especially when the instrument is directly exposed to the solar radiation, both ISO 7726 (ISO Standard 7726 1998) and ASHRAE Handbook of Fundamentals (Ashrae Standard 2001) evidenced that a medium-sized grey-painted globe is more suited, compared to the standard black globe, to represent the outer surface of a clothed person (Johansson et al. 2014).

According to a balance equation between the globe and the surrounding environment, the MRT is calculated as follows:

$$MRT = \left[(T_g + 273,15)^4 + \frac{h_{conv}}{\varepsilon_g \sigma} (T_g - T_{air}) \right]^{1/4} - 273.15 \quad (0.5)$$

Where:

- h_{conv} is the coefficient of convective heat exchange between air and globe [W/(m²K)]
- T_{air} is the air temperature [K]
- T_g is the globe temperature at the equilibrium [K]
- ε_g is the emissivity of the globe [-]
- σ is the Stefan-Boltzmann constant and it is equal to 5.67×10^{-8} [Wm⁻²K⁻⁴]

Since h_{conv} comes from empirical analysis, different values are reported in literature (Kuehn, Stubbs, and Weaver 1970; E. L. Krüger, Minella, and Matzarakis 2014; Kántor, Kovács, and Lin 2015; Thorsson et al. 2007), leading to different MRT results. In this thesis different coefficients were adopted in the calculations of the MRT and a comparison were made between their results.

Before carrying out each measurement, it was necessary to place the support equipment (a tripod equipped with an adjustable height pole) in the measurement environment. The net radiometers, the globe thermometers and the All-in-one sensor (a sensor of the LSI-LASTEM Company, which allows measuring the meteorological parameters needed for the outdoor thermal comfort analysis) were then mounted on it (*Figure 0. 1*). Once the instrumentation was positioned, it was left in the measurement environment for the entire duration of the test. The parameters detected during the measurements were then downloaded from the acquisition system to a laptop where a specific software was installed.

The MRT is calculated starting from the data recorded by each instrument at our disposal. As already noted, the lack of a universal standard that defines a univocal method of calculating MRT in outdoor environments has led to the adoption of different calculation methods. In this thesis it was therefore decided to develop the data analyses initially by choosing only a single calculation method for each instrument and, only subsequently, to compare the results obtained with different approaches (e.g. varying view factors in net radiometers measurements and convective heat exchange coefficient in globe thermometer measurements). In particular, in the calculation of the MRT using three net radiometers it was decided to initially adopt the so-called "standing man" view factors, since they are the most commonly used in literature. These factors attribute a greater relevance to the lateral radiative fluxes than to the vertical ones, according to F_i values of 0.22 and 0.06 respectively. The absorption coefficient for short-wave radiant fluxes (α_k) and the emissivity of the human body (ε_p) are assumed equal to 0.7 and 0.97 respectively, according to the standard values reported in *VDI 2008*. For the single net radiometer measuring the upward/downward direction the F_i factors adopted are equal to 0.5 for both upward and downward directions.

For the MRT evaluation with globe thermometers we decided to use h_{conv} equal to 1.06 W/m²K, according to Kuhen et al.'s method (Kuehn, Stubbs, and Weaver 1970).

The UTCI was then calculated, starting from the MRT of each individual instrument and the meteorological parameters detected by the All-in-one sensor.

The analysis proceeded with a comparison of the results between the MRT values obtained through the combination of the three net radiometers (taken as reference) and those provided by the other instruments at our disposal. The analysis is aimed at defining how much the results provided by the cheaper alternatives differ from the reference ones, as well as in which conditions and environments they can be used to approximate the net radiometers results with greater accuracy.

This is followed by a correlation study between the results obtained through the data analysis and the variables measured. In particular, we investigate the correlation between the UTCI values calculated in the different measurement environments and the parameters involved in its calculation (i.e. air temperature, relative humidity, air velocity, global radiation).

A final analysis was then carried out in order to compare different approaches adopted in literature in the evaluation of the MRT by using the instruments at our disposal. At first, a comparison was made between the results provided by the net radiometers adopting the spherical view factors instead of the "standing man" ones. In particular, this analysis is aimed at open field measurements, where the greater influence of vertical radiative fluxes may be not correctly described by the "standing man" view factors.

This was then followed by a comparison between the results obtained using the balance equation for globe thermometers proposed by Kuhen et al. (Kuehn, Stubbs, and Weaver 1970) and those deriving from the correction suggested by Thorsson et al. (Thorsson et al. 2007). The difference between the two approaches lies in the different way of evaluating the convective heat exchanges between the globe thermometers and the surrounding environment.



Figure 0. 1. Positioning and setup of the instruments on support equipment

Chapter 3: experimental campaigns and results

The chapter describes the different measurement environments in which our surveys were carried out and show the results obtained.

The individual instruments were evaluated for their ability to provide accurate MRT assessments in different urban settings. The experimental campaigns took place in nine different environments, all located in the city of Milan, in July, August, September and October. They were carried out in open fields, in street canyons and in the proximity of different building envelope technologies, in order to observe how the radiative properties of the above-mentioned environments may influence the outdoor thermal comfort.

A brief description of the measurement sites, the day and hour in which the campaigns were carried out, the sampling frequency and the instruments adopted are all included in *Table 0. 1*.

Table 0. 1. Measurement environments, day and hours of the surveys, measurement frequency and instruments adopted.

Building Envelope/ Environment	Location	Measurement date and hour	Measurement frequency	Instruments		
				Black globe (150 mm)	Grey globe (50 mm)	3 net radiometers
Flat rooftop with a waterproofing membrane	Milan, Via Feltrinelli	20/07/2020 12:00-19:30	10 min	X		X
		21/07/2020 9:00-15:40	10 min	X		X
Light plaster wall	Milan, Via Lambruschini	23/07/2020 13:00-16:30	1 min	X		X
Porcelain stoneware Facade Cladding	Milan, Via Lambruschini	27/07/2020 12:00-16:30	1 min	X		X
		18/09/2020 11:10-17:15	1 min	X	X	X
Park	Milan, Cascina Merlata district	28/07/2020 11:50-16:30	1 min	X		X
Green rooftop	Milan, Via G. Ponzio	26/08/2020 day 15:20-21:00	1 min	X		X
		26-27/08/2020 night 21:00-8:00	1 min	X	X	X
		27/08/2020 day 8:00-17:15	1 min	X	X	X
Blue plaster wall	Milan, Cascina Merlata district	01/09/2020 11:30-17:10	1 min	X	X	X
Street Canyon	Milan, Bovisa district	09/09/2020 10:40-17:15	1 min	X	X	X
Green wall	Milan, Via G. La Masa	17/09/2020 11:10-17:15	1 min	X	X	X
	Milan, Via Bovisasca	06/10/2020 10:10-17:45	1 min	X	X	X

In *Chapter 3. Experimental campaigns and results* of this thesis, the single measurement campaigns are described individually, investigating the behaviour of the instruments in the different measurement environments. The purpose is to define, through the data collected, the difference, in terms of MRT and UTCI, found between the results of the net radiometers and those provided by the other "cheaper alternatives". For each measurement, it will then be possible to observe the MRT values calculated at the corresponding sampling frequency, as well as the maximum, minimum and average values. *Figure 0. 2* graphically shows the comparison between the average MRT values of each instrument and those obtained by means of the three net radiometers, for each measurement carried out. According to the figure, the MRT of the three net radiometers (reference values) is indicated in yellow, the MRT of the single radiometer measuring upward/downward direction in blue, the MRT of the black globe in red and the one of the grey globe in purple.

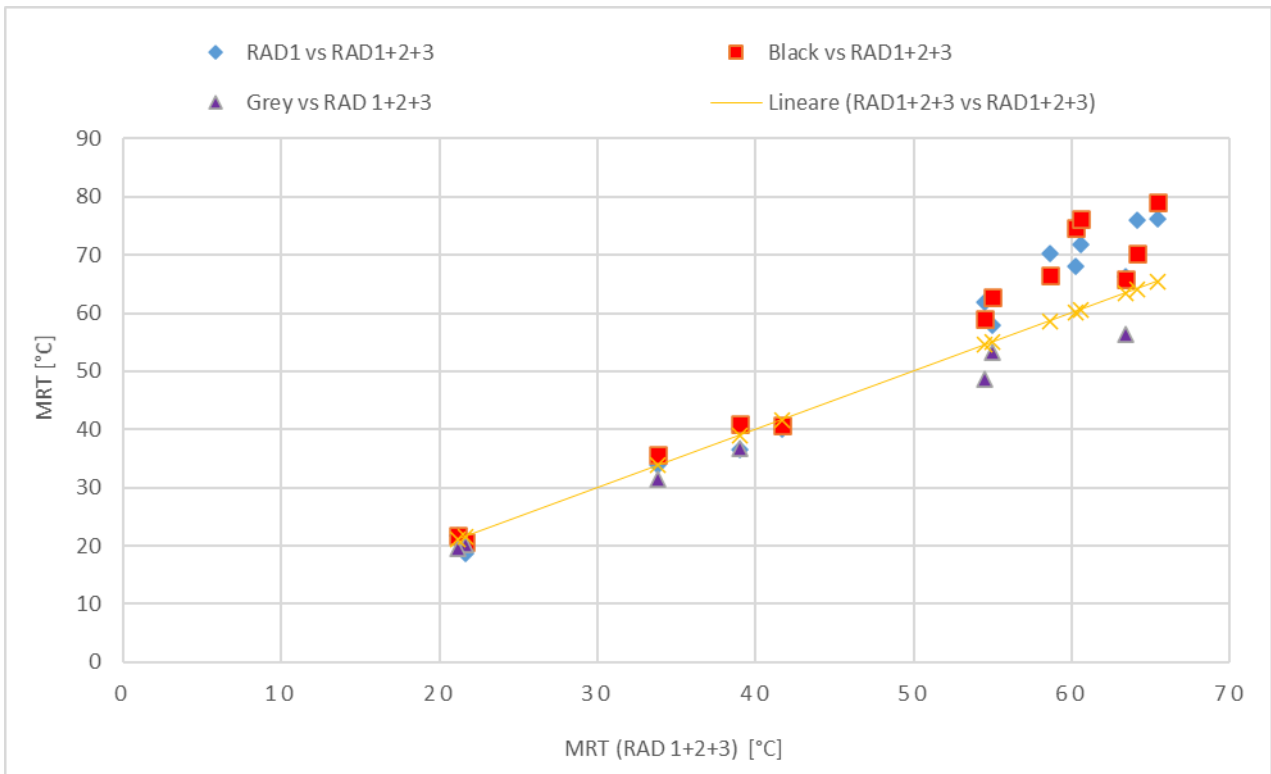


Figure 0. 2. Average MRT values obtained with each instrument in each measurement campaign.

The figure allows us to observe that the average MRT values obtained with the black globe and the single net radiometer are -in the majority of the measurements- higher than the average MRT obtained with the combination of the three net radiometers. On the contrary, the grey globe always tends to underestimate the MRT with respect to the reference values. The differences between one instrument and another are even more evident as MRT increases. In particular, when the reference MRT exceeds 50 °C, the average difference with respect to the black thermometer globe is higher than 15 °C; albeit in a reduced way and in opposite sign, also the difference with respect to the grey globe increases, in absolute value, up to 7 °C. On the other hand, these differences tend to vanish in measurements where the MRT obtained falls below 30 °C. These correspond to measurements made during night or with the instrumentation in shade, therefore in absence of direct solar radiation on the instrumentation.

Another factor influencing the difference in MRT obtained turned out to be the variation in solar height over the course of the day. As an explanatory example, it is possible to consider *Figure 0. 3*, which indicates the trend of the MRT obtained by means of net radiometers, black globe and grey globe during the measurement campaign carried out on 01/09/2020. In the hours corresponding to a greater solar height, between 12:00 and 15:00, the black globe provided MRT values up to 20 °C higher than the reference values. Similarly, by using the grey globe we obtained MRT values up to 20 °C lower than those recorded with the three net radiometers. As the solar height decreases, and in particular after 3:30 pm, the difference between one instrument and another is considerably reduced, until it disappears.

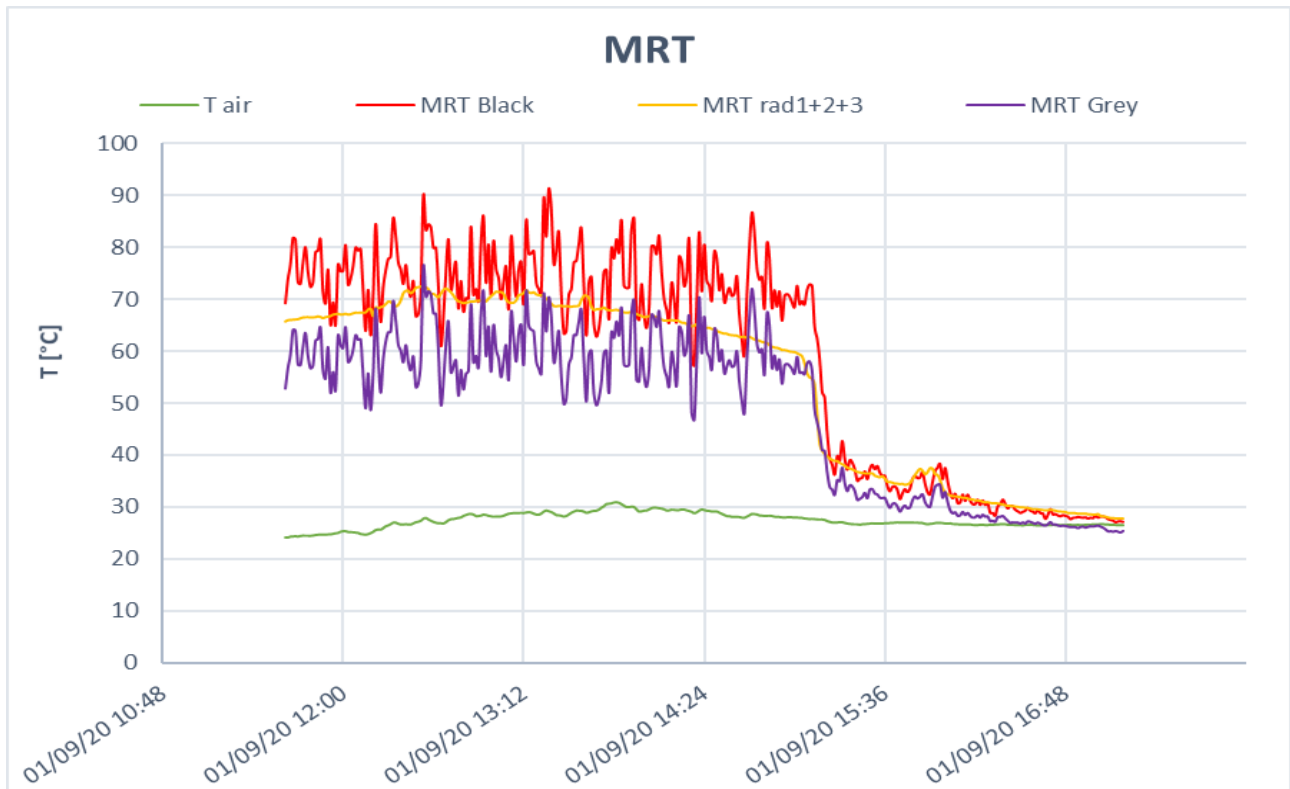



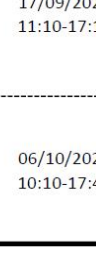
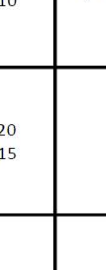
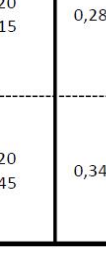
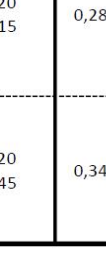
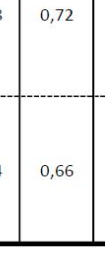
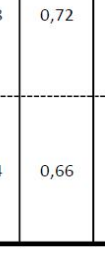
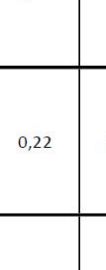
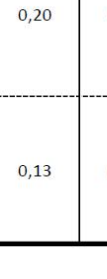
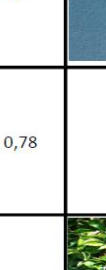








Figure 0. 3. MRT values obtained with three net radiometers, black globe thermometer and grey globe thermometer.

As described in *Chapter 2. Instruments and Methodology*, through the data regarding the radiation received by the net radiometers sensors it was possible to evaluate the radiative properties of the surfaces characterizing the measurement environment. *Table 0. 2* shows the photos of the vertical and horizontal surfaces examined, as well as their reflectivity and absorptivity. These values were then related to the UTCI calculated in the different measurement sites, in order to evaluate how the outdoor thermal comfort is influenced by the radiative properties of the materials present in each specific environment.

The results in the table allow to see that the highest UTCI values obtained (above 40 °C) were found in the presence of environments with a high reflectivity of both the soil and the vertical surfaces present near the instrumentation. In particular, on 23/07/2020, in correspondence with an average reference UTCI equal to 40.95 °C, a ground reflectivity of 0.31 and a reflectivity of the light plaster wall of 0.48 were calculated.

Table 0. 2. Radiative properties of the measurement environments and mean UTCI values.

Building Envelope/ Environment	Measurement date and hour	Radiative properties				Building envelope	Ground surface	UTCI (mean values) [°C]		
		ρ (wall)	α (wall)	ρ (ground)	α (ground)			RAD 1+2+3	Black globe	Grey globe
Flat rooftop with a waterproofing membrane	20/07/2020 12:00-19:30			0,11	0,89			36,76	40,36	
	21/07/2020 9:00-15:40							36,06	38,03	
Light plaster wall	23/07/2020 13:00-16:30	0,48	0,52	0,31	0,69			40,95	44,42	
Porcelain stoneware Facade Cladding	27/07/2020 12:00-16:30	0,30	0,70	0,24	0,76			40,87	42,40	
	18/09/2020 11:10-17:15	0,28	0,72	0,24	0,76			39,14	39,76	37,37
Park	28/07/2020 11:50-16:30			0,20	0,80			38,77	42,58	
Green rooftop	26/08/2020 day 15:20-21:00			0,22	0,78			33,54	33,31	
	26-27/08/2020 night 21:00-8:00							24,75	24,50	24,35
	27/08/2020 day 8:00-17:15							36,33	38,23	35,91
Blue plaster wall	01/09/2020 11:30-17:10	0,31	0,69	0,23	0,77			33,69	34,79	32,19
Street Canyon	09/09/2020 10:40-17:15			0,22	0,78			28,60	29,06	27,99
Green wall	17/09/2020 11:10-17:15	0,28	0,72	0,20	0,80			32,30	32,77	31,70
	06/10/2020 10:10-17:45	0,34	0,66	0,13	0,87			19,27	19,46	18,69

Chapter 4: Discussions and further elaborations

The chapter is aimed at deepening the findings of Chapter 3. *Experimental campaigns and results*, in which the results of the analyses were presented. A first correlation study was performed between the average UTCI values and the recorded meteorological parameters. From this it emerged that the parameters having the greatest influence on the thermal index are the outdoor air temperature and the global radiation impacting the instrumentation. In fact, both of these variables show a strong and positive correlation with the UTCI, as shown in Figure 0. 4. Weaker correlations were identified between UTCI and V_{air} and between UTCI and RH, as shown by the analyses in Chapter 4. *Discussions and further elaborations*.

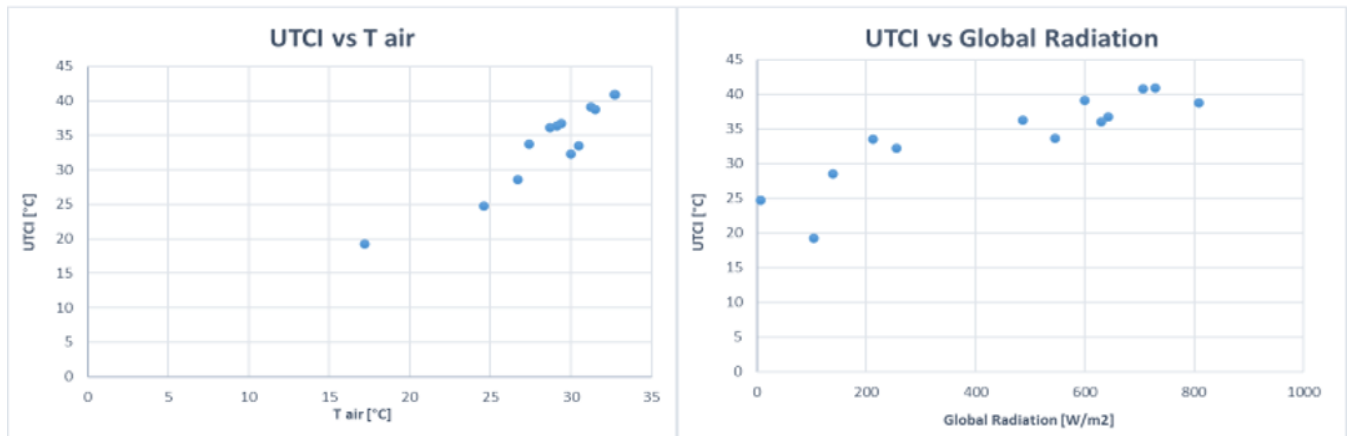


Figure 0. 4. Correlation between UTCI and air temperature and between UTCI and global radiation.

During the analyses it was possible to see how, in open field measurements, the results provided by the globe thermometers differed greatly from the reference values provided by the three net radiometers. In particular, the single net radiometer measuring the radiative fluxes coming from the upward/downward direction has been shown to better approximate the MRT than the black globe thermometer in open field, while the opposite occurs in all the other measurement environments. This has therefore evidenced the importance of vertical radiative fluxes in open field measurements, not correctly described by the "standing man" view factors chosen for the analyses of Chapter 3. *Experimental campaigns and results* and commonly adopted in literature. It was therefore decided to re-evaluate MRT in open field measurements using, as suggested by Thorsson et al. (Thorsson et al. 2007), the spherical view factors. Table 0. 3 shows that, with the new view factors, the differences between the MRT provided by the three net radiometers and the ones provided by the black globe thermometer and by the single radiometer were reduced, approaching the difference generally found in the other measurement environments.

Table 0. 3. Comparison between "standing man" and "spherical" view factors in open field.

Building Envelope/ Environment	Measurement date and hour	Instrumentation directly exposed to the solar radiation	MRT (mean values) [°C]			
			RAD 1+2+3 standing man	RAD 1	Black globe	RAD 1+2+3 sphere
Flat rooftop with a waterproofing membrane	20/07/2020 12:00-19:30	yes	60,22	68,16	74,62	62,44
	21/07/2020 9:00-15:40	yes	58,63	70,17	66,55	61,74
Park	28/07/2020 11:50-16:30	yes	60,61	71,70	76,17	63,58
Green rooftop	27/08/2020 day 8:00-17:15	yes	54,96	57,87	62,66	55,87

Finally, we wanted to investigate the possible causes of the differences found between the globe thermometers and the net radiometers. In particular, the shape of the globe and the method used to evaluate the convective heat exchange between the globe and the measuring environment have been identified as the main causes. Regarding the shape, as already noted, the spherical shape of the globe is not suitable for evaluating the radiative loads acting on a standing person, which are instead considered in the three net radiometers solution: the black globe weights in equal measure the radiative fluxes coming from every direction, while the view factors adopted in net radiometers calculations attribute a greater weight to the horizontal radiative fluxes, as they impact on a greater surface of the human body (modelled as a parallelepiped).

A further problem lies in the convective heat exchange coefficients commonly adopted in the literature. As discussed above, the lack of a univocal method for evaluating the exchanges between the globe and the environment in outdoor conditions has led several researchers to adopt different convective coefficients. Different coefficients lead to different results in terms of MRT obtained by means of the globe thermometer and therefore to more or less marked differences compared to the three radiometers solution. Furthermore, the most commonly used values of h_{conv} come from studies in indoor environments and only subsequently adapted for outdoors. For this purpose, Thorsson et al. (Thorsson et al. 2007) suggested a correction which aims to propose h_{conv} more suitable for outdoor measurements.

In this thesis it was decided to make a comparison between the convective heat transfer coefficient adopted by Kuhen et al. (Kuehn, Stubbs, and Weaver 1970) -and used in the analyses of *Chapter 3. Experimental campaigns and results*- and the one proposed by Thorsson et al. (Thorsson et al. 2007).

According to the results obtained, the correction proposed by Thorsson et al. always increases the MRT calculated both when applied to the black globe and the grey globe. Starting from this consideration, we can establish that, when the new h_{conv} is applied to the black globe results, we face an undesired effect, since it increases the MRT of the globe, already higher than the reference MRT. On the contrary, when the Thorsson et al.'s correction is applied to the grey globe, which generally provided lower MRT values, we are able to reach results more similar to the ones obtained with the three net radiometers. In this way, the grey globe will be able to approximate, with a quite good accuracy, the reference values for the MRT.

This thesis work therefore tried to provide information about possibilities and limitations of individual instruments commonly used in literature for the evaluation of outdoor thermal comfort parameters, investigating the criticalities of measurement methods less accurate but cheaper than the integral radiation measurements, such as globe thermometers. This is followed by an attempt of identifying applicability criteria of corrections which could improve the results of these cheaper methods, in order to approach the reference results obtained with three net radiometers.

In conclusion, the ultimate goal of this thesis is to highlight critical aspects of outdoor thermal comfort assessments, which do not have yet a universally recognized solution, such as which view factors are more suitable to describe the actual radiative fluxes in open field for the calculation of MRT by net radiometers or which convective coefficient better represents the heat exchange between globe thermometer and the surrounding environment. This will lead us to identify possible directions in which to move for future insights, research and studies.

Table of Contents

Abstract	2
Sommario	3
Extended Abstract	4
Table of Contents	16
List of Figures.....	18
List of Tables.....	21
1. Outdoor Thermal Comfort assessment.....	23
1.1 Urban Heat Island effect.....	23
1.1.1 Main causes of UHI effect and mitigation strategies	23
1.2 Outdoor thermal comfort assessment.....	25
1.2.1 Heat balance of the human body.....	25
1.2.2 Mean Radiant Temperature assessment.....	26
1.2.3 Thermal Indices	34
1.3 Lack of standardization in outdoor thermal comfort assessments.....	37
1.3.1 Standards, guidelines and handbooks.....	37
1.3.2 Variety of instruments and methods applied in outdoor thermal comfort assessments.....	38
1.3.3 Need for standardization.....	40
2. Instruments and Methodology.....	41
2.1 Net Radiometers.....	41
2.1.1 Net radiometers NR01.....	43
2.1.2 NR01 governing equations	47
2.1.3 Mean radiant Temperature calculation using net radiometers	48
2.1.4 Solar Reflectivity and solar Absorptivity of a surface calculated with net radiometers	49
2.2 Globe thermometer.....	51
2.2.1 Black globe thermometer.....	51
2.2.2 Grey globe thermometer.....	52
2.2.3 Mean Radiant Temperature calculation using globe thermometers	53
2.3 Multi-parameters sensor	55
2.4 Datalogger	57
2.5 Support equipment	59
2.6 Methodology	60
3. Experimental campaigns and results.....	63

3.1 Mean Radiant Temperature and UTCI assessment	63
3.1.1 Flat rooftop with a waterproofing membrane	65
3.1.2 Light plaster wall.....	69
3.1.3 Porcelain stoneware façade cladding.....	72
3.1.4 Park.....	77
3.1.5 Green rooftop.....	80
3.1.6 Blue plaster building envelope	87
3.1.7 Street canyon.....	90
3.1.8 Green wall.....	93
3.2 Summary of results, mean and peak values.....	99
4. Discussions and further elaborations	105
4.1 Outdoor thermal comfort and thermal perception in different environments and meteorological conditions	105
4.2 Three net radiometers vs Globe thermometers: causes of the different results	111
4.3 Influence of view factors in the evaluation of MRT by using the six-directional method.....	112
4.4 Influence of convective heat exchange coefficient in the evaluation of MRT by using the globe thermometers	115
5. Conclusions.....	130
Nomenclature.....	132
Acronyms.....	132
Symbols.....	133
Bibliography.....	137

List of Figures

Figure 0. 1. Positioning and setup of the instruments on support equipment.....	9
Figure 0. 2. Average MRT values obtained with each instrument in each measurement campaign.....	11
Figure 0. 3. MRT values obtained with three net radiometers, black globe thermometer and grey globe thermometer.	12
Figure 0. 4. Correlation between UTCI and air temperature and between UTCI and global radiation.	14
Figure 1. 1. Main causes of UHI effect (Kleerekoper, Van Esch, and Salcedo 2012).	24
Figure 1. 2 Instruments setup for measuring short-wave and long-wave radiation, using pyranometers and pyrgeometers (Thorsson et al. 2007).	27
Figure 1. 3. Globe thermometer consisting of a flat grey 40 mm celluloid table tennis ball around a Pt100 temperature probe (Thorsson et al. 2007).....	29
Figure 2. 1. Disposition and numbering of the three net radiometers.	42
Figure 2. 2. Wires connecting the net radiometers and the datalogger must avoid interferences with the measurements of the radiometers themselves.	43
Figure 2. 3. Dimensions of NR01 in 10-3 m (Hukseflux NR01 manual).	44
Figure 2. 4. Overview of NR01 (Hukseflux NR01 manual).	45
Figure 2. 5. Spectral response of the pyranometer compared to the solar spectrum. The pyranometer only cuts off a negligible part of the total solar spectrum (Source: Hukseflux 2016).....	46
Figure 2. 6. Atmospheric radiation as a function of wavelength. Long-wave radiation is mainly present in the 4 to 50×10^{-6} m range, whereas solar radiation is mainly present in the 0.3 to 3×10^{-6} m range. The two are measured separately using pyrgeometers and pyranometers (Source: Hukseflux 2016).	47
Figure 2. 7. Disposition of the net radiometers near a vertical/horizontal surface.....	50
Figure 2. 8. Black-painted globe thermometer.	52
Figure 2. 9. Grey-painted globe thermometer.	53
Figure 2. 10. All-in-one sensor able to measure wind velocity and direction, air temperature, solar radiation, air humidity and pressure.	55
Figure 2. 11. Datalogger Alpha-Log and one terminal block extension ALIEM.	58
Figure 2. 12. Datalogger Alpha-Log and the two extensions ALIEM in the shockproof suitcases.....	58
Figure 2. 13. Datalogger Alpha-Log and terminal block.	58
Figure 2. 14. Whole instrumentation used in this thesis work.....	59
Figure 2. 15. Diagram describing the methodology followed in each measurement campaigns.	62
Figure 3. 1. Flat rooftop with a waterproofing membrane, Via Feltrinelli 16/50, Milan.	65
Figure 3. 2. MRT calculated with net radiometers and globe thermometers; 20/07/2020.....	66
Figure 3. 3. MRT calculated with net radiometers and globe thermometers; 21/07/2020.....	66
Figure 3. 4. MRT calculated with three radiometers and one radiometer measuring upward/downward direction; 20/07/2020.	67
Figure 3. 5. MRT calculated with three radiometers and one radiometer measuring upward/downward direction; 21/07/2020.	67
Figure 3. 6. UTCI calculated with net radiometers and globe thermometers; 20/07/2020.	68
Figure 3. 7. UTCI calculated with net radiometers and globe thermometers; 21/07/2020.	68
Figure 3. 8. Light plaster wall, Via Lambruschini 4, Milan.	69
Figure 3. 9. MRT calculated with net radiometers and globe thermometers; 23/07/2020.....	70

Figure 3. 10. MRT calculated with three radiometers and one radiometer measuring upward/downward direction; 23/07/2020.	70
Figure 3. 11. UTCI calculated with net radiometers and globe thermometers; 23/07/2020.	71
Figure 3. 12. Porcelain stoneware facade cladding, Via Lambruschini, Milan.	72
Figure 3. 13. MRT calculated with net radiometers and globe thermometers; 27/07/2020.....	73
Figure 3. 14. MRT calculated with net radiometers and globe thermometers; 18/09/2020.....	74
Figure 3. 15. MRT calculated with three radiometers and one radiometer measuring upward/downward direction; 27/07/2020.	74
Figure 3. 16. MRT calculated with three radiometers and one radiometer measuring upward/downward direction; 18/09/2020.	75
Figure 3. 17. UTCI calculated with net radiometers and globe thermometers; 27/07/2020.	75
Figure 3. 18. UTCI calculated with net radiometers and globe thermometers; 18/09/2020.	76
Figure 3. 19. Park, Cascina Merlata district, Milan.	77
Figure 3. 20. MRT calculated with net radiometers and globe thermometers; 28/07/2020.....	78
Figure 3. 21. MRT calculated with three radiometers and one radiometer measuring upward/downward direction; 28/07/2020.	78
Figure 3. 22. UTCI calculated with net radiometers and globe thermometers; 28/07/2020.	79
Figure 3. 23. Green rooftop, Via G. Ponzio, Milan.....	80
Figure 3. 24. MRT calculated with net radiometers and globe thermometers; day 26/08/2020.....	82
Figure 3. 25. MRT calculated with net radiometers and globe thermometers; night 26-27/08/2020.	82
Figure 3. 26. MRT calculated with net radiometers and globe thermometers; day 27/08/2020.....	83
Figure 3. 27. MRT calculated with three radiometers and one radiometer measuring upward/downward direction; day 26/08/2020.....	83
Figure 3. 28. MRT calculated with three radiometers and one radiometer measuring upward/downward direction; night 26-27/08/2020.....	84
Figure 3. 29. MRT calculated with three radiometers and one radiometer measuring upward/downward direction; day 27/08/2020.....	84
Figure 3. 30. UTCI calculated with net radiometers and globe thermometers; day 26/08/2020.....	85
Figure 3. 31. UTCI calculated with net radiometers and globe thermometers; night 26-27/08/2020.....	85
Figure 3. 32. UTCI calculated with net radiometers and globe thermometers; day 27/08/2020.....	86
Figure 3. 33. Blue plaster building envelope, Cascina Merlata district, Milan.	87
Figure 3. 34. MRT calculated with net radiometers and globe thermometers; 01/09/2020.....	88
Figure 3. 35. MRT calculated with three radiometers and one radiometer measuring upward/downward direction; 01/09/2020.	88
Figure 3. 36. UTCI calculated with net radiometers and globe thermometers; 01/09/2020.	89
Figure 3. 37. Street canyon, Bovisa district, Milan.	90
Figure 3. 38. MRT calculated with net radiometers and globe thermometers; 09/09/2020.....	91
Figure 3. 39. MRT calculated with three radiometers and one radiometer measuring upward/downward direction; 09/09/2020.	91
Figure 3. 40. UTCI calculated with net radiometers and globe thermometers; 09/09/2020.	92
Figure 3. 41. Green wall, Via G. La Masa, Milan.	93
Figure 3. 42. MRT calculated with net radiometers and globe thermometers; 17/09/2020.....	94
Figure 3. 43. MRT calculated with three radiometers and one radiometer measuring upward/downward direction; 17/09/2020.	94
Figure 3. 44. UTCI calculated with net radiometers and globe thermometers; 17/09/2020.	95
Figure 3. 45. Green wall, Via Bovisasca, Milan.	96

Figure 3. 46. MRT calculated with net radiometers and globe thermometers; 06/10/2020.....	97
Figure 3. 47. MRT calculated with three radiometers and one radiometer measuring upward/downward direction; 06/10/2020.	97
Figure 3. 48. UTCI calculated with net radiometers and globe thermometers; 06/10/2020.	98
Figure 3. 49. MRT mean values for each instrument in relation to the MRT obtained by using three net radiometers.	101
Figure 4. 1. UTCI vs T_{air} (mean values).	108
Figure 4. 2. UTCI vs V_{air} (mean values).	108
Figure 4. 3. UTCI vs RH (mean values).	109
Figure 4. 4. UTCI vs Global radiation (mean values).	109
Figure 4. 5. UTCI vs ground reflectivity (mean values).	110
Figure 4. 6. UTCI vs wall reflectivity (mean values).	110
Figure 4. 7. Comparison between standing man and spherical view factors; flat rooftop with a waterproofing membrane, 20/07/2020.	113
Figure 4. 8. Comparison between standing man and spherical view factors; flat rooftop with a waterproofing membrane, 21/07/2020.	113
Figure 4. 9. Comparison between standing man and spherical view factors; park, 28/07/2020.	114
Figure 4. 10. Comparison between standing man and spherical view factors; green rooftop, 27/08/2020.	114
Figure 4. 11. Difference between Kuhen et al.'s and Thorsson et al.'s convective heat transfer coefficients for globe thermometers MRT measurements; 20/07/2020.	117
Figure 4. 12. Difference between Kuhen et al.'s and Thorsson et al.'s convective heat transfer coefficients for globe thermometers MRT measurements; 21/07/2020.	117
Figure 4. 13. Difference between Kuhen et al.'s and Thorsson et al.'s convective heat transfer coefficients for globe thermometers MRT measurements; 23/07/2020.	118
Figure 4. 14. Difference between Kuhen et al.'s and Thorsson et al.'s convective heat transfer coefficients for globe thermometers MRT measurements; 27/07/2020.	118
Figure 4. 15. Difference between Kuhen et al.'s and Thorsson et al.'s convective heat transfer coefficients for globe thermometers MRT measurements; 28/07/2020.	119
Figure 4. 16. Difference between Kuhen et al.'s and Thorsson et al.'s convective heat transfer coefficients for globe thermometers MRT measurements; day 26/08/2020.	120
Figure 4. 17. Difference between Kuhen et al.'s and Thorsson et al.'s convective heat transfer coefficients for globe thermometers MRT measurements; night 26-27/08/2020.	121
Figure 4. 18. Difference between Kuhen et al.'s and Thorsson et al.'s convective heat transfer coefficients for globe thermometers MRT measurements; day 27/08/2020.	122
Figure 4. 19. Difference between Kuhen et al.'s and Thorsson et al.'s convective heat transfer coefficients for globe thermometers MRT measurements; 01/09/2020.	123
Figure 4. 20. Difference between Kuhen et al.'s and Thorsson et al.'s convective heat transfer coefficients for globe thermometers MRT measurements; 09/09/2020.	124
Figure 4. 21. Difference between Kuhen et al.'s and Thorsson et al.'s convective heat transfer coefficients for globe thermometers MRT measurements; 18/09/2020.	125
Figure 4. 22. Difference between Kuhen et al.'s and Thorsson et al.'s convective heat transfer coefficients for globe thermometers MRT measurements; 17/09/2020.	126
Figure 4. 23. Difference between Kuhen et al.'s and Thorsson et al.'s convective heat transfer coefficients for globe thermometers MRT measurements; 06/10/2020.	127

List of Tables

Table 0. 1. Measurement environments, day and hours of the surveys, measurement frequency and instruments adopted.....	10
Table 0. 2. Radiative properties of the measurement environments and mean UTCI values.	13
Table 0. 3. Comparison between “standing man” and “spherical” view factors in open field.	14
Table 1. 1. Examples of rational thermal comfort indices that have been used in outdoor thermal comfort studies (Johansson et al. 2014).	35
Table 1. 2. UTCI ranges and stress categories	36
Table 1. 3. Topics of different standards, guidelines and handbooks (ASHARE 2013; Ashrae Standard 2001; Standard 1998; ISO 2005; VDI 2008) (Johansson et al. 2014).	38
Table 1. 4. Ways to measure and/or model the MRT in the reviewed studies (Johansson et al. 2014).....	39
Table 2. 1. General description of the variables measured in the analysis, including the measuring principle and range, accuracy and resolution of the instruments adopted.....	41
Table 2. 2. NR01 general specifications (Source: Hukseflux 2016).	44
Table 2. 3. Dimensions, colours and emissivity of the globe thermometers used in this work.....	51
Table 2. 4. General specifications of the All-in-one sensor and parameters which can be measured.	56
Table 2. 5. Technical specifications of the All-in-one sensor, including the measuring principle and range, the accuracy and the resolution of the instrument for each meteorological parameter measured.....	56
Table 3. 1. Measurement campaigns: environment, location, date and hour, sampling frequency and instrumentation used.	64
Table 3. 2. UTCI thermal stress categories and colours of the corresponding band in the UTCI graphs in Chapter 3.	64
Table 3. 3. Radiative properties of the horizontal/vertical surfaces tested; flat rooftop with a waterproofing membrane; 20/07/2020.	69
Table 3. 4. Radiative properties of the horizontal/vertical surfaces tested; light plaster wall; 23/07/2020. .	71
Table 3. 5. Radiative properties of the horizontal/vertical surfaces tested; porcelain stoneware façade cladding; 27/07/2020.	76
Table 3. 6. Radiative properties of the horizontal/vertical surfaces tested; park; 28/07/2020.	79
Table 3. 7. Radiative properties of the horizontal/vertical surfaces tested; green rooftop; 26-27/08/2020.	86
Table 3. 8. Radiative properties of the horizontal/vertical surfaces tested; blue plaster building envelope; 01/09/2020.....	89
Table 3. 9. Radiative properties of the horizontal/vertical surfaces tested; street canyon; 09/09/2020.	92
Table 3. 10. Radiative properties of the horizontal/vertical surfaces tested; green wall; 17/09/2020.....	95
Table 3. 11. Radiative properties of the horizontal/vertical surfaces tested; street canyon; 06/10/2020. ...	98
Table 3. 12. Mean, maximum and minimum values of MRT for each measurement by using all the instruments at our disposal.....	101
Table 3. 13. Mean, maximum and minimum values of UTCI for each survey by using all the instruments at our disposal.	103
Table 3. 14. Pictures of the measurement environments and radiative properties of the horizontal/vertical surfaces characterizing each environment.....	104
Table 4. 1. Mean, maximum and minimum values of UTCI obtained starting from the MRT results provided by the three net radiometers method.	107

Table 4. 2. Comparison between standing man and spherical view factors adopted in the MRT evaluation by using net radiometers. 115

Table 4. 3. Mean values of MRT obtained by means of net radiometers and globe thermometers by adopting different convective heat exchange coefficients. 129

1. Outdoor Thermal Comfort assessment

1.1 Urban Heat Island effect

There is a strong relationship between cities and climate: climate conditions affect both the life of the people living in a city and how the urban area is used. The increase in urban air temperatures due to urbanization has a huge impact on the buildings' energy performance and demand (e.g. by increasing the consumption for cooling) and, in the long run, can affect the people health too (e.g. by adding stress on human physiology, by causing fatigue, heat stress and strokes) (Georgatou and Kolokotsa 2016; Kleerekoper, Van Esch, and Salcedo 2012).

Public spaces designed to be used by pedestrians such as parks, squares and residential streets will be more used and enjoyed if their climate is comfortable and healthy (Kleerekoper, Van Esch, and Salcedo 2012). Thus, it is significant for urban planners to gain an understanding of air temperature variations between different land-use categories for both extreme and average climate conditions (Georgatou and Kolokotsa 2016; Svensson and Eliasson 2002).

These are just a few among many reasons behind the rising interest in outdoor thermal comfort, a field that is becoming more crucial since climate change projections suggest that summer heatwaves will become more frequent and severe during this century, consistent with the observed trends of the past decades (Fischer and Schär 2010; van Hove et al. 2015).

Therefore, urban environments become one of the main research topics of scientific and technical communities, since urban areas are the most affected environments by the so-called Urban Heat Island (UHI) effect. This is the phenomenon for which the urban air temperature is higher than the one of the surrounding rural environment (Sangiorgio, Fiorito, and Santamouris 2020). The extent of this temperature difference varies in time and space as a result of meteorological characteristics and urban geometries (Kleerekoper, Van Esch, and Salcedo 2012). One of the most discussed issues related to the UHI effect is the increase in the peak and global electricity demand for cooling, ventilation and air conditioning systems. In Santamouris et al.' study (Santamouris et al. 2001), up to tripled peak building electricity demand were detected due to the effects of the UHI. The increasing worsening of urban thermal conditions thus increases the importance of urgently improving the techniques for assessing outdoor comfort.

1.1.1 Main causes of UHI effect and mitigation strategies

Nowadays, the following phenomena are considered to be the main causes of the UHI effect (*Figure 1. 1*) (Santamouris et al. 2001; Kleerekoper, Van Esch, and Salcedo 2012; Georgatou and Kolokotsa 2016; Oke and Cleugh 1987):

1. Amplified short-wave radiation gain. This means that more solar radiation is absorbed because of multiple reflections in the urban environment. In a built environment, solar energy is absorbed into paving, roofs, and façades of different materials, causing an increase in the surface temperature of urban structures.
2. Air pollution in the urban atmosphere absorbs and re-emits long-wave radiation in the urban environment.
3. Decrease of long-wave radiation loss, through the atmospheric window, due to obstruction of the sky by buildings. The radiation is trapped within the street canyon.
4. Anthropogenic heat released as a result of traffic, industry emissions, and human activities.
5. Highly polluted areas. The pollution blocks the infrared (IR) radiation from the earth and buildings and transforms the radiative energy into convective energy, causing a further rise in the average atmospheric temperature.
6. Decrease in evaporation in urban areas because of 'waterproofed surfaces', less permeable materials, and less vegetation than rural areas. This leads to less moisture availability.

7. Decreased turbulent heat transport due to the reduction of wind velocity. Street canyons reduce convective heat transfer and urban ventilation.

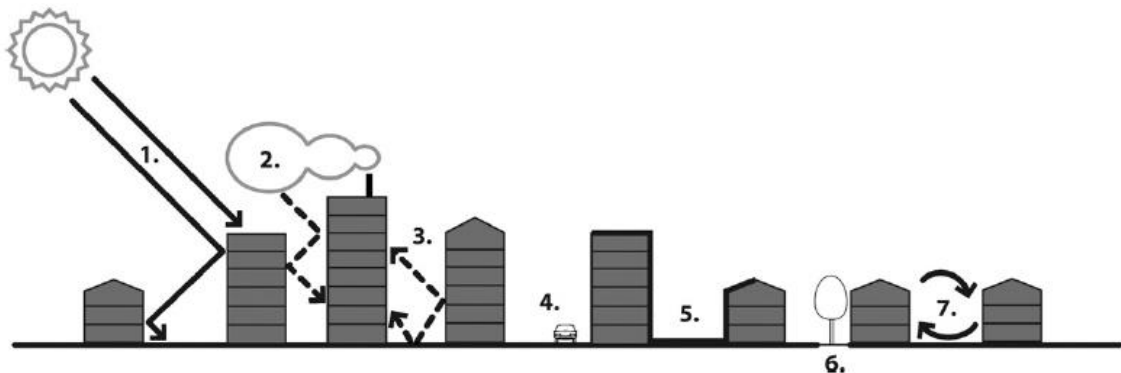


Figure 1. 1. Main causes of UHI effect (Kleerekoper, Van Esch, and Salcedo 2012).

Scientific communities put in place huge effort in developing and implementing several mitigation techniques and strategies of the UHI effect, many of these have already been tested in urban areas and concern blue/green infrastructures (e.g., vegetation and water bodies), and building structures and materials of the built environment (Kleerekoper, Van Esch, and Salcedo 2012).

Green Infrastructures

Vegetation allows cooling the environment actively through evaporation and transpiration and passively through shading surfaces that otherwise would absorb short-wave radiation. The most used applications of vegetation in urban areas are parks, street trees, green roofs or façades, and private gardens. Covering a roof or a façade with vegetation has a cooling effect on both the outdoor urban environment and the building itself: it prevents the absorption of short-wave radiation by the low albedo materials of the building through the shading effect of the vegetation and, during summer, reduces the indoor temperature of the building thanks to the high insulation value of the canopy. The most effective green solutions seem to be street trees (Savio et al. 2006), while the promotion of green in private spaces has a higher effect in the case of high-density cities. In this regard, in Europe, numerous initiatives have started defining a good trend for the implementation of green strategies: one in Paris promoting green façades and green terraces (Mairie de Paris 2014), or the European project CLEVER cities (Clever cities, <https://clevercities.eu>), involving Milan, London, and Hamburg.

Blue infrastructures

Blue infrastructures allow cooling the environment through evaporation processes, by absorbing heat. Water applications are usually more effective when involving a large surface or when the water is flowing or dispersed, like from a fountain (besides, fountains represent an optimum compromise between cost and effectiveness) (Kleerekoper, Van Esch, and Salcedo 2012). The promotion of permeable pavements and water storage infrastructures is also a good strategy in case of droughts and flooding.

Building structure

Building density and geometry affect the incidence of radiation on materials that can store heat and trap the radiation by multiple reflections between the buildings and the urban environment. The obstruction of the sky by building structures reduces the long-wave radiation loss so that heat intercepted will be absorbed or re-radiated into urban canyons. Built form has also an impact on wind speed and ventilation, which are important cooling factors in many warm countries (Kleerekoper, Van Esch, and Salcedo 2012). Space heating/cooling building energy consumption is strongly dependent on the ratio between buildings' surface and volume (S/V) (Martilli 2014). However, even if compact cities are energetically efficient, from a heat stress point of view instead, very compact cities, with no vegetation, are the most uncomfortable, because tall buildings and narrow street canyons make the spatial density of the anthropogenic heat fluxes

higher than the ones of less dense cities (Martilli 2014). Furthermore, from a policy standpoint, it is rather difficult to act on the built form of a city; nevertheless, certain cities tried to include precise spatial parameters in their urban planning guidelines.

Materials

Materials used in the urban area can play an important role in the mitigation of UHI effects. Although surface temperatures may be closely linked to the air temperature, in presence of strong solar fluxes and in absence of evapotranspiration or strong wind the difference may be very substantial and dependent on the material in question (Erell et al. 2014). While permeable materials allow cooling by evaporation, hard materials accumulate heat. It is also important to underline that low albedo materials are responsible for the absorption of short-wave radiation. Some numerical simulating models in Sacramento and California showed that an increase in the albedo city-wide from 25 to 40% leads to a temperature drop of 1-4 °C; while increasing the building albedo from 9 to 70% can reduce the annual cooling demand by 19% (Taha 1997). The effect of albedo modification on air temperature at urban scale has been modelled using mesoscale models. In the majority of the case, achieving a substantial increase in the urban albedo assumed extensive implementation of cool roofs, while cool paving is generally considered as a second strategy (Erell et al. 2014). However, the mentioned strategies could imply an issue for the comfort of people: if it is true that an increase in the albedo city-wide results in a reduction of the UHI effect and consequently leads to a lower cooling consumption, higher albedo means a greater reflection of visible light and thus the risk of glare for the people (Erell et al. 2014). Although the use of high-albedo materials for urban surfaces may reduce the air temperature to which pedestrians are exposed, their radiant balance with the environment is affected too. The reduction in surface temperatures, which leads to reduced long-wave emission, is offset by the increased reflection of solar radiation. The net effect of increasing the albedo of urban surfaces may thus increase the stresses to which pedestrians are exposed, rather than the expected improvement in the thermal comfort (Erell et al. 2014). This can lead to a scenario in which energy policies and citizens' well-being are at odds, differently from the green solutions which both reduce the UHI effect and have a positive impact on the comfort of the people.

Heat-related problems should be evaluated and addressed in the design of outdoor spaces (Lai, Maing, and Ng 2017; Tan, Wong, and Jusuf 2013) and urban planning (Matzarakis, Rutz, and Mayer 2007). Designers and urban and regional planners are thus recently demanding easy methods to assess the thermal characteristic of outdoor environments and their relation with human comfort (Gulyás, Unger, and Matzarakis 2006). For this purpose, this thesis will focus on different methodologies for assessing outdoor thermal comfort.

1.2 Outdoor thermal comfort assessment

Compared to indoor thermal comfort, the outdoor one presents a higher complexity in terms of variability of the environmental conditions (Johansson et al. 2014). Several studies have led to the identification of air temperature (T_{air}), relative humidity (RH), air velocity (V_{air}), and radiant fluxes as the most influential parameters for outdoor thermal comfort (Lai, Maing, and Ng 2017; Thorsson et al. 2007).

In particular, the radiant fluxes are not easy to keep under control because of their rapid changes in both space and time due to the meteorological conditions and the properties of the surrounding elements.

1.2.1 Heat balance of the human body

For a better understanding of the relevance of outdoor thermal comfort and its relationship with the well-being of the people, a brief description of the fluxes involved in the heat exchange between the human body and the surrounding environment is needed. The heat balance is described in *Equation (1. 1)*:

$$(M + \dot{Q}_R + \dot{Q}_C + \dot{Q}_K + \dot{Q}_{SW} + \dot{Q}_{Re}) - \dot{W} = S \left[W/m^2 \right] \quad (1. 1)$$

Where:

- M is the metabolic rate of the human body and it is always positive
- \dot{Q}_R is the radiative flux and, by convention, it is assumed positive if entering in the thermodynamic system (the human body)
- \dot{Q}_C is the convective flux and, by convention, it is assumed positive if entering in the thermodynamic system
- \dot{Q}_K is the conductive flux and, by conduction, it is assumed positive if entering in the thermodynamic system
- \dot{Q}_{SW} is the flux of latent heat due to the perspiration
- \dot{Q}_{Re} is the heat flux due to the respiration (latent and sensible)
- \dot{W} is the rate of work density and, by convention, it is assumed positive if performed by the system.

To better manage the complexity and the diversity of the radiation fluxes, the concept of the Mean Radiant Temperature (MRT) was adopted in studies concerning outdoor thermal comfort assessments.

The MRT is defined as “the uniform temperature of an imaginary enclosure made of black surfaces in which the radiant heat transfer from the human body (with emissivity $\epsilon=1$) equals the radiant heat transfer in the actual non-uniform enclosure” (ASHRAE 55 2017).

This parameter abridges all the radiative fluxes reaching a human body in an outdoor environment: the incoming and reflected radiation, the direct and diffuse short-wave radiation and the long-wave radiation coming from surrounding surfaces, ground and sky. It is thus the most important meteorological input parameter for the human energy balance, especially during sunny weather in summer, since the combined effect of radiant and convective heat gains/losses greatly affect the human energy balance in outdoor spaces (Matzarakis, Rutz, and Mayer 2007; Matzarakis and Endler 2010; Mayer and Höppe 1987; Lai, Maing, and Ng 2017).

The MRT, being closely related to the human body energy balance, has become the target of several assessments regarding outdoor thermal comfort (Lai, Maing, and Ng 2017) and it will be one of the main focus of this thesis, too.

1.2.2 Mean Radiant Temperature assessment

The measurement techniques of the meteorological parameters T_{air} , RH, and V_{air} are defined according to international standards (International Organization for Standardization 1990; International Organization for Standardization 2007; International Organization for Standardization 2007b; International Organization for Standardization 2015; ISO 19926 2015; International Organization for Standardization 2012; International Organization for Standardization 2017; International Organization for Standardization 2018), however, a standardized in-field technique for the MRT in outdoor environments is not yet developed. The lack of an international standard leads thus to the adoption of different methods -with different accuracy- for measuring the MRT in outdoor environments, hindering the comparison of results from different studies (Johansson et al. 2014).

1.2.2.1 Integral radiation measurements

The most accurate method to estimate outdoor MRT is employing integral radiation measurements (Krüger, Minella, and Matzarakis 2014; Thorsson et al. 2007). The method requires simultaneous measurements of

short-wave and long-wave radiation from six directions (east, west, north, south, upward, and downward) using pyranometers and pyrgeometers, as shown in *Figure 1. 2*.



Figure 1. 2 Instruments setup for measuring short-wave and long-wave radiation, using pyranometers and pyrgeometers (Thorsson et al. 2007).

The mean radiant flux density S_{str} [W/m^2] of a human body is firstly calculated by multiplying the six individual measurements of the short-wave and long-wave radiant fluxes with the corresponding weights, the view factor F_i ($i=1-6$), between the body and the surrounding surfaces according to *Equation (1. 2)* (Lai, Maing, and Ng 2017; Lin, Matzarakis, and Hwang 2010), reformulated from the German standard VDI 3787 (VDI 2008) (derived from Fanger' studies on thermal comfort) (Ole Fanger 1970):

$$S_{str} = \alpha_k \sum_{i=1}^6 F_i K_i + \varepsilon_p \sum_{i=1}^6 F_i L_i \quad (1. 2)$$

Where:

- F_i is the view factor for the i -th direction between the human body and the surrounding surfaces, determined by both the position and the orientation of the person
- K_i is the short-wave radiant fluxes from the i -th direction
- L_i is the long-wave radiant fluxes from the i -th direction
- α_k is the absorption coefficient for short-wave radiant fluxes (assuming 0.7 as standard value) (VDI 2008)
- ε_p is the emissivity of the human body. According to Kirchoff's laws, ε_p is equal to the absorption coefficient for short-wave radiant fluxes (assuming 0.97 as standard value) (VDI 2008).

The F_i factor allows considering different reference shapes, e.g. a standing man and a sphere. In the latter case, all fluxes are weighted identically with a value of 0.167. In the "standing man" case, instead, the role of the lateral fluxes become relatively greater than the vertical ones according to F_i values of 0.22 and 0.06 respectively, as suggested by Hoppe's analysis (Höppe 1992; Peter Höppe 1999), assuming that a standing person is attributable to a square-based parallelepiped with a ratio $H/L = 3.5$.

There are some remarkable differences between the MRT values characterizing the radiation load of a spherical body and a standing man. In the case of a standing shape, the MRT obtained will result higher than the MRT with "sphere factors" during the time of the day of lower sun elevation (Kántor, Kovács, and Lin

2015), accordingly to the different weights attributed to the lateral fluxes. *Chapter 3. Experimental campaigns and results* of the thesis analyses this aspect more in detail.

The MRT, according to VDI 3787 (VDI 3787 2008), is calculated as the temperature of an ideal black cavity in which the human body (modelled with a lumped-parameter approximation) is absorbing long-wave radiation, equal to the summation of the absorbed radiation in the real environment considering both the short-wave and long-wave radiation in Equation (1. 2):

$$S_{str} = \varepsilon_p * \sigma * MRT^4 \quad (1. 3)$$

Arranging (1. 3), the MRT (°C) is obtained from Stefan-Boltzmann law (VDI 3787 2008):

$$MRT = \left(\frac{S_{str}}{\varepsilon_p * \sigma} \right)^{0.25} - 273.15 \quad (1. 4)$$

Where:

- σ is the Stefan-Boltzmann constant and it is equal to $5.67 \times 10^{-8} \text{ Wm}^{-2}\text{K}^{-4}$.

The short-wave and long-wave radiation are measured by pyranometers and pyrgeometers respectively (Johansson et al. 2014), which is, however, an expensive, complex and not always feasible method.

The German guideline VDI 3787 suggests a similar but simpler and cheaper method where one pyranometer and one pyrgeometer are mounted on a moveable axis. During the observation period, the instruments are oriented alternatively to the six directions (VDI 3787 2008).

1.2.2.2 Globe thermometer measurements

Another less expensive method to determine the MRT is by using a globe thermometer (*Figure 1. 3*) combined with measurements of air temperature and wind speed (Thorsson et al. 2007), according to ISO 7726 (ISO Standard 7726 1998) for forced convection:

$$MRT = \left[(T_g + 273.15)^4 + \frac{h_{cg}}{h_{Rg}} (T_g - T_{air}) \right]^{1/4} - 273.15 \quad [^{\circ}\text{C}] \quad (1. 5)$$

Where:

- T_g is the globe temperature at the equilibrium with the surrounding environment (°C)
- T_{air} is the air temperature (°C)
- $h_{cg} = \frac{6.3 * v^{0.6}}{D^{0.4}}$ is the coefficient of heat transfer in forced convection at the level of the globe (ISO Standard 1998). Since the coefficient comes from empirical analysis, different values are reported in the literature (Kuehn, Stubbs, and Weaver 1970; Krüger, Minella, and Matzarakis 2014; Kántor, Kovács, and Lin 2015), leading to different MRT results. This aspect will be subsequently treated in this thesis.
- $h_{Rg} = \varepsilon * \sigma$ is the coefficient of heat transfer by radiation at the level of the globe.

The standard globe thermometer for indoors is black painted with a diameter of 150 mm and a wall thickness of 0.4 mm, often made of copper (ISO Standard 7726 1998). However, such large and heavy globe thermometers implies a large response time, up to 20-30 min to reach its equilibrium temperature with the

surrounding environment (ISO Standard 7726 1998; Spagnolo and de Dear 2003). The detailed energy balance will be discussed in *Section 2.2.3 Mean Radiant Temperature calculation using globe thermometers*.

Although the measurement of the MRT through a globe thermometer is more convenient than that made through a net radiometer, researchers have pointed out several shortcomings using this technique in outdoor thermal comfort assessments. The most important issues can be listed as follows (ASHRAE Standard 55 2017); Spagnolo and de Dear 2003; Kántor, Lin, and Matzarakis 2014):

- Because of the rapidly variable conditions (radiation and wind field) in outdoor environments, the globe has no time to reach its equilibrium (response time of the standard black globe ca. 15 min).
- Because of the shape of the globe, the resulted MRT cannot perfectly represent the radiation load on a standing man (more similar to the solution with the “sphere view factor” of the integral radiation measurements).
- Because of the black colour of the globe, it absorbs too much short-wave radiation compared to the clothed human body.

Both ISO 7726 (ISO Standard 7726 1998) and ASHRAE Handbook of Fundamentals (Ashrae Standard 2001) recommended a medium grey colour, instead of black, when the globe is exposed to solar radiation, to better agree with the outer surface of a clothed person (Johansson et al. 2014). The 40 mm flat grey globe thermometer (response time ca. 5-10 min) shown in *Figure 1. 3*, made of a grey painted table tennis ball, has been used in several studies (e.g. Thorsson et al. 2007; Yahia and Johansson 2013) and has been proven to be accurate, mobile and cheap (Thorsson et al. 2007; Johansson et al. 2014).

As already evidenced, to be able to register sudden variations in MRT with a globe thermometer, the globe needs to have a sufficiently short response time. To achieve this, the globe should be of small size and have a small heat capacity (Johansson et al. 2014; Nikolopoulou, Baker, and Steemers 1999). However, the smaller is the globe, the greater is the effect of convective heat exchange (i.e. air temperature and wind velocity) on the resulted globe temperature, which reduces the accuracy of the MRT calculation (Kántor, Lin, and Matzarakis 2014).



Figure 1. 3. Globe thermometer consisting of a flat grey 40 mm celluloid table tennis ball around a Pt100 temperature probe (Thorsson et al. 2007)

1.2.2.3 Simulating Software: Urban Thermal Environment Models

Traditionally the investigation of the urban microclimate has been performed only by observational and empirical means (Blocken 2015), but the significant advances in computational resources of the last decades have permitted the application of numerical simulation approaches involving computational fluid dynamics and thermal energy balance models (Tsoka, Tsikaloudaki, and Theodosiou 2018; Mirzaei and Haghighat 2010).

The basis of the creation of numerical micro-scale models relies on the complex interactions between urban fabric (i.e. buildings and ground surfaces) and the local weather parameters (Tsoka, Tsikaloudaki, and Theodosiou 2018). To support the experimental assessment and measurements carried out through in-field monitoring, different simulating software could be adopted. They can provide numerical simulations to extend the main findings of the experimental campaigns and they are also useful to elaborate predictions for future scenarios.

The ENVI-met and the RayMan models are two examples of these kinds of software and they will be analysed in detail.

1.2.2.3.1 ENVI-met

The ENVI-met model was developed by Michael Bruse at the Ruhr University of Bochum and the first official release was in 1998 (Bruse and Fleer 1998). It is a three-dimensional microclimate model able to simulate urban environment interactions between surfaces, vegetation and air with variable resolution in space and time. Its high spatial resolution allows a fine analysis of the microclimate at street level and the possibility of representing complex geometries including galleries and horizontal overhangs as well as various vegetation covers (Georgatou and Kolokotsa 2016; Eliasson 2000).

In the majority of the existing studies, the model has been applied not only for the investigation of current microclimate conditions but also for the comparative assessment of the performance of various mitigation strategies towards the UHI effect (Tsoka, Tsikaloudaki, and Theodosiou 2018). It is a prognostic model based on fundamental laws of fluid-dynamics and thermo-dynamics, capable to represent the diurnal cycle of the major climatic variables, involving air and soil temperature and humidity, wind speed and direction, radiative fluxes, etc. with a typical horizontal resolution ranging from 0.5 to 5 m and a time step of 1 to 5 s (Tsoka, Tsikaloudaki, and Theodosiou 2018; Bruse and Fleer 1998; Envi-met, 2018, <https://www.envi-met.com/>; Huttner 2012). The model geometry is realized by means of a grid numerical discretization (considering that due to its horizontal grid resolution, all objects become cuboids).

According to Georgatou and Kolokotsa's analysis in 2016 (Georgatou and Kolokotsa 2016), the model is able to accurately simulate: flow between building structures and street canyons, exchanges processes of heat and vapour at the ground surface and walls, turbulence effects, vegetation parameters, pollutant dispersion, bioclimatology.

ENVI-met model consists of the following sub-models (Tsoka, Tsikaloudaki, and Theodosiou 2018):

- The 1D boundary model, used for initializing the simulation and for the definition of the boundary conditions of the 3D atmospheric model.
- The 3D atmospheric model, which allows modelling short-wave and long-wave radiation fluxes, air temperature, air humidity, wind flow, turbulence and pollutant dispersion and deposition.
- The soil model, simulating the surface temperature and the distribution of the natural soil temperature.
- The vegetation model, including the simulation of the transpiration rates, the leaf temperatures of trees and the heat and vapour exchanges between the plants and the atmosphere.

The soil types and surfaces can be assigned for each grid cell, considering the individual thermodynamic and hydraulic properties (Pioppi et al. 2020). Both the vegetation and the soil are schematized as a one-dimensional column with a certain height and a given leaf and root (respectively) normalized area density profile (Pioppi et al. 2020). The outdoor temperature and the relative humidity are based on the 3D wind field, described as a three-dimensional turbulent flow given by the non-hydrostatic incompressible Navier-Stokes equations (Bruse and Fleer 1998). The interaction between the built surfaces and the atmosphere can be carried out considering all the thermo-physical properties as input parameters, like albedo, thermal emissivity, absorption capability, transmission capability, heat transfer coefficient and heat capacity. The interaction between plants and surroundings is provided instead in terms of direct heat flux, evaporation flux and transpiration flux (Pioppi et al. 2020).

The simulation requires two main input files (Tsoka, Tsikaloudaki, and Theodosiou 2018):

- the area input file, in which it is possible to define the building structure, the vegetation and the soil characteristics
- the configuration file, containing simulation settings about initialization values for meteorological parameters, the simulation timing and the definition of output folder names.

The first version of the ENVI-met model was announced in 1998 (Bruse and Fler 1998), while the latest one (v.4.0) was released in 2014. This latest version has overcome an important limitation of the previous one, giving the option of adding thermal mass and heat inertia on the building elements. A 3D vegetation model has been also implemented in the latest version, which is able to simulate complex vegetation geometries and also water spray simulation like fountains. Finally, version v.4.0 provides a new forcing scheme of air temperature and relative humidity input parameters, involving the definition of the hourly evolution of the respective variables along the simulation period in the configuration file (Tsoka, Tsikaloudaki, and Theodosiou 2018).

Despite the significant advantages illustrated and the improvements reached with the latest version of the software, some inaccuracies are still present in the model. More precisely, the weak points involve (Tsoka, Tsikaloudaki, and Theodosiou 2018):

- The calculation of radiant fluxes (Huttner 2012; Kleerekoper et al. 2017; Roth and Lim 2017)
- The turbulence model Yamada and Mellor E-ε, tending to overestimate the turbulent prediction in high acceleration areas (Acero and Herranz-Pascual 2015; Huttner 2012)
- The grid generation (Acero and Arrizabalaga 2018)
- The lack of information concerning the near-wall phenomena (Toparlar et al. 2017)
- The hypothesis of static clouds and wind conditions during the simulation period (Morakinyo et al. 2017; Maggiotto et al. 2014).

Another drawback consists of the fact that its high complexity makes the model slow. To reduce the time, it is possible to either limit the calculated time span or the model resolution, or the size of the area of interest. However, the limitation resolution leads to inaccuracy (Georgatou and Kolokotsa 2016).

According to the data reported in the literature, the software has been widely used for the evaluation of the effects of different implementation strategies in urban environments (i.e. addition of urban greenery, application of cool materials, water-based mitigation strategies, etc.) thanks to the capability of the model to provide an accurate calculation of the main parameters affecting the outdoor thermal comfort such as MRT, air temperature, wind speed and relative humidity, along with the possibility to calculate thermal comfort indices such as the Predicted Mean Vote (PMV) and Physiological Equivalent Temperature (PET).

Several studies have demonstrated that the model can predict the MRT with good accuracy if compared to the one obtained by experimental integral radiation measurements. The model provides an approximation of MRT at the pedestrian's level (Ali-Toudert and Mayer 2006; Yang, Lau, and Qian 2011) described by Equation (1. 6) (Bruse and Fler 1998):

$$MRT = \left[\frac{1}{\sigma} \left(E(z) + \frac{\alpha_k}{\varepsilon_p} (D(z) + I(z)) \right) \right] \quad (1. 6)$$

Where:

- σ is the Stefan Boltzmann constant
- α_k is the body's total absorption coefficient for shortwave radiation
- ε_p is the emissivity
- $E(z)$ is the long-wave radiation flux absorbed by a body at height z
- $D(z)$ is the total diffuse short-wave radiation flux absorbed by a body at height z
- $I(z)$ is the direct short-wave radiation flux absorbed by a body at height z

The results of different studies about the ENVI-met's performances on MRT calculation indicate that the model tends to overestimate daytime MRT values and underestimate night-time ones (Forouzandeh 2018; Lee, Mayer, and Chen 2016; Morakinyo et al. 2017; Salata et al. 2017; Yang, Lau, and Qian 2011; S. R. Yang

and Lin 2016; Zhao and Fong 2017); while the magnitude of the daytime maximum MRT values was always accurately reproduced (Acero and Arrizabalaga 2018; Roth and Lim 2017; Sharmin, Steemers, and Matzarakis 2017).

The reported discrepancies between simulated and experimental values of MRT may be attributed to several factors (Tsoka, Tsikaloudaki, and Theodosiou 2018):

- Inaccuracies on the calculation of radiant fluxes: the model tends to overestimate the daytime short-wave radiation, except peak values at midday. As a result, morning and afternoon MRT values will be also overestimated (Acero and Arrizabalaga 2018; Huttner 2012; Salata et al. 2016; (Sharmin, Steemers, and Matzarakis 2017).
- Assumption of static sky condition and steady-state wind profile: as already mentioned, the model does not consider transient clouds and the consequent variability of incoming solar radiation along the day (Acero and Herranz-Pascual 2015; Morakinyo et al. 2017; Salata et al. 2016).
- Potential inaccuracies on the definition of the urban geometry involving building height, the definition of the street canyon and the selected resolution of vertical and horizontal grid size: this would affect the exposure of surfaces on solar radiation and consequently the MRT calculation.

However, the ENVI-met model is continuously evolving in recent years and an increasingly high number of researchers are analysing it, its strength and its weakness, feeling incline to adopt it in their studies as an important supporting tool (Georgatou and Kolokotsa 2016).

1.2.2.3.2 RayMan Model

RayMan is a bioclimatic model, developed in the Meteorological Institute, University of Freiburg, according to the guidelines of the German Engineering Society (VDI 1998). It is well suited to calculate radiation fluxes, using as input parameters data related to the incoming global radiation and geometrical features of the monitoring site, such as Sky View Factor (SVF) and solid-angle proportions of the surrounding surfaces (Krüger, Minella, and Matzarakis 2014; Georgatou and Kolokotsa 2016). The SVF is a dimensionless quantity, ranging from 0 to 1, representing the degree of obstruction of the sky from the perspective of a single observation point in the urban environment. According to the definition, lower values of SVF means a more obstructed area and vice versa (Lai, Maing, and Ng 2017; (Oke and Cleugh 1987).

Kruger et al. (E. L. Krüger, Minella, and Matzarakis 2014) compared different methods implemented in the RayMan model for MRT calculations and their degree of accuracy. Here are reported four different approaches applied in previous publications and analysed by Kruger et al.' study:

- **Method 1:**
It consists of using as input parameters exclusively the data measured at an urban site, using integral radiation measurements. Measured global short-wave radiation already incorporates the effect of local geometry, so the MRT can be calculated directly from integral radiation measurement carried out in the urban areas.
- **Method 2:**
It considers as input parameters the urban data excluding solar radiation, along with the estimated SVF and the solar radiation data measured at a rural site. This is possible since RayMan is capable of accounting for morphology effects on predicted global short-wave radiation and thus provide the estimated MRT through integral radiation measurements carried out in rural areas and local SVF.
- **Method 3:**
It uses as input parameters the urban data excluding solar radiation, with SVF data for each site. The use of SVF as input with no solar radiation data relies on the capability of the RayMan model to use

the SVF and the solar path as a starting point to predict shadowing effects and therefore estimate MRT.

- **Method 4:**

It consists of using as input the urban data excluding urban solar radiation but including solar radiation at the rural site, without taking into account of SVF information. This kind of approach tests how the SVF data in method 2 contribute effectively to a better estimation than using the trivial solar radiation data measured at the rural site.

In general, according to the information obtained from the studies, it results that all the four methods tested in the RayMan model tend to overestimate the MRT (E. L. Krüger, Minella, and Matzarakis 2014). Method 4 showed a very weak correlation with respect to the ISO calculation values (taken as reference) and should not, therefore, be applied. Method 2 suggests that using global radiation data measured at a rural location and accounting for urban morphology aspects, expressed as local SVF data, improves the results when compared to the simple adoption of global radiation data collected at a rural location with no morphology corrections. However, the correlation is still weaker than method 1.

The information collected with these analyses could be summarized as follows (E. L. Krüger, Minella, and Matzarakis 2014):

- Integral radiation measurements are still the best option for correctly estimating the MRT
- Globe temperature measurements could be carried out instead when integral radiation measurements are not viable
- In case of a lack of integral radiation measurement results or globe temperature data recorded in the urban area, global radiation data measured at a rural location could be used.

Finally, some considerations can be made about the relevance of urban geometry information. While it seems that urban geometry attributes do not give a high contribution for a better estimation of the MRT in a generic scenario, it is possible to observe that, under a clear sky and sunny conditions, SVF data become much more relevant.

In general, once the limitations of different inputs formats are known, as well as the degree of overestimation in MRT values, the best choice for performing the analysis can be defined.

1.2.2.4 Relation between Sky View Factor and Mean Radiant Temperature

Several researchers pointed out that shading, by buildings or trees, is important for providing daytime outdoor thermal comfort in open spaces (Lai, Maing, and Ng 2017; Lin et al. 2012; Tan, Wong, and Jusuf 2013; Pearlmutter, Bitan, and Berliner 1999).

The level of shading by buildings is usually quantified utilizing urban geometrical parameters such as the height-to-width ratio (H/W) for simple canyon geometry (Lai, Maing, and Ng 2017; Lin et al. 2012; Johansson and Emmanuel 2006; Jamei et al. 2016) or the SVF for complex urban canyons (Lai, Maing, and Ng 2017; Lin, Matzarakis, and Hwang 2010; Lin et al. 2012; Tan, Wong, and Jusuf 2013).

About the relationship between SVF and MRT, several studies have shown that higher SVF causes higher MRT under sunny conditions when exposed to beam solar radiation (Lai, Maing, and Ng 2017; Tan, Wong, and Jusuf 2013; Krüger, Minella, and Rasia 2011; Lee, Mayer, and Schindler 2014). In particular, Tan et al. (Tan, Wong, and Jusuf 2013) reported there are simple and positive correlations between SVF and MRT with a coefficient of determination $R^2=0.61$ and $R^2=0.32$ in two sites in Singapore at the same hour (14:00), while Lee et al. (Lee, Mayer, and Schindler 2014) experienced a similar correlation with $R^2=0.57$ in the southwest of Germany.

Besides, Kruger et al. (E. L. Krüger, Minella, and Rasia 2011) examined the correlation between SVF and the temperature difference ($\Delta MRT-T$), which is the difference between SVF and the ambient temperature at the

reference station. The difference ($\Delta MRT-T$) increases with larger SVF with a coefficient of determination $R^2=0.57$. Kruger attributed this correlation to the strong dependence of MRT on solar radiation.

The findings of the above studies suggest that the short-wave component of MRT is largely attributed to the direct solar radiation from the sun in the unblocked sky (under unshaded conditions). This indicates that the effect of the SVF is mainly acting as an opening of outdoor space for the direct short-wave fluxes from the sun. This is analogue to a large opening of a room exposed to the sun allowing more sunlight entering into the room (Lai, Maing, and Ng 2017).

Although a high level of shading can block the direct solar radiation, on the other hand, an overly restricted sky view limits the radiative loss from the built environment, resulting in more solar heat absorption (Lai, Maing, and Ng 2017; David Pearlmutter, Berliner, and Shaviv 2006). The resulting densely built environment may cause the retention of the radiant fluxes, especially the long-wave one: a higher level of shading (less sky view) causes more absorption of long-wave fluxes by the deeper canyon (Lai, Maing, and Ng 2017; David Pearlmutter, Berliner, and Shaviv 2006).

It should be noted, however, that there have been very few attempts, in literature, to establish a direct relationship between SVF and daytime downward and horizontal radiant fluxes, especially long-wave fluxes (Lai, Maing, and Ng 2017).

1.2.3 Thermal Indices

1.2.3.1 Thermal indices classification

Over the years, more than 100 different thermal indices have been developed to describe the heat exchange between a human body and the surrounding environment (Blazejczyk et al. 2012). The great majority of these indices were developed for indoor conditions and just later tried to be adapted for outdoor environments (Johansson et al. 2014).

Thermal comfort indices can be divided into rational and empirical indices (D.A. McIntyre 1980). Empirical indices are derived from subjective estimates (D.A. McIntyre 1980): one example is the correlation between subjective thermal perception and measured meteorological variables determined through multiple regression analysis (Givoni et al. 2003; Metje, Sterling, and Baker 2008; Johansson et al. 2014).

Rational thermal comfort indices are based instead on the analysis of the physics of the heat transfer, i.e. based on the heat balance equation of the human body (Johansson et al. 2014). Some of these indices are reported in *Table 1. 1*.

Although many of the indices described were developed for indoor conditions (i.e. PMV, SET and ET), they have also been applied outdoors (Johansson et al. 2014).

Table 1. 1. Examples of rational thermal comfort indices that have been used in outdoor thermal comfort studies (Johansson et al. 2014).

Index	References	Description
Predicted Mean Vote (PMV)	(ASHARE 55 2013), (Ashrae Standard 2001), (ISO 2005), (Blazejczyk et al. 2012), (D.A. McIntyre 1980).	Mainly for indoors. It includes the meteorological variables affecting thermal comfort (air temperature, air humidity, wind speed and MRT) as well as personal variables (clothing and activity).
Standard Effective Temperature (SET)	(Ashrae Standard 2001), (Blazejczyk et al. 2012), (D.A. McIntyre 1980).	Mainly for indoors. It includes the meteorological variables affecting thermal comfort as well as personal variables.
Effective Temperature (ET)	(Ashrae Standard 2001), (Blazejczyk et al. 2012), (D.A. McIntyre 1980).	Mainly for indoors. It only takes into account the four meteorological variables, while clothing and activity are standardised for indoor sedentary.
Perceived Temperature (PT)	(VDI 2008), (Blazejczyk et al. 2012).	Based on PMV equation, but it can be used for outdoor environments.
Physiologically Equivalent Temperature (PET)	(VDI 2008), (Blazejczyk et al. 2012), (Peter Höppe 1999).	Applied for outdoors. It only uses the four meteorological variables. Clothing and activity level are standardised for indoor sedentary.
Universal Thermal Climate Index (UTCI)	(Blazejczyk et al. 2012), (Havenith et al. 2012), (G. Jendritzky, A. Maarouf 2001).	Intended for outdoors. No information on clothing insulation level of the surveyed population is required. Reference condition for activity: metabolic rate of 135 W/m ² and a walking speed of 1.1 m/s.

Both ISO 7730 (ISO 7730 2005) and ASHRAE 55 (ASHRAE 55 2013), which were designed for indoor environments, suggest the use of the Predicted Mean Vote (PMV), while the German guidelines VDI 3787 (VDI 2008), developed for outdoor environments, suggest the use of PMV, PT, and PET (Johansson et al. 2014).

PET is one of the most popular thermal indices and was developed based on the Munich Energy-balance Model for Individuals (MEMI) (Peter Höppe 1999). It is defined as the air temperature at which, in a typical indoor setting (taken as a reference environment), the heat budget of the human body is balanced with the same core and skin temperature as under the actual complex outdoor conditions (VDI 2008; Peter Höppe 1999; Kántor and Unger 2010).

1.2.3.2 Universal Thermal Climate Index (UTCI)

Among the indices listed in *Table 1. 1*, the UTCI was developed by Jendritzky et al. (G. Jendritzky, A. Maarouf 2001) with the specific aim to elaborate a new universal climate index to cover the whole range of heat exchanges between the human body and the outdoor thermal environment, in different climate and seasons. Its universality also depends on the applicability in situations in which the weather is well known, but not the characteristic of the human body and/or its activity. It was developed based on a multi-node model of human thermoregulation (Havenith et al. 2012; Fiala et al. 2012; Fang et al. 2018).

The UTCI is calculated through an equation in which the unknown parameters are the air temperature, the relative humidity, the wind speed, and the MRT. The equation that combines these measured variables results in the UTCI equivalent temperature, which is eventually associated with a stress category (*Table 1. 2*). The stress category tries to translate the UTCI equivalent temperature in the sensation that the human body feels in the considered environment.

For these reasons the UTCI will be adopted in this work as the reference thermal comfort index, where the meteorological variables are recorded via dedicated sensors and the MRT is evaluated by means of different experimental instrumentations (globe thermometer and net radiometers), to make a comparison.

Table 1. 2. UTCI ranges and stress categories

UTCI (°C) range	Stress Category
above +46	Extreme heat stress
+38 to +46	Very strong heat stress
+32 to +38	Strong heat stress
+26 to +32	Moderate heat stress
+9 to +26	No thermal stress
+9 to 0	Slight cold stress
0 to -13	Moderate cold stress
-13 to -27	Strong cold stress
-27 to -40	Very strong cold stress
below -40	Extreme cold stress

Fang et al.' study in 2018 (Fang et al. 2018) analysed the UTCI index dependence on the input parameters used for its calculation. The results of the above-mentioned study can be summarized as follows:

- **UTCI under different air velocities:**
To offset the risen temperature, an increased in v_a improved the thermal comfort condition, according to some previous investigations. In particular, Fang et al.'s publication noticed that when the operative temperature (T_{op}) was lower than 26 °C, the UTCI decreased with the rise of V_{air} . The lower the T_{op} , the higher the decrease in the UTCI. However, when T_{op} exceeded 26 °C, the change of UTCI with V_{air} was not evident anymore. This result is similar to the one obtained from Tseliou et al.'s analysis in 2016 (Tseliou et al. 2016).
- **UTCI against relative humidity:**
The change of RH causes a linear increase in the UTCI. In particular, the effects of RH on the UTCI is much stronger in warm conditions. However, in the case of warm temperature, the negative effects of RH on thermal comfort have to be considered. In an outdoor thermal environment, pedestrians should avoid staying in hot and humid conditions.
Compared with other thermal indices (such as PET), the linear relationship between UTCI and RH is more relevant and significant.
- **UTCI against operative temperature:**
There is an exponential relationship between UTCI and T_{op} , acquired via regression in Fang et al.'s publication. Under different RH, the exponential relationship is significantly different.
As already described, T_{op} affects also the relationship between UTCI and RH and between UTCI and V_{air} .

The dependence of the UTCI on the meteorological parameters used for its calculation will be further investigated in this thesis too, to make a comparison with the results reported in the literature from other studies.

1.2.3.3 Benefits of geographic information system (GIS) applications in thermal comfort index-based assessments

Thermal sensations of people are not only based on generic thermo-physiological reactions triggered by the actual thermal environment, but also on several subjective psychological and behavioural features (Kántor and Unger 2010). This fact has led recent urban environmental comfort studies to apply human monitoring (using unobtrusive observation and/or structured interviews) to the thermal comfort index-based assessment, as reported in Kantor and Unger's publication in 2010 (Kántor and Unger 2010), in which the benefits of simultaneous observations of the visitors who came to the surveyed area (human monitoring) - along with thermal indices measurements- are analysed.

To estimate the thermal comfort conditions of a site in an objective way, human biometeorological stress indices need to be calculated from meteorological parameters influencing thermal sensations. Nevertheless, a subjective approach, besides the objective one, could be included in the thermal comfort examination, involving not only the above mentioned meteorological parameters but also different subjective features. There are two main types of methods to collect additional information about subjects included in a thermal comfort assessment: social surveys (questionnaires and/or structured interviews) and human unobtrusive observation (Kántor and Unger 2010).

This kind of monitoring can provide valuable and useful information, particularly if it is followed by geo-informatical data processing. Human observation consists of marking the visitors' exact locations on the map of the study area and recording some of their individual characteristics (i.e. age, clothing, type of activity, exposition to the sun). GIS applications, like ArcView, can be used to create the area usage map for further descriptive and inferential statistical treatment and the measured data can be visualized graphically in the view windows of the software. The area usage can be showed on the whole or can be separated and presented according to any of the objective or subjective parameters. Consequently, the spatio-temporal presence of certain groups or the attendance of particular sub-areas becomes easy to analyse (Kántor and Unger 2010). The area usage maps created in this way are much more expressive than the pure statistical measures (commonly used by theoretical studies) without graphical representations. This investigation design is particularly suitable for the thermal comfort examination of small-sized urban parks and squares since in a relatively short time a lot of information can be obtained (Kántor and Unger 2010).

The final aim of Kantor and Unger's publication is intended to enhance - by exploiting the georeferenced data processing in GIS software as well as the global informational network- the establishment of a common and international database, supposing that researchers feel inclined to share their database. Such a common database would summarize the results of scientists dealing with applied urban climatology, thermal comfort, and environmental psychology in different geographical regions, with different architectural and cultural backgrounds, facilitating thus the international comparison in this field (Kántor and Unger 2010).

1.3 Lack of standardization in outdoor thermal comfort assessments

As evidenced in the previous sections, one of the most critical aspects concerning the outdoor thermal comfort assessments is the lack of a standardized approach and methodology. There is a great variety of instruments and methods used to measure meteorological variables, especially for the MRT. This large variety of methods hinders the comparison of results from different studies.

Thus, there is a need for standardization and guidelines regarding how to design field surveys in outdoor environments. Such standards should advise on the choice of measurement sites, type and positioning of instruments, appropriate methods to determine MRT, and suitable thermal comfort indices, as evidenced by Johansson et al.'s study in 2014 (Johansson et al. 2014).

1.3.1 Standards, guidelines and handbooks

Even if there is not a unique standardized approach, a huge variety of national and international standards, guidelines and handbooks is present, concerning measurements of meteorological variables, questionnaire design and calculation of thermal comfort indices. Each of them covers different aspects, summarized in *Table 1. 3*, which extrapolates the main topics of Johansson's analysis (Johansson et al. 2014).

Table 1. 3. Topics of different standards, guidelines and handbooks (ASHARE 2013; Ashrae Standard 2001; Standard 1998; ISO 2005; VDI 2008) (Johansson et al. 2014).

Standards, guidelines, handbooks	Topics covered
ASHRAE 55 (Ashrae Standard 55 2017)	Thermal comfort indices; requirements for thermal comfort evaluation; metabolic rate definition; subjective scales definition for questionnaires and human monitoring; clothing insulation. Refers to indoors.
ASHRAE handbook (Ashrae Standard 2001)	Instruments and methodology for determination of MRT; thermal comfort indices definition; requirements for thermal comfort evaluation; metabolic rate definition.
ISO 7726 (ISO Standard 7726 1998)	Instruments for determination of MRT; required measuring range; accuracy and response time of the instruments; methodology for evaluation of MRT.
ISO 7730 (ISO 7730 2005)	Thermal comfort indices; requirements for thermal comfort evaluation; metabolic rate definition; clothing insulation. Refers to indoors.
VDI 3787 (VDI 3787 2008)	Thermal comfort indices; requirements for thermal comfort evaluation; metabolic rate definition.

However, in the standards, guideline and handbooks reported in *Table 1. 3*, there are no recommendations on how to design the field survey in terms of site selection, appropriate number of sites, appropriate time of the day, minimum period of time for each survey, description and classification of the characteristics of the sites, etc (Johansson et al. 2014).

1.3.2 Variety of instruments and methods applied in outdoor thermal comfort assessments

Johansson's publication (Johansson et al. 2014) also focused on reviewing instruments and methods (described in *Section 1.2* Outdoor thermal comfort assessment) used to assess outdoor thermal comfort and subjective thermal perception, by analysing several studies reported in the literature in the last decade. As shown in *Table 1. 4* (which summarizes and expands Johansson's work), the great majority of the studies (80%) measured or modelled the MRT, since it represents a significative parameter for thermal comfort in outdoor environments. However, the instruments and methods used to determine MRT varied greatly between the studies available in the literature.

Table 1. 4. Ways to measure and/or model the MRT in the reviewed studies (Johansson et al. 2014).

Measurements	Studies
MRT calculation using globe thermometers, along with measurements of air temperature and wind speed	(Marialena Nikolopoulou, Baker, and Steemers 2001), (Marialena Nikolopoulou and Lykoudis 2006), (Thorsson et al. 2007), (Eduardo L. Krüger and Rossi 2011), (Lin, De Dear, and Hwang 2011), (Bröde et al. 2012), (Cheng et al. 2012), (Makaremi et al. 2012), (Ng and Cheng 2012), (Xi et al. 2012), (E. Krüger et al. 2013), (Yahia and Johansson 2013b), (W. Yang, Wong, and Jusuf 2013).
Integral radiation measurements	(Thorsson et al. 2007).
Incoming short-wave and long-wave radiation from six directions using 1 radiometer on a movable axis	(Thorsson et al. 2007), (Oliveira and Andrade 2007), (Andrade, Alcoforado, and Oliveira 2011), (Kántor, Unger, and Gulyás 2012).
Incoming short-wave and long-wave radiation from two directions (upward and downward)	(Spagnolo and de Dear 2003).
Global short-wave radiation and modelling with RayMan	(Thorsson, Lindqvist, and Lindqvist 2004), (Thorsson et al. 2007), (Lin 2009), (Lin, De Dear, and Hwang 2011), (Mahmoud 2011).
MRT calculation form global radiation and ground surface temperature	(Becker, Potchter, and Yaakov 2003).
No calculation of MRT	(Givoni et al. 2003), (Stathopoulos, Wu, and Zacharias 2004), (Eliasson et al. 2007), (Metje, Sterling, and Baker 2008), (Yin et al. 2012).

The most commonly used method to determine MRT is by using a globe thermometer combined with measurements of air temperature and wind speed, probably due to a compromise between accuracy, instrument cost and availability. The types of globe thermometers also varied greatly between different studies, as regard material, size and colour of the globe and, in general, the characteristics of the globe thermometers were not well described (Johansson et al. 2014).

The VDI method described above (VDI 3787 2008) -which uses just one pyranometer and one pyrgeometer on a movable axis- was adopted in three studied. In one of the studies reviewed (Spagnolo and de Dear 2003) a similar method was used, where incoming (downward) and outgoing (upward) short-wave (direct and diffuse) and long-wave radiation was measured, without considering the east, west, north and south directions. This method will be further discussed in this thesis, especially in comparison to the integral radiation measurement method from the six directions (*Section 2.1.3.1 Mean radiant Temperature calculation using only one net radiometer*).

Although the integral measurement method described by Thorsson et al. (Thorsson et al. 2007) and analysed in *Section 1.2.2.1* Integral radiation measurements of this thesis is the most accurate one, its cost and complexity are the reason why numerous researchers chose other methods for their studies.

1.3.3 Need for standardization

Johansson's study (Johansson et al. 2014) evidenced thus the presence of a great variety of instruments and methods adopted in outdoor thermal comfort surveys, both as regards micrometeorological instruments and thermal indices. It has also noted that measurement equipment, accuracy and response time of the methods adopted in literature to evaluate the MRT and wind speed – two of the most important meteorological variables that influence the human energy balance and assessment of thermal comfort – varied greatly. It was also noted that measurement equipment, accuracy and response time were not stated in the majority of the existing studies. Furthermore, the subjective judgment scales to determine thermal perception were different from study to study, and the description of the sites is often poor (Johansson et al. 2014).

A further problem is that many researchers use parts of many different standards since there is no single complete standard for outdoor thermal comfort surveys (Johansson et al. 2014). There is thus a need for standardization regarding how to perform field surveys in outdoor environments. In particular, Johansson et al.'s review (Johansson et al. 2014) evidenced a need of:

- Giving guidance on the experimental design, which should include site selection, season and time-period of the survey.
- Standardizing micrometeorological instruments and measurements method. Instruments should be standardized as regard shape, size, material, colour and type of temperature sensor.
- Standardizing MRT and wind speed measurements, as regard methods used in the evaluation, required accuracy and response time of instruments adopted.
- Recommending suitable thermal comfort indices. Standards and/or guidelines should define suitable indices depending on the aim of the study.
- Standardizing reports on outdoor thermal comfort surveys, including minimum requirements on the description of measurement sites and surroundings, measurement method (i.e. type and positioning of instruments and their accuracy), choice of thermal comfort index, questionnaire design, etc.

According to Johansson et al., wider participation in the development of a standardization process would ensure wider acceptance and deployment by the researcher community and easier comparison of the results obtained from different surveys (Johansson et al. 2014).

Starting from what was discussed in previous sections, this thesis will aim to identify and analyse the most accurate methods for carrying out experimental campaigns concerning the evaluation of outdoor thermal comfort and, at the same time, provide alternatives that can represent a good compromise between accuracy and cost of the instruments, highlighting their strengths and weaknesses.

In this work, therefore, an attempt was made to cover the wide range of instruments used in recent studies. The instrumentation adopted, which will be discussed in detail in the next paragraphs, mainly consists of three net radiometers, two globe thermometers of different sizes and colours and a sensor providing the meteorological parameters needed for the analysis.

2. Instruments and Methodology

Once defined the main parameters and measurement techniques to assess the outdoor thermal comfort, it becomes crucial focusing on the instrumentation capable to measure all the parameters needed for a detailed analysis.

In this chapter, the instrumentation adopted during the experimental campaign, in accordance with the considerations resulting from the previous paragraphs, is presented.

Table 2. 1 shows the parameters that were evaluated during our analysis, with the relative principle of measurement and the technical characteristics of the measuring instrument. A multiparameter sensor, able to measure the air temperature, relative humidity, wind speed and direction, solar irradiance and atmospheric pressure was installed, besides three net radiometers and two globe thermometers. A more detailed description of the individual instruments will be provided in this chapter.

Table 2. 1. General description of the variables measured in the analysis, including the measuring principle and range, accuracy and resolution of the instruments adopted.

Variable	Code	UoM	Measuring principle	Range	Accuracy	Resolution
Air temperature	T _{air}	°C	Diode	-40 ÷ +80 °C	± 0.3 °C	0.1 °C
Wind velocity	V _{air}	m/s	Ultrasonic	0 ÷ 60 m/s	± 0.3 m/s	0.01 m/s
Wind direction	DIR _a	°	Ultrasonic	0 ÷ 360 °	± 3°	0.1°
Relative Humidity	RH	%	Capacitive	0 ÷ 100%	± 3%	0.10%
Pressure	P _{atm}	hPa	Piezoresistive	600 ÷ 1100 hPa	± 0.5 hPa @25 °C	0.1 hPa
Solar radiation	R _{sol}	W/m ²	Photodiode	0 ÷ 2000 W/m ²	± 5 %	1 W/m ²
Short-wave radiation fluxes	SW _i	W/m ²	Pyranometer	0 ÷ 2000 W/m ²	± 10 % (daily)	1 W/m ²
Short-wave radiation fluxes	LW _i	W/m ²	Pyrgeometer	-300 ÷ 300 W/m ²	not yet formalised	1 W/m ²
Globe thermometer temperature	T _g	°C	Black or grey painted globe	-40 ÷ +80 °C	± 0.15 °C	0.01 °C

2.1 Net Radiometers

The most accurate but also the most expensive method to estimate outdoor MRT is by means of integral radiation measurements from six directions (east, west, north, south, upward and downward) using net radiometers, as stated in Section 1.2.2.1 Integral radiation measurements.

The short-wave and long-wave radiant fluxes are measured by pyranometers and pyrgeometers respectively. The pyranometer measures the solar irradiance incident on a surface in the range 0.3 – 3 μm, while the pyrgeometer is suited for radiation fluxes in the range 4.5 – 100 μm. By combining the two typologies of sensors it is possible to obtain the integral measurement of the radiation coming from the hemisphere seen by the sensors themselves.

Different setups have been used and discussed in recent studies. The difference is mainly about the number of sensors, which implies simultaneous or sequential measurements.

As previously described in *Section 1.2.2.1 Integral radiation measurements*, Thorsson et al.'s study (Thorsson et al. 2007) adopted three radiometers, mounted on perpendicular and fixed axis, to simultaneously measure short-wave and long-wave radiation coming from the six directions.

The German guideline VDI 3787 (VDI 3787 2008) suggests instead a cheaper method, adopting only one pyranometer and one pyrgeometer mounted on moveable axes; during the observation period, the instruments are oriented alternatively to the six directions (VDI 3787 2008). This approach is made possible thanks to the low thermal inertia of the pyranometer and pyrgeometer, allowing them to have a quite short response time. On the other hand, since the sensors do not detect the radiation coming from the six directions simultaneously, the time window of the measurements is about 10 minutes (VDI 3787 2008) and it could be not suitable with the time variation of outdoor meteorological conditions, in particular for the direct solar radiation (i.e. due to the passage of clouds).

In Spagnolo and de Dear's work (Spagnolo and de Dear 2003), a similar method with only one radiometer was adopted, where incoming (downward) and outgoing (upward) short-wave (direct and diffuse) and long-wave radiation were measured, but without considering the east, west, north and south directions.

In this thesis, three net radiometers were installed and Thorsson's method were adopted as a reference, due to its accuracy in outdoor MRT assessments. The three radiometers were mounted on 2 perpendicular axes, at a height of 1.1 m from the ground surface, corresponding to the centre of gravity of a standing person. When the instrumentation is used to measure the thermal comfort parameters in proximity to a vertical wall, the radiometer indicated with the number 2 (*Figure 2. 1*) is located 1 m away from the wall.



Figure 2. 1. Disposition and numbering of the three net radiometers.

2.1.1 Net radiometers NR01

The model of the net radiometer chosen for the measurement campaign is the Hukseflux NR01, a 4-component net radiometer, consisting of 2 pyranometers type SR01, 2 pyrgeometers type IR01, a heater, a levelling assembly for x- and y-axis, and a Pt100 instrument body temperature sensor.

Pyranometers and pyrgeometers (the latter with additional input of the body temperature measurement) measure the short-wave and long-wave radiation received by a plane surface, in W/m^2 .

For compensation of pyrgeometer emission in the long-wave calculation and calculation of sky and surface temperatures, a Pt100 temperature sensor is included in the instrument body. Working completely passive, using a thermopile sensor, the two sensors generate a small output voltage proportional to the radiative fluxes. To prevent condensation of water on the pyrgeometer windows, the NR01 has internal heating close to the pyrgeometers. This keeps the instrument above the dew point.

To operate, NR01 should be connected to a measurement system, typically a datalogger (*Section 2.4 Datalogger*).

The instrument should be used following the recommended practices of ISO, IEC, WMO and ASTM (ISO 1990; WMO 2008; ASTM; Hukseflux 2016).

Cables could act as a source of distortion. It is recommended to keep the distance between a data logger and the sensor as short as possible. Another precaution to take into account is the fact that the wires must not obstruct the field of view of the net radiometers, in particular the one that measures the upward/downward direction (*Figure 2. 2*).



Figure 2. 2. Wires connecting the net radiometers and the datalogger must avoid interferences with the measurements of the radiometers themselves.

2.1.1.1 Dimensions, main components and general specifications of NR01

In *Table 2. 2* the general specifications of a single NR01 net radiometer are listed, including the range of the measured parameters, the operating ranges of the instrument and the standards regulating its use.

The dimensions, expressed in mm, of the NR01 model are indicated in *Figure 2. 3*.

Table 2. 2. NR01 general specifications (Source: Hukseflux 2016).

NR01 Specifications	
Spectral short-wave range	285 to 3000×10^{-9} m
Spectral long-wave range	4.5 to 40×10^{-6} m
Levelling	Bubble level and a levelling assembly for x- and y-axis are included
Temperature sensor	Pt100
Heater on pyrgeometer	12 Vdc; 1.5 W
Rated operating temperature range	-40 to +80 °C
Rated operating relative humidity range	0 to 100%
Required readout	4x differential voltage channel or 4x single-ended voltage channel, input resistance $> 10^6 \Omega$
Standards for the use of the instrument	ISO 1990; WMO 2008; ASTM

In Figure 2. 4 the main components constituting the NR01 net radiometer are reported. The numbers indicated in the above-mentioned figure represent:

1. Up-facing pyrgeometer IR01
2. Sun screens
3. Levelling assembly for the x-axis
4. Levelling assembly for the y-axis
5. Up-facing pyranometer SR01
6. Down-facing pyranometer SR01
7. 4x hex bolts for levelling adjustment
8. Down-facing pyrgeometer IR01

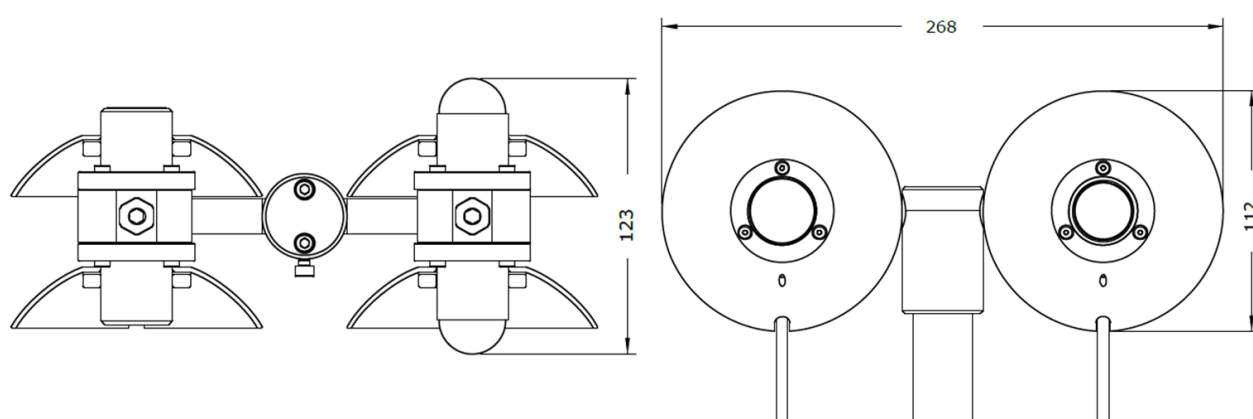


Figure 2. 3. Dimensions of NR01 in 10-3 m (Hukseflux NR01 manual).

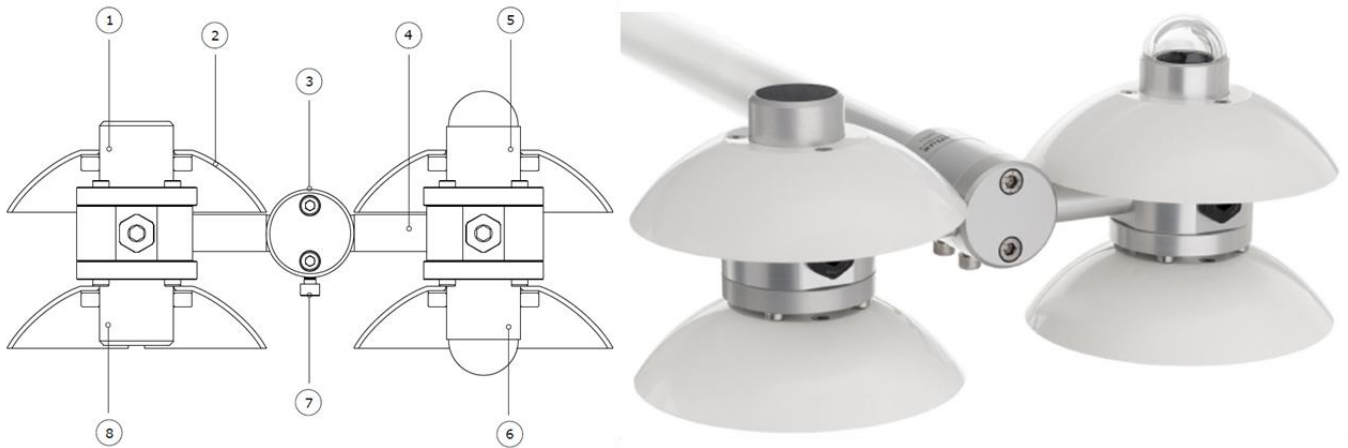


Figure 2. 4. Overview of NR01 (Hukseflux NR01 manual).

2.1.1.2 Pyranometers SR01

SR01 is the model of the pyranometers installed in the NR01 radiometer. The pyranometer measures the solar radiation received by a plane surface from a 180° field of view angle and this quantity, expressed in W/m^2 , is called “hemispherical” solar radiation.

The solar radiation spectrum extends roughly from 285 to $3000 \times 10^{-9} m$. By definition, a pyranometer should cover that spectral range with a spectral selectivity that is as “flat” as possible.

In an irradiance measurement, the response to “beam” radiation varies with the cosine of the angle of incidence; it should have a full response when the solar radiation hits the sensor perpendicularly (normal to the surface, the sun at zenith, 0° angle of incidence), zero response when the sun is at the horizon (90° angle of incidence, 90° zenith angle) and 50 % of full response at 60° angle of incidence.

A pyranometer should have a so-called “directional response” (older documents mention “cosine response”) that is as close as possible to the ideal cosine characteristic.

To attain the proper directional and spectral characteristics, a pyranometer’s main components are (Hukseflux 2016):

- a thermal sensor with a black coating. It has a flat spectrum covering the 200 to $50000 \times 10^{-9} m$ range and has a near-perfect directional response. The coating absorbs all the solar radiation and, at the moment of absorption, converts it into heat. The heat flows through the sensor to the sensor body. The thermopile sensor generates a voltage output signal that is proportional to the solar irradiance.
- A glass dome that limits the spectral range from 285 to $3000 \times 10^{-9} m$ (cutting off the part above $3000 \times 10^{-9} m$), while preserving the 180° field of view angle. Another function of the dome is the shielding of the thermopile sensor from the environment (i.e. from convection and rain).

Pyranometers can be manufactured with different specifications and different levels of verification and characterization during production. The ISO 9060 - 1990 standard (International Organization for Standardization 9060 1990), “Solar energy - specification and classification of instruments for measuring hemispherical solar and direct solar radiation”, distinguishes between 3 classes; secondary standard (highest accuracy), first-class (second highest accuracy) and second class (third highest accuracy). SR01 is a second-class pyranometer.

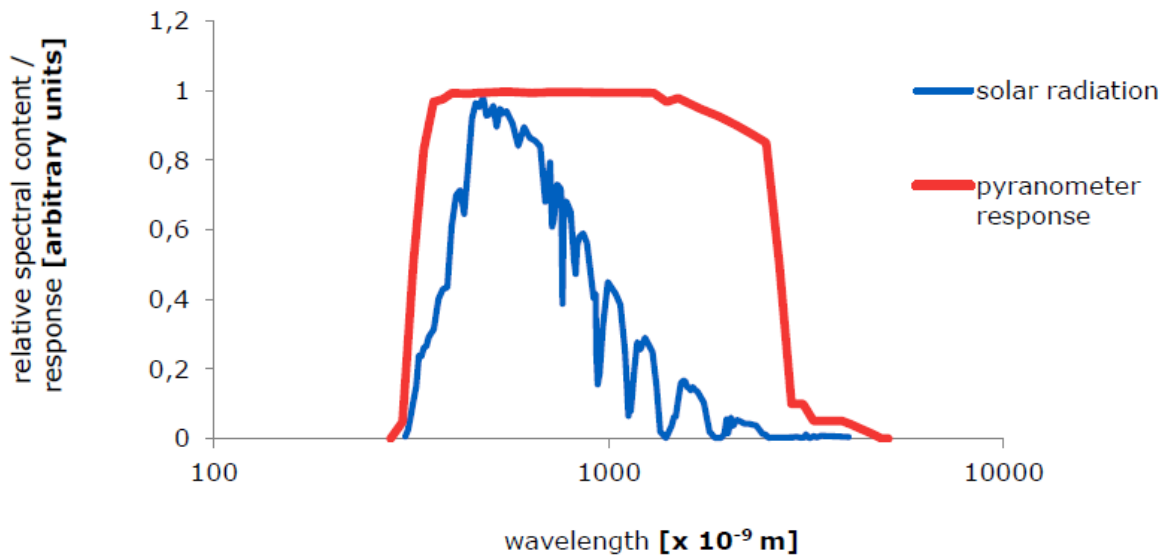


Figure 2. 5. Spectral response of the pyranometer compared to the solar spectrum. The pyranometer only cuts off a negligible part of the total solar spectrum (Source: Hukseflux 2016).

2.1.1.3 Pyrgeometers IR01

IR01 is the model of the pyrgeometers installed in the NR01 radiometer. It measures the long-wave or far-infra-red (FIR) radiation received by a plane surface, in W/m^2 , ideally from a 180° field of view angle.

In the case of IR01, the ideal 180° field of view angle has been reduced to 150° . This makes it possible to offer an instrument at a lower price level, while the loss of accuracy is relatively small.

As secondary measurands, the sky temperature (T_{sky}), and the equivalent surface temperature ($T_{surface}$) can be measured. Both are so-called equivalent blackbody radiative temperatures, temperatures calculated from the pyrgeometer assuming these are uniform-temperature black-bodies with an emission coefficient of 1.

Long-wave radiation is the part of the radiation budget that is not emitted by the sun. The spectral range of the long-wave radiation is not standardized; a practical cut-on is in the range of 4 to $50 \times 10^{-6} m$ (Figure 2. 6).

In the long-wave spectrum, the sky can be seen as a temperature source, colder than the ground level ambient air temperature, with its lowest temperatures at the zenith, getting warmer (closer to ambient air temperature) at the horizon.

The uniformity of this long-wave source is much better than the one in the range of the solar spectrum, where the sun is a dominant contributor. The “equivalent blackbody” temperature, as a function of zenith angle, roughly follows the same pattern, independent of the actual sky condition (cloudy or clear). This explains why for pyrgeometers the directional response is not very critical.

The most important factors determining downward long-wave irradiance are:

- ambient air temperature
- sky condition/cloud cover
- atmospheric moisture content

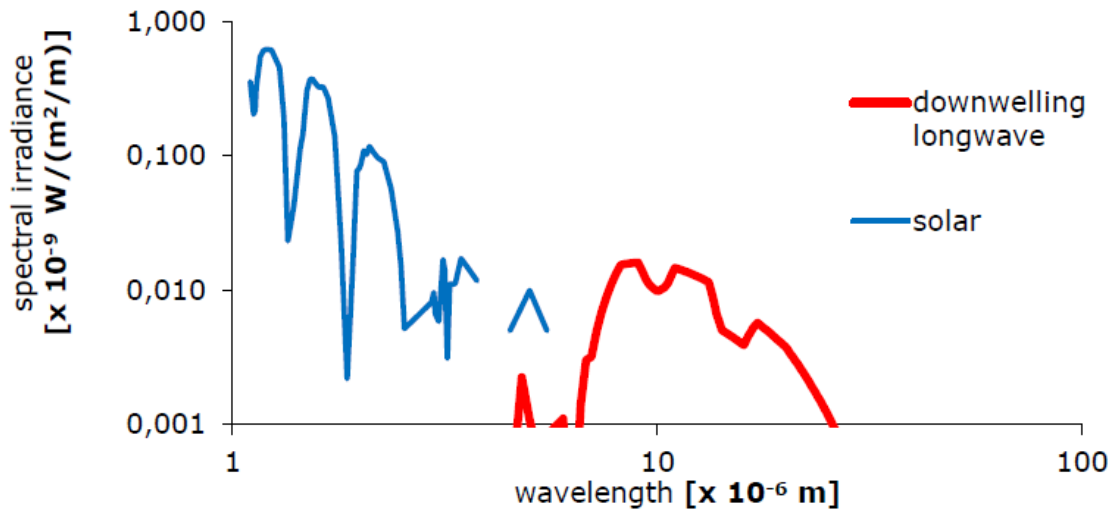


Figure 2. 6. Atmospheric radiation as a function of wavelength. Long-wave radiation is mainly present in the 4 to 50 x 10⁻⁶ m range, whereas solar radiation is mainly present in the 0.3 to 3 x 10⁻⁶ m range. The two are measured separately using pyrgeometers and pyranometers (Source: Hukseflux 2016).

2.1.2 NR01 governing equations

The solar irradiance in W/m² is calculated by dividing the SR01 output, a small voltage, by the sensitivity of the instrument (provided with the calibration certificate of SR01).

The central measurement equation governing solar radiation measurement with pyranometers is described in Equation (2. 1):

$$E = \frac{U}{S_s} \quad (2. 1)$$

Where:

- E is the short-wave irradiance [W/m²]
- U is the output of the SR01 sensor [V]
- S_s is the sensitivity of the SR01 sensor [Vm²/W]

The long-wave irradiance in W/m² is calculated by dividing the IR01 output, a small voltage, by the sensitivity of the instrument (provided with the calibration certificate of IR01) and taking in account the irradiated heat by the sensor itself (Stefan-Boltzmann law).

The central measurement equation governing long-wave measurement with pyrgeometers is described in Equation (2. 2):

$$E = \frac{U}{S_s} + \sigma \cdot (T_s + 273.15)^4 \quad (2. 2)$$

Where:

- E is the long-wave irradiance [W/m²]
- U is the output of the IR01 sensor [V]
- S_s is the sensitivity of the IR01 sensor [Vm²/W]
- σ is the Stefan-Boltzmann constant
- T_s is the temperature of the sensor [°C]

2.1.3 Mean radiant Temperature calculation using net radiometers

The simultaneous measurements of short-wave and long-wave radiation fluxes, with the corresponding weight F_i between the body and the surrounding elements, coming from the six directions, provided by the three net radiometers, are taken into account to evaluate the MRT according to (2. 3), which sums up all the intermediate steps described in detail in *Section 1.2.2.1 Integral radiation measurements*:

$$MRT = \left(\frac{\sum_{i=1}^3 \left[F_i \left(\alpha_k (SW_{UP,i} + SW_{DOWN,i}) + \varepsilon_p (LW_{UP,i} + LW_{DOWN,i}) \right) \right]}{\sigma * \varepsilon_p} \right)^{0.25} - 273.15 \quad [^{\circ}C] \quad (2. 3)$$

Where:

- F_i is the view factor for the i-th direction between the human body and the surrounding surfaces, determined by both the position and the orientation of the person.
- $SW_{UP,i}$ is the short-wave radiant fluxes recorded by the i-th radiometer, measured by the correspondent up-facing pyranometer.
- $SW_{DOWN,i}$ is the short-wave radiant fluxes recorded by the i-th radiometer, measured by the correspondent down-facing pyranometer.
- $LW_{UP,i}$ is the long-wave radiant fluxes recorded by the i-th radiometer, measured by the correspondent up-facing pyrgeometer.
- $LW_{DOWN,i}$ is the long-wave radiant fluxes recorded by the i-th radiometer, measured by the correspondent down-facing pyrgeometer.
- α_k is the absorption coefficient for short-wave radiant fluxes (assuming 0.7 as standard value) (VDI 2008).
- ε_p is the emissivity of the human body. According to the Kirchoff's laws, ε_p is equal to the absorption coefficient for short-wave radiant fluxes (assuming 0.97 as standard value)(VDI 2008)
- σ is the Stefan-Boltzmann constant and it is equal to $5.67 \times 10^{-8} \text{ Wm}^{-2}\text{K}^{-4}$.

The F_i factors allow considering different reference shapes, e.g. a standing man and a sphere. In the latter case, all fluxes are weighted identically with a value of 0.167, while in the “standing man” case, the role of the lateral fluxes become relatively greater than the vertical ones according to F_i values of 0.22 and 0.06 respectively, as suggested by Hoppe’s analysis (P Höppe 1992; Peter Höppe 1999), assuming that a standing person is attributable to a square-based parallelepiped with a ratio H/L = 3.5.

In this work both the approaches have been adopted, making a comparison between the two different solutions. Remarkable differences between the MRT values characterizing the radiation load of a spherical body and a standing man have been found and will be analysed in detail in *Chapter 3. Experimental campaigns and results*.

2.1.3.1 Mean radiant Temperature calculation using only one net radiometer

Along with the integral radiation measurement method, a simpler approach adopting only one net radiometer, measuring the upward and downward direction, has been adopted in our analysis.

A similar approach was suggested by Spagnolo and de Dear in their work in 2003 (Spagnolo and de Dear 2003), aiming to evaluate the vertical radiative fluxes. Although the equation proposed by Spagnolo and de Dear was somehow similar to that proposed in the German guideline VDI 3787 (VDI 3787 2008), in this thesis work it was decided to use an equation more similar to *Equation (2. 3)*, but focusing only on vertical radiative fluxes. This made it possible to evaluate their relevance in different environments and meteorological conditions, leading to further discussions on the importance attributed to the view factors adopted in the calculation of MRT with net radiometers. In this thesis, their approach is also studied as a cheaper alternative to the solution with the three net radiometers, trying to define its limits and the field of applicability.

The MRT is then calculated according to (2. 4):

$$MRT = \left(\frac{F_1 \left(\alpha_k (SW_{UP,1} + SW_{DOWN,1}) + \varepsilon_p (LW_{UP,1} + LW_{DOWN,1}) \right)}{\sigma * \varepsilon_p} \right)^{0.25} - 273.15 \text{ [}^\circ\text{C]} \quad (2.4)$$

Where:

- F_1 is the view factor for the single net radiometer 1 (number indicated in *Figure 2. 1*). It is assumed equal to 0.5 for both upward and downward directions.
- $SW_{UP,1}$ is the short-wave radiant fluxes measured by up-facing pyranometer of the net radiometer 1 (number indicated in *Figure 2. 1*).
- $SW_{DOWN,1}$ is the short-wave radiant fluxes measured by down-facing pyranometer of the net radiometer 1 (number indicated in *Figure 2. 1*).
- $LW_{UP,1}$ is the long-wave radiant fluxes measured by up-facing pyrgeometer of the net radiometer 1 (number indicated in *Figure 2. 1*).
- $LW_{DOWN,1}$ is the long-wave radiant fluxes measured by down-facing pyrgeometer of the net radiometer 1 (number indicated in *Figure 2. 1*).
- α_k is the absorption coefficient for short-wave radiant fluxes (assuming 0.7 as standard value) (VDI 2008).
- ε_p is the emissivity of the human body. According to the Kirchoff's laws, ε_p is equal to the absorption coefficient for short-wave radiant fluxes (assuming 0.97 as standard value)(VDI 2008).
- σ is the Stefan-Boltzmann constant and it is equal to $5.67 \times 10^{-8} \text{ Wm}^{-2}\text{K}^{-4}$.

2.1.4 Solar Reflectivity and solar Absorptivity of a surface calculated with net radiometers

The calculation of the radiative properties of the surfaces surrounding the environments studied in every single analysis carried out in this thesis has been considered relevant, in order to better characterize the conditions of the environment itself and the parameters which have an impact on it.

Different properties of the surrounding surfaces imply a different amount of radiation absorbed and re-emitted in the environment, causing variations in the thermal sensations. In this work, the radiative properties were calculated through a rough estimate, using the radiative fluxes detected by the net radiometers as input data. Different types of surfaces (i.e. green surfaces, concrete, porcelain, etc.) and their impact on the MRT and thermal indices have been studied for this purpose.

The three net radiometers, as shown in *Figure 2. 7*, were disposed always in the same position during all the measurements carried out.

The net radiometers indicated with the number 1 and 2 in *Figure 2. 7*, were always placed parallel respectively to the horizontal and vertical surface to be analysed. The radiative properties of vertical/horizontal surfaces were calculated as described in (2. 5) and (2. 6):

$$\rho = \frac{SW_{DOWN}}{SW_{UP}} \quad (2.5)$$

$$\alpha = 1 - \rho \quad (2.6)$$

Where:

- ρ is the reflectivity of the surface examined
- α is the absorptivity of the surface examined
- SW_{UP} is the short-wave radiant flux measured by the pyranometer facing the rest of the environment.
- SW_{DOWN} is the short-wave radiant flux measured by the pyranometer facing the examined vertical or horizontal surface.



Figure 2. 7. Disposition of the net radiometers near a vertical/horizontal surface.

(2. 5) and (2. 6) move from the following assumptions:

- The total short-wave radiation incident on a vertical or horizontal surface is equal to the amount of short-wave radiation that reaches the up-facing sensor of the net radiometer.
- The short-wave radiation reflected by a vertical or horizontal surface is equal to the amount of short-wave radiation measured by the down-facing sensor of the net radiometer). The distance between the vertical or horizontal surface and the sensor has been considered sufficiently low to validate this assumption.
- The transmissivity of the vertical surface examined is equal to zero.

2.2 Globe thermometer

Another cheaper method to determine the MRT is by using a globe thermometer, combined with measurements of air temperature and wind speed. As previously described in *Section 1.2.2.2 Globe thermometer measurements* and *Section 1.3.2 Variety of instruments and methods applied in outdoor thermal comfort assessments* in literature there is a great variety of globe thermometers in terms of (Johansson et al. 2014):

- Size, with variable diameters ranging from 38 mm to 150 mm.
- Material, which can be plastic or metallic (generally copper).
- Colour, which can be black or grey.

The standard globe thermometer for indoor environments is black, but both ISO 7726 (ISO Standard 7726 1998) and ASHRAE Handbook of Fundamentals (Ashrae Standard 2001) recommended a medium grey colour, instead of black, when the globe is exposed to the solar radiation, to better agree with the outer surface of a clothed person (Johansson et al. 2014).

In *Section 1.2.2.2 Globe thermometer measurements*, it was evidenced that, to be able to register sudden variations in MRT, the globe needs to have a sufficiently short response time. To achieve this, the globe should be of small size and have a small heat capacity (Johansson et al. 2014; M. Nikolopoulou, Baker, and Steemers 1999).

However, the smaller is the globe, the greater is the effect of convective heat exchange (i.e. air temperature and wind velocity) on the resulted globe temperature, which reduces the accuracy of the MRT calculation (Kántor, Kovács, and Lin 2015).

For a more detailed analysis that could offer a comparison between the different solutions reported in the literature, this thesis aims to study the behaviour of globes with different shape and colour (*Table 2. 3*).

Table 2. 3. Dimensions, colours and emissivity of the globe thermometers used in this work.

Colour of the globe thermometer	Emissivity ϵ [-]	Diameter D [mm]
Black	0,963	150
Grey	0,93	50

2.2.1 Black globe thermometer

The black thermometer used in this analysis is the standard globe thermometer for indoors, which is black painted with a diameter of 150 mm and a wall thickness of 0.4 mm, made of copper (ISO Standard 1998) (*Figure 2. 8*). The emissivity of the globe is $\epsilon_g = 0.963$.

Although the globe technique is more convenient and cheaper than the six-directional method, researchers have pointed out several shortcomings using this technique in outdoor thermal comfort assessments.

The most important issues, as previously observed in *Section 1.2.2.2 Globe thermometer measurements*, regard the response time (ca. 15 min for the standard black globe), the shape (not suitable for representing the radiation load on a standing man) and the black colour of the globe (which absorbs too much short-wave radiation if compared to the clothed human body) (Ashrae Standard 2001; Spagnolo and de Dear 2003; Kántor, Kovács, and Lin 2015).

The large size of this globe will negatively affect the response time and so the capability of the instrument to follow sudden variations in the measured variables. On the other hand, the large dimensions of the globe allow having a lower susceptibility to the effects of convective heat exchange, leading to better accuracy in MRT evaluation.

The globe uses a PT100 (platinum 100 Ohm) resistance. It is a thermo-resistive sensor: it exploits an electrical resistance that is a function of the temperature we want to evaluate.

The position of the black globe thermometer in the equipment set up was studied to avoid interferences between the globe and the net radiometers, in particular the one indicated with the number 3 in *Figure 2. 1*. The rod that supports the globe is placed at 45° from the two rods supporting the net radiometers indicated with the numbers 1 and 3, perpendicular to each other. Also, the wire connecting the globe to the data logger is placed in a way to prevent any kind of disturb to the field of view of pyranometers and pyrgeometers.

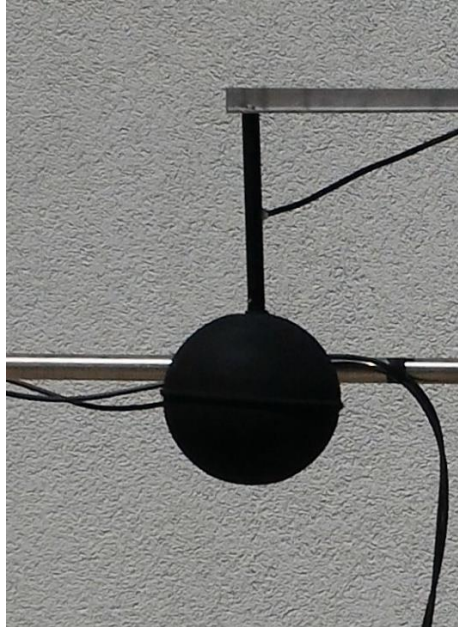


Figure 2. 8. Black-painted globe thermometer.

2.2.2 Grey globe thermometer

The grey globe thermometer adopted in this work has a diameter of 50 mm and an emissivity $\epsilon_g = 0.93$ (*Figure 2. 9*), similar to those used in several studies previously listed in *Section 1.3.2 Variety of instruments and methods applied in outdoor thermal comfort assessments* (i.e. Thorsson et al. 2007; Yahia and Johansson 2013a).

In outdoor thermal comfort assessment, especially when the instrument is directly exposed to the solar radiation, both ISO 7726 (ISO Standard 7726 1998) and ASHRAE Handbook of Fundamentals (Ashrae Standard 2001) evidenced that a medium-sized grey-painted globe is more suited, compared to the standard black globe, to represent the outer surface of a clothed person (Johansson et al. 2014).

The smaller dimension of this globe, compared to the black globe adopted, also allows to have a shorter response time (ca. 5-10 min) but it is more affected by the effects of convective heat exchange.

Moreover, the position and the small size of the globe ensure that it does not interfere with the field of view of the three net radiometers. As for the black globe, a wire is needed for the connection of the instrument to the acquisition system.

Unfortunately, the instrument was not available during the first measurement campaigns carried out and, therefore, the first analyses will take into consideration only the MRT values obtained using the black globe, which will be compared to the results provided by the six-directional method, taken as reference values.



Figure 2. 9. Grey-painted globe thermometer.

2.2.3 Mean Radiant Temperature calculation using globe thermometers

The MRT in outdoor conditions is measured through the thermal balance equation of the globe, by considering the heat exchange between the surrounding environment and the globe itself, according to Equation (2. 7):

$$q_{conv} + q_{rad} + q_{sol} = 0 \quad (2. 7)$$

Where q_{conv} represents the contribution of convective effects, q_{rad} is the contribution of the radiative fluxes and q_{sol} is related to the absorption of solar radiation. All the terms in the equation are expressed in W/m^2 .

At the equilibrium, all the fluxes are balanced and the globe reaches its equilibrium temperature. By making explicit the terms in (2. 7), we get:

$$h_{conv}(T_{air} - T_g) + \varepsilon_g \sigma (T_{rad}^4 - T_g^4) + \alpha_g G_g = 0 \quad (2. 8)$$

Where:

- h_{conv} is the coefficient of convective heat exchange between air and globe [$W/(m^2K)$]
- T_{air} is the air temperature [K]
- T_g is the globe temperature at the equilibrium [K]
- ε_g is the emissivity of the globe [-]
- σ is the Stefan-Boltzmann constant and it is equal to $5.67 \times 10^{-8} Wm^{-2}K^{-4}$
- T_{rad} is the radiant temperature [K]
- α_g is the solar absorption coefficient of the globe [-]
- G_g is the solar irradiance incident on the globe [W/m^2]

(2. 8) can be re-written by using the concept of MRT previously described, that resumes all the short-wave and long-wave radiant fluxes, according to (2. 9):

$$h_{conv}(T_{air} - T_g) + \varepsilon_g \sigma (MRT^4 - T_g^4) = 0 \quad (2. 9)$$

Therefore, the MRT can be determined re-arranging the previous equation, according to (2. 10):

$$MRT = \left[(T_g + 273.15)^4 + \frac{h_{conv}}{\varepsilon_g \sigma} (T_g - T_{air}) \right]^{1/4} - 273.15 \quad (2. 10)$$

Since h_{conv} comes from empirical analysis, different values are reported in the literature (Kuehn, Stubbs, and Weaver 1970; E. L. Krüger, Minella, and Matzarakis 2014; Kántor, Kovács, and Lin 2015; Thorsson et al. 2007), leading to different MRT results.

In this thesis it was decided to adopt various solutions present in the literature. The following publications have been taken into account for evaluating h_{conv} .

- Thorsson et al. (Thorsson et al. 2007) and Kantor et al. (Kántor, Kovács, and Lin 2015) assumed forced convection conditions in their analyses and thus applied the same correlation for the convective heat exchange suggested by the standard ISO 7726 for indoor environments:

$$h_{conv} = 6.3 * \frac{V_{air}^{0.6}}{D^{0.4}} \quad (2. 11)$$

By using the convective heat exchange coefficient of (2. 11), the MRT in (2. 10) can be re-written, by making explicit the Stefan-Boltzmann constant, as:

$$MRT = \left[(T_g + 273.15)^4 + \frac{1.1 * 10^8 V_{air}^{0.6}}{\varepsilon_g D^{0.4}} (T_g - T_{air}) \right]^{1/4} - 273.15 \quad [^{\circ}C] \quad (2. 12)$$

Where:

- V_{air} is the air velocity [m/s]
- D is the diameter of the globe [m]

- Thorsson et al. (Thorsson et al. 2007) also proposed a correction for h_{conv} in outdoor environments. In Thorsson et al.'s first analysis, the MRT values obtained with the globe thermometer were compared to those obtained using the integral radiation measurements, considered to be the most accurate way for estimating MRT. The correction proposed was thus intended to make the globe thermometer results closer to the radiometers ones. By adopting a new h_{conv} , the coefficient 1.1 and the exponent of the air velocities in (2. 12) were changed according to (2. 13):

$$MRT = \sqrt[4]{(T_g + 273.15)^4 + \frac{1.34 \cdot 10^8 V_{air}^{0.71}}{\varepsilon_g D^{0.4}} \cdot (T_g - T_{air})} - 273.15 \quad [^{\circ}C] \quad (2. 13)$$

Anyway, it has to be considered that Thorsson et al. applied the h_{conv} correction on the analysis carried out in October and in July, observing that, before the coefficient correction, in most of the cases the globe thermometer provided MRT values lower than those obtained by means of the six-directional method. The results that will be presented in this thesis show that this is true, in case of black globe thermometer measurements, only during cold seasons and in the hours of the day corresponding to a lower solar altitude. On the other hand, during the central hours of the day, the black globe tends to overestimate the MRT. The correction proposed is instead more suitable for the

grey globe, whose results show MRT values usually equal or slightly lower than those obtained with the net radiometers (see *Chapter 3. Experimental campaigns and results*).

- Kuhen et al. (Kuehn, Stubbs, and Weaver 1970), through a detailed analysis of the convective forces acting on the globe, obtained a similar but slightly lower h_{conv} compared to the one presented in the Equation (2. 12). The resulting MRT is:

$$MRT = \left[(T_g + 273.15)^4 + \frac{1.06 * 10^8 V_{air}^{0.6}}{\varepsilon_g D^{0.4}} (T_g - T_{air}) \right]^{1/4} - 273.15 \text{ [}^\circ\text{C]} \quad (2. 14)$$

2.3 Multi-parameters sensor

The multi-parameters or the All-in-sensor of the LSI-LASTEM Company (*Figure 2. 10*) allows measuring the meteorological parameters needed for the outdoor thermal comfort analysis performed in this work.

It integrates a sonic anemometer with a fast response capacitive to measure wind velocity and direction, an air temperature and relative humidity sensor, a barometric pressure sensor and a photodiode solar radiation sensor. To conduct the wind measurements properly, on the top of the sensor there is a hollow arrow that has to be positioned to point the North direction. *Table 2. 4* and *Table 2. 5* list the general specifications of the sensor and the technical description of how the desired parameters are detected respectively.

All-in-one has been placed on the top of the pole which supports all the other sensors, in order to avoid any kind of disturb from the rest of the equipment. Also, the cable, connecting the sensor to the acquisition system, must not obstruct the field of view of the three net radiometers.



Figure 2. 10. All-in-one sensor able to measure wind velocity and direction, air temperature, solar radiation, air humidity and pressure.

Table 2. 4. General specifications of the All-in-one sensor and parameters which can be measured.

All-in-one general specifications	
Parameters measured	Wind velocity, wind direction, relative humidity, dew point, pressure, solar radiation
Material	Luran
Supply	12-30 Vdc
Size	170x126 mm
Weight	0.95 kg

Table 2. 5. Technical specifications of the All-in-one sensor, including the measuring principle and range, the accuracy and the resolution of the instrument for each meteorological parameter measured.

Technical specifications		
<i>Wind velocity</i>	Principle	Ultrasonic
	Range	0-60 m/s
	Accuracy	± 0.3 m/s
	Resolution	0.01 m/s
<i>Wind direction</i>	Principle	Ultrasonic
	Range	0-360 °
	Accuracy	± 3°
	Resolution	0.1°
<i>Air temperature</i>	Principle	Diode
	Range	-40 - +80 °C
	Accuracy	± 0.3 °C
	Resolution	0.1 °C
<i>RH</i>	Principle	Capacitive
	Range	0-100%
	Accuracy	3%
	Resolution	0.10%
<i>Dew point</i>	Principle	Calculated
<i>Pressure</i>	Principle	Piezoresistive
	Range	600-1100 hPa
	Accuracy	± 0.5 hPa @25 °C
	Resolution	0.1 hPa
<i>Solar radiation</i>	Principle	Photodiode
	Range	0-2000 W/m ²
	Accuracy	5%
	Resolution	1 W/m ²

2.4 Datalogger

An acquisition system is required to receive and process the outputs provided in terms of voltage by the sensors described in *Section 2.1 Net Radiometers*, *Section 2.2 Globe thermometer* and *Section 2.3 Multi-parameters sensor*.

For this purpose, it was decided to use the Alpha-Log datalogger from LSI-LASTEM Company, to whose terminal block (*Figure 2. 11*) the wires and the cables coming from the net radiometers, the globes and the All-in-one sensor are connected. In order to receive the outputs of all the previously described instrumentation at the same time, two extensions - named ALIEM – have been added to expand the number of terminals available. Data acquisition of the Alpha-Log model is in the range 1 sec - 12 h.

It has an internal memory of 400 MB, which can be expanded with external memory up to 32 GB.

The datalogger has a series of acquisition channels and a local display for viewing in real-time the data acquired. Every single channel is numbered and, in general, a sensor must be connected to several channels. The display shows the following information:

- List of the parameters measured in real-time
- Last 20 alarms and errors
- Starting and actual data/hour
- Operating status
- Battery status
- Internal/external memory status
- List of servers

Before being able to carry out the measurements in field, it was necessary to configure the acquisition system to acquire through the sensors described. The configuration consists of physically connecting the sensors to the datalogger and programming the acquisition system using the 3DOM software, which can be downloaded for free from the LSI-LASTEM website. Once the system has been configured, the control unit becomes able to acquire and record the data, which will be downloaded by connecting the data logger to the computer on which the software has been installed. At any time it is possible to modify the configuration via computer, connecting it to the serial communication port 1 with the 3DOM software.

During the surveys, Alpha-Log and the ALIEM extensions are put in two shockproof suitcases of 340x270x140 mm (*Figure 2. 12*) to avoid knocks and/or overheating of the control unit.

Figure 2. 13 illustrates the main components of the datalogger and the terminal block.

The numbers in figure represent:

1. On/off switch
2. Input I²C
3. USB
4. Ethernet
5. Serial port modem
6. Serial port ALIEM
7. Display LCD 4x20
8. Keyboard
9. LED indicating the operating status
10. Terminal block

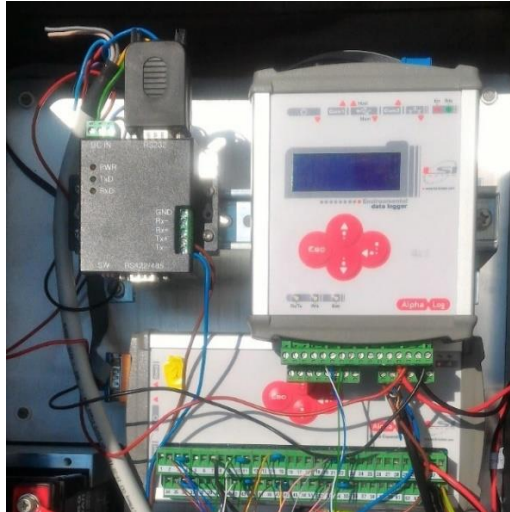


Figure 2. 11. Datalogger Alpha-Log and one terminal block extension ALIEM.

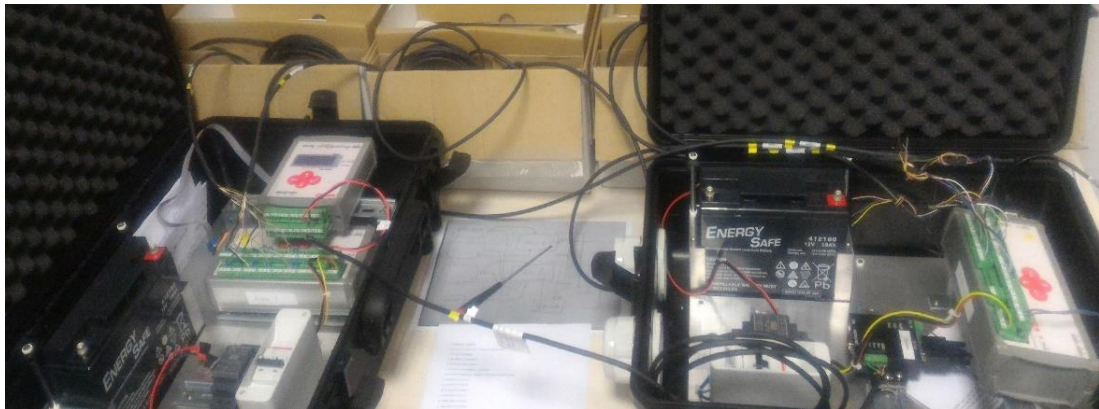


Figure 2. 12. Datalogger Alpha-Log and the two extensions ALIEM in the shockproof suitcases.

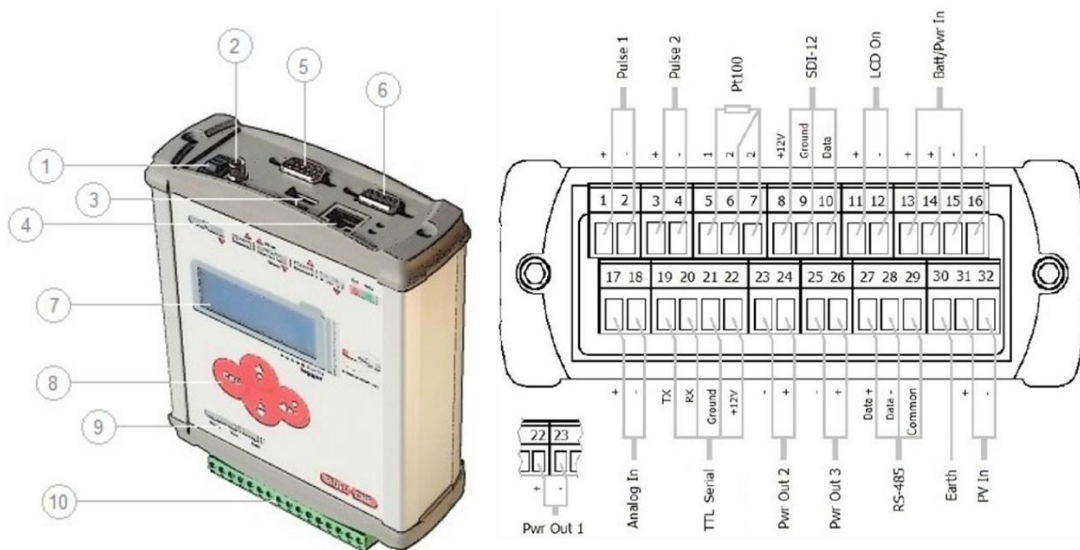


Figure 2. 13. Datalogger Alpha-Log and terminal block.

2.5 Support equipment

Once all the instruments are available, it is necessary having a support able to keep the instrumentation fixed during the experimental measurement campaigns. A tripod equipped with an adjustable height pole has been adopted for this purpose.

Two perpendicular rods, at the extremities of which are put the three net radiometers, are attached to the pole by means of two metallic plates, fixed with screws. The midpoint between the two plates is positioned 1.1 meters above the ground, corresponding to the centre of gravity of a standing person.

A further bar, smaller in size than the 2 rods with the net radiometers, is placed slightly above, to support the black globe thermometer. The bar is placed at such a height that the centre of gravity of the black thermometer globe is at a height of 1.1 m.

A metal support is also needed to position the grey globe thermometer. The same criterion is applied for the black globe and the three radiometers are applied to it: the centre of gravity must be positioned 1.1 m above the ground.

Finally, on the top of the pole, the All-in-one sensor is fixed to a metal plate so that the arrow recessed on the surface of the sensor points the North direction.

In order not to damage the cables connecting the radiometers to the datalogger and, at the same time, to ensure that they do not create an obstacle to the view field of the radiometers, a black scotch tape was used to attach the cables to the two perpendicular bars supporting the sensors.



Figure 2. 14. Whole instrumentation used in this thesis work.

2.6 Methodology

In this paragraph the description of the methodology, followed in each experimental test performed, is reported, as well as the equations adopted in the calculation of the MRT starting from the parameters measured with the instrumentation described in *Chapter 2. Instruments and Methodology*.

Before carrying out each measurement, it was necessary to place the support equipment (*Section 2.5 Support equipment*) in the measurement environment. The net radiometers (*Section 2.1 Net Radiometers*), the globe thermometers (*Section 2.2 Globe thermometer*) and the All-in-one sensor (*Section 2.3 Multi-parameters sensor*) were then fixed to it with screws and bolts. Position and height at which the instruments were positioned are those described in *Section 2.5 Support equipment*.

The two shockproof suitcases containing the data logger and the terminal blocks (*Section 2.4 Datalogger*) were positioned close to the instrumentation, but at a distance such as not to interfere with the measurements.

Once the instrumentation was positioned, it was left in the measurement environment for the entire duration of the experimental test, at the end of which it was disassembled and the individual instruments were placed in the appropriate containers.

The parameters detected during the course of the measurements were then downloaded from the acquisition system to the laptop where the 3DOM software was installed, as described in *Section 2.4 Datalogger*.

The first step of data analysis therefore consisted in the evaluation of the parameters of interest. In particular, for each measurement the following were calculated:

- The MRT using three net radiometers ($MRT_{Rad1+2+3}$), according to Equation (2. 3). The absorption coefficient for short-wave radiant fluxes (α_k) and the emissivity of the human body (ε_p) are assumed equal to 0.7 and 0.97 respectively, according to the standard values reported in the *VDI 2008*. In the analysis of *Chapter 3. Experimental campaigns and results*, we decided to adopt the so-called “standing man” view factors, since they are the most commonly adopted in literature. These factors attribute a greater relevance to the lateral radiative fluxes than to the vertical ones, according to F_i values of 0.22 and 0.06 respectively. *Section 4.3 Influence of view factors in the evaluation of MRT by using the six-directional method* will aim to investigate the difference between the MRT obtained using the “standing man” factors ($MRT_{Rad1+2+3,standing\ man}$) and the “sphere” ones ($MRT_{Rad1+2+3,sphere}$), which weight equally all the fluxes from the six directions, according to a value of 0.167.
- The MRT using a single net radiometer (MRT_{Rad1}), according to Equation (2. 4). The F_i factors adopted are equal to 0.5 for both upward and downward directions.
- MRT using the black (MRT_{Black}) and the grey (MRT_{Grey}) globe thermometers, according to Equation (2. 10). The black globe we used has an emissivity of 0.963 and a diameter of 150 mm. The grey globe has an emissivity of 0.93 and a diameter of 50 mm. The nomenclature MRT_{Globe} will be used to indicate the MRT values calculated with a generic globe thermometer, regardless its colour. In the analysis of *Chapter 3. Experimental campaigns and results*, we decided to adopt h_{conv} equal to 1.06, according to Kuhen et al.’s approach (Kuehn, Stubbs, and Weaver 1970), as described in Equation (2. 14). In *Section 4.4 Influence of convective heat exchange coefficient in the evaluation of MRT by using the globe thermometers*, a comparison is made between the results -in terms of MRT- provided by the Kuhen et al.’s method and the ones obtained after applying a correction proposed by Thorsson et al. (Thorsson et al. 2007), according to Equation (2. 13). The results obtained with this approach will be indicated as $MRT_{Black.Th.}$ for the black globe and $MRT_{Grey.Th.}$ for the grey globe.

- UTCI starting from the MRT of each individual instrument and the meteorological parameters detected by the All-in-one sensor.
- Radiative properties of the surrounding environment. In particular, the reflectivity and absorptivity of the horizontal and vertical surfaces (according to Equation (2. 5) and Equation (2. 6), respectively) characterizing the measurement environment were evaluated.

Then, the analysis proceeded with a comparison of the results between the MRT values obtained through the combination of the three net radiometers (taken as reference) and those provided by the other instruments at our disposal. Initially a comparison is made between $MRT_{Rad1+2+3}$, MRT_{Black} and MRT_{Grey} , in order to define how much the results provided by the globe thermometers differ from those obtained with the three net radiometers. The analysis is also aimed at defining in which conditions and environments the thermometers can be used to approximate the reference results with greater accuracy. A similar analysis was then carried out between $MRT_{Rad1+2+3}$ and MRT_{Rad1} , in particular as regards the measurements carried out in open field, where the vertical radiative fluxes have a greater importance and, consequently, the single radiometer 1 can be more reasonably adopted to assess the MRT. This is followed by a correlation study between the results obtained and the variables involved, as well as a search for the causes determining the differences in results between one instrument and another. In particular, the correlation between the UTCI values obtained in the different measurement environments and the parameters involved in its calculation (T_{air} , RH, v_{air} , global radiation) will be studied.

A final analysis was then carried out in order to compare different approaches in the evaluation of the MRT by using the instruments at our disposal.

At first, we wanted to observe how much the view factors chosen to calculate the $MRT_{Rad1+2+3}$ influenced the results obtained. A comparison was thus made between $MRT_{Rad1+2+3,standing\ man}$ and $MRT_{Rad1+2+3,sphere}$, in particular for measurements carried out in open field, where the greater influence of vertical radiative fluxes may be not correctly described by the "standing man" view factors. This was followed by a comparison between the results obtained using the equations for globe thermometers proposed by Kuhen et al. (MRT_{Black} and MRT_{Grey}) and those deriving from the correction by Thorsson et al. ($MRT_{Black,Th.}$ and $MRT_{Grey,Th.}$). The two methods tend to evaluate the convective heat exchanges between the globe thermometers and the surrounding environment in a different way and, consequently, to provide different results.

The diagram in *Figure 2. 15* summarizes all the steps carried out in this thesis work, from the setup of the instrumentation to the analysis of the results.

The results of these analyses will be presented in the following chapters of this thesis work.

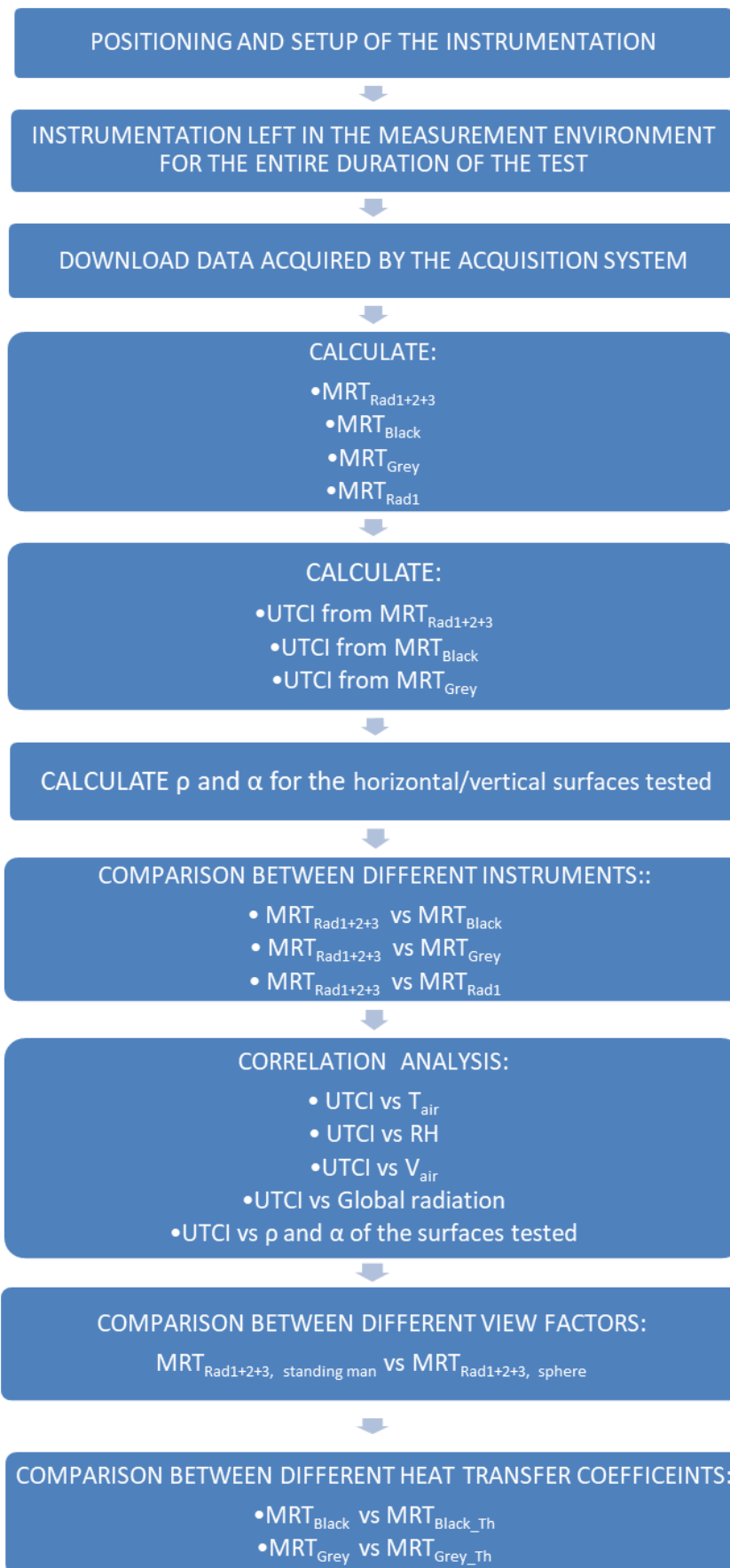


Figure 2. 15. Diagram describing the methodology followed in each measurement campaigns.

3. Experimental campaigns and results

The instrumentation described in *Chapter 2. Instruments and Methodology* was used in this thesis work to evaluate the parameters most affecting the outdoor thermal comfort. This chapter aims to describe different tested environments and show the results obtained through experimental campaigns carried out in July, August, September, and October 2020. The final purpose, in the light of the measurements and related analyses, is to provide information about the most suitable instruments to assess the MRT. The measurement campaign is designed to evaluate the ability of the sensors to provide accurate MRT assessments in different urban settings against the 6-directional net radiometer intended as ground truth. The measurements were carried out in open fields, in street canyons, and in the proximity of different building envelope technologies, to observe how the radiative properties of the above-mentioned environments may influence the outdoor thermal comfort. The UTCI, calculated starting from the evaluation of the MRT provided by the different instruments, was used as the main index describing the thermal comfort.

3.1 Mean Radiant Temperature and UTCI assessment

The experimental campaigns took place in nine different locations in the city of Milan. Each set differs from the others in the radiative properties of the soil and the envelope of the buildings surrounding the measurement environments, as well as in the different exposure of the instrumentation to direct solar radiation (i.e. open field or street canyon).

Table 3. 1 includes the locations and times on which the measurements were carried out, the equipment used in each of them, and the sampling frequency.

In the following sub-chapters, each measurement campaign will be analysed individually, according to their environmental characteristics.

By following the methodology described in *Section 2.6 Methodology*, the results will be represented as follows:

- MRT trend calculated with the three net radiometers and the globe thermometers, in contrast with the air temperature.
- MRT trend calculated with a single net radiometer measuring the upward and downward radiation and the combination of the three net radiometers.
- UTCI calculated through the MRT provided by radiometers and globes. The UTCI defines a category of thermal stress which tries to translate the UTCI equivalent temperature in the sensation that the human body feels in the considered environment.
- Radiative properties of the horizontal and/or vertical surface examined.

The graphs representing the UTCI trends calculated by net radiometers and globe thermometers will have bands of different colours, to highlight the different categories of thermal stress. *Table 3. 2* indicates, for each UTCI value, which is the corresponding category and the relative colour used in the graphs of this chapter.

Table 3. 1. Measurement campaigns: environment, location, date and hour, sampling frequency and instrumentation used.

Building Envelope/ Environment	Location	Measurement date and hour	Measurement frequency	Instruments		
				Black globe (150 mm)	Grey globe (50 mm)	3 net radiometers
Flat rooftop with a waterproofing membrane	Milan, Via Feltrinelli	20/07/2020 12:00-19:30	10 min	X		X
		21/07/2020 9:00-15:40	10 min	X		X
Light plaster wall	Milan, Via Lambruschini	23/07/2020 13:00-16:30	1 min	X		X
Porcelain stoneware Facade Cladding	Milan, Via Lambruschini	27/07/2020 12:00-16:30	1 min	X		X
		18/09/2020 11:10-17:15	1 min	X	X	X
Park	Milan, Cascina Merlata district	28/07/2020 11:50-16:30	1 min	X		X
Green rooftop	Milan, Via G. Ponzio	26/08/2020 day 15:20-21:00	1 min	X		X
		26-27/08/2020 night 21:00-8:00	1 min	X	X	X
		27/08/2020 day 8:00-17:15	1 min	X	X	X
Blue plaster wall	Milan, Cascina Merlata district	01/09/2020 11:30-17:10	1 min	X	X	X
Street Canyon	Milan, Bovisa district	09/09/2020 10:40-17:15	1 min	X	X	X
Green wall	Milan, Via G. La Masa	17/09/2020 11:10-17:15	1 min	X	X	X
	Milan, Via Bovisasca	06/10/2020 10:10-17:45	1 min	X	X	X

Table 3. 2. UTCI thermal stress categories and colours of the corresponding band in the UTCI graphs in Chapter 3.

UTCI (°C) range	Stress Category	Colour of the corresponding band
above +46	Extreme heat stress	Orange
+38 to +46	Very strong heat stress	Blue
+32 to +38	Strong heat stress	Green
+26 to +32	Moderate heat stress	Grey
+9 to +26	No thermal stress	White

3.1.1 Flat rooftop with a waterproofing membrane

The measurements here analysed were carried out on the roof of a public residential building in Via Feltrinelli in Milan, from 12:00 to 19:30 on 20/07/2020 and from 9:00 to 15:40 on 21/07/2020. The measurement environment consists of a flat rooftop equipped with a waterproof slate membrane. The instrumentation was located in a place where the surrounding elements did not interfere with the measurements.

Figure 3. 1 shows a view of the measuring environments and the arrangement of the instrumentation. As illustrated in Table 3. 1, the meteorological parameters were provided thanks to a control unit with a measurement frequency of 10 minutes. For this reason, also MRT and UTCI were computed every 10 minutes.



Figure 3. 1. Flat rooftop with a waterproofing membrane, Via Feltrinelli, Milan.

Figure 3. 2 (day 20/07/2020) and Figure 3. 3 (day 21/07/2020) show the MRT values calculated during the two days of measurements.

From the two figures it can be seen that the black globe thermometer (red line) tends to overestimate the MRT with respect to the values calculated using the net radiometers (yellow line). During the first day of measurements, we found a minimum difference between MRT_{Black} and $MRT_{Rad1+2+3}$ equal to 0.7 °C (recorded at 19:30) and a maximum difference of 24.15 °C (recorded at 14:40); the average MRT calculated by means of the black globe is equal to 74.62 °C, while we obtain an average $MRT_{Rad1+2+3}$ of 60.22 °C. During the second day of measurements, on 21/07/2020, the difference between MRT_{Black} and $MRT_{Rad1+2+3}$ varies between -6.6 °C and 22.7 °C. The average values recorded are equal to 66.55 °C for MRT_{Black} and 58.63 °C for $MRT_{Rad1+2+3}$. Observing the two figures, it can be seen that the difference between the two trends increases in the hours corresponding to a greater solar height, while it decreases when the solar height is lower. In the evening and early morning hours the difference between MRT_{Black} and $MRT_{Rad1+2+3}$ is in fact at its minimum. During the early morning we can also detect a MRT_{Black} lower than $MRT_{Rad1+2+3}$.

In Figure 3. 4 (20/07/2020) and Figure 3. 5 (21/07/2020) we can see instead the trends of $MRT_{Rad1+2+3}$ and MRT_{Rad1} : according to the two figures, the single radiometer (blue line) measuring upward and downward directions tends to overestimate the MRT in the hours of the day corresponding to a greater solar height, while it underestimates it when the solar height is lower. During the first day of measurements, we recorded a maximum MRT_{Rad1} of 78.93 °C, in correspondence to a $MRT_{Rad1+2+3}$ of 58.32 °C (at 13:50); the minimum MRT_{Rad1} was recorded at 19:30 and it is equal to 38.75 °C, lower than the corresponding $MRT_{Rad1+2+3}$ of 49.37 °C. The average MRT_{Rad1} on 20/07/2020 was equal to 68.16 °C. During the second day, MRT_{Rad1} assumes a maximum value of 77.61 °C and a minimum of 50.81 °C, obtained at 14:10 and 9:30 respectively; the average value is equal to 70.17 °C, higher than the corresponding average $MRT_{Rad1+2+3}$ value of 58.63 °C.

The same comparison was also made in terms of UTCI in Figure 3. 6 and Figure 3. 7. The trend of the UTCI calculated considering the data measured by the black globe thermometer (red line) and the one calculated

from $MRT_{Rad1+2+3}$ (yellow line) follow the same trend observed for the MRT. During the first day of measurements (20/07/2020) the two UTCIs fall within two different thermal stress categories for the majority of the day (“Very strong heat stress” for black globe and “Strong heat stress” for net radiometers), while they belong to the same stress category only from around 19:00 onwards. On this day, the average UTCI assumes a value of 40.36 °C if calculated by means of black globe and 36.76 °C if calculated using net radiometers. During the second day of measurements, the indices fall within the same stress category (“Strong heat stress, $32 \text{ °C} \leq \text{UTCI} < 38 \text{ °C}$) only in the early hours of the morning, until 11:15. On this day, the average UTCI is equal to 38.03 °C if obtained through MRT_{Black} and 36.06 °C using the data recorded by the net radiometers.

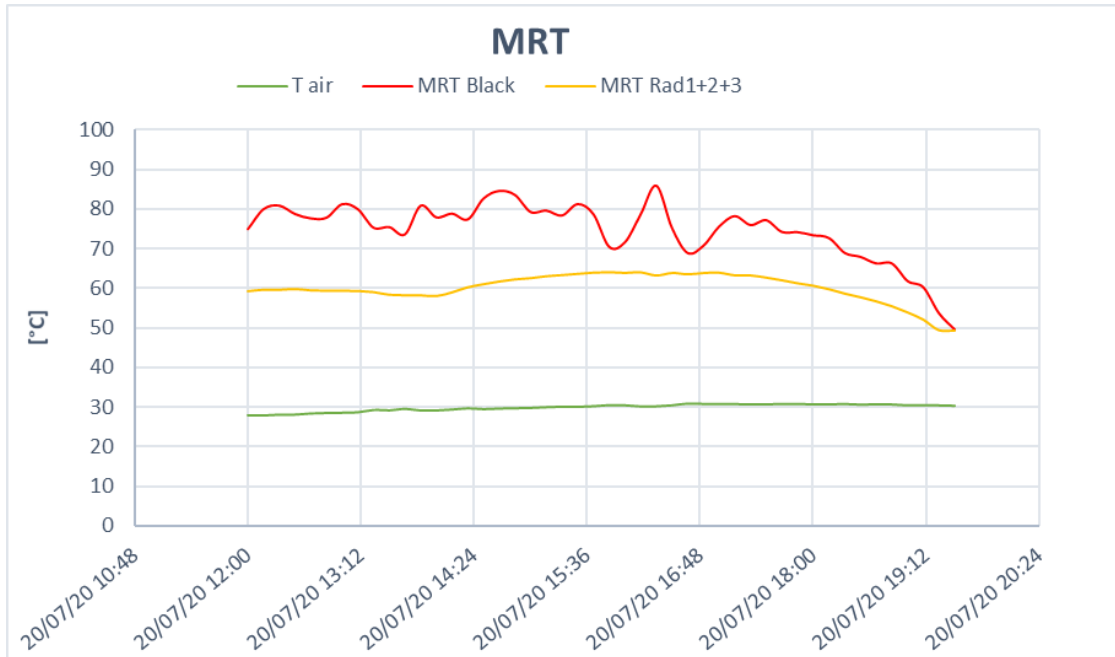


Figure 3. 2. MRT calculated with net radiometers and globe thermometers; 20/07/2020.

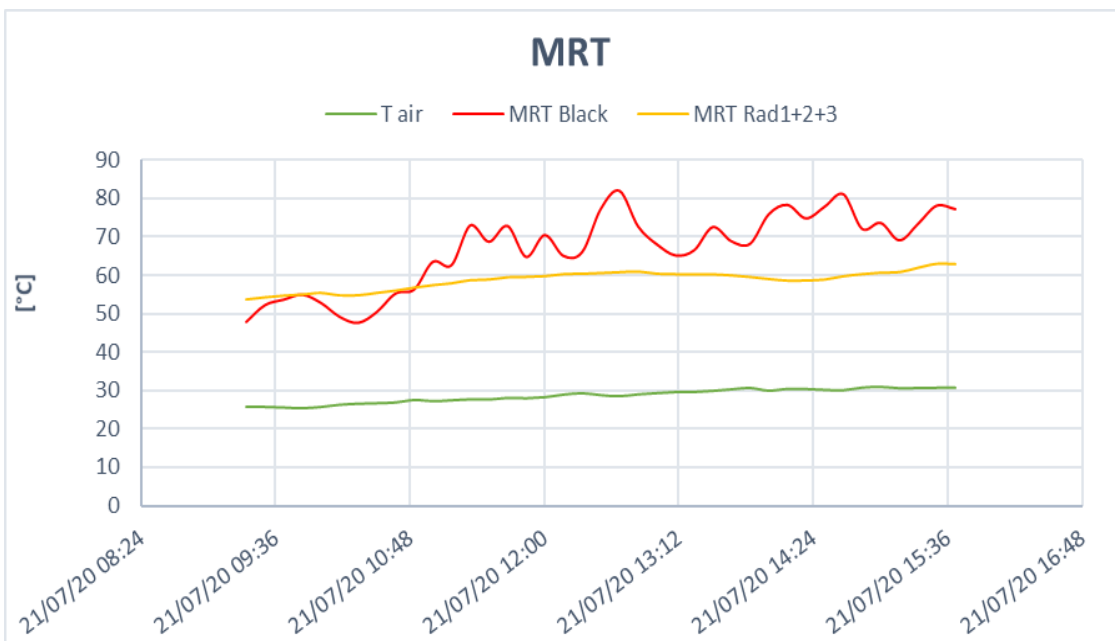


Figure 3. 3. MRT calculated with net radiometers and globe thermometers; 21/07/2020.

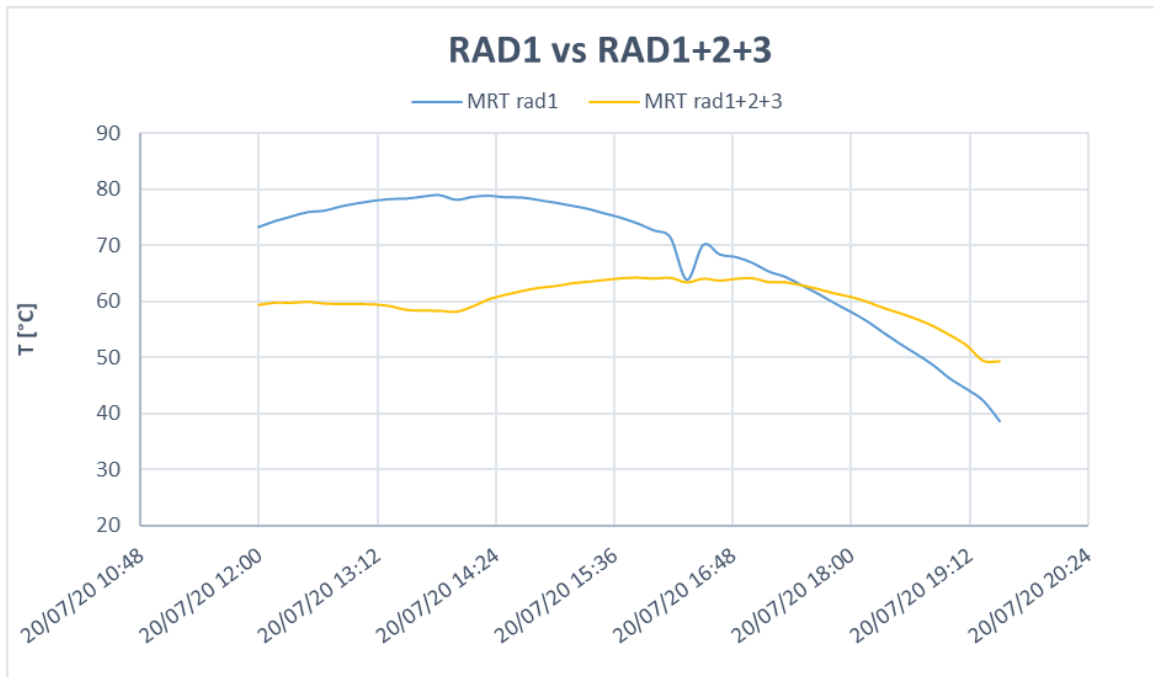


Figure 3. 4. MRT calculated with three radiometers and one radiometer measuring upward/downward direction; 20/07/2020.

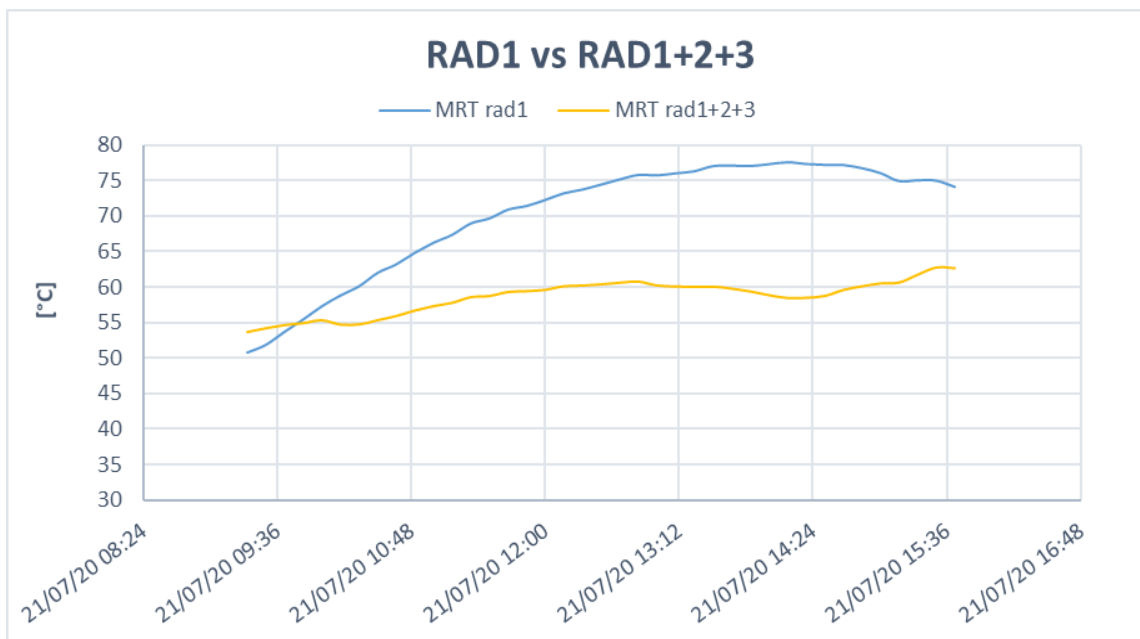


Figure 3. 5. MRT calculated with three radiometers and one radiometer measuring upward/downward direction; 21/07/2020.

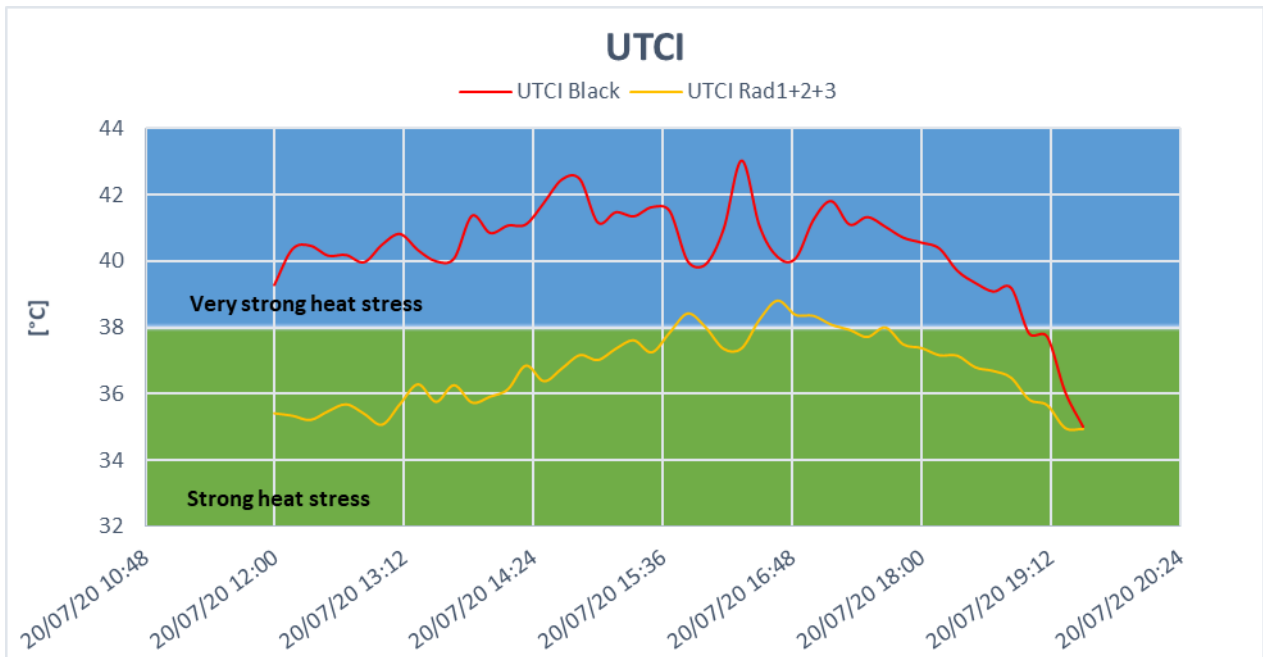


Figure 3. 6. UTCI calculated with net radiometers and globe thermometers; 20/07/2020.

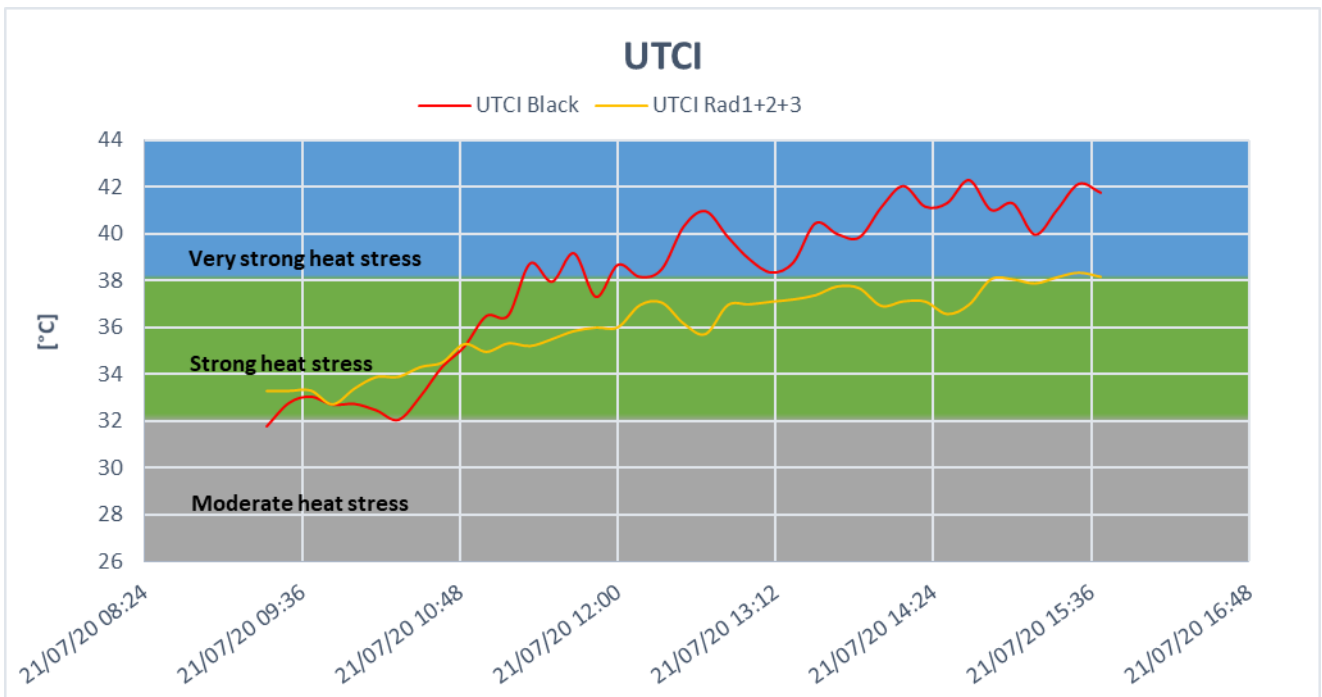



Figure 3. 7. UTCI calculated with net radiometers and globe thermometers; 21/07/2020.

According to methodology described in *Section 2.6 Methodology*, the radiative properties of the roof surface were calculated and reported in *Table 3. 3*, along with a picture of the rooftop surface. We obtained an average reflectivity $\rho = 0.11$ (calculated as the average over the entire duration of the measurements) and, consequently, an average absorptivity $\alpha = 0.89$. As expected, considering the colour of the ground surface, we recorded a low reflectivity and a high absorptivity.

Table 3. 3. Radiative properties of the horizontal/vertical surfaces tested; flat rooftop with a waterproofing membrane; 20/07/2020.

Horizontal/vertical surface	Image of the surface	ρ [-]	α [-]
Waterproofing membrane		0.11	0.89

3.1.2 Light plaster wall

The campaign took place in Via Lambruschini in Bovisa district, in Milan, on 23/07/2020, from 13:00 to 16:30, near a building characterised by a light plaster envelope; the flooring is light-coloured too. In the measurement environment there are no other elements that obstruct the direct solar radiation. The measurement was carried out near a building belonging to the campus of the “Politecnico di Milano”. The instrumentation was positioned 1 meter from the wall of the building as shown in *Figure 3. 8*. The meteorological parameters were detected by the All-in-one sensor every minute, allowing to carry out the analysis concerning MRT and UTCI.

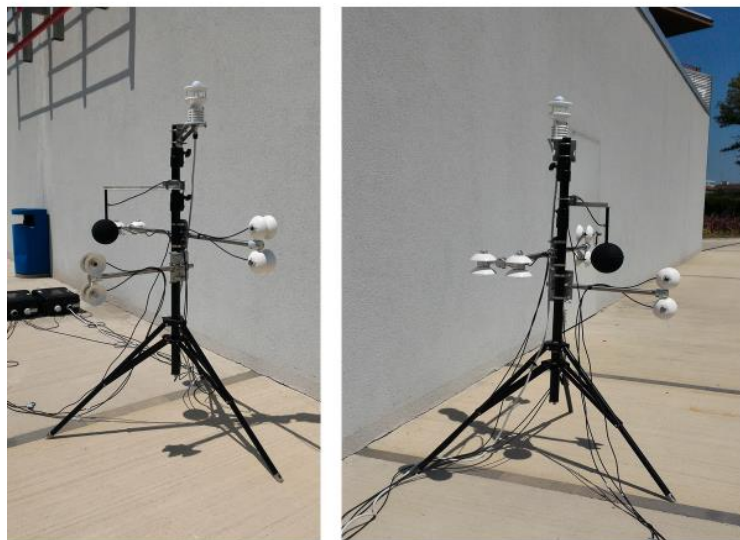


Figure 3. 8. Light plaster wall, Via Lambruschini, Milan.

Figure 3. 9 shows the trend of the MRT calculated both by black globe thermometer and net radiometers. According to the figure, the black globe (red line) overestimates the MRT in hours corresponding to a greater solar height, with respect to the three net radiometers (yellow line) solution; as the solar height decreases, this difference is considerably reduced until it disappears. The minimum MRT_{Black} recorded (at 16:30) was equal to 41.47 °C, in correspondence to a minimum $MRT_{Rad1+2+3}$ of 41.66 °C. On the other hand, when the solar height was higher, we get a maximum MRT_{Black} of 108.28 °C (recorded at 13:50) and a maximum $MRT_{Rad1+2+3}$ of 72.66 °C, facing a great difference between the two solutions. The average

MRT calculated by the black globe is equal to 79.00°C, while we obtain an average $MRT_{Rad1+2+3}$ of 65.41°C. A similar discrepancy in the results is evidenced in the *Figure 3. 10*, showing the difference between $MRT_{Rad1+2+3}$ and MRT_{Rad1} . The single radiometer (blue line) provides greater values of MRT when the vertical radiant fluxes prevail on the lateral ones, while the trend is reversed - even if with a small difference in magnitude - as lateral fluxes gain relevance. In particular, we recorded a maximum MRT_{Rad1} of 89.16 °C, in correspondence to a $MRT_{Rad1+2+3}$ of 72.42 °C (at 13:15); the minimum MRT_{Rad1} was recorded at 16:30 and it is equal to 37.36 °C, lower than the corresponding $MRT_{Rad1+2+3}$ of 46.14 °C. The average MRT_{Rad1} was equal to 76.28 °C.

The UTCI (*Figure 3. 11*), being closely related to the MRT results, have a similar behaviour: the large difference experienced between MRT_{Black} and $MRT_{Rad1+2+3}$ is reflected in the UTCI trend, by changing the stress category to which the UTCI belongs to (“Very strong heat stress” category for the net radiometers solution and “Extreme heat stress” category for the globe thermometer one), during the hours corresponding to a greater solar height. The average UTCI value assumes a value of 44.42 °C if calculated by means of the black globe and 40.95 °C if calculated using net radiometers, both falling in the “Very strong heat stress” category.

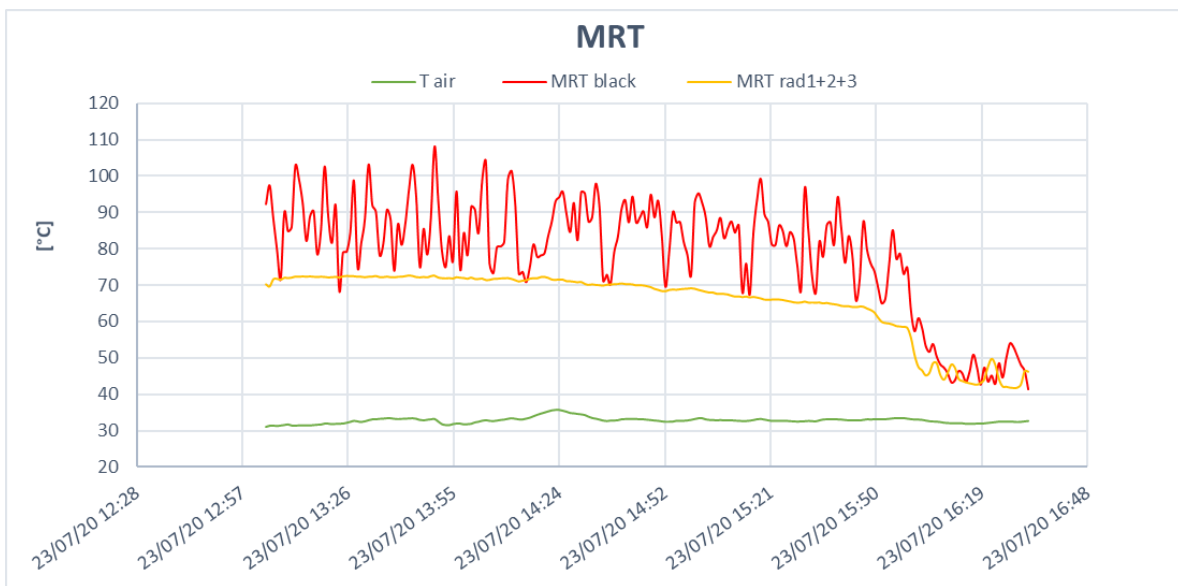


Figure 3. 9. MRT calculated with net radiometers and globe thermometers; 23/07/2020.

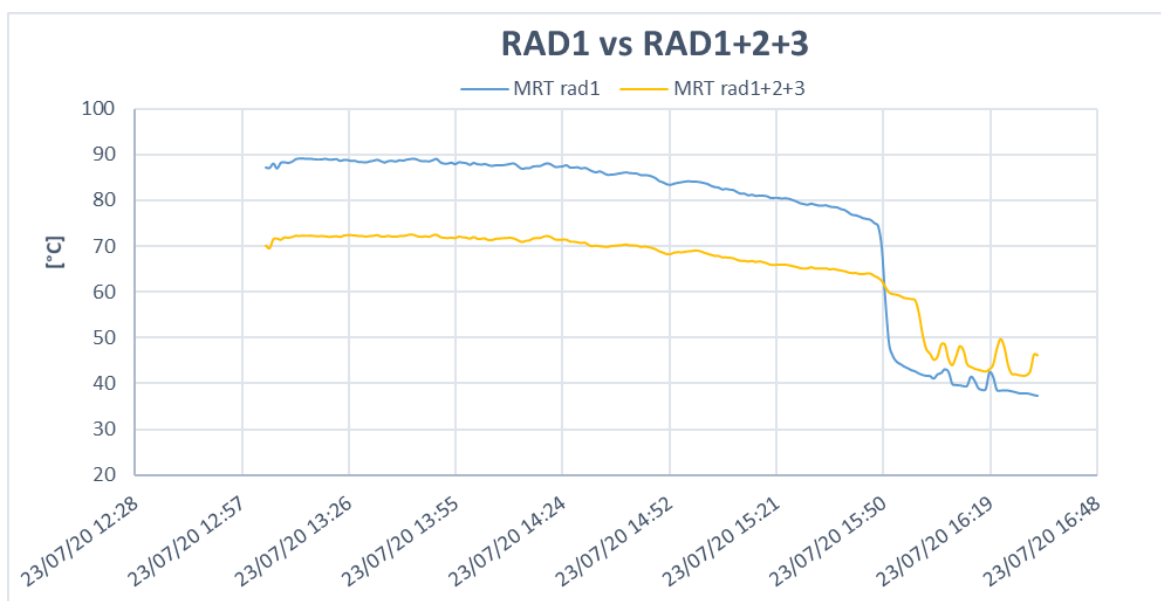


Figure 3. 10. MRT calculated with three radiometers and one radiometer measuring upward/downward direction; 23/07/2020.

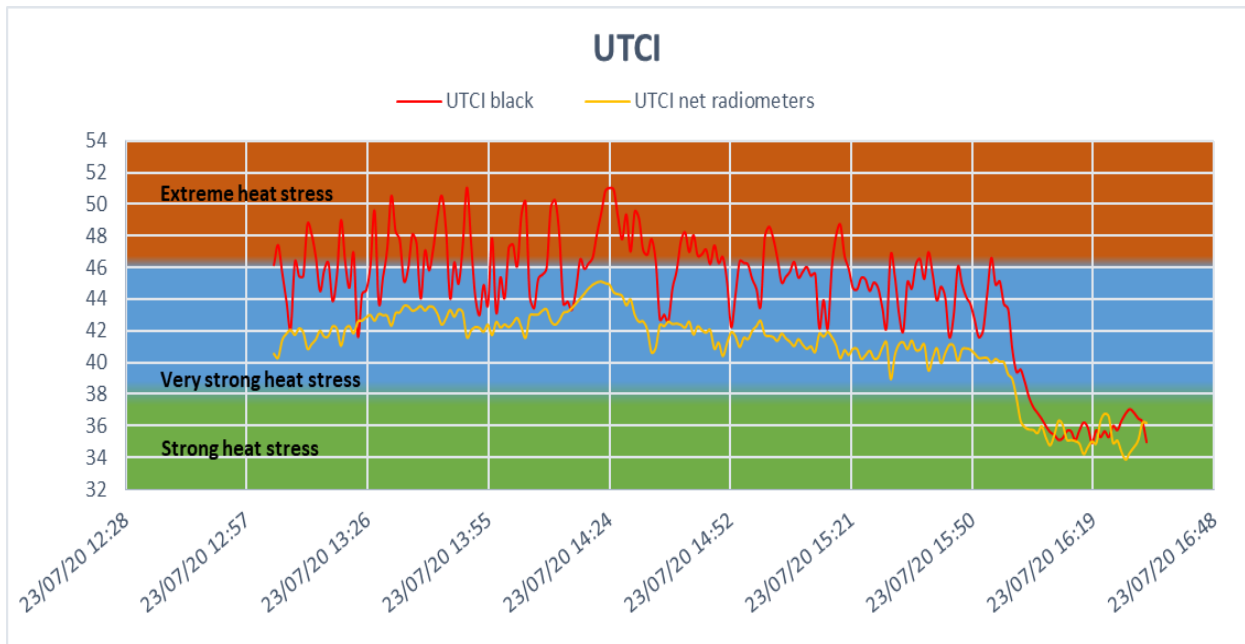




Figure 3. 11. UTCI calculated with net radiometers and globe thermometers; 23/07/2020.

The radiative properties of both the ground surface and the light-coloured plaster wall were then calculated and reported in *Table 3. 4*. For the wall, we obtain an average reflectivity of 0.48 and, consequently, an average absorptivity of 0.52. The results are consistent with the light colour of the building envelope. The average reflectivity and the average absorptivity of the ground surface are 0.31 and 0.69 respectively.

Table 3. 4. Radiative properties of the horizontal/vertical surfaces tested; light plaster wall; 23/07/2020.

Horizontal/vertical surface	Image of the surface	ρ [-]	α [-]
Ground surface		0.31	0.69
Light plaster building envelope		0.48	0.52

3.1.3 Porcelain stoneware façade cladding

This section deals with the measurements carried out on 27/07/2020 and 18/09/2020 in Via Lambruschini, in Milan, near a building with a porcelain stoneware envelope. A small grassy area is present about 1.50 m away from the instrumentation. The purpose of carrying out the analysis at the same point but in different months is to highlight how the instruments' responses vary at different times of the year, with different meteorological conditions.

As described in Section 2.1.4 *Solar Reflectivity and solar Absorptivity of a surface calculated with net radiometers*, to measure the radiative properties of the building envelope, the instrumentation was positioned 1 meter from the porcelain stoneware wall (Figure 3. 12).

The meteorological parameters were detected by the All-in-one sensor every minute and therefore also the interpolations between the data represented in Figure 3. 13, Figure 3. 14, Figure 3. 15, Figure 3. 16, Figure 3. 17, and Figure 3. 18 are per minute.



Figure 3. 12. Porcelain stoneware facade cladding, Via Lambruschini, Milan.

Figure 3. 13 and Figure 3. 14 show the trend of the MRT calculated with globe thermometers and net radiometers, on 27/07/2020 and 18/09/2020 respectively. From the two figures it can be seen that the black globe (red line) tends to overestimate the MRT, compared to the results provided by the net radiometers (yellow line), in the hours corresponding to a greater solar height, while the difference between the two solutions vanishes as solar height decreases. Differently from the black globe behaviour, the grey globe (purple line) trend in Figure 3. 14 seems to underestimate the MRT, if compared to $MRT_{Rad1+2+3}$, in the central hours of the day, when the solar height is at its maximum.

On 27/07/2020, the minimum MRT_{Black} recorded (at 13:45) was equal to 43.93 °C, in correspondence to a $MRT_{Rad1+2+3}$ of 45.86 °C. On the other hand, when the solar height was higher, we get a maximum MRT_{Black} of 97.59 °C (recorded at 12:55) and a maximum $MRT_{Rad1+2+3}$ of 72.41 °C, facing a great difference between the two solutions. The average MRT calculated by the black globe is equal to 70.19 °C, while we obtain an average $MRT_{Rad1+2+3}$ of 64.16 °C. During the measurements carried out on 18/09/2020, we recorded an average MRT_{Black} of 65.86 °C, higher than the average $MRT_{Rad1+2+3}$ equal to 63.38 °C. On the contrary, with the grey globe we obtained an average MRT_{Grey} value of 56.38 °C, lower than the reference value and with an higher absolute difference $MRT_{Globe} - MRT_{Rad1+2+3}$ with respect to the black globe. The maximum values obtained with the three instruments are 72.01 °C for $MRT_{Rad1+2+3}$, 88.07 °C for MRT_{Black} and 76.60 °C for the grey globe. Even if the average value of MRT_{Grey} was lower than the average reference value, however, the maximum value obtained during the day was higher than the maximum $MRT_{Rad1+2+3}$, due to the large fluctuations that can be observed in Figure 3. 14 in the trends of the MRT obtained with the two globe thermometers.

As regards the difference between $MRT_{Rad1+2+3}$ and MRT_{Rad1} (Figure 3. 15 and Figure 3. 16), the behaviour is analogue to the black globe one. In the hours of greatest solar height, the single radiometer 1 (blue line) overestimates the MRT and this is even more pronounced in the measurements carried out in July (Figure 3. 15) rather than in September (Figure 3. 16). In particular, on 27/07, we recorded a maximum MRT_{Rad1} of 91.20 °C, in correspondence to a $MRT_{Rad1+2+3}$ of 69.00 °C (at 13:15); the minimum MRT_{Rad1} was recorded at 16:30 and it is equal to 47.31 °C, corresponding to a $MRT_{Rad1+2+3}$ value of 45.54 °C. The average MRT_{Rad1} was equal to 75.99 °C, even greater than the average MRT_{Black} of 70.19 °C. On 18/09/2020, we obtained an average MRT_{Rad1} of 66.33 °C, still greater than the average MRT_{Black} , equal to 65.86 °C. For measurements carried out near a vertical wall it therefore seems that the single radiometer 1 overestimates the MRT too much with respect to the reference solution, even more than the black globe does.

The comparison was also made in terms of UTCI in Figure 3. 17 and Figure 3. 18. As can be observed in Figure 3. 17, during the first day of measurements (27/07/2020) the two UTCI fall within the same thermal stress category (“Very strong heat stress”) for the majority of the day, with average values equal to 42.40 °C for the black globe measurements and 40.87 °C for the net radiometers. On 18/09, the average values calculated for the UTCI are similar for the black globe and the net radiometers solutions, with values equal to 39.76 °C and 39.14 °C, while we get a lower average value for the grey globe (37.37 °C). While the UTCI trends obtained through $MRT_{Rad1+2+3}$ and MRT_{Black} fall within the same stress category (“Very strong heat stress”) for the majority of the day, the UTCI trend of the grey globe continuously oscillates between the “Very strong heat stress” and the “Strong heat stress” categories.

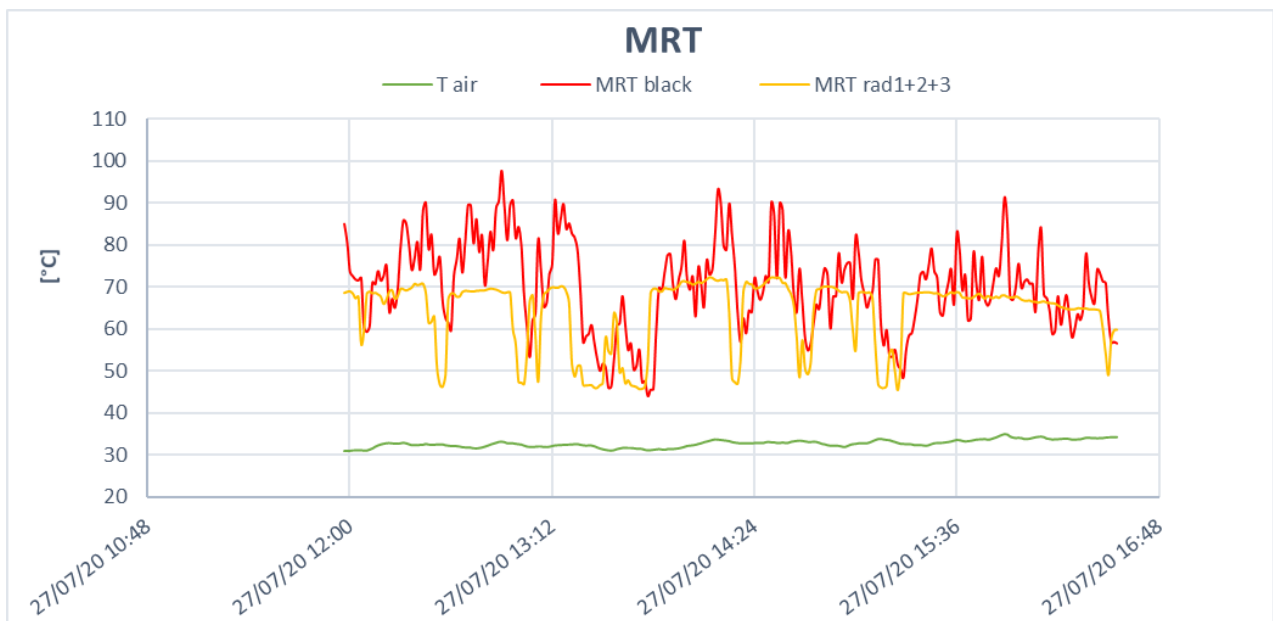


Figure 3. 13. MRT calculated with net radiometers and globe thermometers; 27/07/2020.

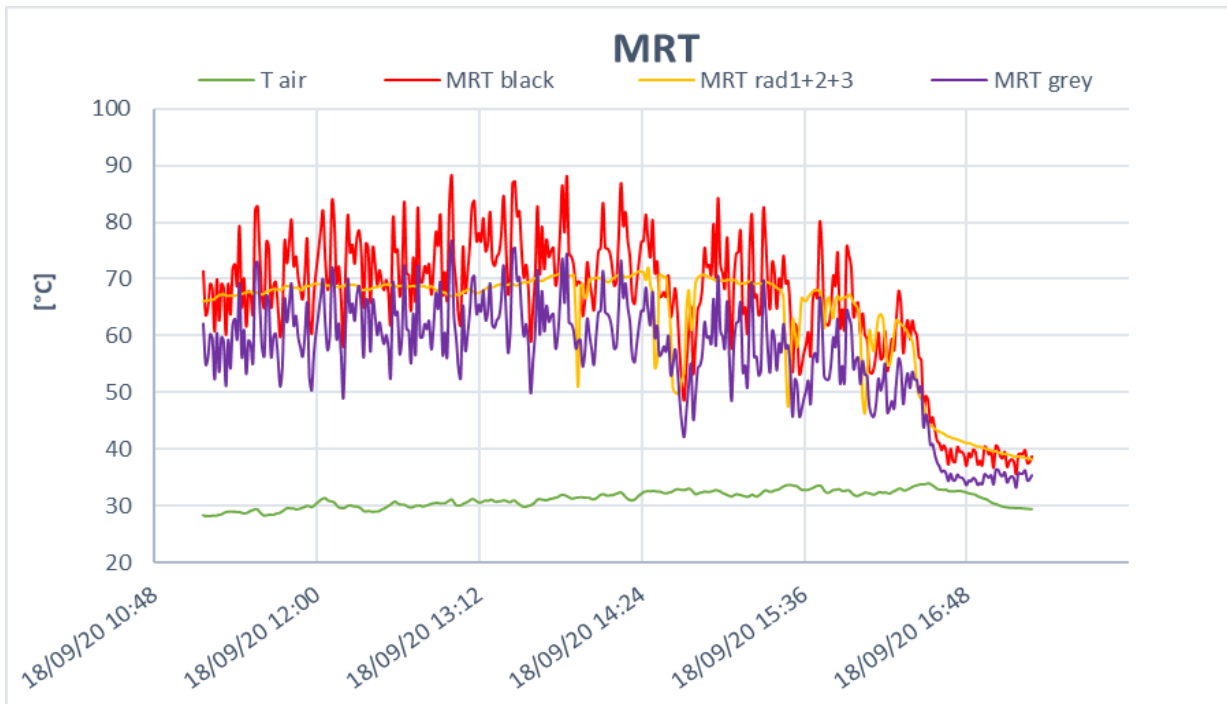


Figure 3. 14. MRT calculated with net radiometers and globe thermometers; 18/09/2020.

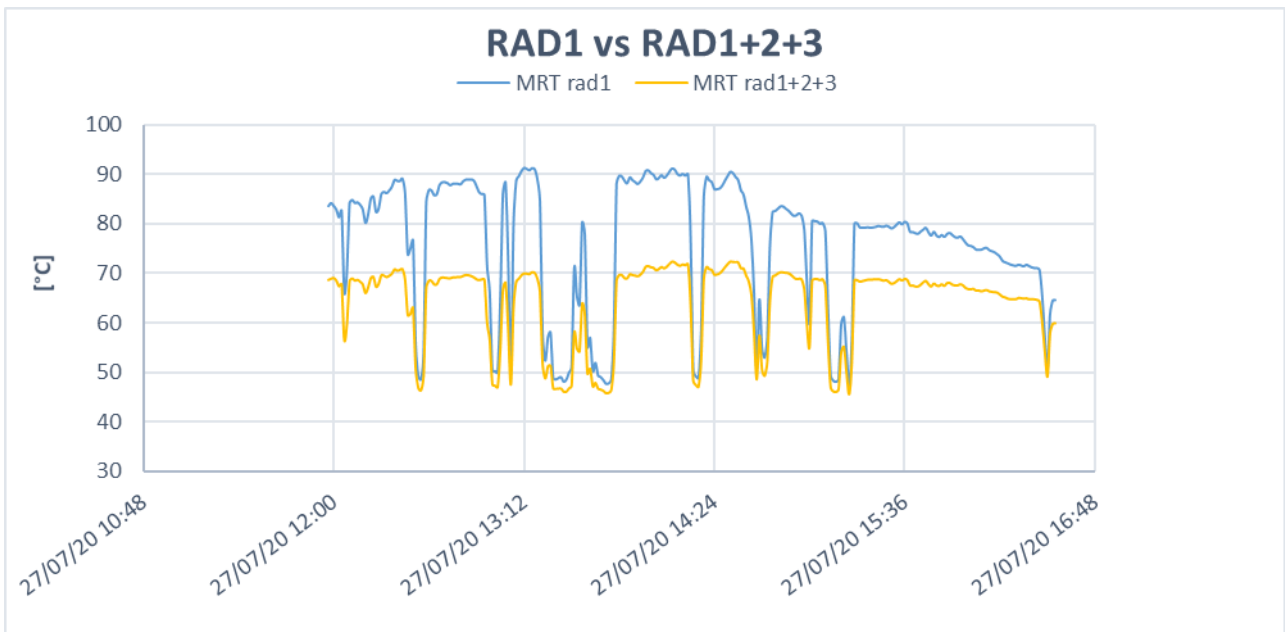


Figure 3. 15. MRT calculated with three radiometers and one radiometer measuring upward/downward direction; 27/07/2020.

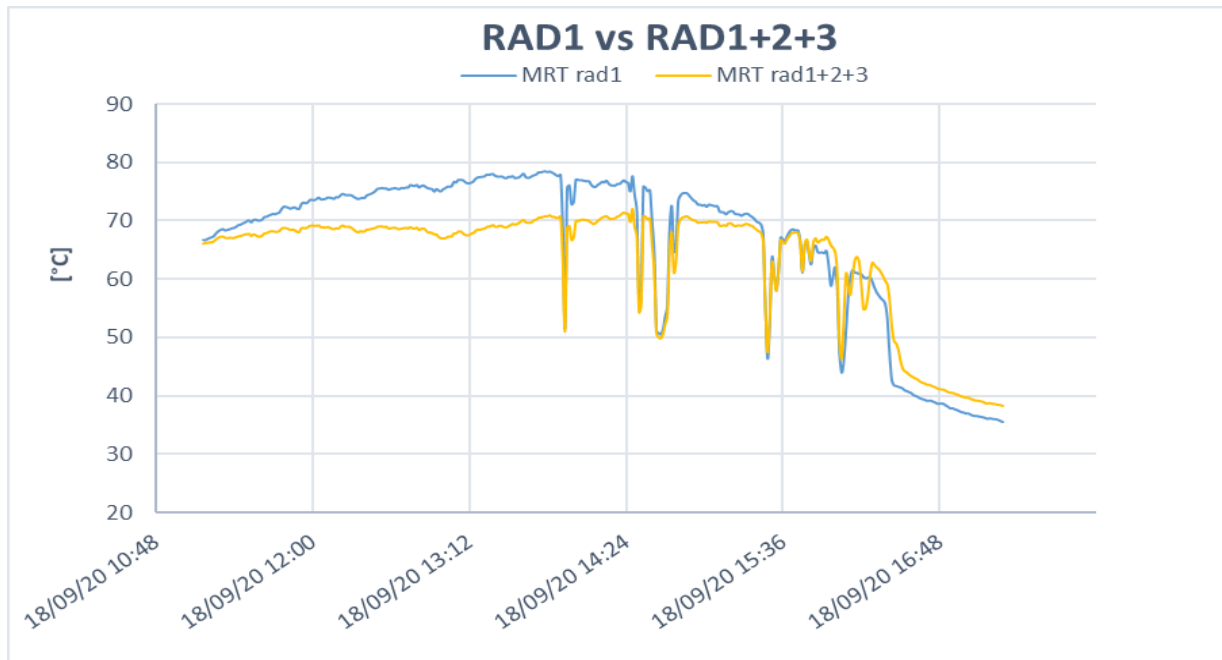


Figure 3. 16. MRT calculated with three radiometers and one radiometer measuring upward/downward direction; 18/09/2020.

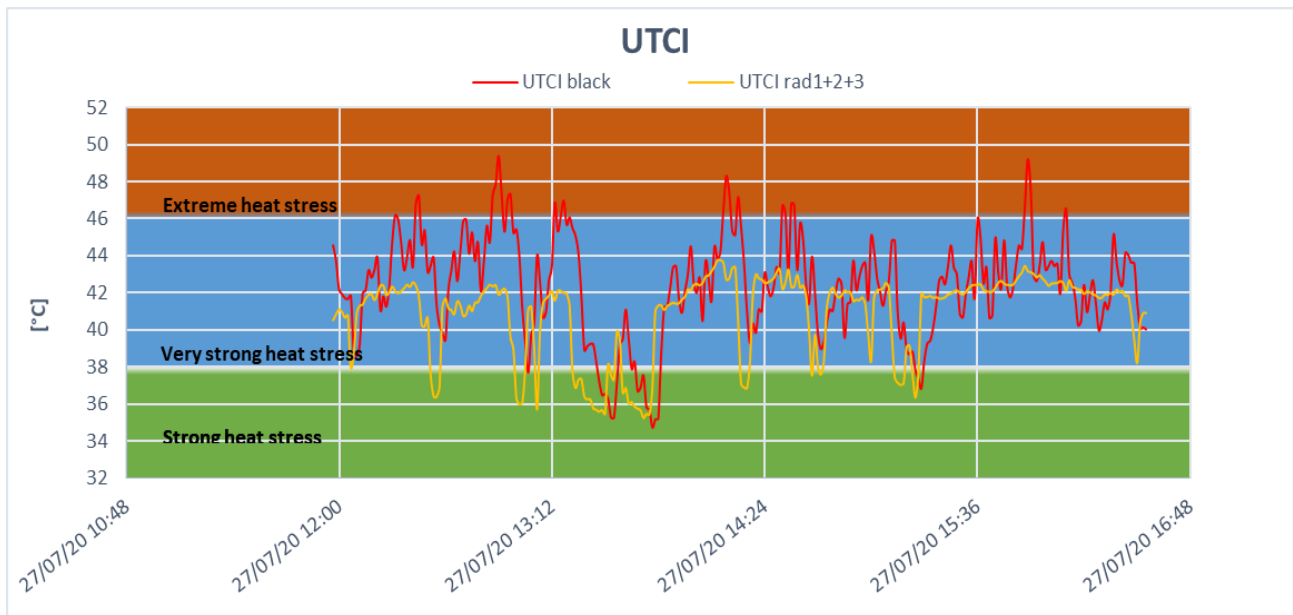


Figure 3. 17. UTCI calculated with net radiometers and globe thermometers; 27/07/2020.

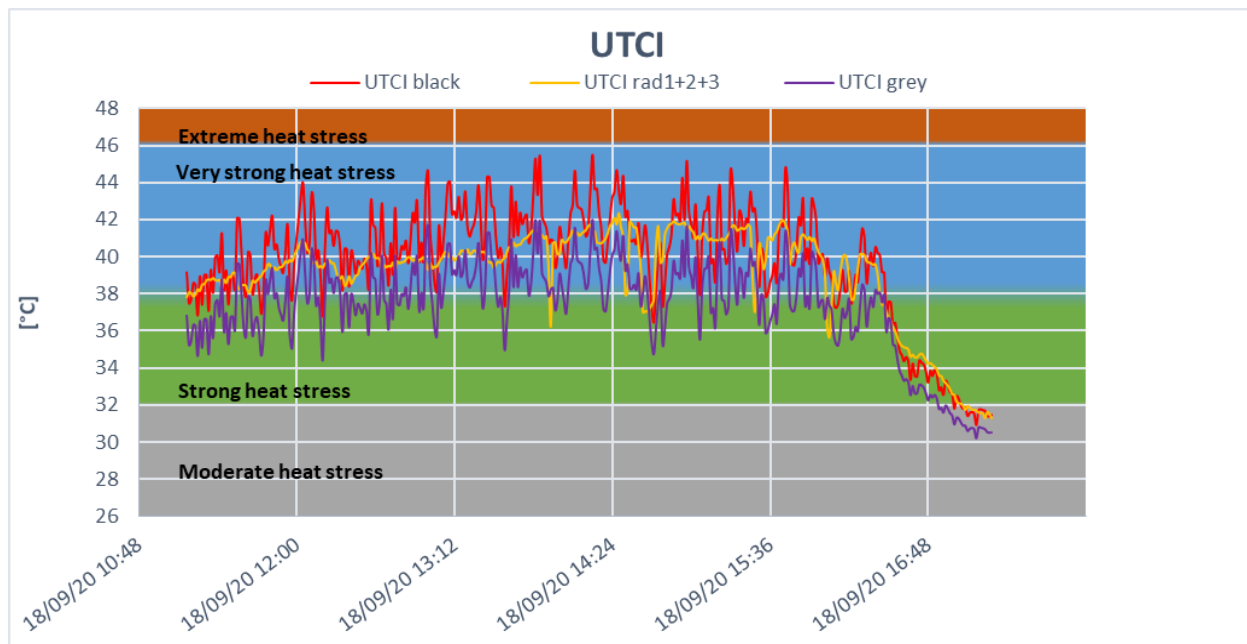




Figure 3. 18. UTCI calculated with net radiometers and globe thermometers; 18/09/2020.

Finally, the radiative properties of the building envelope and the ground surface were calculated and their pictures reported in *Table 3. 5*. For the vertical wall examined, we obtain a value equal to 0.30 on 27/07/2020 and equal to 0.28 on 18/09/2020. Accordingly, the average absorptivity over the measurement period is 0.70 in July and 0.72 in September. For the ground surface, instead, we get an average reflectivity of 0.24 (and, consequently, an average absorptivity of 0.76) for both the days of measurement.

Table 3. 5. Radiative properties of the horizontal/vertical surfaces tested; porcelain stoneware façade cladding; 27/07/2020.

Horizontal/vertical surface	Image of the surface	ρ [-]	α [-]
Ground surface		0.24	0.76
Porcelain stoneware building envelope		0.30	0.70

3.1.4 Park

The measurements analysed in this section took place in a park in Cascina Merlata district in Milan, from 11:50 am to 4:30 pm on 28/07/2020. The analysis is aimed at evaluating how the instruments measure the parameters of interest in an open field, in absence of obstacles to direct solar radiation and without elements that could overshadow the instrumentation.

Figure 3. 19 shows a picture of the measurement environment. As can be seen, the instrumentation was positioned on the lawn grass, away from any element that could obstruct the direct radiation.

The meteorological parameters were measured per minute by the All-in-one sensor and therefore the interpolation in the Excel graphs (Figure 3. 20, Figure 3. 21, and Figure 3. 22) was made starting from per-minute input data.



Figure 3. 19. Park, Cascina Merlata district, Milan.

Figure 3. 20 shows the trend of the MRT calculated both by black globe thermometer and net radiometers. The figure evidences that, in open field, in absence of elements obstructing the direct solar radiation, the black globe thermometer records a much higher MRT than the one measured by net radiometers, with an average difference of 15.56 °C between the two curves. In particular, the average MRT_{Black} is equal to 76.17 °C, while for the net radiometers we obtain an average $MRT_{Rad1+2+3}$ of 60.61 °C. The minimum MRT_{Black} recorded (at 12:20) was equal to 57.51, higher than the minimum $MRT_{Rad1+2+3}$ of 49.69 °C. The maximum MRT values calculated are equal to 96.12 °C for MRT_{Black} (recorded at 12:50) and 65.96 °C (at 12:30) for $MRT_{Rad1+2+3}$, evidencing again the great difference between the two solutions in open field.

Figure 3. 21 shows the comparison between $MRT_{Rad1+2+3}$ and MRT_{Rad1} . It can be seen that, for open field measurements, the single radiometer provides results with a higher accuracy than those obtained with the black globe thermometers. In particular, the average MRT_{Rad1} is equal to 71.70 °C, closer to the reference values with respect to the average MRT_{Black} . Furthermore, the maximum MRT_{Rad1} obtained is equal to 79.74 °C, much lower than the value of 96.12 °C obtained with the black globe.

The UTCI (Figure 3. 22), being closely related to the MRT results, shows a similar trend and the large difference experienced between MRT_{Black} and $MRT_{Rad1+2+3}$ is reflected here, even if both the curves fall in the same thermal stress category (“Very strong heat stress”) for the majority of the measurement duration. The average UTCI assumes a value of 42.58 °C if calculated by means of the black globe and 38.77 °C if calculated using net radiometers.

However, some researchers (i.e. Thorsson et al. 2007) have pointed out that, in open field measurements, the vertical radiative fluxes have a greater importance, not correctly described by the view factors

commonly adopted (0.06 for both upward and downward direction). This topic will be discussed more in detail in *Chapter 4. Discussions and further elaborations*.

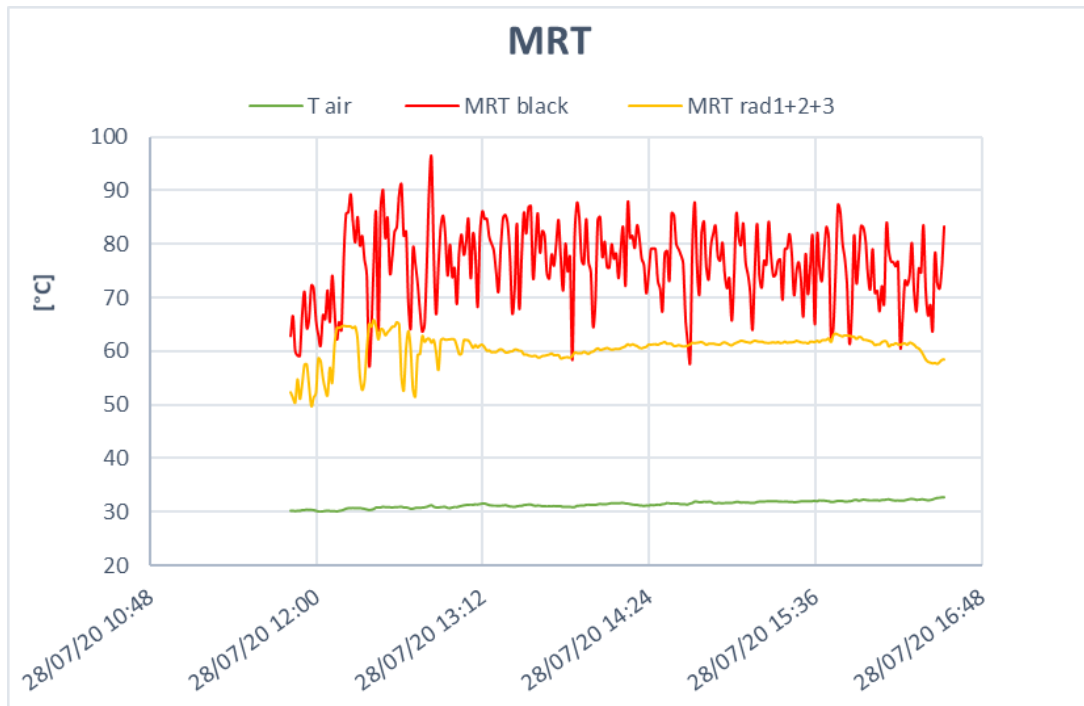


Figure 3. 20. MRT calculated with net radiometers and globe thermometers; 28/07/2020.

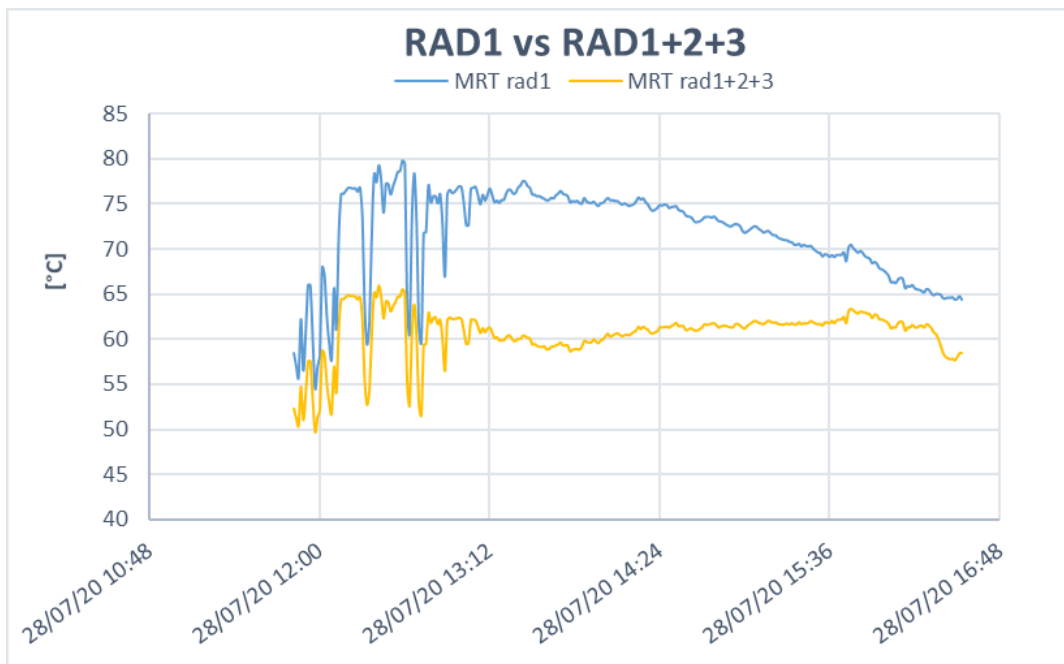


Figure 3. 21. MRT calculated with three radiometers and one radiometer measuring upward/downward direction; 28/07/2020.

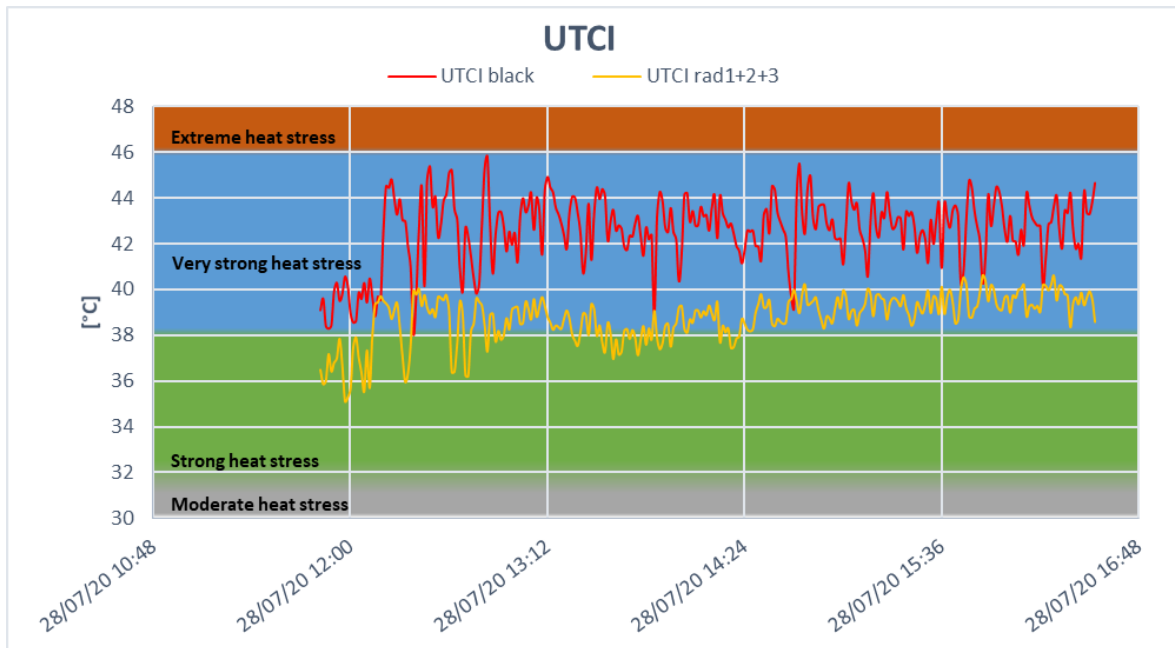



Figure 3. 22. UTCI calculated with net radiometers and globe thermometers; 28/07/2020.

The radiative properties of the lawn grass were finally calculated and reported in *Table 3. 6*. According to the data recorded by the net radiometer 1, we calculated an average reflectivity of the ground surface equal to 0.20 and, therefore, an average absorptivity value of 0.80. The results are consistent with the typical reflectivity values for this type of soil (usually between 0.20 and 0.25) (<http://www.intelligence.tuc.gr/>).

Table 3. 6. Radiative properties of the horizontal/vertical surfaces tested; park; 28/07/2020.

Horizontal/vertical surface	Image of the surface	ρ [-]	α [-]
Lawn grass		0.20	0.80

3.1.5 Green rooftop

The measurements took place on the roof of a building, belonging to the campus of “Politecnico di Milano”, in Via G. Ponzio, in Milan, from 15:20 on 26/08/2020 to 17:15 on 27/08/2020 continuously. The measurement environment (*Figure 3. 23*) consists of a flat rooftop covered with grass. During the night, the instrumentation was fixed to a pole using tie rods, to prevent sudden gusts of wind from causing it to fall. The measurements took place in an environment similar to the one analysed in *Section 3.1.4 Park* (grassy ground and open field). Therefore, in this section, we will evaluate if there is an actual analogy in terms of thermal comfort (evaluated by UTCI). Furthermore, with measurements lasting 26 hours, it is possible to understand how the instruments behave during night hours too, in absence of solar radiation.

For better graphical visualization, the results of this analysis have been divided as follows:

- 26/08/2020 DAY:
 - Measurement duration: 15:20 - 21:00
 - Instrumentation: 3 net radiometers, black globe, All-in-one sensor
- 26-27/08/2020 NIGHT:
 - Measurement duration: 21:01 (26/08/2020) - 8:00 (27/08/2020)
 - Instrumentation: 3 net radiometers, black globe, grey globe, All-in-one sensor
- 27/08/2020 DAY:
 - Measurement duration: 8:01 - 17:15
 - Instrumentation: 3 net radiometers, black globe, grey globe, All-in-one sensor



Figure 3. 23. Green rooftop, Via G. Ponzio, Milan.

Figure 3. 24 and *Figure 3. 25* represent the trend of the MRT calculated by using globe thermometers and net radiometers during the last hours of the first day of measurement (26/08/2020) and during night. In these hours, the difference between MRT_{Black} and $MRT_{Rad1+2+3}$ is almost zero. On 26/08, the average $MRT_{Rad1+2+3}$ is equal to 41.65 °C, while the average MRT_{Black} is 40.74 °C; during night we obtained an average $MRT_{Rad1+2+3}$ of 21.66 °C and an average MRT_{Black} of 20.77 °C. From the two figures it can be seen that, during the hours of low solar height and during the night, the $MRT_{Black} - MRT_{Rad1+2+3}$ difference is greatly reduced, until it becomes negative but still small in magnitude. The maximum values recorded during the first day were 71.90 °C (at 16:15) for the net radiometers and 86.57 °C (at 15:25) for the black globe; the minimum values recorded at 21:00 were 24.11 °C if calculated with the radiometers and 21.69 °C with the black globe.

According to *Figure 3. 25*, during night the minimum values calculated fell to 18.09 °C for $MRT_{Rad1+2+3}$, 15.20 °C for MRT_{Black} and 14.72 °C for MRT_{Grey} . Also in terms of average values, the grey globe, during night measurements, provides a MRT_{Grey} equal to 20.27 °C, thus having a $MRT_{Globe} - MRT_{Rad1+2+3}$ difference greater, in absolute value, than the one obtained with the black globe.

Figure 3. 26 shows instead the MRT trend obtained with the two globe thermometers and the net radiometers on the second day of measurements (27/08/2020). During this day, the minimum values recorded are 31.32 °C for the black globe, 26.64 °C for the grey globe and 27.19 °C for the net radiometers; the maximum values are 88.14 °C, 75.67 °C and 68.83 °C with the black globe, the grey globe and the three net radiometers respectively. In terms of average values we observed an $MRT_{Rad1+2+3}$ equal to 54.96 °C, an MRT_{Black} of 62.66 °C and an MRT_{Grey} of 53.36 °C. The figure thus shows that the black thermometer globe tends to overestimate the MRT with respect to the reference solution, while the grey globe underestimates it. The difference between $MRT_{Rad1+2+3}$ and MRT_{Grey} is however very small, with an average value over the day of 1.60 °C. This seems to confirm what has been reported in literature (Standard 1998; Ashrae Standard 2001): in outdoor condition and, in particular, in open field measurements, with the instrumentation directly exposed to solar radiation, the grey globe is more suitable than the black globe to evaluate the MRT.

As regards the difference between $MRT_{Rad1+2+3}$ and MRT_{Rad1} , from *Figure 3. 27* and *Figure 3. 28* we can observe that, during evening and night measurements, the single net radiometer provides lower value than $MRT_{Rad1+2+3}$. In particular, we obtained an average value of MRT_{Rad1} equal to 40.07 °C on 26/08 and 18.73 °C during the night between 26/08 and 27/08. As the solar height increases, MRT_{Rad1} increases accordingly, becoming higher than the corresponding $MRT_{Rad1+2+3}$. In *Figure 3. 29*, showing the trends on 27/08, the average MRT_{Rad1} is equal to 57.87 °C. The result obtained is therefore greater than the average $MRT_{Rad1+2+3}$, but still lower than MRT_{Black} , confirming that, in open field, the single radiometer approximates the reference solution better than the black globe.

The comparison was also made in terms of UTCI in *Figure 3. 30*, *Figure 3. 31* and *Figure 3. 32*. During late afternoon and night (*Figure 3. 30* and *Figure 3. 31*), consistently with the small difference in the MRT trends, the UTCI values are very similar to each other and the difference is smaller than 1°C between one instrument and another.

On the second day of measurements, according to *Figure 3. 32*, the UTCI average values are equal to 36.33 °C for net radiometers, 38.23 °C for black globe and 35.91 °C for grey globe. During the majority of the measurement duration, the UTCI trends obtained with the net radiometers and the grey globe fell into the “Strong heat stress” category, while the UTCI calculated from the data provided by the black globe continuously oscillated between the above mentioned category and the “Very strong heat stress” one. Only until 8:30, all three curves fall into the “Moderate heat stress” category.

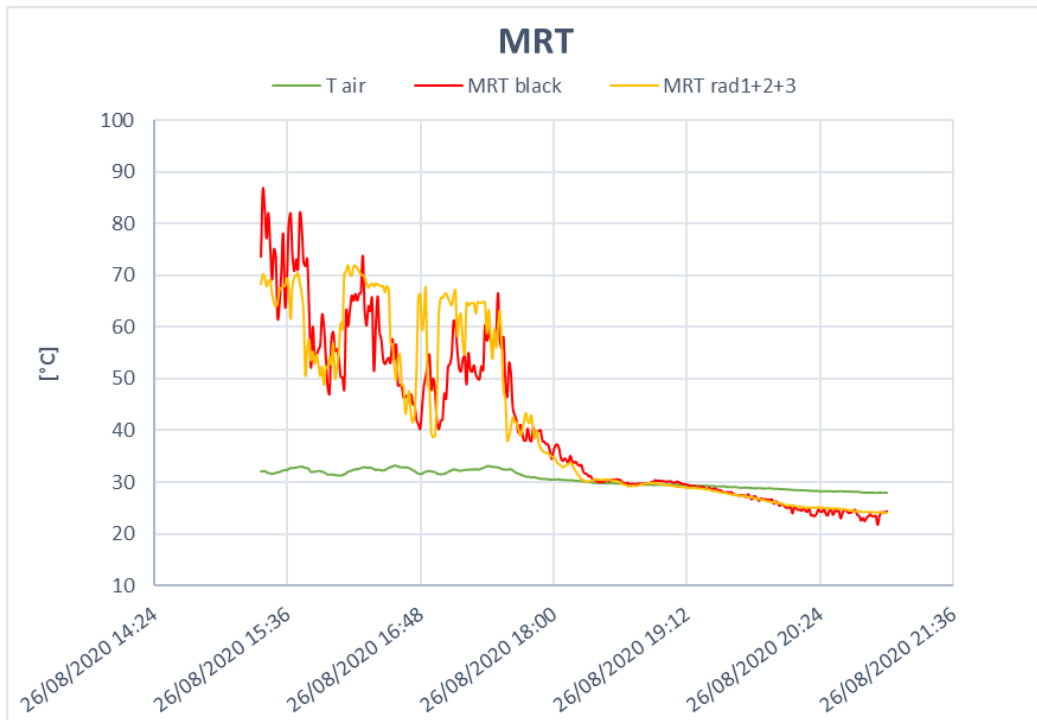


Figure 3. 24. MRT calculated with net radiometers and globe thermometers; day 26/08/2020.

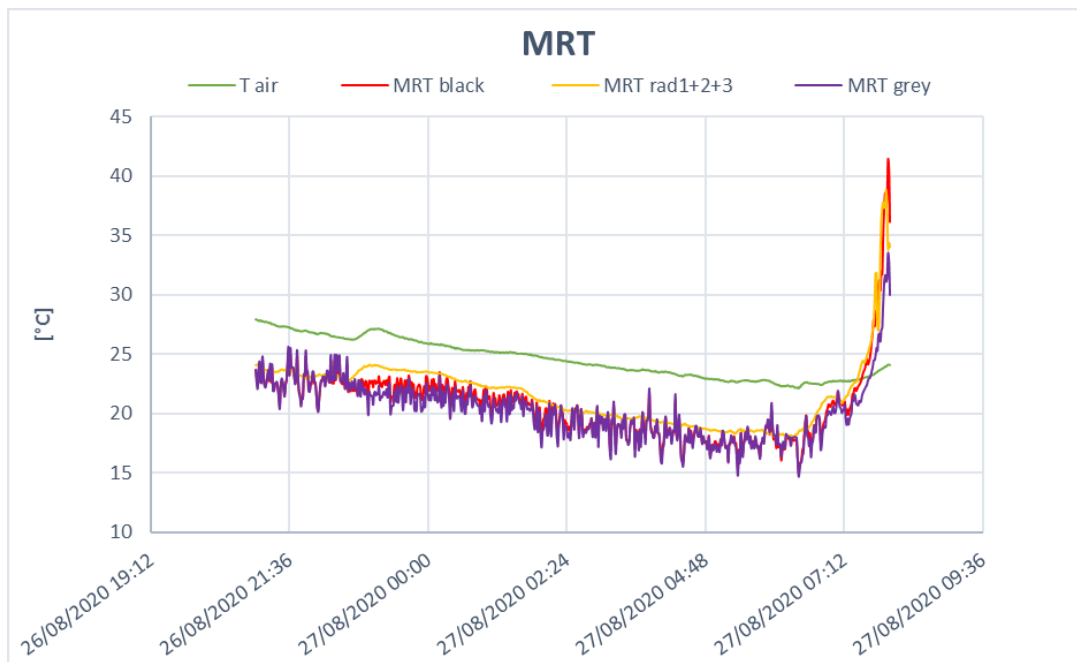


Figure 3. 25. MRT calculated with net radiometers and globe thermometers; night 26-27/08/2020.

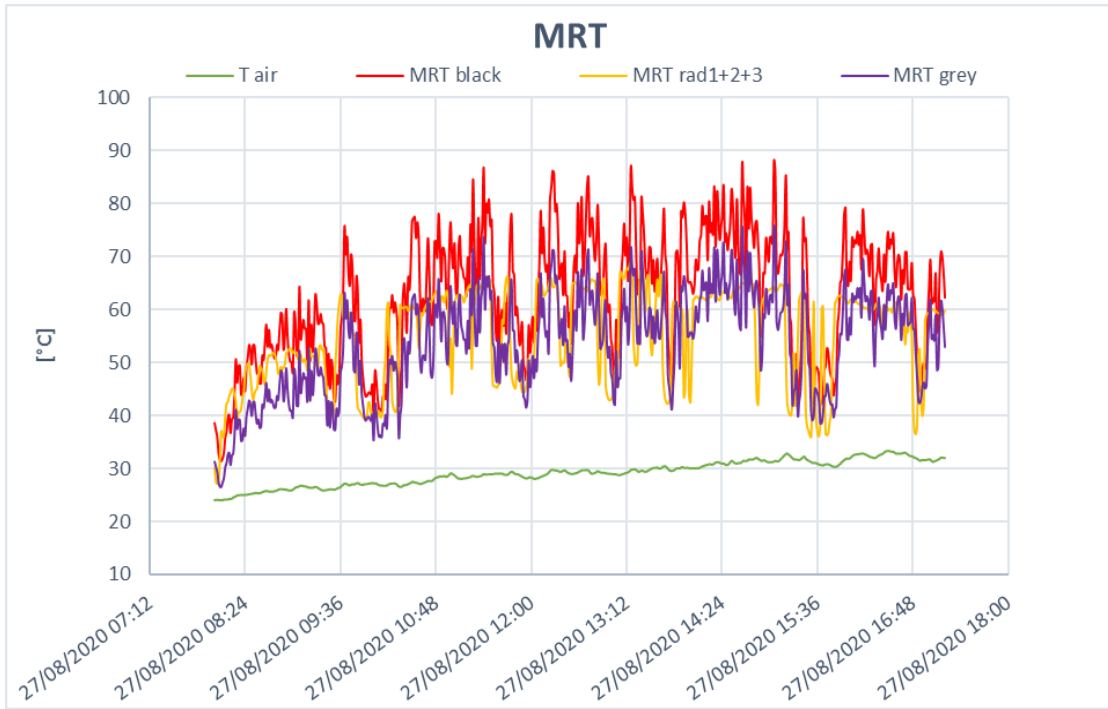


Figure 3. 26. MRT calculated with net radiometers and globe thermometers; day 27/08/2020.

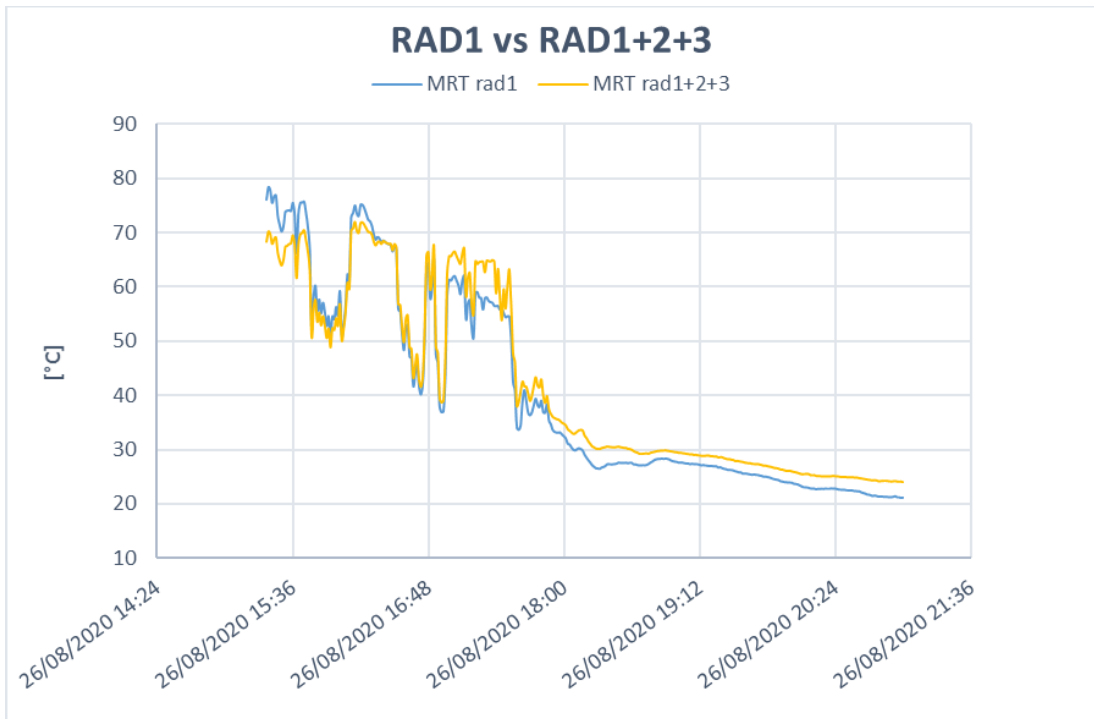


Figure 3. 27. MRT calculated with three radiometers and one radiometer measuring upward/downward direction; day 26/08/2020.

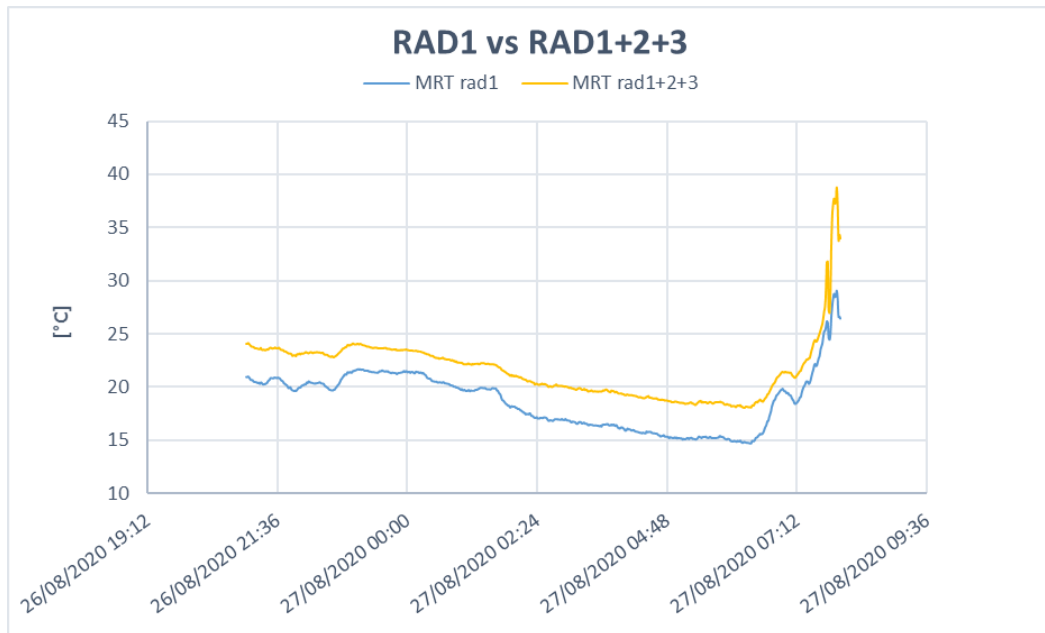


Figure 3. 28. MRT calculated with three radiometers and one radiometer measuring upward/downward direction; night 26-27/08/2020.

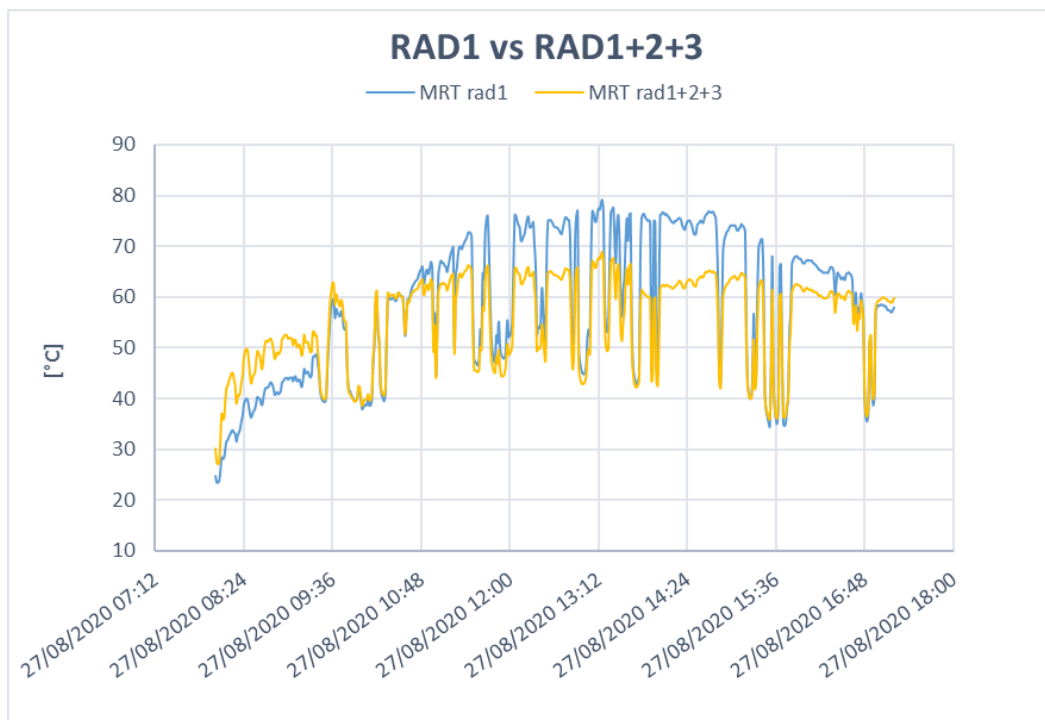


Figure 3. 29. MRT calculated with three radiometers and one radiometer measuring upward/downward direction; day 27/08/2020.

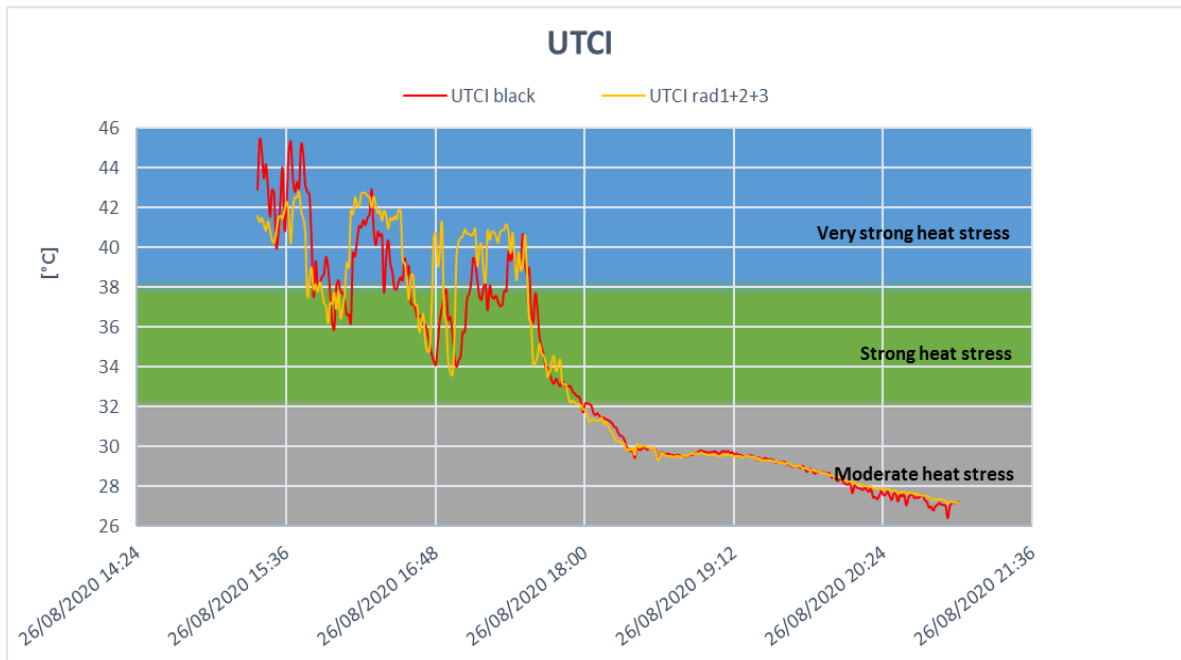


Figure 3. 30. UTCI calculated with net radiometers and globe thermometers; day 26/08/2020.

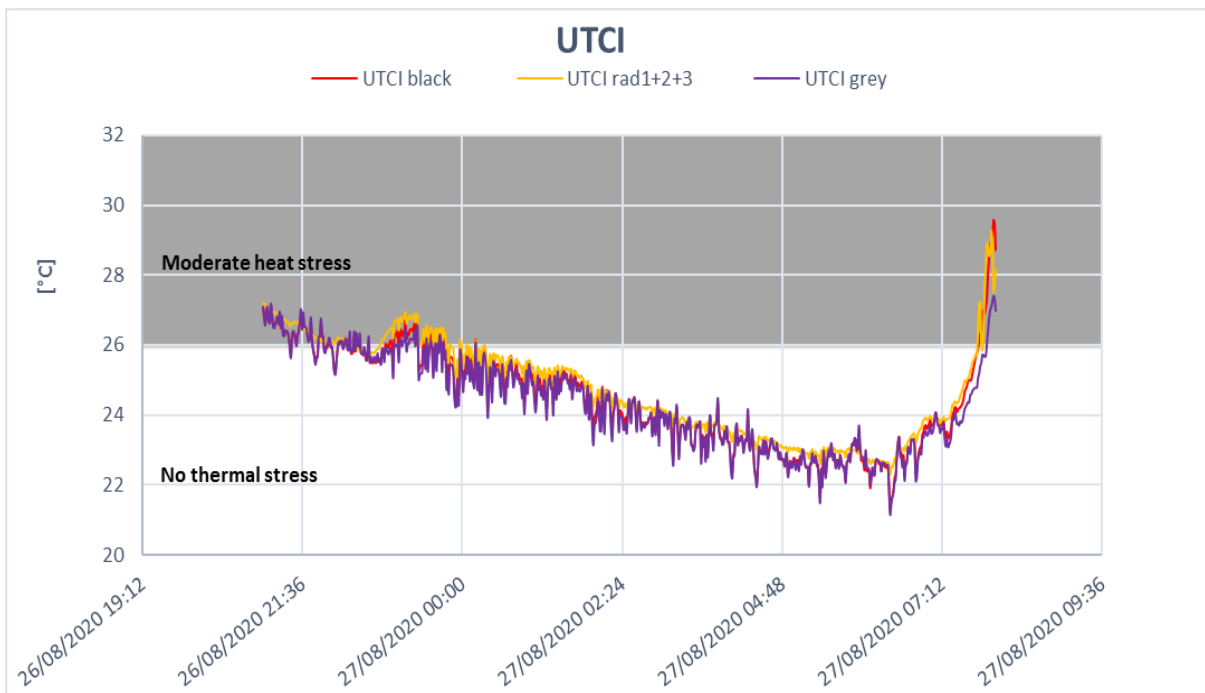


Figure 3. 31. UTCI calculated with net radiometers and globe thermometers; night 26-27/08/2020.

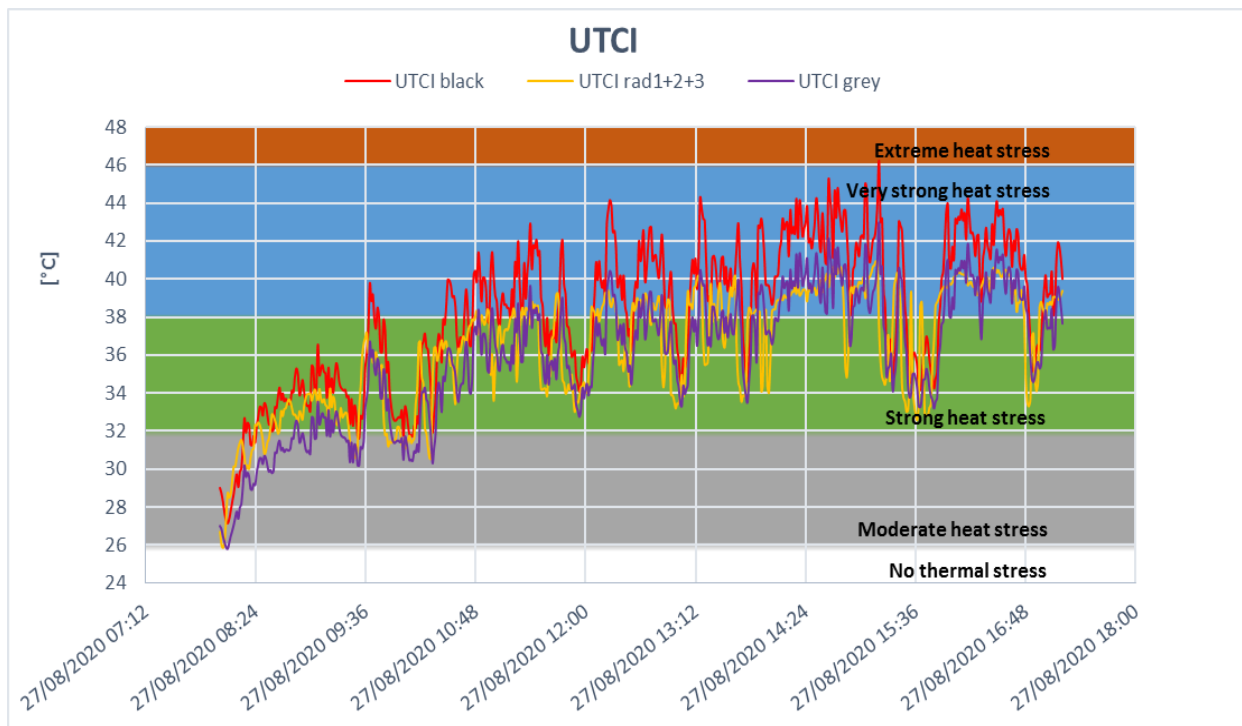



Figure 3. 32. UTCI calculated with net radiometers and globe thermometers; day 27/08/2020.

Finally, the radiative properties of the grass covering the rooftop were calculated. As reported in *Table 3. 7*, we obtained an average reflectivity of 0.22 and, consequently, an average absorptivity of 0.78. The results are consistent with the typical reflectivity values of grassy soils (0.20 - 0.30) (<http://www.intelligence.tuc.gr/>).

Table 3. 7. Radiative properties of the horizontal/vertical surfaces tested; green rooftop; 26-27/08/2020.

Horizontal/vertical surface	Image of the surface	ρ [-]	α [-]
Grass		0.22	0.78

3.1.6 Blue plaster building envelope

This section focuses on a measurement campaign taking place on 01/09/2020 in Cascina Merlata district, in Milan, from 11:30 to 17:10. The measurement aims to study the outdoor thermal comfort parameters in an environment similar to the one of *Section 3.1.2 Light plaster wall* and *Section 3.1.3 Porcelain stoneware façade cladding* but with different colour and material of the building envelope near which the survey was carried out. The vertical surfaces tested is a blue plaster wall of a residential building (*Figure 3. 33*). No other element that could interfere with the field of view of the net radiometers was present in the proximity of the instrumentation.



Figure 3. 33. Blue plaster building envelope, Cascina Merlata district, Milan.

Figure 3. 34 shows the trend of the MRT calculated by using globe thermometers and net radiometers. According to the figure, the black globe (red line) overestimates the MRT especially in central hours of the day, corresponding to a greater solar height, with respect to the three net radiometers (yellow line) solution. As the solar height decreases, this difference is considerably reduced until it vanishes after 15:30. The black globe thermometer provided an average MRT_{Black} equal to 58.98 °C, with a minimum of 27.16 °C (recorded at 17:10) and a maximum value of 91.20 °C (recorded at 13:22). On the contrary, the grey globe (purple line) underestimated the MRT with respect to the reference solution, providing an average MRT_{Grey} of 48.71 °C. By using the net radiometers, we found an MRT that was in the middle between the two solutions provided by the globes: the average $MRT_{Rad1+2+3}$ is equal to 54.53 °C, with a minimum value of 27.84 °C and a maximum value of 72.55 °C.

Figure 3. 35, showing the MRT_{Rad1} trend, evidenced that, when we are not in open field, the single net radiometer is not suitable to approximate the reference results. The average MRT_{Rad1} is equal to 61.94 °C, experiencing a difference of 7.41 °C with respect to the average $MRT_{Rad1+2+3}$.

The UTCI trend obtained through the measurements carried out with the three instruments is shown in *Figure 3. 36*. Until 15:00, the UTCI calculated with the black globe falls into the “Very strong heat stress” category, while the grey globe provided UTCI values belonging to the “Strong heat stress” category. The reference UTCI values obtained with the net radiometers are perfectly in the middle, oscillating between the two thermal stress ranges mentioned. After 15:00 all the curves in *Figure 3. 36* falls into the “Moderate heat stress” category.

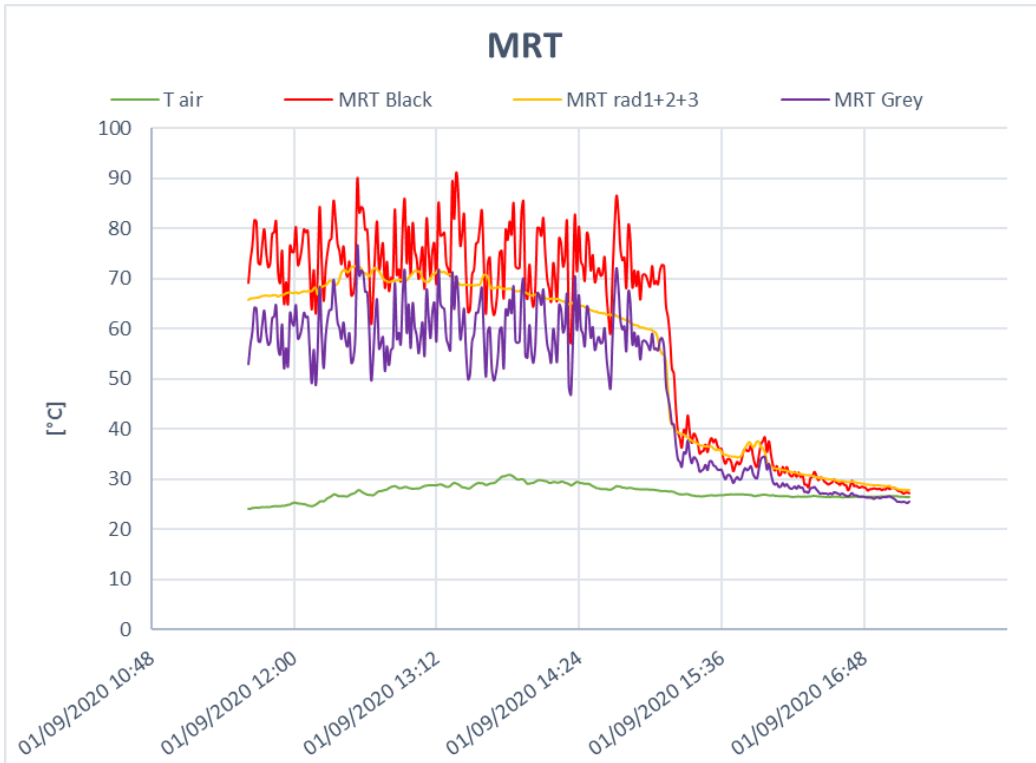


Figure 3. 34. MRT calculated with net radiometers and globe thermometers; 01/09/2020.

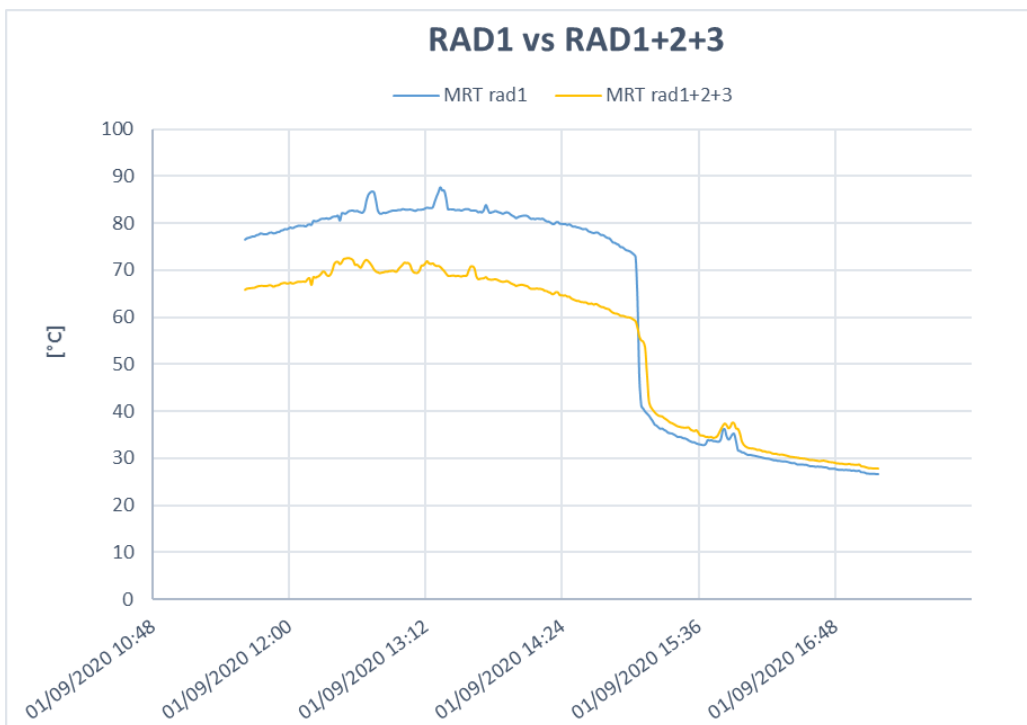


Figure 3. 35. MRT calculated with three radiometers and one radiometer measuring upward/downward direction; 01/09/2020.

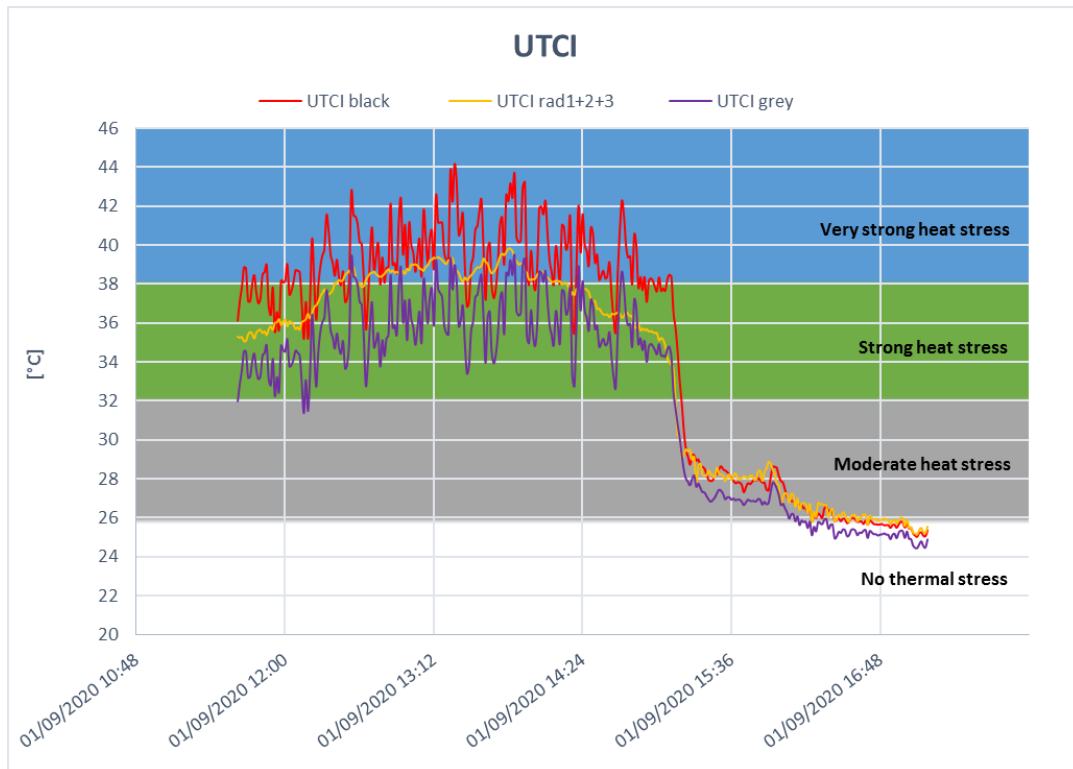




Figure 3. 36. UTCI calculated with net radiometers and globe thermometers; 01/09/2020.

Finally, the radiative properties of both the building envelope and the ground surface were calculated. And reported in *Table 3. 8*, which also shows pictures of both the horizontal and the vertical surfaces examined. We obtained an average reflectivity of the wall equal to 0.31 and, consequently, an average absorptivity of 0.69. For the porphyry flooring, we get a value of 0.23 for the average reflectivity and 0.77 for the absorptivity.

Table 3. 8. Radiative properties of the horizontal/vertical surfaces tested; blue plaster building envelope; 01/09/2020.

Horizontal/vertical surface	Image of the surface	ρ [-]	α [-]
Ground surface		0.23	0.77
Blue plaster building envelope		0.31	0.69

3.1.7 Street canyon

The measurements were carried out in the campus of the “Politecnico di Milano”, in Bovisa district, on 09/09/2020, from 10:40 to 17:15, in a road simulating a street canyon, in which students and professors passed through. The study of this type of environment aims to understand how the instrumentation behaves when solar radiation does not reach it directly.

Figure 3. 37 provides a view of the measurement site. On one side of the street there is a wall of a building with a porcelain stoneware envelope, while, on the other side, a grate covered with leaves and flowers separates the road and a little grassy area. The buildings acted as a barrier to solar radiation, leaving the instrumentation in shadow.



Figure 3. 37. Street canyon, Bovisa district, Milan.

Figure 3. 38 shows the trend of the MRT calculated by using black globe (red line), grey globe (purple line) and net radiometers (yellow line). The results obtained seem to confirm what was observed in Section 3.1.5 Green rooftop for night measurements: with the instrumentation totally in the shade, the MRT values obtained with the different instruments at our disposal are very similar to each other, with an average difference of 1.76°C between MRT_{Black} and $MRT_{Rad1+2+3}$ and 2.24 °C between $MRT_{Rad1+2+3}$ and MRT_{Grey} . In particular, the mean values obtained were 33.80 °C for the net radiometers, 35.56 °C for the black globe and 31.56 °C for the grey globe. Although with a small difference, it is once again confirmed that the black globe tends to overestimate the MRT, while the grey globe underestimates it. These results evidence that, in absence of direct solar radiation on the instrumentation, the grey globe is less suitable than the black one to approximate the reference values.

In Figure 3. 39 it is possible to see that the single radiometer, with an average MRT_{Rad1} of 33.89 °C, is capable to provide an accurate result.

All the UTCI curves in Figure 3. 40 fall into the “Moderate heat stress” category until 17:00; after that time, the values present a rapid increase, since the sunlight becomes able to reach the instrumentation directly.

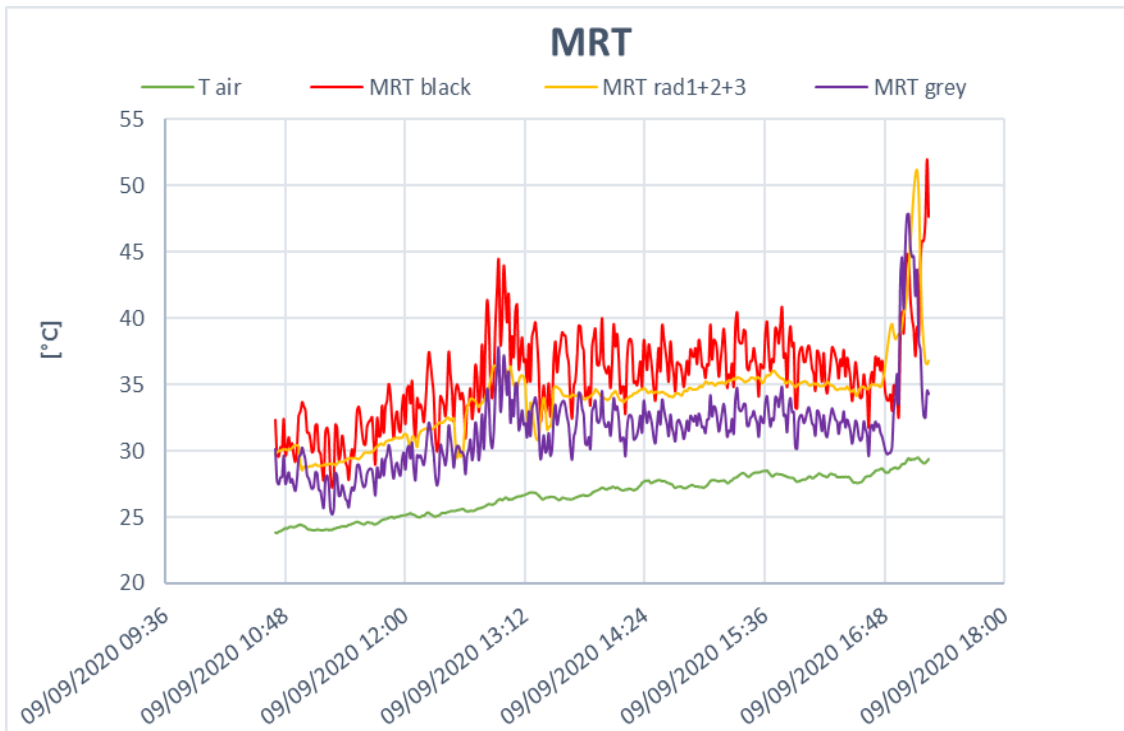


Figure 3. 38. MRT calculated with net radiometers and globe thermometers; 09/09/2020.

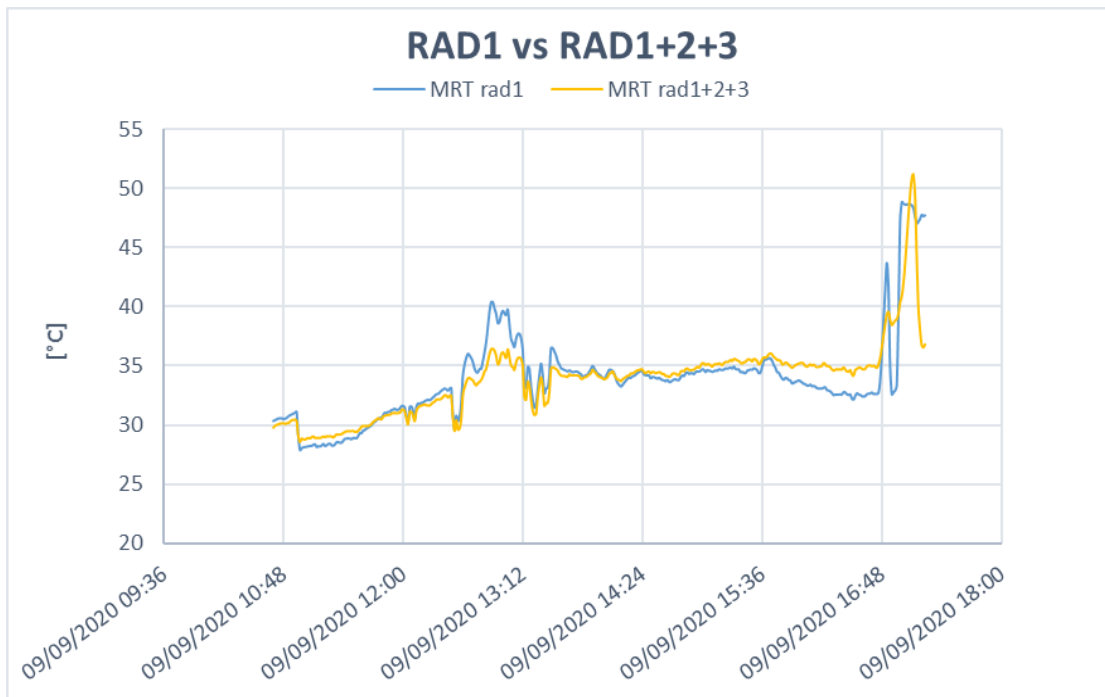


Figure 3. 39. MRT calculated with three radiometers and one radiometer measuring upward/downward direction; 09/09/2020.

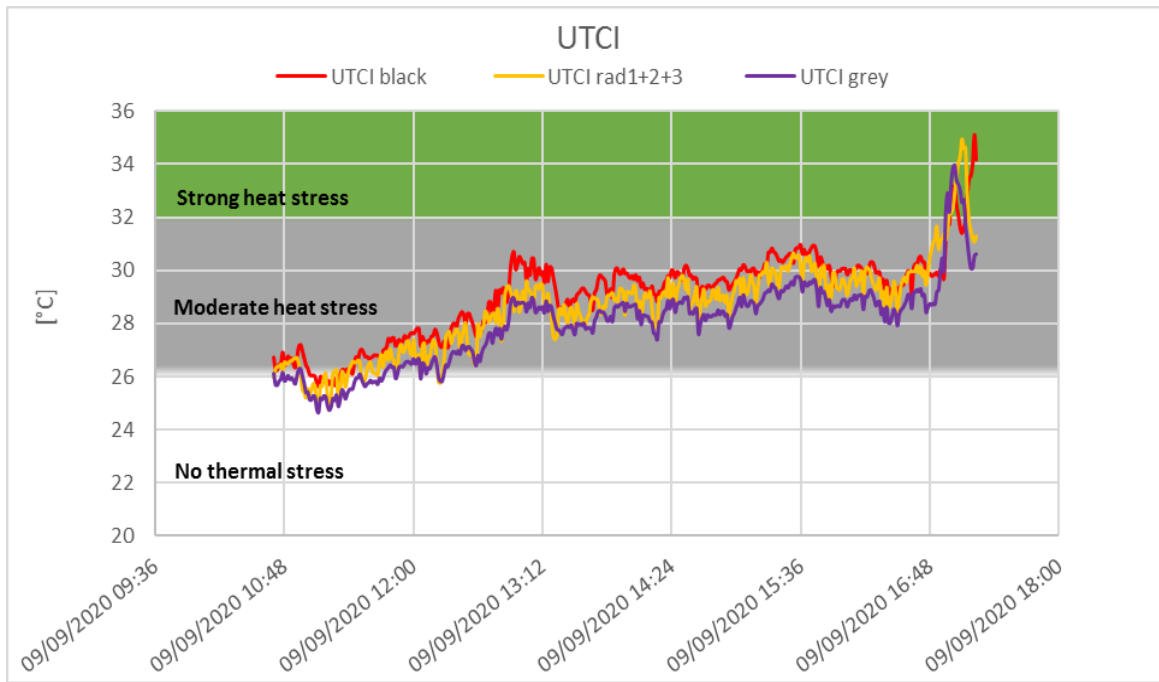

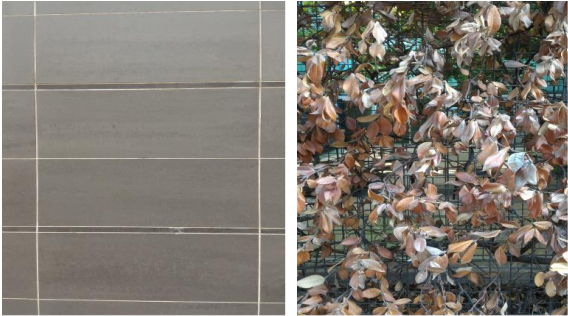


Figure 3. 40. UTCI calculated with net radiometers and globe thermometers; 09/09/2020.

The radiative properties of the ground surface were reported in *Table 3. 9*, along with the pictures of the ground surface and the walls on both sides of the street. The average reflectivity of the ground was equal to 0.22 and, consequently, the average absorptivity was equal to 0.78. The distance greater than 1 m between the instrumentation and the walls did not allow to calculate with an adequate approximation the radiation reflected by the vertical surfaces. It was therefore not possible to apply the methodology described in *Section 2.6 Methodology* for the calculation of reflectivity and absorptivity to these walls.

Table 3. 9. Radiative properties of the horizontal/vertical surfaces tested; street canyon; 09/09/2020.

Horizontal/vertical surface	Image of the surface	ρ [-]	α [-]
Ground surface		0.22	0.78
Walls on the two side of the street			

3.1.8 Green wall

This section deals with two measurement campaigns both taking place in the proximity of green walls. The purpose is to understand how the radiative properties of the leaves covering the wall could affect the outdoor thermal comfort in the surroundings, in terms of MRT and UTCI.

Section 3.1.8.1 Green Wall in Via G. La Masa, Milan and Section 3.1.8.2 Green Wall in Via Bovisasca, Milan will describe the two campaigns individually.

3.1.8.1 Green Wall in Via G. La Masa, Milan

The first analysis was carried out in Via G. La Masa, in Milan, on 17/09/2020 from 11:10 to 17:15. The measurements were carried out near a grate covered by a dense climbing plant, which covered it entirely. The branches reach up to the porphyry pavement. Figure 3. 41 provides a view of the measurement environment.



Figure 3. 41. Green wall, Via G. La Masa, Milan.

In Figure 3. 42 it is possible to see the trend of the MRT calculated by using black globe (red line), grey globe (purple line) and net radiometers (yellow line). The figure shows once again that the black globe overestimates the MRT in the hours of greatest solar height, while the grey globe underestimates it. In particular, the black globe provided an average MRT_{Black} equal to 40.85 °C, with a minimum value 29.23 °C (recorded at 17:15) and a maximum of 67.41 °C (recorded at 11:22). The net radiometer trend shows a maximum value of 55.69 °C at 11:30 and a minimum value of 29.28 °C at the end of the measurement campaign, at 17:15; the average $MRT_{Rad1+2+3}$ is equal to 38.99 °C, 1.86 °C lower than the average MRT_{Black} . A lower average MRT was recorded by the grey globe, with a value of 36.67 °C. Between 12:30 and 13, the curve of the black globe presents a different trend compared to that of the black globe and net radiometers. The latter in fact experiences a sharp sudden drop, while the MRT_{Grey} remains approximately constant. This is due to the fact that in that period of time the black globe and two net radiometers found themselves in the shadow due to the passage of clouds, while the grey globe remained exposed to the direct solar radiation and only for a very short period of time was found in the shade.

Figure 3. 43 instead shows the comparison between $MRT_{Rad1+2+3}$ and MRT_{Rad1} . The latter shows a peak value of 60.35 °C, a minimum of 26.03 °C and an average value equal to 36.52 °C, lower than the average $MRT_{Rad1+2+3}$ (38.99 °C) and very similar to the average MRT_{Grey} (36.67 °C).

All the UTCI curves in Figure 3. 44 fall into the “Strong heat stress” category until 14:00. After this time, the instrumentation was in shadow, facing a decrease in the calculated MRT and, consequently, in the UTCI, which from here on will fall into the “Moderate heat stress” category.

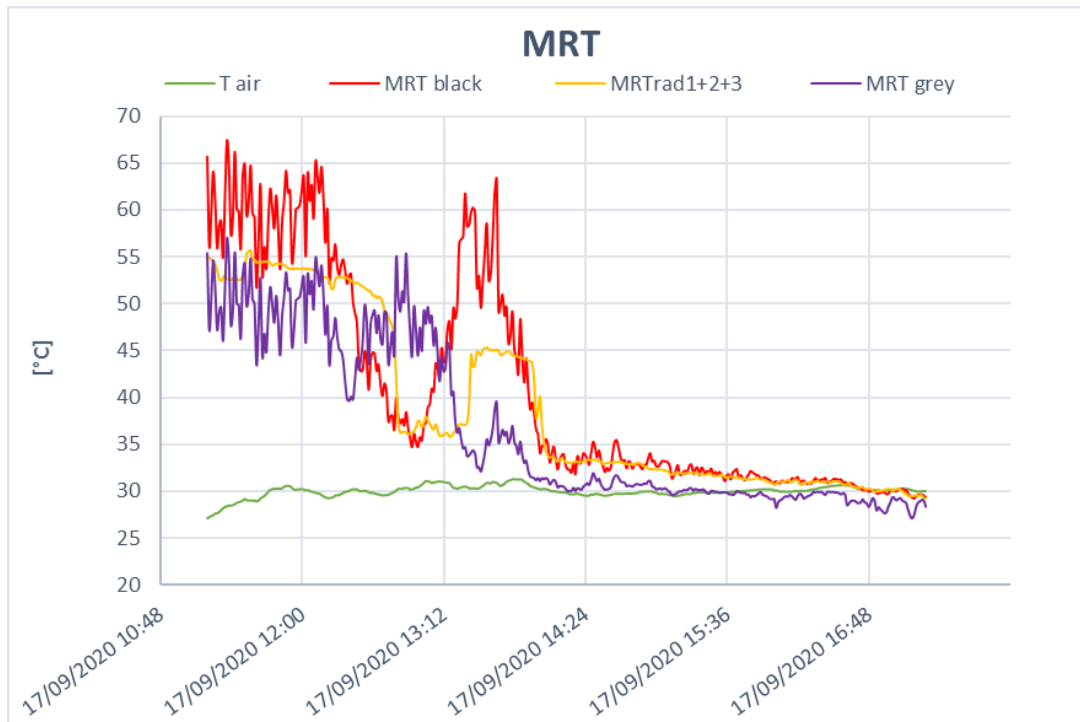


Figure 3. 42. MRT calculated with net radiometers and globe thermometers; 17/09/2020.

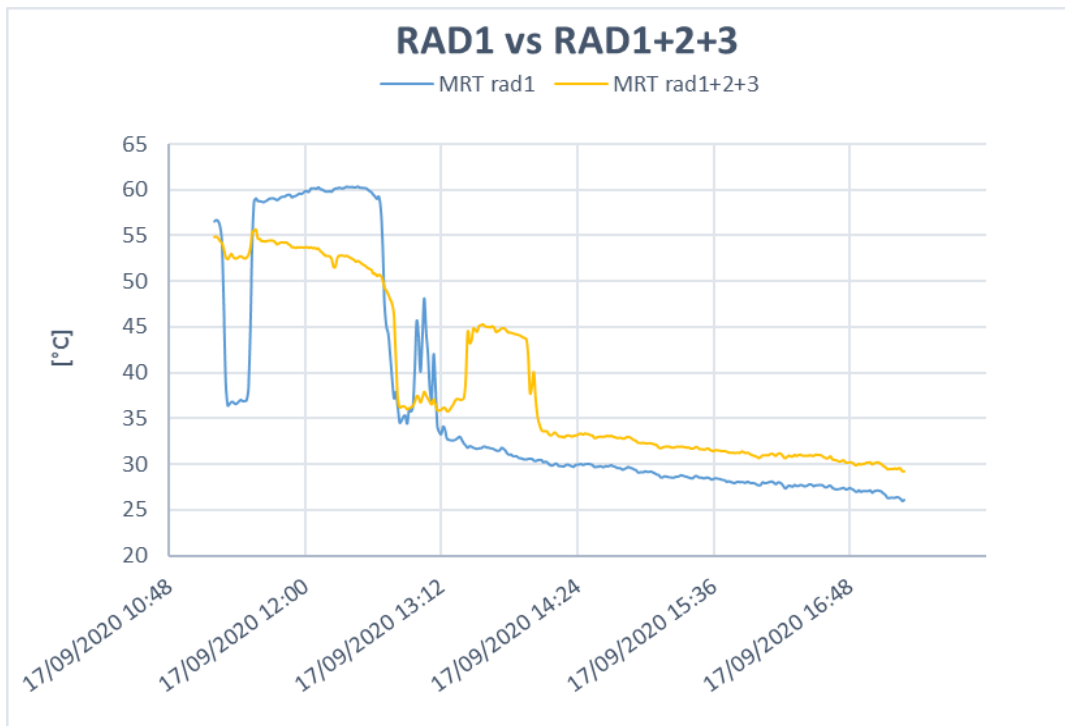


Figure 3. 43. MRT calculated with three radiometers and one radiometer measuring upward/downward direction; 17/09/2020.

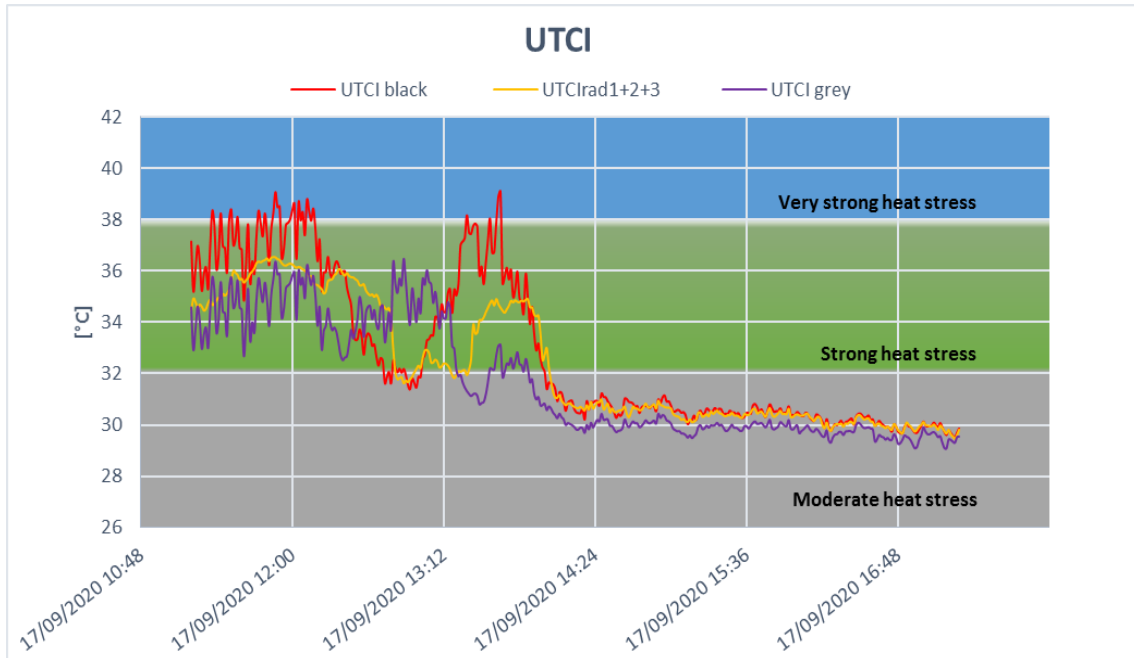




Figure 3. 44. UTCI calculated with net radiometers and globe thermometers; 17/09/2020.

Table 3. 10 shows the radiative properties of the surface tested. We observed an average reflectivity of the green wall tested of 0.28 and an average absorptivity of 0.72. The results are consistent with the typical values reported in literature, between 0.20 and 0.30. For the porphyry pavement, we obtained an average reflectivity equal to 0.20 and an average absorptivity of 0.80.

Table 3. 10. Radiative properties of the horizontal/vertical surfaces tested; green wall; 17/09/2020.

Horizontal/vertical surface	Image of the surface	ρ [-]	α [-]
Ground surface		0.20	0.80
Green wall		0.28	0.72

3.1.8.2 Green Wall in Via Bovisasca, Milan

The second measurement campaign carried out near a green wall took place in Via Bovisasca, in Milan. The survey lasted from 10:10 to 17:45 on 06/10/2020. The examined wall is a white plaster wall thickly covered with leaves, as shown in *Figure 3. 45*. During the measurements, the instrumentation was in shade, since the surrounding buildings acted as obstacles to the direct solar radiation. This leads to irradiation conditions similar to what has been analysed in *Section 3.1.7 Street canyon*.



Figure 3. 45. Green wall, Via Bovisasca, Milan.

Figure 3. 46 shows the trend of the MRT calculated by using black globe (red line), grey globe (purple line) and net radiometers (yellow line). The figure confirms that in case of totally or partially shaded instrumentation, the difference between the MRT calculated by using different instruments is strongly reduced if compared to open field measurements. Furthermore, with the instrumentation in shade, the effect on the MRT of the solar height variation during the day vanishes and the results provided by the globes show almost the same deviation from the net radiometers values during the whole duration of the campaign. The average MRT values obtained are equal to 21.20 °C by using net radiometers, 21.77 °C with black globe and 19.18 °C with grey globe. Although with a very small difference between the results provided by the different instruments, it is still confirmed that the black globe tends to overestimate the MRT, while the grey globe to underestimate it.

According to *Figure 3. 47*, the difference between $MRT_{Rad1+2+3}$ and MRT_{Rad1} is reduced too: the average MRT value provided by the single net radiometer is equal to 21.69 °C, 0.49 °C higher than the average $MRT_{Rad1+2+3}$.

Consistently with the results obtained in terms of MRT, also the UTCI curves in *Figure 3. 48* are close to each other. The average UTCI values are 19.27 °C for net radiometers, 19.46 °C for black globe and 18.69 °C for grey globe. All the curves belong to the “No heat stress” category for the whole duration of the survey.

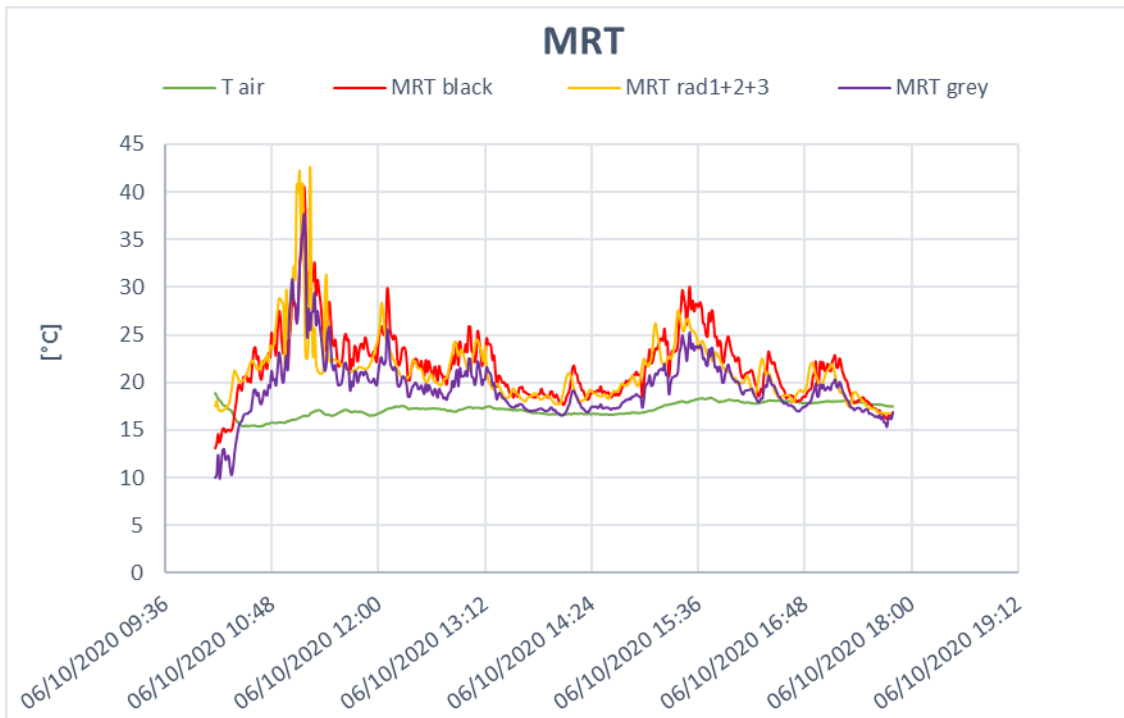


Figure 3. 46. MRT calculated with net radiometers and globe thermometers; 06/10/2020.

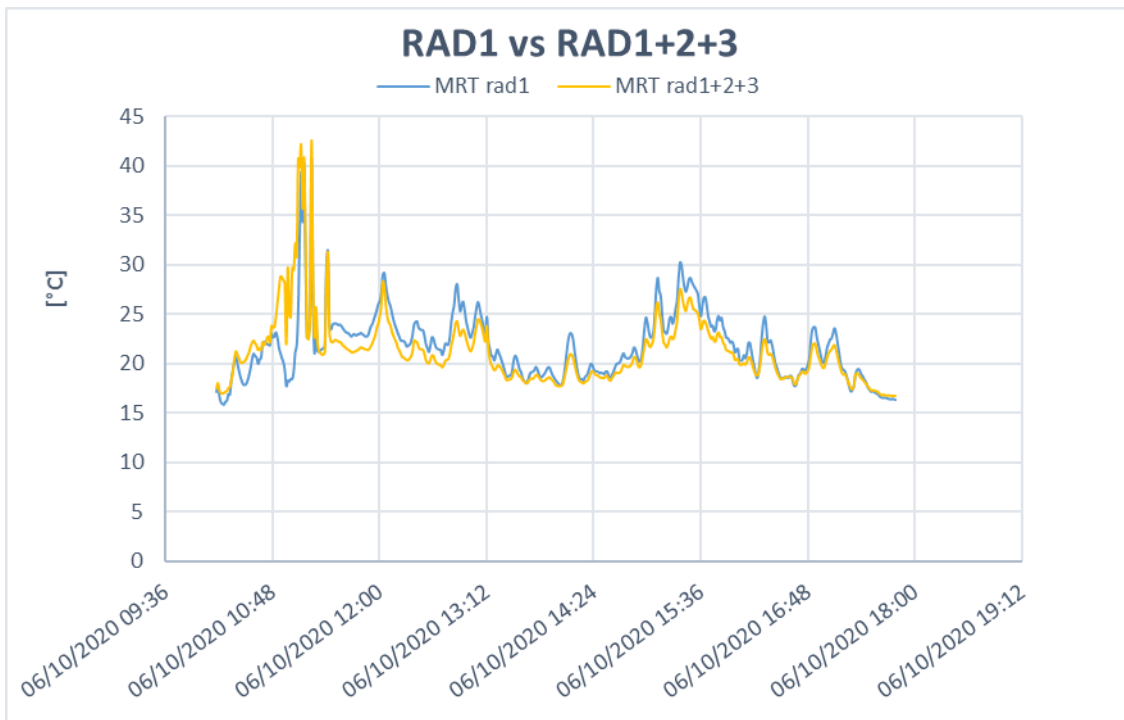


Figure 3. 47. MRT calculated with three radiometers and one radiometer measuring upward/downward direction; 06/10/2020.

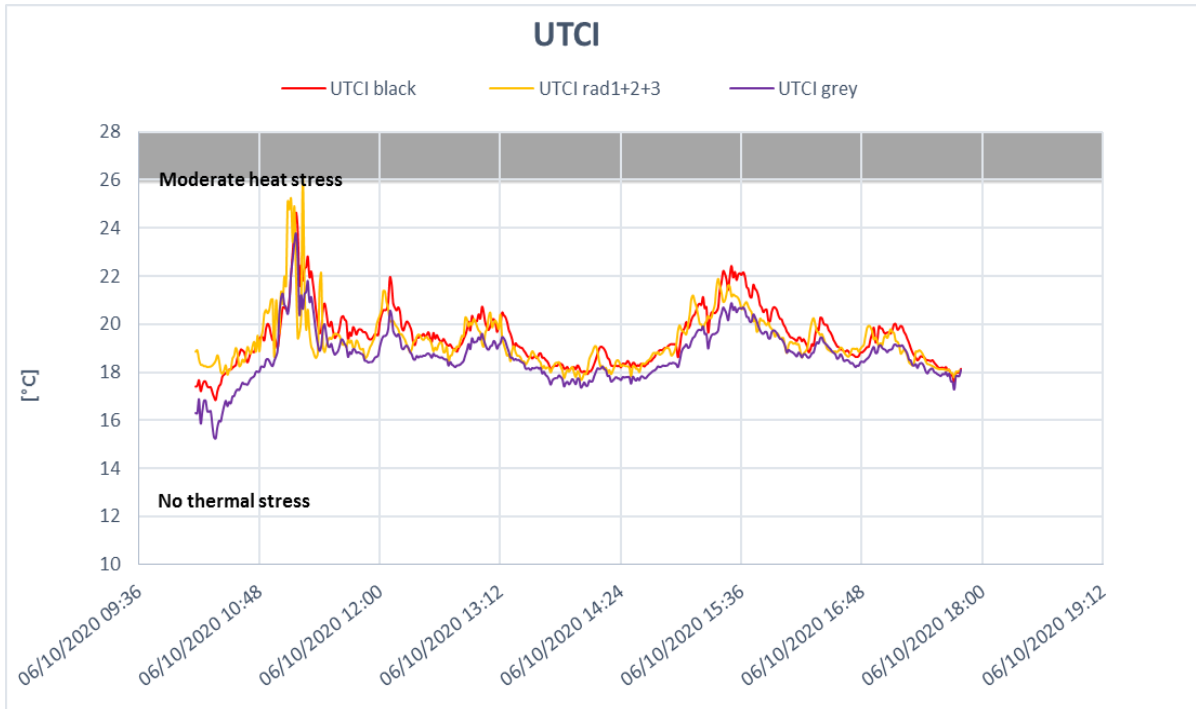




Figure 3. 48. UTCI calculated with net radiometers and globe thermometers; 06/10/2020.

As for previous sections, the radiative properties of both the wall and the ground surface were evaluated. According to *Table 3. 11* we obtained an average reflectivity value of the green wall equal to 0.34 (and therefore an average absorptivity of 0.66). For the flooring, we calculated a value of 0.13 for the reflectivity and 0.87 for the absorptivity.

Table 3. 11. Radiative properties of the horizontal/vertical surfaces tested; street canyon; 06/10/2020.

Horizontal/vertical surface	Image of the surface	ρ [-]	α [-]
Ground surface		0.13	0.87
Green wall		0.34	0.66

3.2 Summary of results, mean and peak values

The purpose of this section is to provide a summary of the results observed in *Section 3.1 Mean Radiant Temperature and UTCI assessment*.

Table 3. 12 provides, for each experimental campaign, the results in terms of MRT, including maximum, minimum and mean values. The direct exposure to solar radiation and the time interval in which the experimental campaigns were carried out are also present in the table since they influenced the results obtained. According to the table, the difference between the average MRT values obtained with the different instruments (i.e. three net radiometer and black/grey globe thermometer) increases when the instrumentation is directly exposed to the sun and in the central hours of the day, as shown in the figures of the previous paragraphs.

Thanks to the table it is also possible to observe how each instrument behaves differently according to the type of environment in which the measurements were carried out. We can see that the results obtained by means of the black globe are always greater, except for the night measurements, of $MRT_{Rad1+2+3}$, taken as a reference. In particular, the $MRT_{Black} - MRT_{Rad1+2+3}$ difference increases considerably in open field, where the average difference is equal to 15.56 °C for the measurements made in the Cascina Merlata park. A smaller deviation from the reference values is instead found in the measurements made near vertical walls; the average differences $MRT_{Black} - MRT_{Rad1+2+3}$ were recorded equal to 13.59 °C near the building with a light plaster envelope, 6.03 °C near the porcelain stoneware wall, 4.45 °C near the blue plaster building and 1.86 °C near the green wall in Via G. La Masa (the second green wall is less significant in this kind of comparison since the measurements were carried out in the absence of direct solar radiation on the instrumentation).

The single radiometer measuring the upward/downward direction, as the black globe thermometer, overestimates the MRT during the hours of maximum solar height, while it slightly underestimates the reference MRT values during late afternoon and night measurement. However, in the open field, the $MRT_{Rad1} - MRT_{Rad1+2+3}$ difference is lower than $MRT_{Black} - MRT_{Rad1+2+3}$, while an opposite trend is found in measurements made in street canyons or near the vertical walls tested. During the measurements carried out in the park in Cascina Merlata, MRT_{Rad1} is 4.47 °C lower than MRT_{Black} and a similar behaviour is found on 27/08/2020, during the survey on the green rooftop, where the single radiometer allowed to obtain an average MRT value which was 4.79 °C closer -with respect to MRT_{Black} - to the reference values. On the contrary, for the two measurements carried out near the building with porcelain stoneware envelope and near the blue plaster wall values we obtained average MRT_{Rad1} values equal to 75.99 °C (on 27/07/2020), 66.33 °C (on 18/09/2020) and 61.94 °C (on 01/09/2020), respectively 5.8 °C, 0.47 °C and 2.96 °C higher than the corresponding MRT_{Black} values. This behaviour is not found in the two measurements carried out near the green walls. However, it should be emphasized that, as observed in *Section 3.1.8 Green wall* in both these measurements, the different exposure of the individual instruments to the direct solar radiation influenced the calculation of the parameters of interest.

The view factors adopted in the calculation of MRT using net radiometers certainly play an important role in these experienced differences and *Section 4.3 Influence of view factors in the evaluation of MRT by using the six-directional method* will try to investigate this topic further.

Differently from what observed for the single radiometer and the black globe, the grey globe thermometer tends to underestimate the MRT if compared to the reference $MRT_{Rad1+2+3}$. During the measurements in the open field carried out on 27/08/2020 on the green roof, an average MRT_{Grey} of 53.36 °C was recorded, corresponding to a $MRT_{Grey} - MRT_{Rad1+2+3}$ difference -in absolute value- equal to 1.6 °C, lower than the corresponding $MRT_{Black} - MRT_{Rad1+2+3}$ of 7.7 °C. Although opposite in sign, the $MRT_{Grey} - MRT_{Rad1+2+3}$ difference results more similar to the $MRT_{Black} - MRT_{Rad1+2+3}$ difference as the total amount of direct radiation on the instrumentation decreases. On 01/09 the mean difference $MRT_{Grey} - MRT_{Rad1+2+3}$ was found to be, in absolute value, equal to 5.82 °C, while the average $MRT_{Black} - MRT_{Rad1+2+3}$ difference was 4.45 °C; on 09/09, during the measurement campaign in the street canyon, the grey globe provided an average value of MRT 2.24 °C lower than the reference value, while MRT_{Black} was 1.76 °C higher. In these last two cases the black globe gave results more similar to the reference $MRT_{Rad1+2+3}$ with respect to the MRT_{Grey} , even if the $MRT_{Grey} - MRT_{Rad1+2+3}$ difference was still minimal.

Finally, by comparing the minimum and maximum values obtained by the individual instruments in the various measurements made, it is possible to note the greater uniformity of the results provided by the three net radiometers compared to the other instruments adopted. In fact, *Table 3. 12* evidences that, for each measurement, the solution with the three radiometers presents the lowest maximum value and the higher minimum value: this allows to have a narrower range of values, less fluctuating than the other approaches used. On the contrary, the other instruments seem to be more susceptible to sudden changes of the external variables, which can lead to rapid increases/decreases in the measured parameters, before settling back to the actual values. This is particularly evident in the measurement campaigns carried out in July, while it gradually becomes less marked in September and October. Considering, for example, the measurements carried out on 20/07/2020 on the flat rooftop with a waterproofing membrane, it can be observed that the difference between the maximum and the minimum value of $MRT_{Rad1+2+3}$ is equal to 14.82 °C, while there is a difference of 36.23 °C and 40.18 °C between the maximum and minimum values of the MRT_{Black} and of MRT_{Rad1} , respectively. In September, instead, considering the measurements carried out on 17/09/2020 near a green wall, this difference is equal to 26.41 °C for $MRT_{Rad1+2+3}$, 34.32 °C for MRT_{Rad1} , 38.18 °C for MRT_{Black} and 29.96 °C for MRT_{Grey} .

In *Figure 3. 49* it is possible to see in a graphical representation the same results discussed for *Table 3. 12*. The figure shows the ratio between the average MRT values of each instrument and those obtained by means of the three net radiometers. This allows to observe, as already discussed, that the average values of MRT_{Black} and MRT_{Rad1} are higher - with the exception of the night measurements - than the average $MRT_{Rad1+2+3}$. On the contrary, the grey globe always tends to underestimate the MRT with respect to the reference values. Furthermore, it is evidenced that, as $MRT_{Rad1+2+3}$ increases, the individual differences $MRT_{Rad1} - MRT_{Rad1+2+3}$, $MRT_{Black} - MRT_{Rad1+2+3}$ and $MRT_{Grey} - MRT_{Rad1+2+3}$ increase in absolute value too.

Table 3. 12. Mean, maximum and minimum values of MRT for each measurement by using all the instruments at our disposal.

Building Envelope/ Environment	Measurement date and hour	Instrumentation directly exposed to the solar radiation	MRT (mean values) [°C]				MRT max [°C]				MRT min [°C]			
			RAD 1+2+3	RAD 1	Black globe	Grey globe	RAD 1+2+3	RAD 1	Black globe	Grey globe	RAD 1+2+3	RAD 1	Black globe	Grey globe
Flat rooftop with a waterproofing membrane	20/07/2020 12:00-19:30	yes	60,22	68,16	74,62		64,19	78,93	85,79		49,37	38,75	49,56	
	21/07/2020 9:00-15:40	yes	58,63	70,17	66,55		62,83	77,61	81,83		53,65	50,81	47,54	
Light plaster wall	23/07/2020 13:00-16:30	yes, until 16:00	65,41	76,28	79,00		72,66	89,16	108,28		41,66	37,36	41,47	
Porcelain stoneware Facade Cladding	27/07/2020 12:00-16:30	yes	64,16	75,99	70,19		72,41	91,20	97,59		45,54	47,31	43,93	
	18/09/2020 11:10-17:15	yes	63,38	66,33	65,86	56,38	72,01	78,50	88,07	76,60	38,24	35,55	35,69	33,16
Park	28/07/2020 11:50-16:30	yes	60,61	71,70	76,17		65,96	79,74	96,12		49,69	54,53	57,51	
Green rooftop	26/08/2020 day 15:20-21:00	yes, until sunset (~ 18:00)	41,65	40,07	40,74		71,90	78,40	86,57		24,11	21,04	21,69	
	26-27/08/2020 night 21:00-8:00	no	21,66	18,73	20,77	20,27	38,82	29,06	41,43	33,48	18,09	14,73	15,20	14,72
	27/08/2020 day 8:00-17:15	yes	54,96	57,87	62,66	53,36	68,83	79,00	88,14	75,67	27,19	23,57	31,32	26,64
Blue plaster wall	01/09/2020 11:30-17:10	yes	54,53	61,94	58,98	48,71	72,55	87,64	91,20	76,32	27,84	26,49	27,16	25,19
Street Canyon	09/09/2020 10:40-17:15	no, until 16:30	33,80	33,89	35,56	31,56	51,18	48,83	51,97	47,81	28,52	27,91	27,25	25,24
Green wall	17/09/2020 11:10-17:15	yes	38,99	36,52	40,85	36,67	55,69	60,35	67,41	57,03	29,28	26,03	29,23	27,07
	06/10/2020 10:10-17:45	no	21,20	21,69	21,77	19,48	42,60	40,71	40,50	37,57	16,67	15,79	13,15	9,89

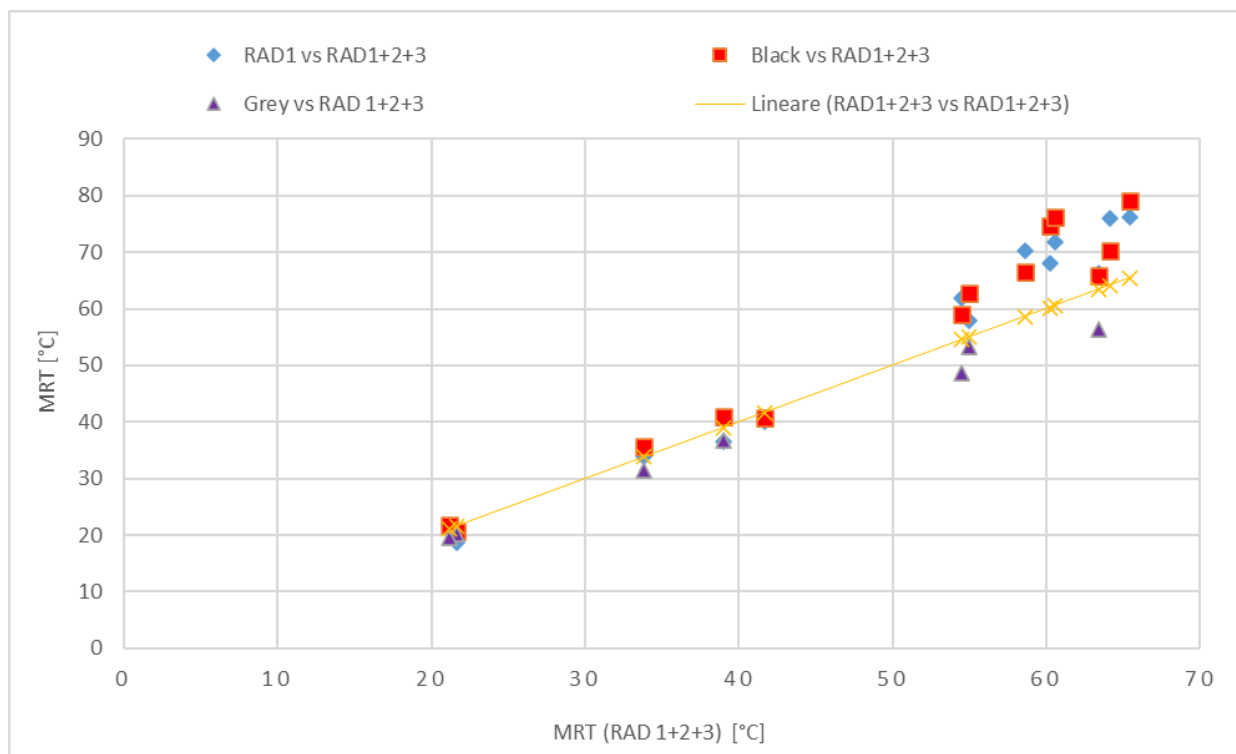


Figure 3. 49. MRT mean values for each instrument in relation to the MRT obtained by using three net radiometers.



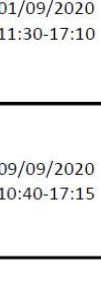
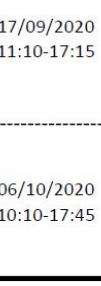

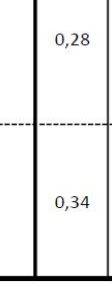

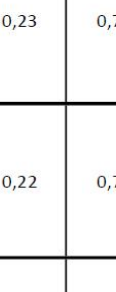








Similar to what observed in *Table 3. 12* for MRT, *Table 3. 13* shows the maximum, minimum and average values of UTCI obtained in each measurement campaign. The strong relationship between MRT and UTCI leads us to the same conclusions discussed above: the UTCI obtained through the data provided by the black globe will be higher - especially in the hours of greatest solar height - compared to the UTCI values calculated starting from $MRT_{Rad1+2+3}$, while the opposite trend is found for the grey globe. A correlation study between the UTCI and the parameters used in its calculation will be performed in *Section 4.1 Outdoor thermal comfort and thermal perception in different environments and meteorological conditions*.

In this sense, it is appropriate to start observing how the calculated UTCI values can be influenced by the radiative properties of the measurement environment. *Table 3. 14* shows the images of the surfaces tested in each survey, as well as their radiative properties. It can be seen that the highest UTCI values are found in the presence of ground surfaces with a high reflectivity. In particular, the three highest values of mean UTCI calculated with the three radiometers (40.95 °C, 40.87 °C and 39.14 °C) are found in the presence of horizontal surfaces with a reflectivity of 0.31 (corresponding to the UTCI of 40.95 °C) and 0.24 (in measurements made near the porcelain stoneware envelope, where we obtained UTCI of 40.87 °C and 39.14 °C). It is also noted that the average UTCI value of 40.95 °C occurs in correspondence with the light plaster wall, having the highest reflectivity (equal to 0.48) among the vertical surfaces examined. The wall with the second highest reflectivity is instead the green wall tested on 06/10, in which, nevertheless, we found the lowest UTCI value (19.27 °C). However, it should be noted that this measurement campaign took place with the instrumentation completely in the shade and on the day with the lowest T_{air} ; these factors have certainly contributed to greatly reduce the MRT and, consequently, the UTCI. From a first glance at the results it seems therefore that the meteorological conditions and the quantity of direct radiation impacting on the instrumentation have a greater influence on the comfort index than the radiative properties of the materials characterizing the environment. In order to analyse this aspect further, the correlation between UTCI and reflectivity will be studied in *Section 4.1 Outdoor thermal comfort and thermal perception in different environments and meteorological conditions*.

Table 3. 13. Mean, maximum and minimum values of UTCI for each survey by using all the instruments at our disposal.

Building Envelope/ Environment	Measurement date and hour	Instrumentation directly exposed to the solar radiation	UTCI (mean values) [°C]				UTCI max [°C]				UTCI min [°C]			
			RAD 1+2+3	RAD 1	Black globe	Grey globe	RAD 1+2+3	RAD 1	Black globe	Grey globe	RAD 1+2+3	RAD 1	Black globe	Grey globe
Flat rooftop with a waterproofing membrane	20/07/2020 12:00-19:30	yes	36,76	38,74	40,36		38,81	41,47	43,01		34,94	32,19	34,99	
	21/07/2020 9:00-15:40	yes	36,06	38,93	38,03		38,33	42,20	42,26		32,69	32,53	31,74	
Light plaster wall	23/07/2020 13:00-16:30	yes, until 16:00	40,95	43,73	44,42		45,11	49,30	51,03		33,85	32,95	34,93	
Porcelain stoneware Facade Cladding	27/07/2020 12:00-16:30	yes	40,87	43,89	42,40		43,74	48,62	49,39		35,25	35,71	34,73	
	18/09/2020 11:10-17:15	yes	39,14	39,87	39,76	37,37	42,35	43,79	45,49	42,01	31,31	30,61	30,92	30,23
Park	28/07/2020 11:50-16:30	yes	38,77	41,47	42,58		40,65	43,53	45,82		35,11	36,28	38,06	
Green rooftop	26/08/2020 day 15:20-21:00	yes, until sunset (~ 18:00)	33,54	33,11	33,31		42,75	44,11	45,40		27,13	26,30	26,43	
	26-27/08/2020 night 21:00-8:00	no	24,75	23,89	24,50	24,35	29,26	26,53	29,58	27,42	22,29	21,24	21,29	21,14
	27/08/2020 day 8:00-17:15	yes	36,33	37,02	38,23	35,91	40,94	43,55	46,21	43,00	25,87	24,84	27,16	25,83
Blue plaster wall	01/09/2020 11:30-17:10	yes	33,69	35,49	34,79	32,19	39,80	43,45	44,16	39,47	25,15	24,77	25,05	24,44
Street Canyon	09/09/2020 10:40-17:15	no, until 16:30	28,60	28,62	29,06	27,99	34,94	34,36	35,10	33,98	24,78	24,66	25,66	24,64
Green wall	17/09/2020 11:10-17:15	yes	32,30	31,63	32,77	31,70	36,52	37,93	39,09	36,46	29,47	28,57	29,50	29,10
	06/10/2020 10:10-17:45	no	19,27	19,43	19,46	18,69	26,04	25,47	24,67	23,76	17,66	17,05	16,83	15,26

Table 3. 14. Pictures of the measurement environments and radiative properties of the horizontal/vertical surfaces characterizing each environment.

Building Envelope/ Environment	Measurement date and hour	Radiative properties				Building envelope	Ground surface	UTCI (mean values) [°C]		
		ρ (wall)	α (wall)	ρ (ground)	α (ground)			RAD 1+2+3	Black globe	Grey globe
Flat rooftop with a waterproofing membrane	20/07/2020 12:00-19:30			0,11	0,89			36,76	40,36	
	21/07/2020 9:00-15:40							36,06	38,03	
Light plaster wall	23/07/2020 13:00-16:30	0,48	0,52	0,31	0,69			40,95	44,42	
Porcelain stoneware Facade Cladding	27/07/2020 12:00-16:30	0,30	0,70	0,24	0,76			40,87	42,40	
	18/09/2020 11:10-17:15	0,28	0,72	0,24	0,76			39,14	39,76	37,37
Park	28/07/2020 11:50-16:30			0,20	0,80			38,77	42,58	
Green rooftop	26/08/2020 day 15:20-21:00			0,22	0,78			33,54	33,31	
	26-27/08/2020 night 21:00-8:00							24,75	24,50	24,35
	27/08/2020 day 8:00-17:15							36,33	38,23	35,91
Blue plaster wall	01/09/2020 11:30-17:10	0,31	0,69	0,23	0,77			33,69	34,79	32,19
Street Canyon	09/09/2020 10:40-17:15			0,22	0,78			28,60	29,06	27,99
Green wall	17/09/2020 11:10-17:15	0,28	0,72	0,20	0,80			32,30	32,77	31,70
	06/10/2020 10:10-17:45	0,34	0,66	0,13	0,87			19,27	19,46	18,69

4. Discussions and further elaborations

This chapter provides a discussion of the results obtained in the experimental campaigns described in *Chapter 3. Experimental campaigns and results*.

The additional elaborations presented in this section aim at defining how the outdoor thermal comfort is influenced by the radiative properties of the surrounding environment and, at the same time, at investigating the main causes underlying the difference in results - in terms of MRT and UTCI - provided by the individual measuring instruments used.

Table 3. 12 and *Table 3. 13* had already shown some differences between the results obtained with the instruments at our disposal, in relation to the place, date, and time in which the measurements took place. Starting from what we have already seen, we will therefore try to investigate the influence of each variable involved.

4.1 Outdoor thermal comfort and thermal perception in different environments and meteorological conditions

This section deals with evaluating the outdoor thermal comfort and its relation with the meteorological parameters and the radiative properties of the surfaces surrounding the tested environment. This type of analysis starts from the calculation of the UTCI, obtained in each of the experimental campaigns described in *Chapter 3. Experimental campaigns and results*.

Table 4. 1 shows the maximum, minimum and average values of UTCI obtained through the solution with three net radiometers (reference results for our analysis). According to the table, the situations that present a more severe thermal discomfort, i.e. those having average values of UTCI falling into the category "Very strong heat stress" ($38\text{ °C} < \text{UTCI} < 46\text{ °C}$, according to *Table 3. 2*), are found for the measurements carried out in conditions of the total exposure of the instrumentation to the direct solar radiation and with an air temperature (which seems to be one of the most influential meteorological parameter on the thermal index) $T_{\text{air}} > 31\text{ °C}$. The strong and positive correlation between the UTCI and the T_{air} is shown in *Figure 4. 1*. Weaker correlations are instead found between the other two meteorological parameters involved in the UTCI equation: *Figure 4. 2* and *Figure 4. 3* respectively show the average values of UTCI as V_{air} and RH vary.

As previously observed from the measurements described in *Chapter 3. Experimental campaigns and results* and highlighted in *Table 4. 1*, the exposure of the instrument to the direct solar radiation proved to be one of the factors that most influenced the results obtained in terms of UTCI. We, therefore, tried to analyse the relation between the global radiation on the instrumentation and the chosen thermal comfort index.

Figure 4. 4 evidences, as expected, a strong correlation between the two variables. In fact, although there is no real direct proportionality between the UTCI values and the global radiation impacting the instrumentation, the values reported in *Table 4. 1* show that, for UTCI values falling within the "Very strong heat stress" category, we recorded global radiation values equal to or greater than 600 W/m^2 . Consistently, in correspondence to UTCI values lower than 30 °C , a global radiation lower than 140 W/m^2 has been recorded. The only exception is found in the two days of measurements on the rooftop with the waterproofing membrane: despite detecting high global radiation values (higher than 600 W/m^2), the UTCI is equal to 36 °C and therefore does not fall within the "Very strong heat stress" category. This can be explained by looking at the external air temperatures in those two days of measurements; the temperature was in fact lower than 30 °C and this confirms how much T_{air} is an important parameter in the evaluation of the UTCI. The combined effect of the impacting global radiation and of the external air temperature turns out to be fundamental for the determination of the thermal stress category.

Once the influence of the weather parameters on the UTCI has been discussed, the different radiative properties of the surfaces characterizing the different measurement environments have been studied, as well as their impact on the perceived thermal comfort sensation. According to *Table 4. 1* and *Figure 4. 5* (showing the relation between UTCI and ground reflectivity), the mean values of UTCI falling into the "Very strong heat stress" category are all belonging to measurements carried out in environments with the highest ground reflectivity values among those obtained. The only exception was found for the measurements carried out in Cascina Merlata park: even if the ground reflectivity value is one of the lowest among those

proposed, the corresponding UTCI value is higher than 38 °C. As already noted, whenever an attempt is made to define a correlation between the results -in terms of MRT and, consequently, UTCI- obtained and the variables involved, the data obtained in the open field assessments deviate from the common trend of this correlation.

It, therefore, seems increasingly necessary to evaluate the correctness of the view factors commonly adopted for the calculation of MRT using net radiometers in the open field, a topic that will be discussed in *Section 4.3 Influence of view factors in the evaluation of MRT by using the six-directional method*.

Figure 4. 6, on the other hand, is intended to show the correlation found between the average values of UTCI obtained and the radiative properties of the vertical surfaces examined. Unlike what was observed for the reflectivity of the flooring, in this case there is no direct proportionality between the two parameters in question. While it is true that the highest UTCI value (40.95 °C) occurs in correspondence with the highest reflectivity value (0.48), this behaviour is not found in the other measurements. Surely the different amount of radiation incident on the instrumentation and the different meteorological conditions contributed to make the comparison between the vertical surfaces tested more difficult. In fact, it is observed that the second highest reflectivity value (0.34) was calculated for a green wall, which was in shade for the entire duration of the measurements, contributing to greatly reduce the corresponding UTCI value (equal to 19.27 °C, the lowest value among those obtained). The UTCI value calculated on 27/07/2020, near the porcelain stoneware envelope, was found to be the second highest and equal to 40.87 °C. This surface had a reflectivity of 0.30, but it is reasonable to think that the high UTCI is given more than anything else by the very high T_{air} recorded (32.71 °C), especially in light of the correlation analysis between the latter and the thermal comfort index.

Table 4. 1. Mean, maximum and minimum values of UTCI obtained starting from the MRT results provided by the three net radiometers method.

Building Envelope/ Environment	Measurement date and hour	Radiative properties				Instrumentation directly exposed to the solar radiation	Meteorological variables (mean values)			Global Radiation (mean values) [W/m ²]	UTCI (RAD1+2+3) [°C]			
		ρ (wall)	α (wall)	ρ (ground)	α (ground)		T air [°C]	V air [m/s]	RH [%]		mean	max	min	
Flat rooftop with a waterproofing membrane	20/07/2020					yes			1,78	39,60	642,89	36,76	38,74	40,36
	12:00-19:30			0,11	0,89									
Light plaster wall	21/07/2020					yes			1,42	48,06	629,64	36,06	38,93	38,03
	9:00-15:40													
Porcelain stoneware	23/07/2020	0,48	0,52	0,31	0,69	yes, until 16:00			1,49	45,67	729,33	40,95	43,73	44,42
	13:00-16:30													
Facade Cladding	27/07/2020	0,30	0,70	0,24	0,76	yes			0,85	44,25	706,31	40,87	43,89	42,40
	12:00-16:30													
Park	18/09/2020	0,28	0,72	0,24	0,76	yes			0,77	39,69	599,68	39,14	39,87	39,76
	11:10-17:15													
Green rooftop	28/07/2020			0,20	0,80	yes			1,81	51,68	808,73	38,77	41,47	42,58
	11:50-16:30													
Green wall	26/08/2020 day					yes, until sunset (~ 18:00)			0,81	48,20	211,65	33,54	33,11	33,31
	15:20-21:00													
Blue plaster wall	26-27/08/2020 night 21:00-8:00			0,22	0,78	no			0,58	68,74	5,49	24,75	23,89	24,50
	27/08/2020 day 8:00-17:15					yes			1,07	57,06	486,32	36,33	37,02	38,23
Street Canyon	01/09/2020	0,31	0,69	0,23	0,77	yes			0,96	39,06	546,01	33,69	35,49	34,79
	11:30-17:10													
Green wall	09/09/2020			0,22	0,78	no, until 16:30			1,21	55,59	138,34	28,60	28,62	29,06
	10:40-17:15													
Green wall	17/09/2020	0,28	0,72	0,20	0,80	yes			0,62	44,84	255,35	32,30	31,63	32,77
	11:10-17:15													
Green wall	06/10/2020	0,34	0,66	0,13	0,87	no			0,41	66,86	103,04	19,27	19,43	19,46
	10:10-17:45													

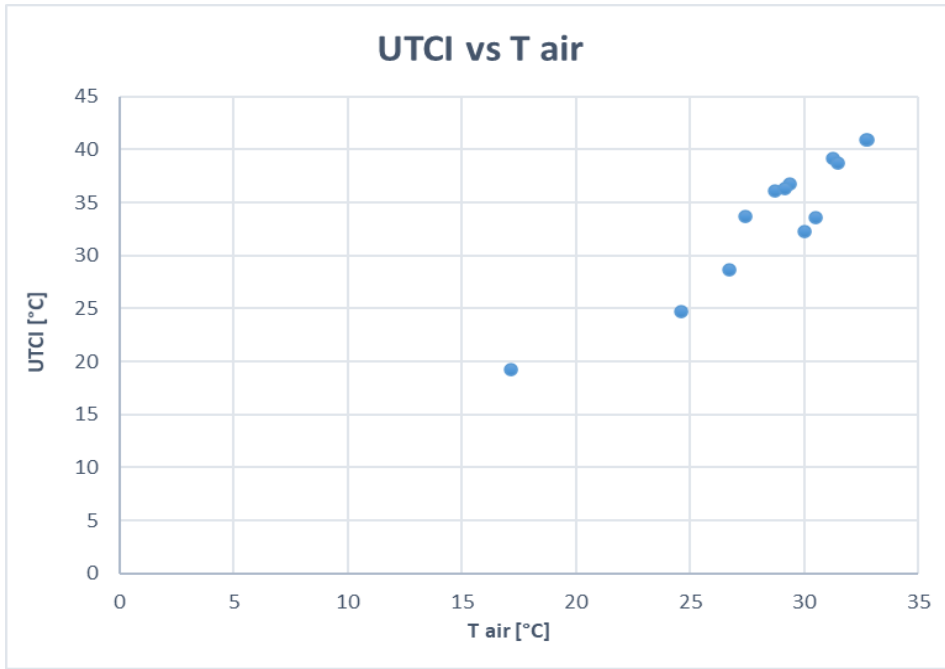


Figure 4. 1. UTCI vs T_{air} (mean values).

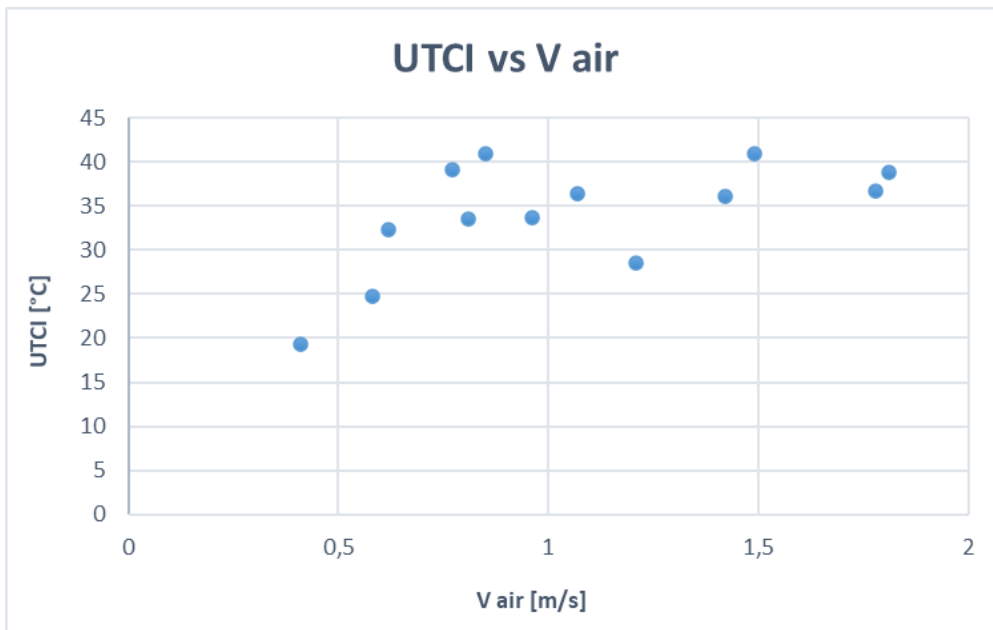


Figure 4. 2. UTCI vs V_{air} (mean values).

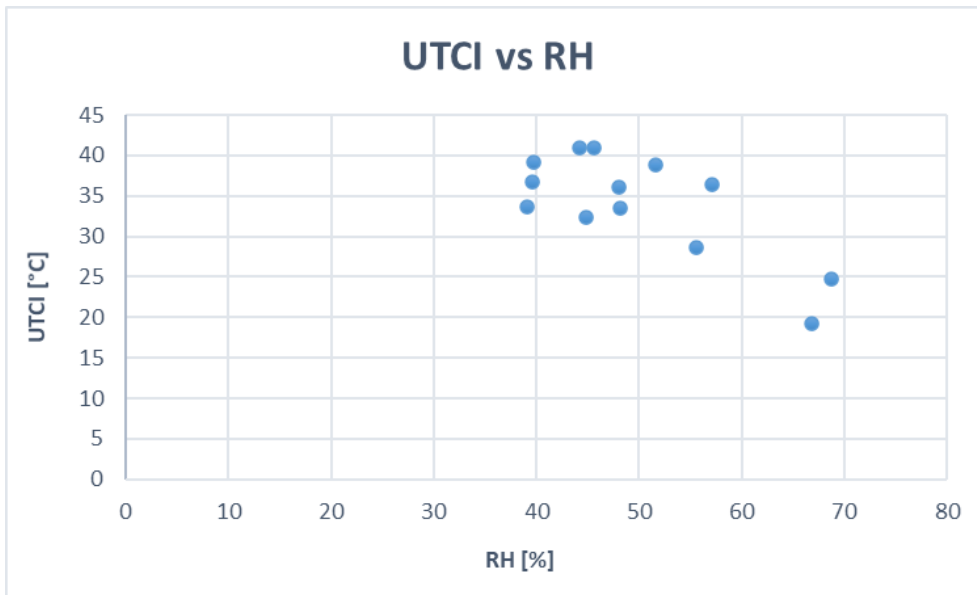


Figure 4. 3. UTCI vs RH (mean values).

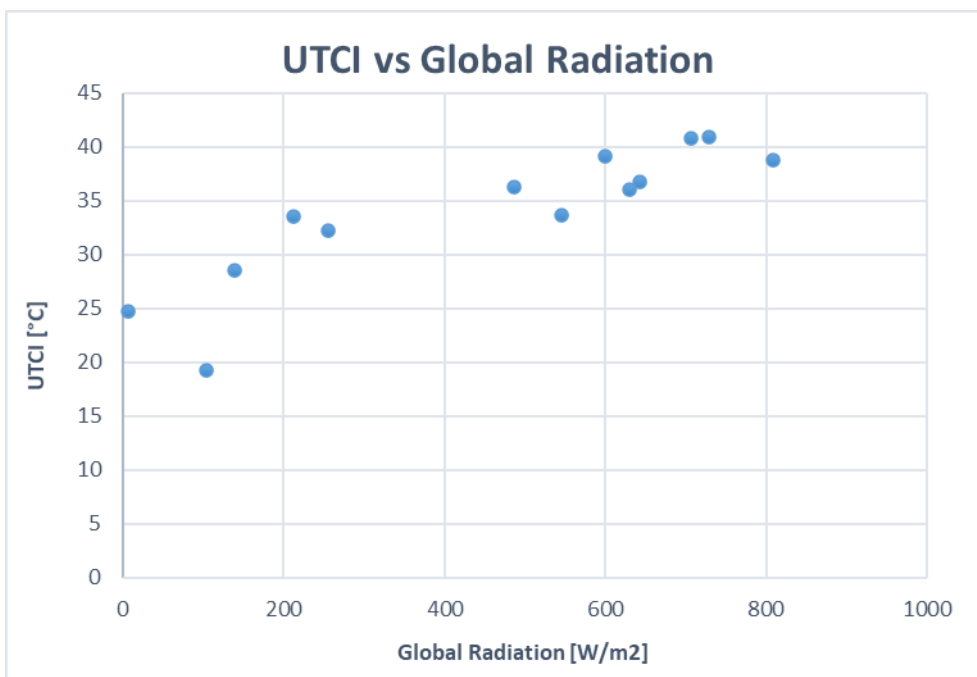


Figure 4. 4. UTCI vs Global radiation (mean values).

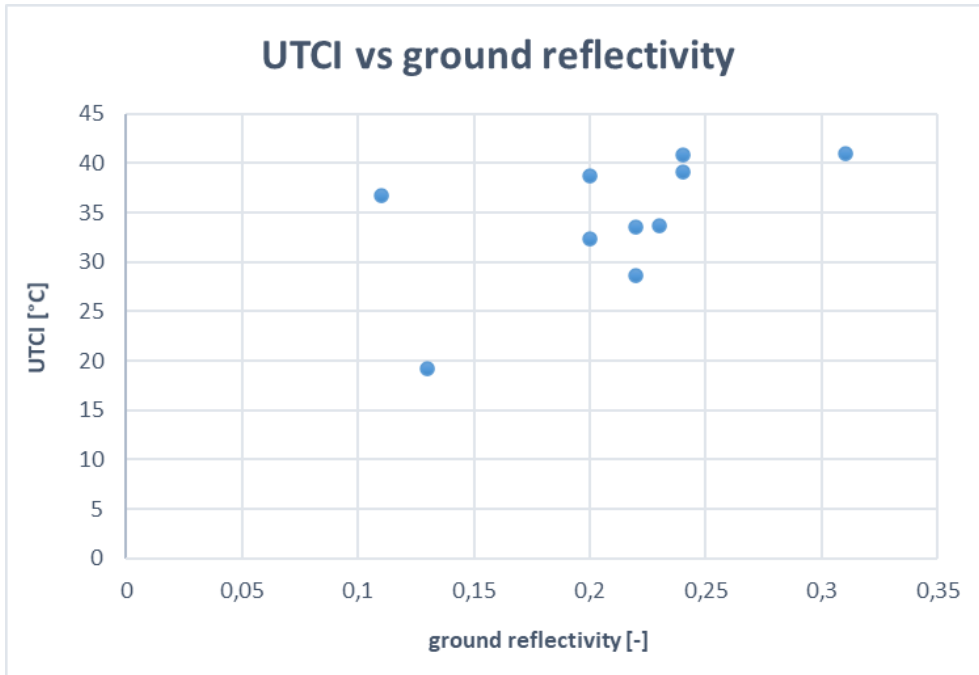


Figure 4. 5. UTCI vs ground reflectivity (mean values).

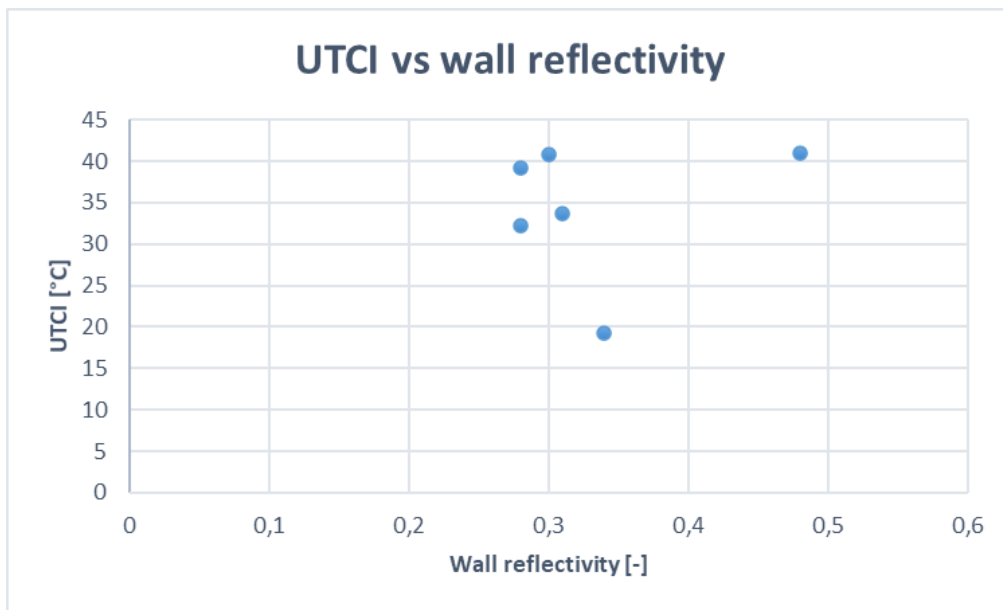


Figure 4. 6. UTCI vs wall reflectivity (mean values).

4.2 Three net radiometers vs Globe thermometers: causes of the different results

From the results reported in *Section 3.1 Mean Radiant Temperature and UTCI assessment*, we can see that the average MRT values calculated using a black globe thermometer are higher than those provided by the three net radiometers solution (regardless of the tested environment) when the analyses are made during the daily hours, while they are lower for measurements carried out during the early morning, late afternoon and night.

More specifically, *Figure 3. 2, Figure 3. 3, Figure 3. 9, Figure 3. 13, Figure 3. 20, Figure 3. 26, Figure 3. 34 and Figure 3. 42* show that the black globe tends to overestimate the MRT in the hours corresponding to a greater solar height (this is even more evident in open field assessment and in the months in which the solar height is higher), while it underestimates the MRT values in the hours in which the solar height decreases.

On the contrary, the analyses in *Section 3.1 Mean Radiant Temperature and UTCI assessment* show that the mean values of MRT and, therefore, of UTCI obtained by means of a grey globe thermometer are lower than those calculated thanks to the data provided by the three net radiometers: the difference between the results obtained with the two instruments oscillates in a range between 1.39 °C and 7.00 °C as regard MRT mean values, while between 0.40 °C and 1.77 °C as regards the UTCI mean values. A smaller difference -in magnitude- is thus observed compared to the $MRT_{Black} - MRT_{Rad1+2+3}$ difference, in particular in the hours corresponding to a greater solar height and when the instrumentation is entirely exposed to the direct solar radiation. This confirms what is reported in the literature (Standard 7726 1998; Ashrae Standard 2001; Johansson et al. 2014): the grey globe thermometer, absorbing less radiation than the black globe, is more suitable to model the outer surface of a clothed person in outdoor environments.

The difference in results between net radiometers and globe thermometers can be attributed to two main causes:

- The shape of the globe. The spherical shape of the globe thermometer is not suitable for evaluating the radiative loads acting on a standing person, which are instead considered in the three net radiometers solution: the globes consider in equal measure the radiative fluxes coming from any direction, while the view factors adopted in net radiometers calculations attribute greater weight to the horizontal radiative fluxes, as they impact on a greater surface of the human body (modelled as a parallelepiped). Finally, the variation of the solar height contributes to vary the relevance of the horizontal radiative fluxes compared to the vertical ones during the day and it is for this reason that the black globe thermometer goes from underestimating to overestimating the MRT as the height of the sun changes. The importance of the different weight attributed to radiative fluxes coming from different directions will be investigated in *Section 4.3 Influence of view factors in the evaluation of MRT by using the six-directional method*.
- The convective heat exchange coefficients commonly adopted in literature. As already noted in *Section 2.2.3 Mean Radiant Temperature calculation using globe thermometers*, several studies have adopted different coefficients, contributing to the increased difficulty in comparing assessments from different authors. Different coefficients, therefore, lead to different results in terms of MRT obtained by means of a globe thermometer (according to Equation (2. 10)) and therefore to more or less marked differences compared to the three radiometers solution. *Section 4.4 Influence of convective heat exchange coefficient in the evaluation of MRT by using the globe thermometers* will aim to analyse the results obtained through the use of different convective heat exchange coefficients, highlighting the criticalities of each.

4.3 Influence of view factors in the evaluation of MRT by using the six-directional method

In *Section 3.1 Mean Radiant Temperature and UTCI assessment*, the MRT measured using the three net radiometers was calculated according to Equation (2. 3), where the view factors adopted were equal to 0.06 for the upward and downward directions (radiometer indicated with the number 1 in *Figure 2. 1*) and 0.22 for the other four directions (radiometers 2 and 3). These factors are commonly used in literature to evaluate the radiative load acting on a standing person, ideally represented as a square base parallelepiped with a ratio $H/L = 3.5$.

However, Thorsson et al.'s study (Thorsson et al. 2007) pointed out that vertical and lateral radiative fluxes have a different relevance according to the measurement environment. In particular, lateral radiative fluxes gain more relevance when measurements are carried out in street canyons or, more generally, in areas where there is a limited SVF. On the other hand, in the open field, without any obstacle to the direct solar radiation, the vertical flows gain greater relevance. This calls into question if the view factors commonly used in MRT evaluation for the six-directional method can be considered universally valid or need to be adapted according to the measurement environment.

For this purpose, this section proposes a comparison between the results obtained in *Section 3.1 Mean Radiant Temperature and UTCI assessment* -adopting the "standing man" view factors- and the MRT values obtained by applying the so-called "spherical" view factors. In the latter case, the fluxes coming from the six directions are weighted equally, according to view factors of 0.167.

For this analysis, we deal with the measurements carried out in open fields, including roofs, parks, or any area without elements that could block the direct solar radiation, overshadowing the instrumentation. As noted in *Section 3.1 Mean Radiant Temperature and UTCI assessment*, in fact, the measurements in open field turned out to be those for which the $MRT_{Black} - MRT_{Rad1+2+3}$ difference was larger, even higher than the $MRT_{Rad1} - MRT_{Rad1+2+3}$ difference, which in the other measurement environments was always higher. The fact that the single radiometer measuring the vertical radiative fluxes is closer, in open field, to the reference values, also underlines how the fluxes in this direction gain importance in this type of measurement environment.

For this purpose, the current section includes the following analyses discussed in *Section 3.1 Mean Radiant Temperature and UTCI assessment*:

- Flat rooftop with a waterproofing membrane (*Section 3.1.1 Flat rooftop with a waterproofing membrane*).
- Park (*Section 3.1.4 Park*).
- Green rooftop (*Section 3.1.5 Green rooftop*).

Figure 4. 7 and *Figure 4. 8* show the MRT trend obtained using integral radiation measurements using both "standing man" ($MRT_{Rad1+2+3,standing\ man}$) and "spherical" view factors ($MRT_{Rad1+2+3,sphere}$), as well as using a single radiometer measuring upward and downward directions (MRT_{Rad1}) and black globe thermometer (MRT_{Black}) on the rooftop with the waterproofing membrane. Similarly, *Figure 4. 9* represents the trends of the same parameters in the Cascina Merlata park, while *Figure 4. 10* is related to the measurements on the green rooftop (considering only the diurnal measurements on 27/08/2020, since night measurements are not explanatory in this kind of analysis).

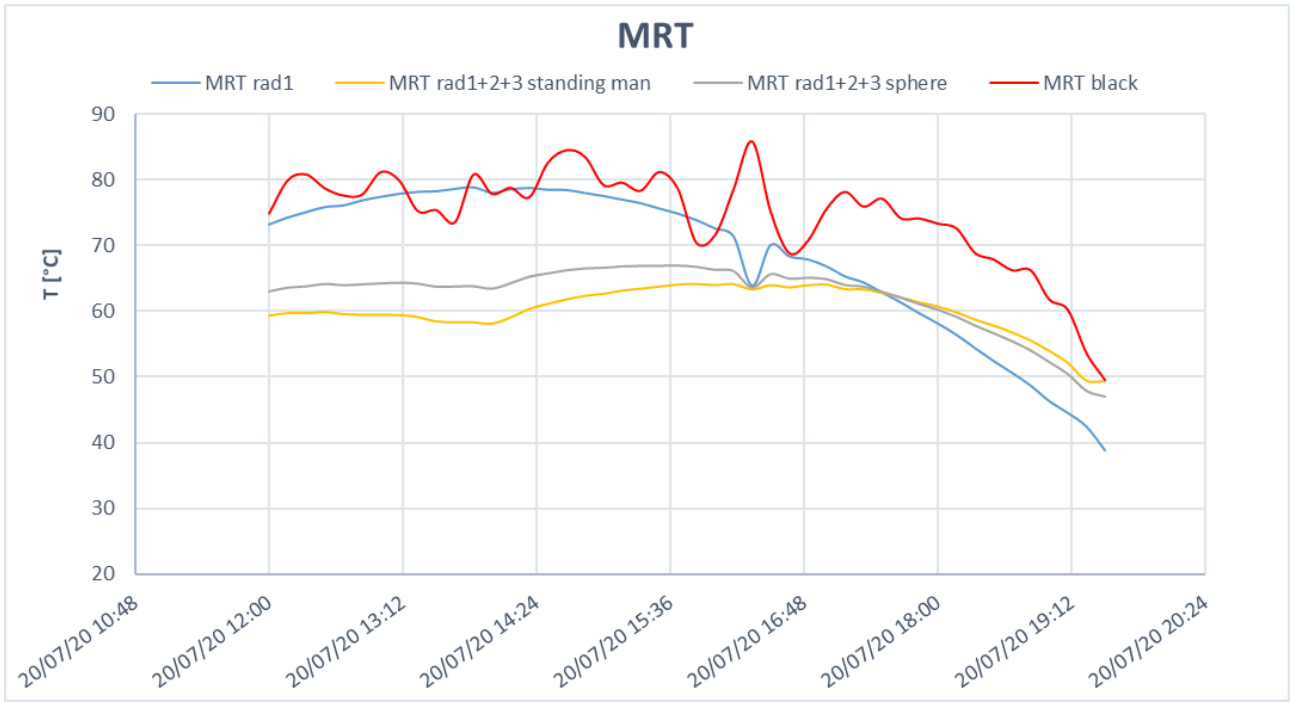


Figure 4. 7. Comparison between standing man and spherical view factors; flat rooftop with a waterproofing membrane, 20/07/2020.

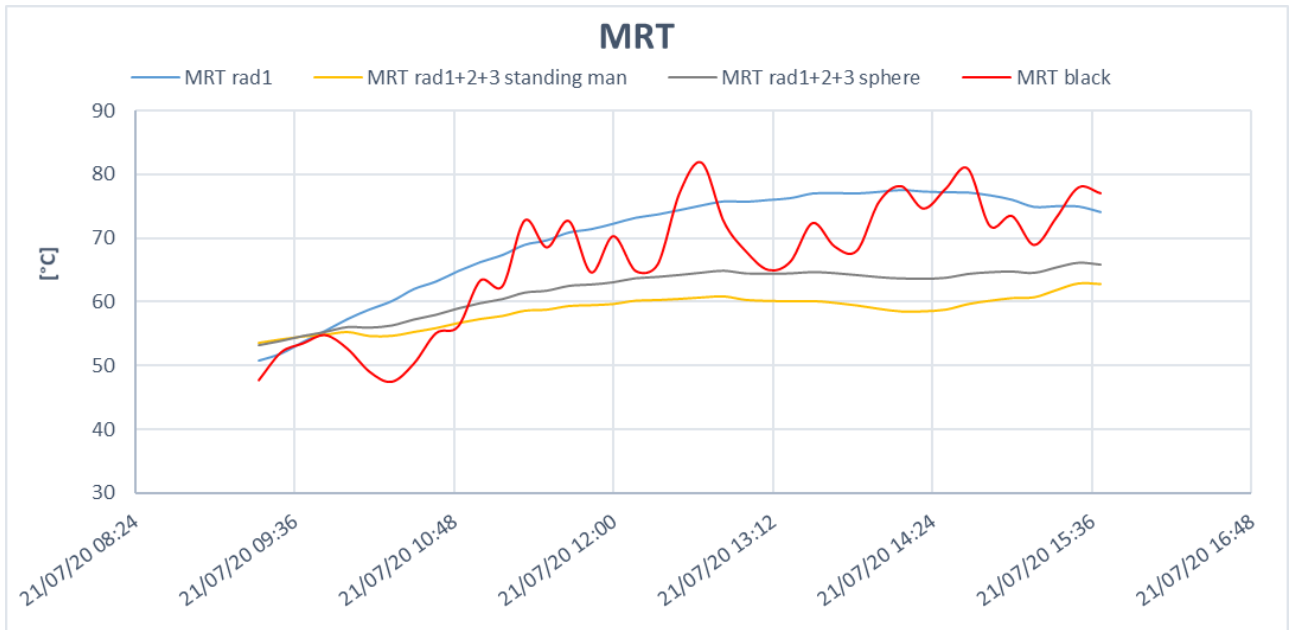


Figure 4. 8. Comparison between standing man and spherical view factors; flat rooftop with a waterproofing membrane, 21/07/2020.

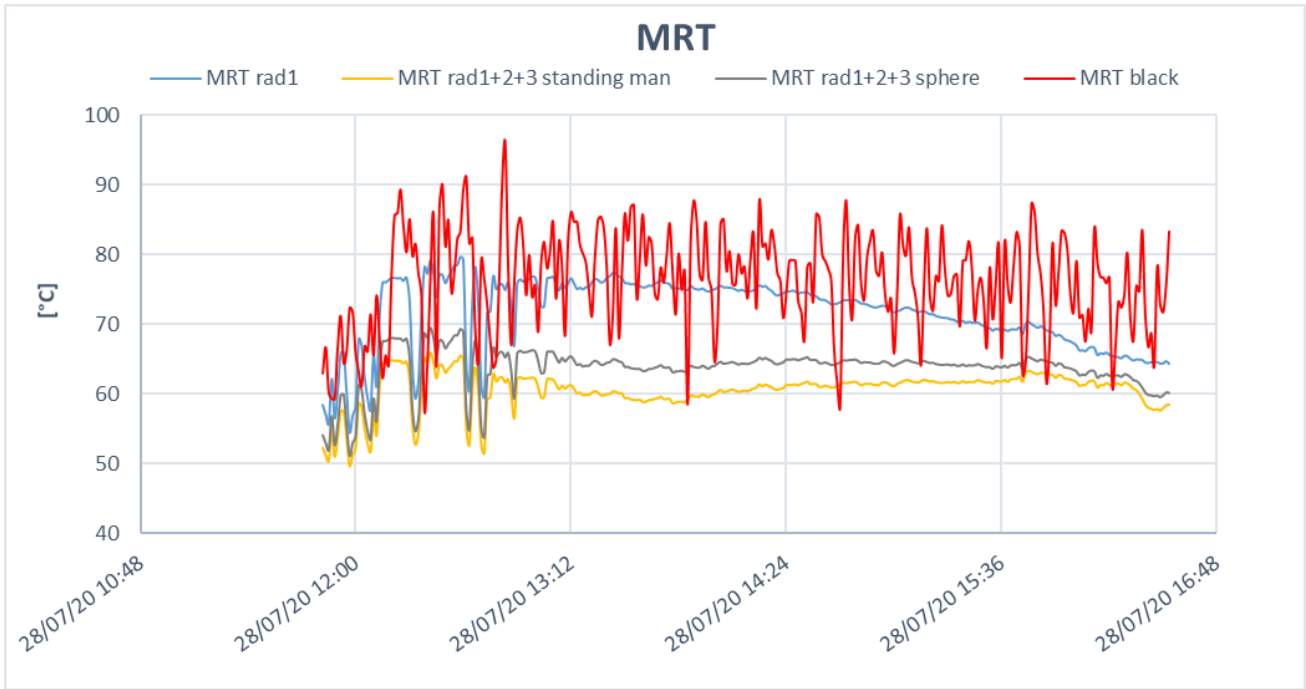


Figure 4. 9. Comparison between standing man and spherical view factors; park, 28/07/2020.

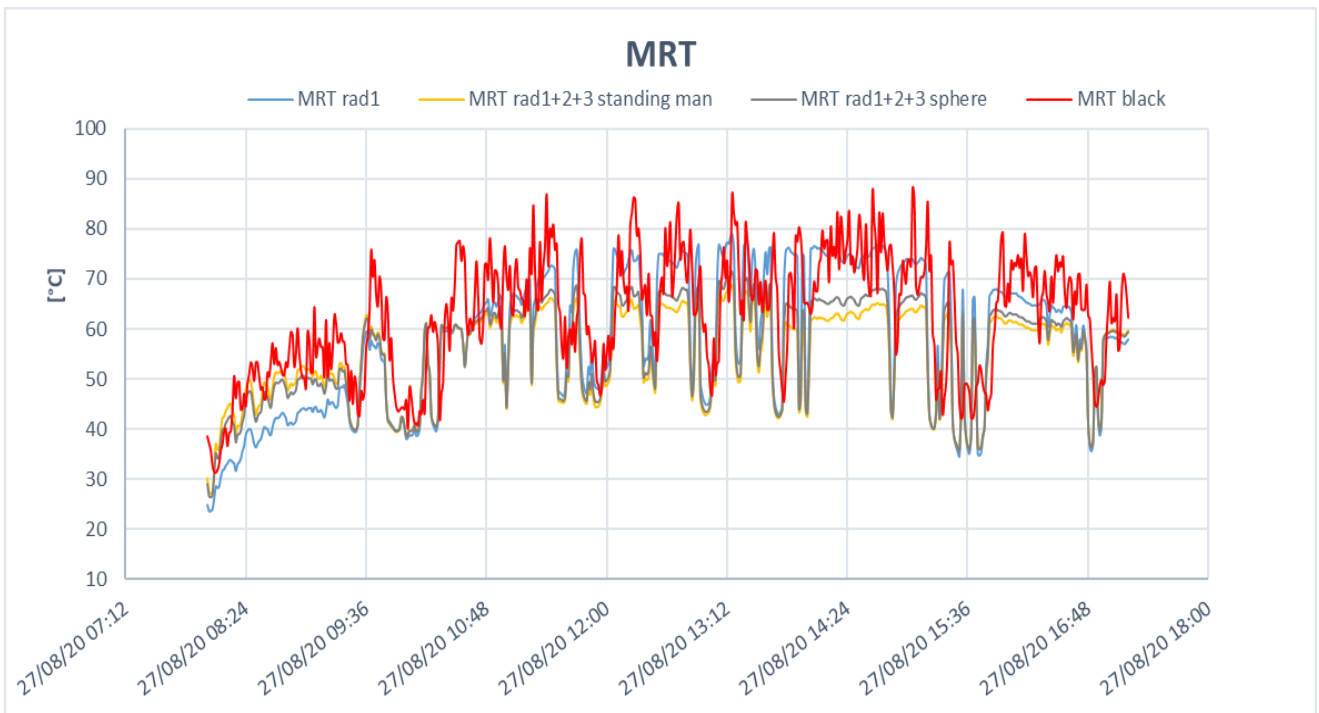


Figure 4. 10. Comparison between standing man and spherical view factors; green rooftop, 27/08/2020.

The environments considered in this section are well suited to the use of spherical view factors, in accordance with what is reported in Thorsson’s study (Thorsson et al. 2007) about the relevance of the different radiative fluxes for the evaluation of outdoor thermal comfort parameters.

According to the graphs reported in this section, we can find confirmation of the behaviour predicted: when the sun is at a greater height, the MRT evaluated with the spherical view factors is higher than the one obtained by using standing man factors, similarly to what was discussed in Chapter 3. *Experimental campaigns and results for MRT_{Rad1} and MRT_{Black}* . In particular, for the measurements in the park of Cascina

Merlata district, we recorded a difference $MRT_{Rad1+2+3,sphere} - MRT_{Rad1+2+3,standing\ man}$ equal or greater than 4 °C between 12:50 and 14:30; after 16:00, that difference is always lower than 1.5 °C.

The average $MRT_{Rad1+2+3,sphere} - MRT_{Rad1+2+3,standing\ man}$ difference resulting from these analyses is equal to 2.22 °C for the measurements on the waterproof slated membrane roof on 20/07, 3.11 °C in the same environment on 21/07, 2.97 °C in the Cascina park Merlata and 0.91 °C on the green rooftop.

The mean MRT values for each measurement considered are reported in *Table 4. 2*. According to the results of the table, the $MRT_{Rad1+2+3,sphere}$ values are always included between MRT_{Rad1} and $MRT_{Rad1+2+3,standing\ man}$.

However, even adopting spherical view factors for open field measurements, giving thus a greater relevance to the vertical radiative fluxes, the difference between $MRT_{Rad1+2+3,sphere}$ and MRT_{Black} or MRT_{Rad1} is still very pronounced, up to a maximum of 12.59 °C and 8.12 °C, respectively. This means that both of these two solutions, which are more economically advantageous than the method with three radiometers, cannot be replaced without facing a great loss of accuracy in the results, especially in open field measurements.

Table 4. 2. Comparison between standing man and spherical view factors adopted in the MRT evaluation by using net radiometers.

Building Envelope/ Environment	Measurement date and hour	Instrumentation directly exposed to the solar radiation	MRT (mean values) [°C]			
			RAD 1+2+3 standing man	RAD 1	Black globe	RAD 1+2+3 sphere
Flat rooftop with a waterproofing membrane	20/07/2020 12:00-19:30	yes	60,22	68,16	74,62	62,44
	21/07/2020 9:00-15:40	yes	58,63	70,17	66,55	61,74
Park	28/07/2020 11:50-16:30	yes	60,61	71,70	76,17	63,58
Green rooftop	27/08/2020 day 8:00-17:15	yes	54,96	57,87	62,66	55,87

4.4 Influence of convective heat exchange coefficient in the evaluation of MRT by using the globe thermometers

This section aims to analyse the correction proposed by Thorsson et al. (Thorsson et al. 2007) about the convective heat exchange coefficients adopted for the calculation of MRT using globe thermometers. The need arises from the fact that the commonly used h_{conv} comes from studies in indoor environments and only subsequently adapted for outdoors. The correction, therefore, aims to propose h_{conv} more suitable for outdoor measurements.

In order to investigate in which conditions the new h_{conv} is more suitable than the one adopted in *Section 3.1 Mean Radiant Temperature and UTCI assessment* to evaluate MRT in outdoor assessments, the graphs reported in this section represent the difference between MRT values obtained using three net radiometers ($MRT_{Rad1+2+3,standing\ man}$) and globe thermometers, with both the convective heat exchange coefficient adopted by Kuhen et al. (Kuehn, Stubbs, and Weaver 1970) (the one adopted for the analyses in *Section 3.1 Mean Radiant Temperature and UTCI assessment*, and equal to 1.06 W/m²K) and the one corrected by Thorsson et al. (Thorsson et al. 2007), according to the following equations:

$$Black - RAD = MRT_{Black} - MRT_{Rad1+2+3} \quad (4.1)$$

$$Black\ Thorsson - RAD = MRT_{Black_{Th.}} - MRT_{Rad1+2+3} \quad (4.2)$$

$$Grey - RAD = MRT_{Grey} - MRT_{Rad1+2+3} \quad (4.3)$$

$$Grey\ Thorsson - RAD = MRT_{Grey_{Th.}} - MRT_{Rad1+2+3} \quad (4.4)$$

The MRT values of the second terms in (4. 1), (4. 2), (4. 3) and (4. 4), as described in *Chapter 2. Instruments and Methodology*, are calculated as follows:

$$MRT_{Rad1+2+3} = \left(\frac{\sum_{i=1}^3 \left[F_i \left(\alpha_k (SW_{UP,i} + SW_{DOWN,i}) + \varepsilon_p (LW_{UP,i} + LW_{DOWN,i}) \right) \right]}{\sigma * \varepsilon_p} \right)^{0.25} - 273.15 \text{ [}^\circ\text{C]} \quad (4.5)$$

$$MRT_{Globe} = \left[(T_g + 273.15)^4 + \frac{1.06 * 10^8 v_{air}^{0.6}}{\varepsilon_g D^{0.4}} (T_g - T_{air}) \right]^{1/4} - 273.15 \text{ [}^\circ\text{C]} \quad (4.6)$$

$$MRT_{Globe_{Th.}} = \sqrt[4]{(T_g + 273.15)^4 + \frac{1.34 \cdot 10^8 v_{air}^{0.71}}{\varepsilon_g D^{0.4}} \cdot (T_g - T_{air})} - 273.15 \text{ [}^\circ\text{C]} \quad (4.7)$$

In Equation (4. 5), the view factors F_i adopted are those representing a standing person (*Section 2.1.3 Mean radiant Temperature calculation using net radiometers*).

Equation (4. 6) and Equation (4. 7) are generic for any type of globe: MRT_{Black} and MRT_{Grey} were calculated with Equation (4. 6) (where the values 0.15 meters and 0.05 meters are used for parameter D , respectively for MRT_{Black} and MRT_{Grey}), while $MRT_{Black_{Th.}}$ and $MRT_{Grey_{Th.}}$ were calculated by means of (4. 7) (where parameter D is set equal to 0.15 m and 0.05 m, for $MRT_{Black_{Th.}}$ and $MRT_{Grey_{Th.}}$ respectively).

Calculation of the globe MRT with Kantor et al.'s coefficients (Kántor, Kovács, and Lin 2015), described in Equation (2. 12), was not included in the analysis proposed in this section, since it provides results that are simply multiplied by a factor $\frac{1.1}{1.06}$ with respect to MRT_{Globe} equation (Equation (2. 14)), without changing any other parameter.

Figure 4. 11 and Figure 4. 12 show that, for the measurements carried out on the rooftop with the waterproofing membrane, the difference in results between black globe thermometer and net radiometers increases if Thorsson et al.'s correction is applied. The use of the new convective heat transfer coefficients increases the MRT_{Black} by a range between 6 °C and 11 °C, moving away from the reference results.

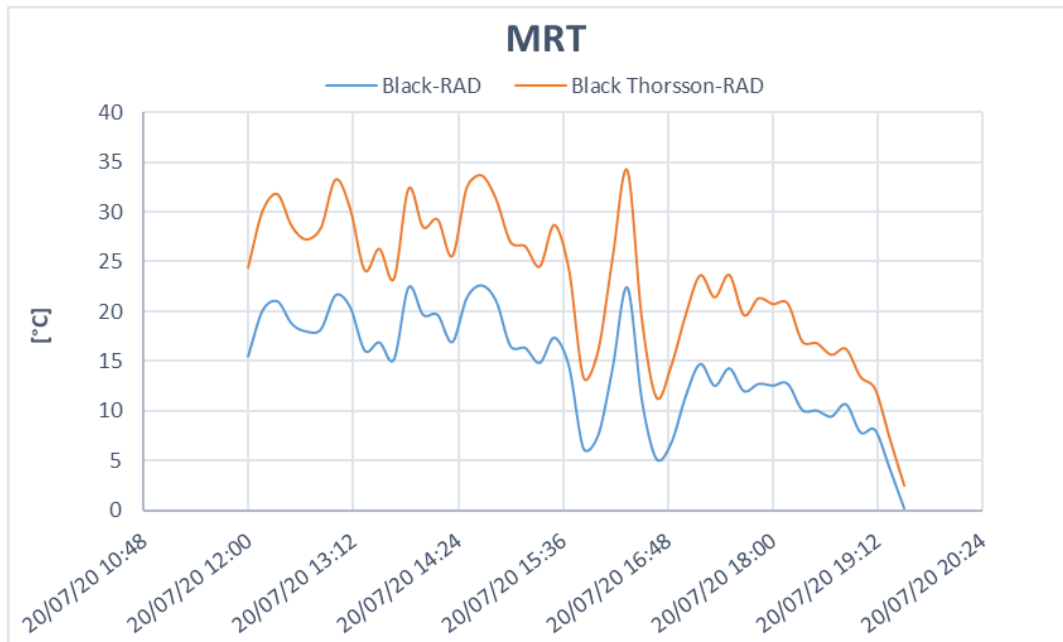


Figure 4. 11. Difference between Kuhen et al.'s and Thorsson et al.'s convective heat transfer coefficients for globe thermometers MRT measurements; 20/07/2020.

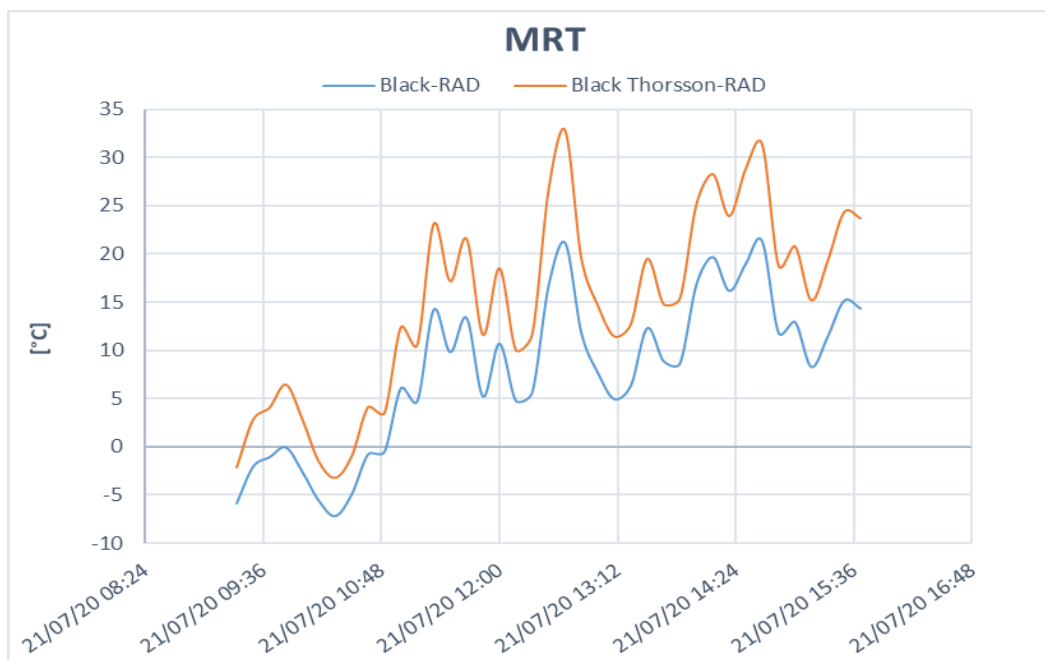


Figure 4. 12. Difference between Kuhen et al.'s and Thorsson et al.'s convective heat transfer coefficients for globe thermometers MRT measurements; 21/07/2020.

Figure 4. 13 and Figure 4. 14 show how the MRT results provided by the black globe thermometer vary with the new convective exchange coefficients, respectively for the measurements near the building with the light plaster envelope and the porcelain stoneware, both held in July. In both the two measurement campaigns very similar values of T_{air} , V_{air} and RH were found, as previously observed in Table 4. 1. For both the measurement environments, Thorsson et al.'s correction applied to the black globe tends to provide results that differ more from $MRT_{Rad1+2+3}$ than the results prior to the correction. In particular, the average $MRT_{Black_Th.}$ is 7.98 °C higher than the previous average MRT_{Black} on 23/07/2020, while the average difference $MRT_{Black_Th.} - MRT_{Black}$ is also higher and equal to 10.72 °C on 27/07/2020.

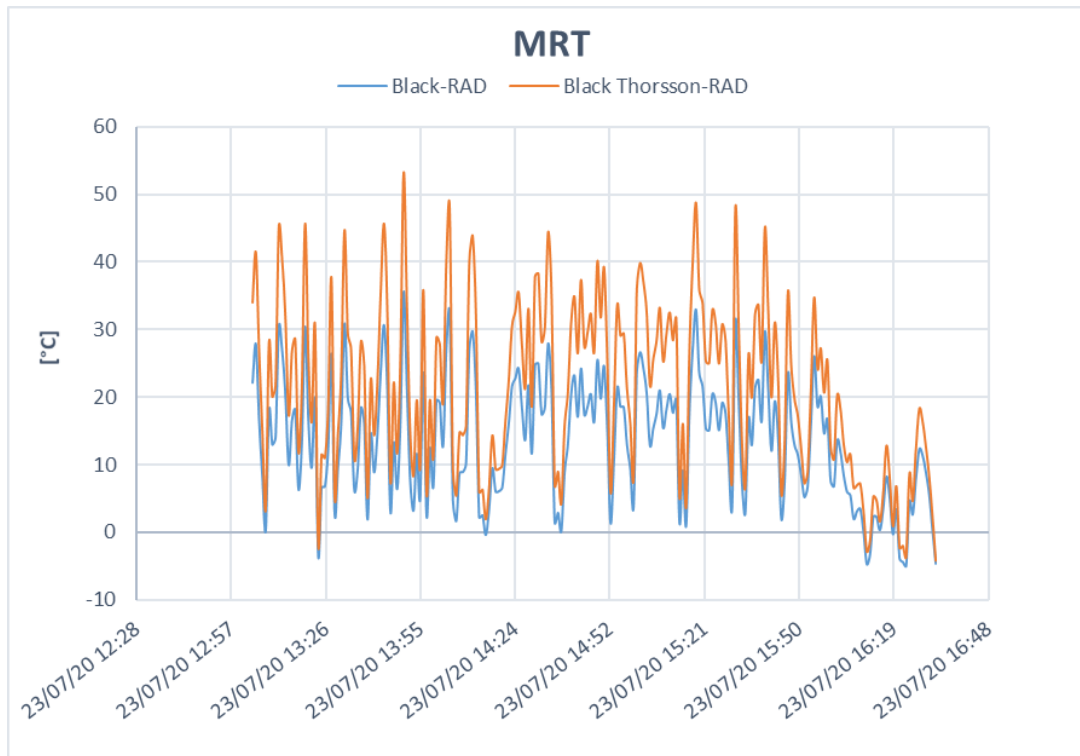


Figure 4. 13. Difference between Kuhen et al.'s and Thorsson et al.'s convective heat transfer coefficients for globe thermometers MRT measurements; 23/07/2020.

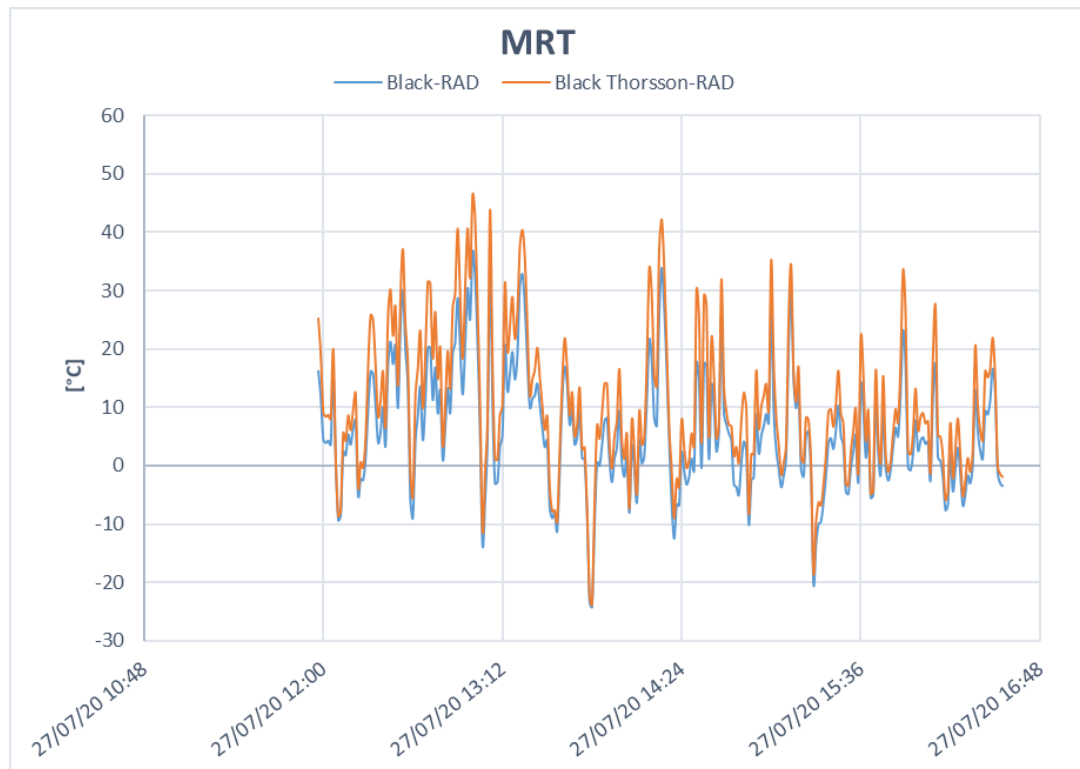


Figure 4. 14. Difference between Kuhen et al.'s and Thorsson et al.'s convective heat transfer coefficients for globe thermometers MRT measurements; 27/07/2020.

Figure 4. 15 shows the results of the measurements carried out in the Cascina Merlata park with the new convective heat exchange coefficient corrected by Thorsson. According to the figure, the new average $MRT_{Black,Th}$ obtained is equal to 85.19 °C, greater than the previous MRT_{Black} (equal to 76.17 °C). Even for measurements in the open field, the new h_{conv} , applied to the black globe thermometer, provides an undesired effect.

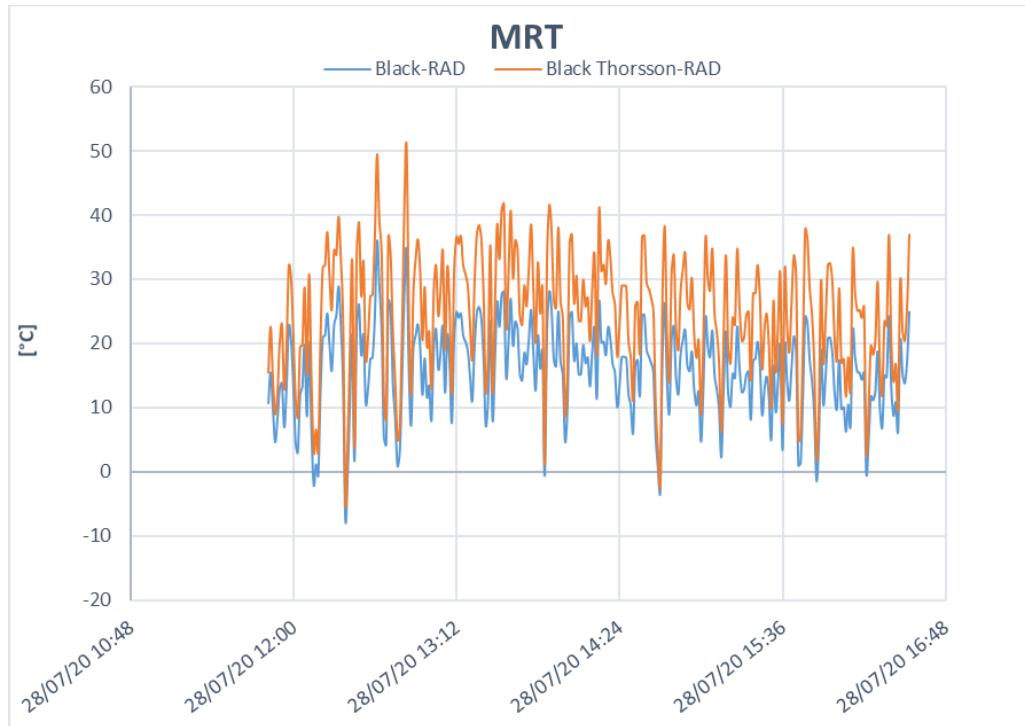


Figure 4. 15. Difference between Kuhen et al.'s and Thorsson et al.'s convective heat transfer coefficients for globe thermometers MRT measurements; 28/07/2020.

Figure 4. 16, Figure 4. 17 and Figure 4. 18 represent the results obtained from the measurements on the green rooftop respectively on 26/08/2020, in the night between 26/08/2020 and 27/08/2020 and on 27/08/2020.

During the first day of measurement (26/08), the new convective coefficient, applied to the black globe, is able to reduce the previous $MRT_{Black} - MRT_{Rad1+2+3}$ average difference in absolute value: *Black Thorsson - RAD* is equal to 0.72 °C, while the average *Black - RAD* previously calculated was equal to -0.91 °C. On the contrary, according to Figure 4. 17, it seems that the Thorsson et al.'s correction applied to the black globe thermometer provides an undesired effect even for night measurements. The difference $MRT_{Black} - MRT_{Rad1+2+3}$, which turns out to be negative during the night, is increased in absolute value after the new h_{conv} is adopted. The average *Black - RAD* was previously equal to -0.89 °C, while with the new coefficient we face a *Black Thorsson - RAD* difference of -1.31 °C.

The second graph in Figure 4. 17 also shows that even the grey globe thermometer is penalized by the new convective heat exchange coefficients during night measurements: the average difference *Grey Thorsson - RAD* (which is negative and equal to -1.97 °C) is greater - in absolute value - than the previous *Grey - RAD* (equal to -1.39 °C).

Also considering daytime measurements on 27/08 (Figure 4. 18), both globe thermometers are penalized by the proposed correction. In particular, the difference between black globe and net radiometers increases, after the correction, by 5.14 °C, while the difference between grey globe and radiometers increases, in absolute value, by 1.26 °C. However, it should be remembered that these measurements are carried out in open field, and therefore it would be possible to choose to adopt the spherical view factors for the net radiometers, in order to give greater relevance to the vertical radiative fluxes. In this way the $MRT_{Rad1+2+3}$ would increase, consequently reducing the differences obtained between radiometers and globe thermometers.

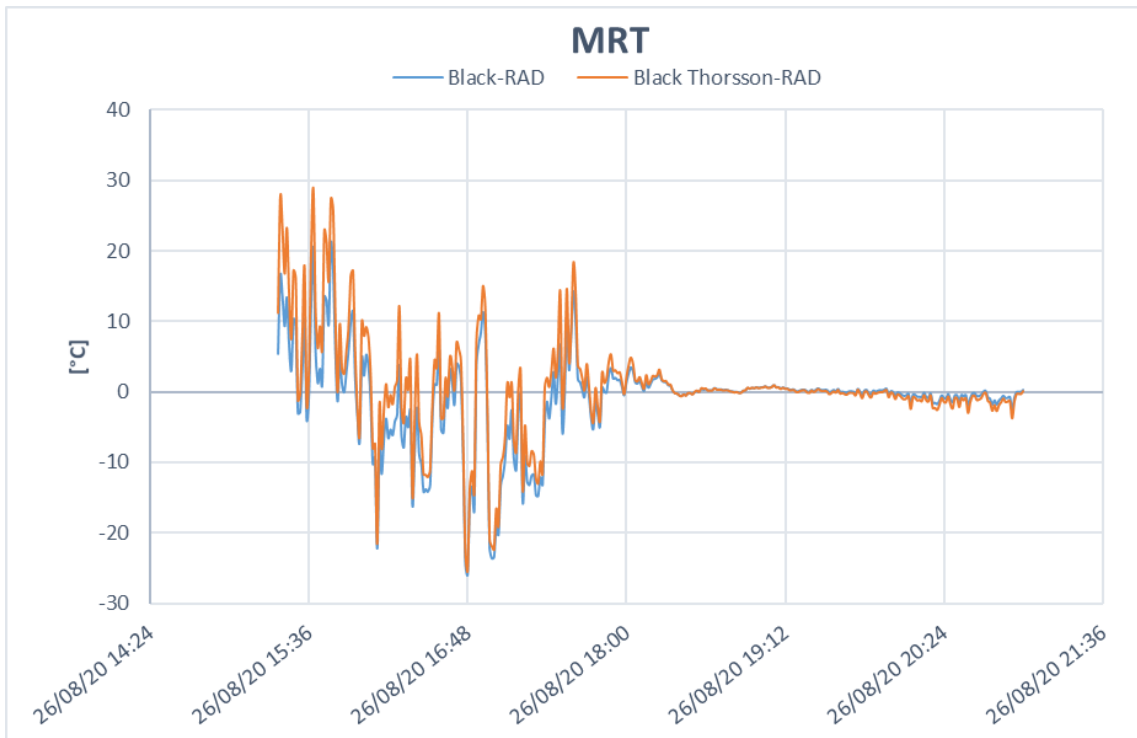


Figure 4. 16. Difference between Kuhnen et al.'s and Thorsson et al.'s convective heat transfer coefficients for globe thermometers MRT measurements; day 26/08/2020.

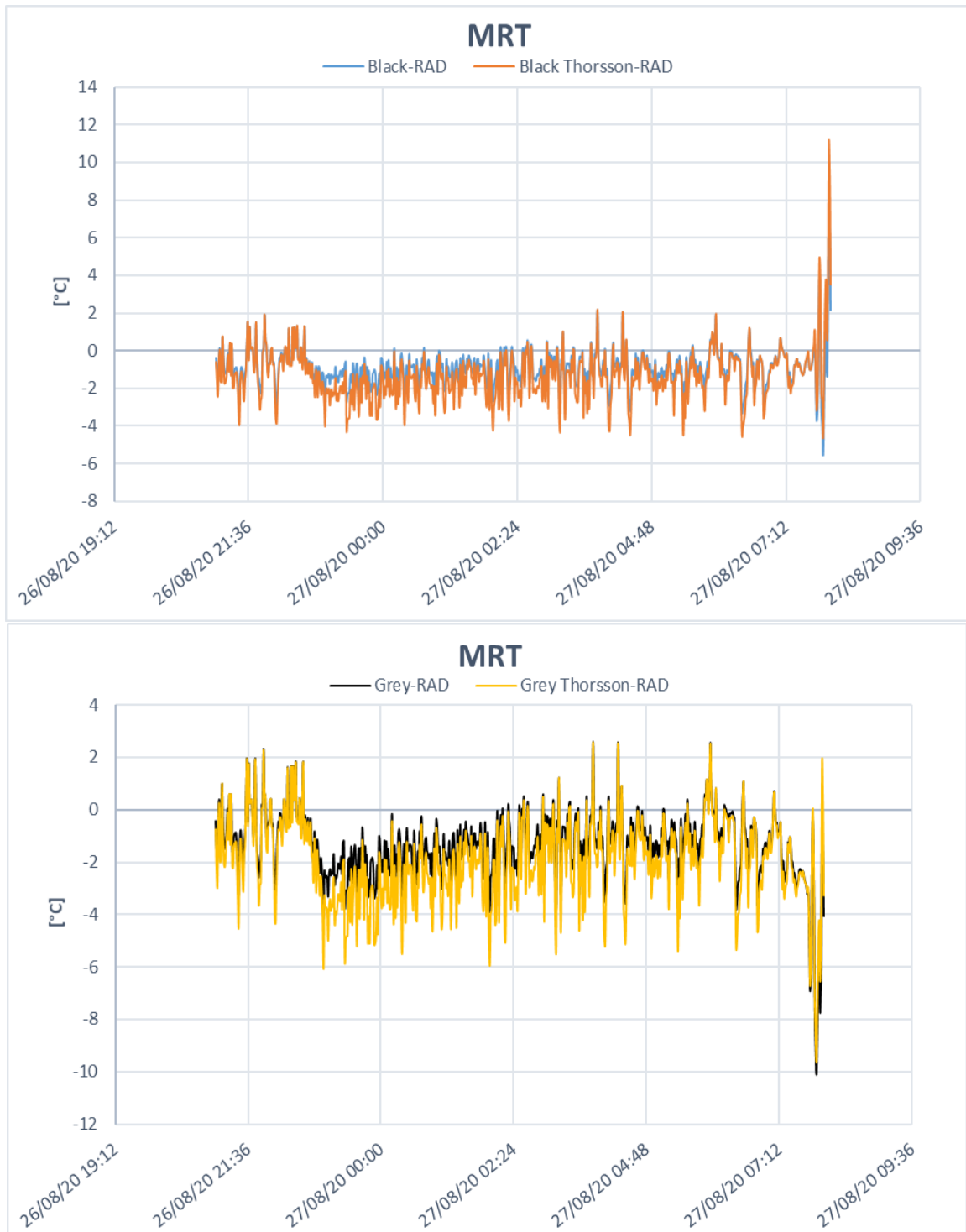


Figure 4. 17. Difference between Kuhen et al.'s and Thorsson et al.'s convective heat transfer coefficients for globe thermometers MRT measurements; night 26-27/08/2020.

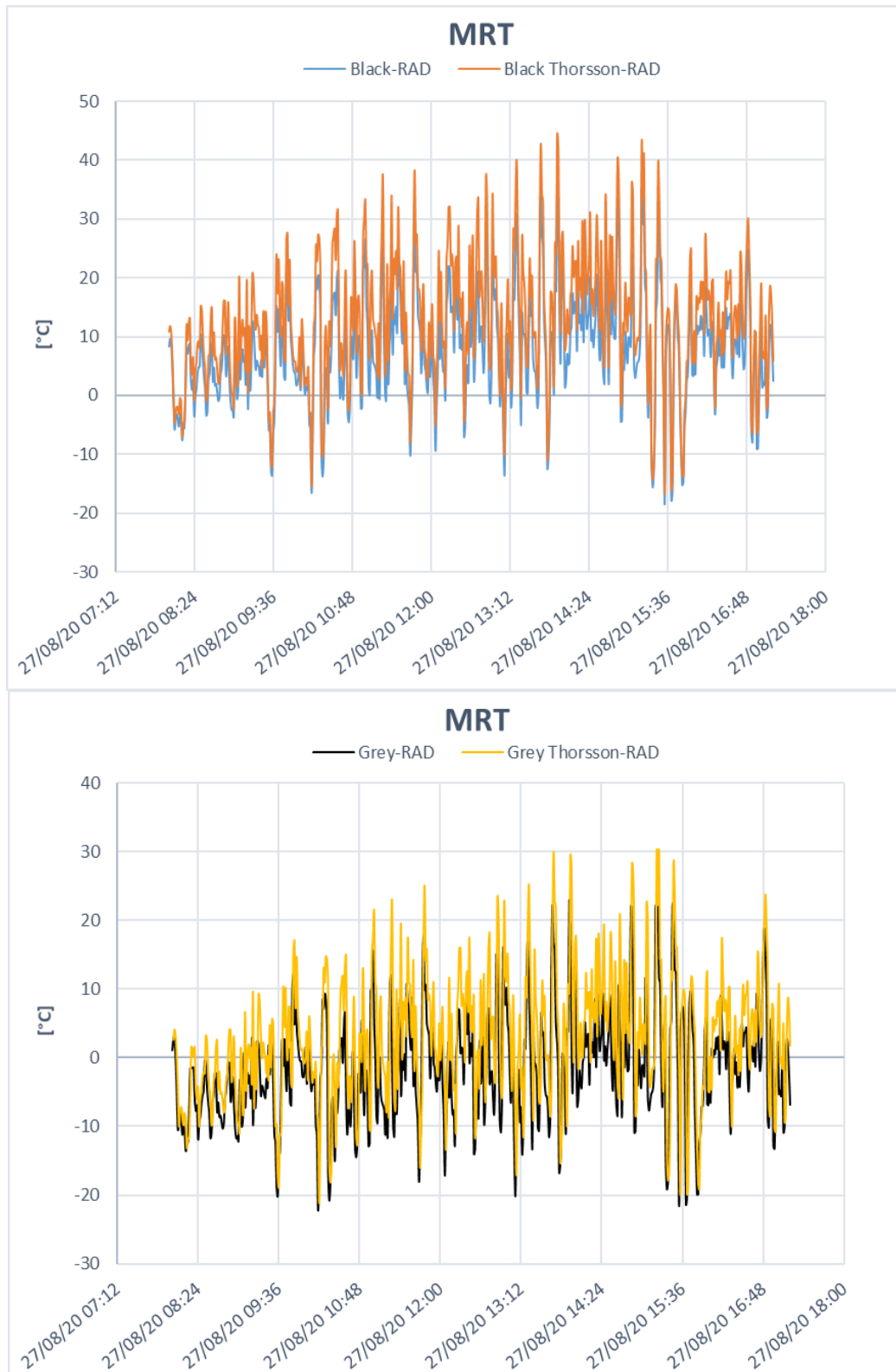


Figure 4. 18. Difference between Kuhen et al.'s and Thorsson et al.'s convective heat transfer coefficients for globe thermometers MRT measurements; day 27/08/2020.

Figure 4. 19 refers to the measurements carried out near the blue plaster wall on 01/09/2020. It shows once again that the Thorsson et al.'s correction is not suitable for the black globe thermometer, as it provides results that deviate further from the reference values provided by net radiometers. The previous average *Black – RAD* equal to 4.45 °C turns into a *Black Thorsson – RAD* average difference of 8.35 °C.

On the contrary, the new h_{conv} applied to the grey globe allows to obtain a *Grey Thorsson – RAD* difference lower than *Grey – RAD*, obtained before the correction. In particular, the new average difference is equal to $-2.60\text{ }^{\circ}\text{C}$, while the previous average difference was equal to $-5.82\text{ }^{\circ}\text{C}$.

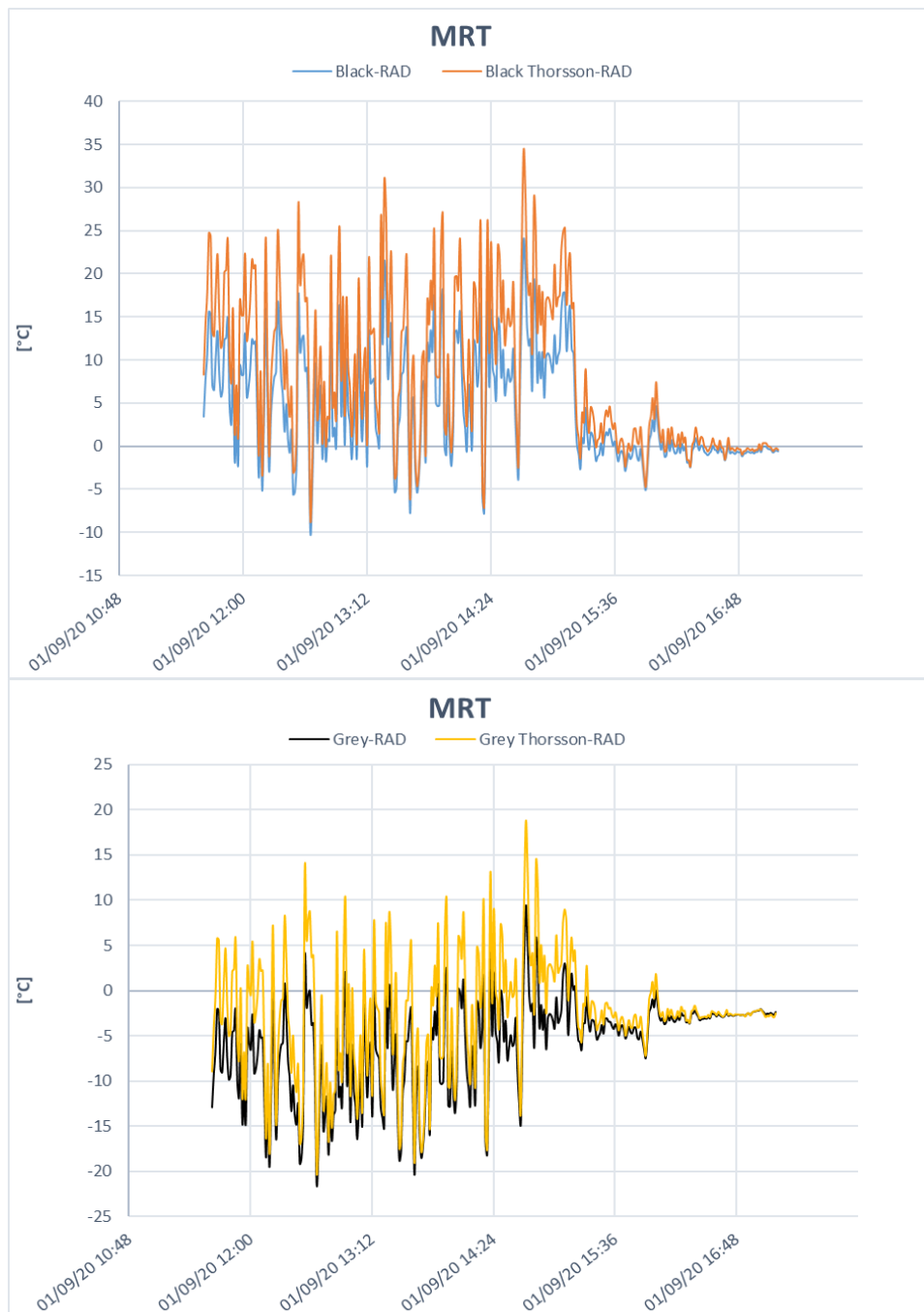


Figure 4. 19. Difference between Kuhen et al.'s and Thorsson et al.'s convective heat transfer coefficients for globe thermometers MRT measurements; 01/09/2020.

Figure 4. 20 compares the differences between the two globe thermometers and the net radiometers, before and after applying the Thorsson et al.'s correction, for the measurements carried out in the street canyon, on 09/09/2020.

From the figure, it is possible to observe that, even for measurements carried out with the instrumentation in a shaded situation, the new h_{conv} turns out not to be suitable for the black globe thermometer, increasing

the difference $MRT_{Black} - MRT_{Rad1+2+3}$. The new *Black Thorsson - RAD* average difference is equal to 3.46 °C, while we had a *Black - RAD* of 1.76 °C before the correction. On the contrary, the grey globe, after applying the proposed correction, gives results more similar to the reference ones: we calculated an average *Grey Thorsson - RAD* of -1.16 °C and a *Grey - RAD* of -2.24 °C.

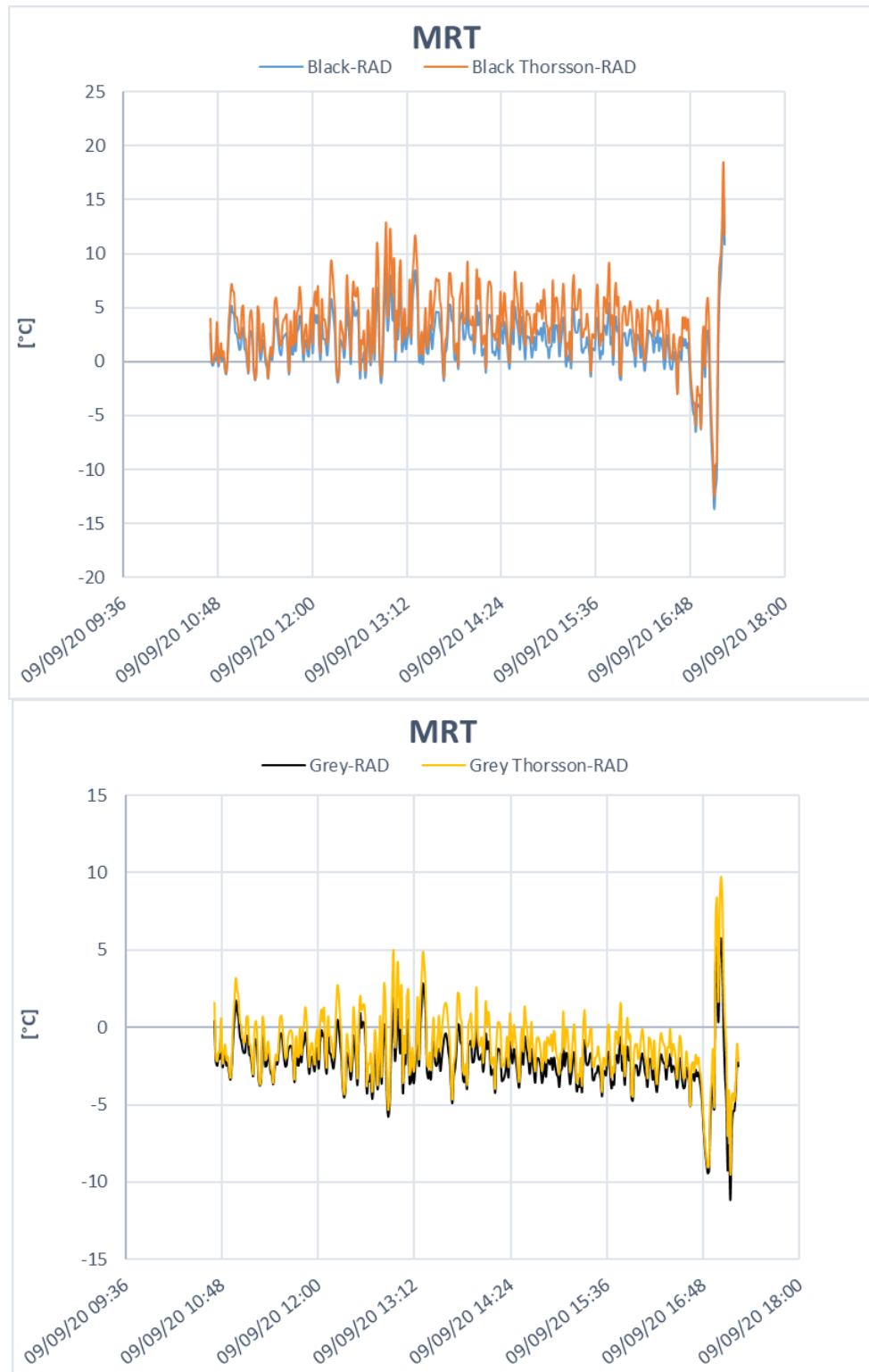


Figure 4. 20. Difference between Kuhén et al.'s and Thorsson et al.'s convective heat transfer coefficients for globe thermometers MRT measurements; 09/09/2020.

Figure 4. 21 refers to the measurement campaign carried out near the building with the porcelain stoneware envelope on 18/09/2020. For the whole duration of the survey the instrumentation was exposed to the direct solar radiation, but the new h_{conv} seems still suitable only for the grey globe thermometer, while, if applied to the black globe, they provide an undesired effect. The average difference between black globe and net radiometers is increased of 4.08 °C after the correction, while the average difference between the grey globe and the net radiometers decreases, in absolute value, of 3.67 °C (from a *Grey – RAD* equal to -7.00 °C to a *Grey Thorsson – RAD* of -3.33 °C).

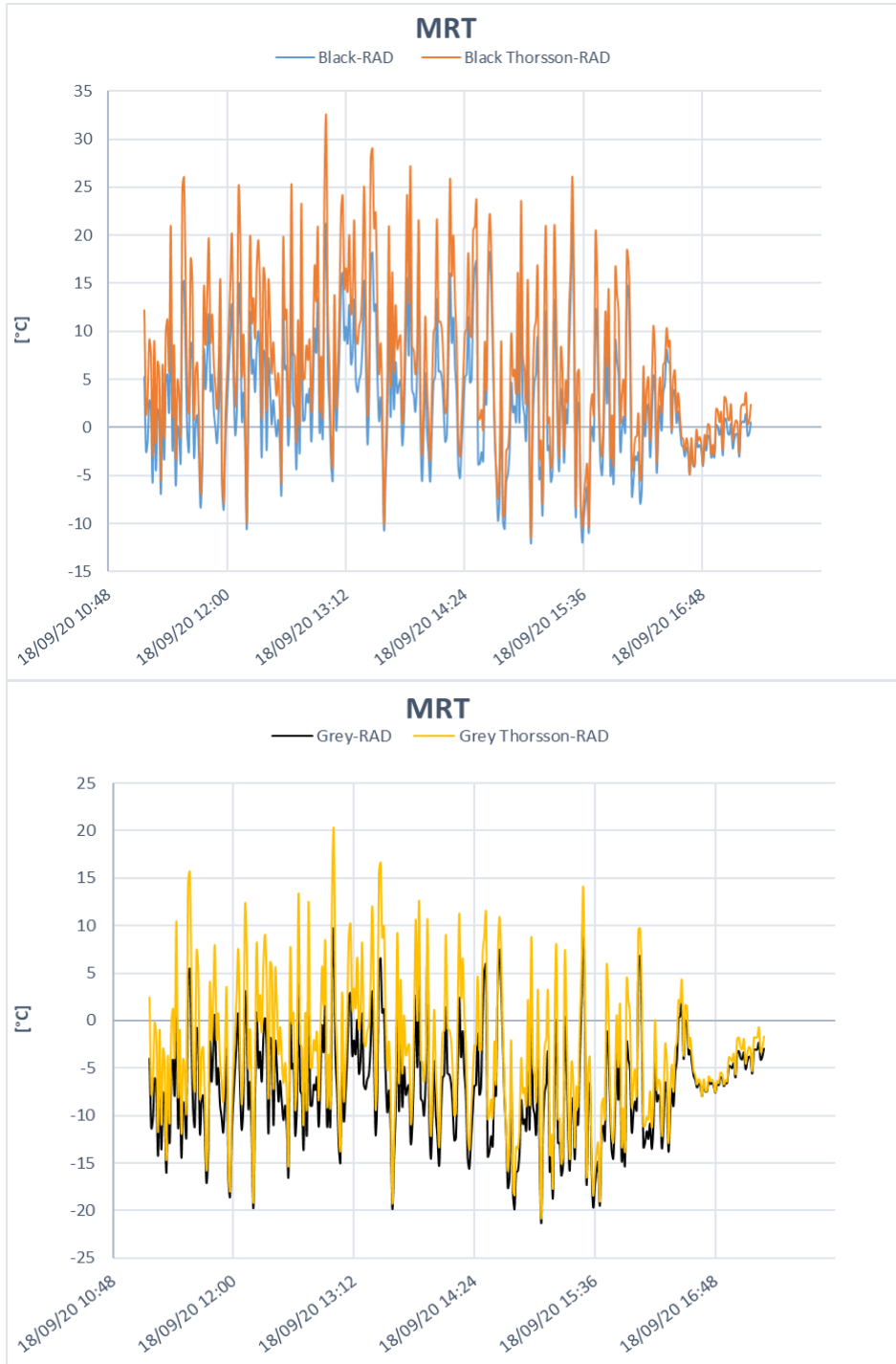


Figure 4. 21. Difference between Kuhen et al.'s and Thorsson et al.'s convective heat transfer coefficients for globe thermometers MRT measurements; 18/09/2020.

Figure 4. 22 and Figure 4. 23 show the MRT results after adopting the Thorsson et al.'s correction to the measurements carried out near the two green walls described in Section 3.1 Mean Radiant Temperature and UTCI assessment, respectively on 17/09/2020 and on 06/10/2020. In both figures it is possible to note that, by adopting the new h_{conv} coefficient, the MRT values obtained with both the black globe and the grey globe are greater than those obtained before applying the Thorsson et al.'s correction. In this way the black globe (having an average difference $Black - RAD$ higher than 0 °C before the correction) moves further from the reference values, while the grey globe (which had an average $Grey - RAD$ lower than 0 °C) approaches them.

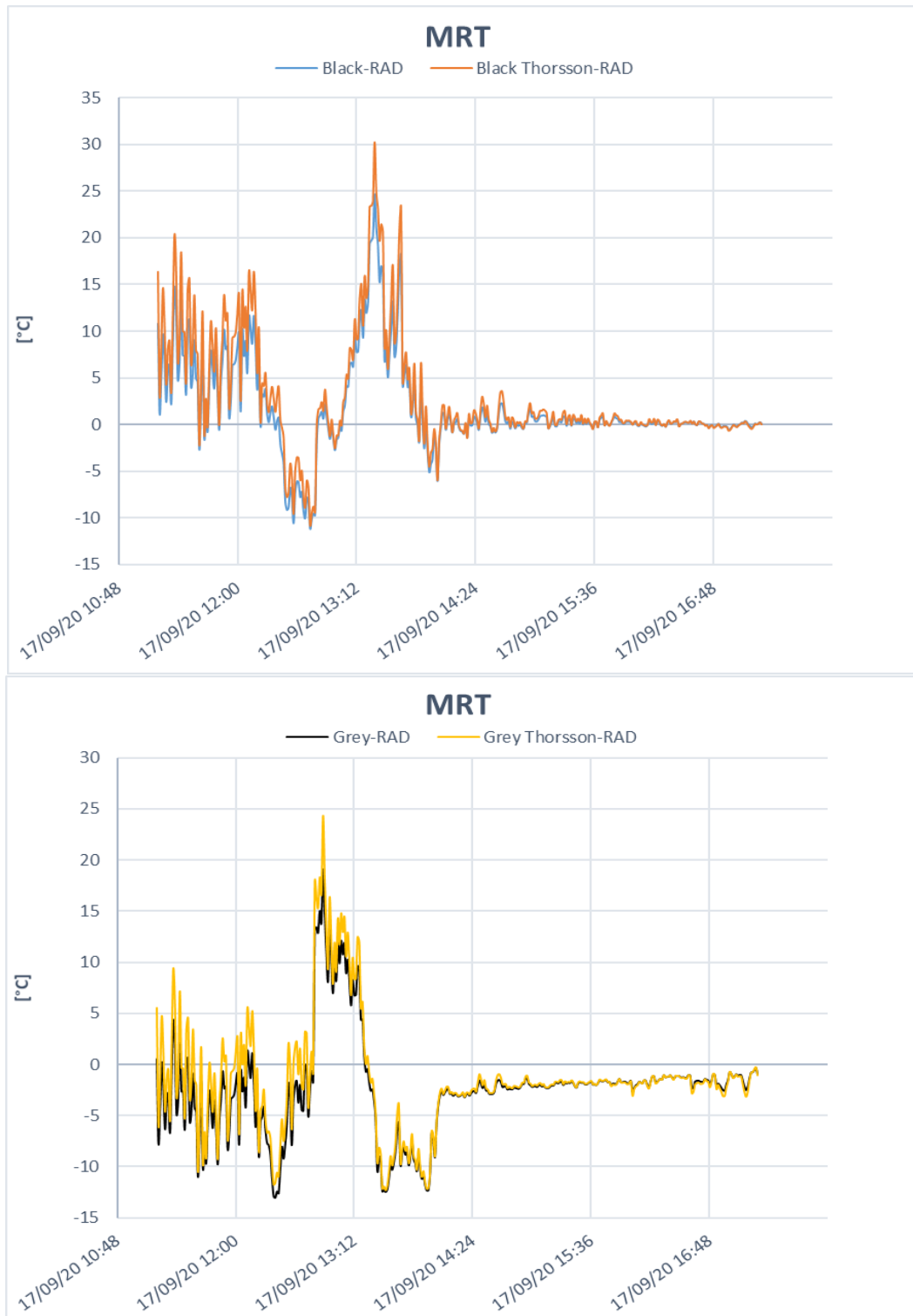


Figure 4. 22. Difference between Kuhen et al.'s and Thorsson et al.'s convective heat transfer coefficients for globe thermometers MRT measurements; 17/09/2020.

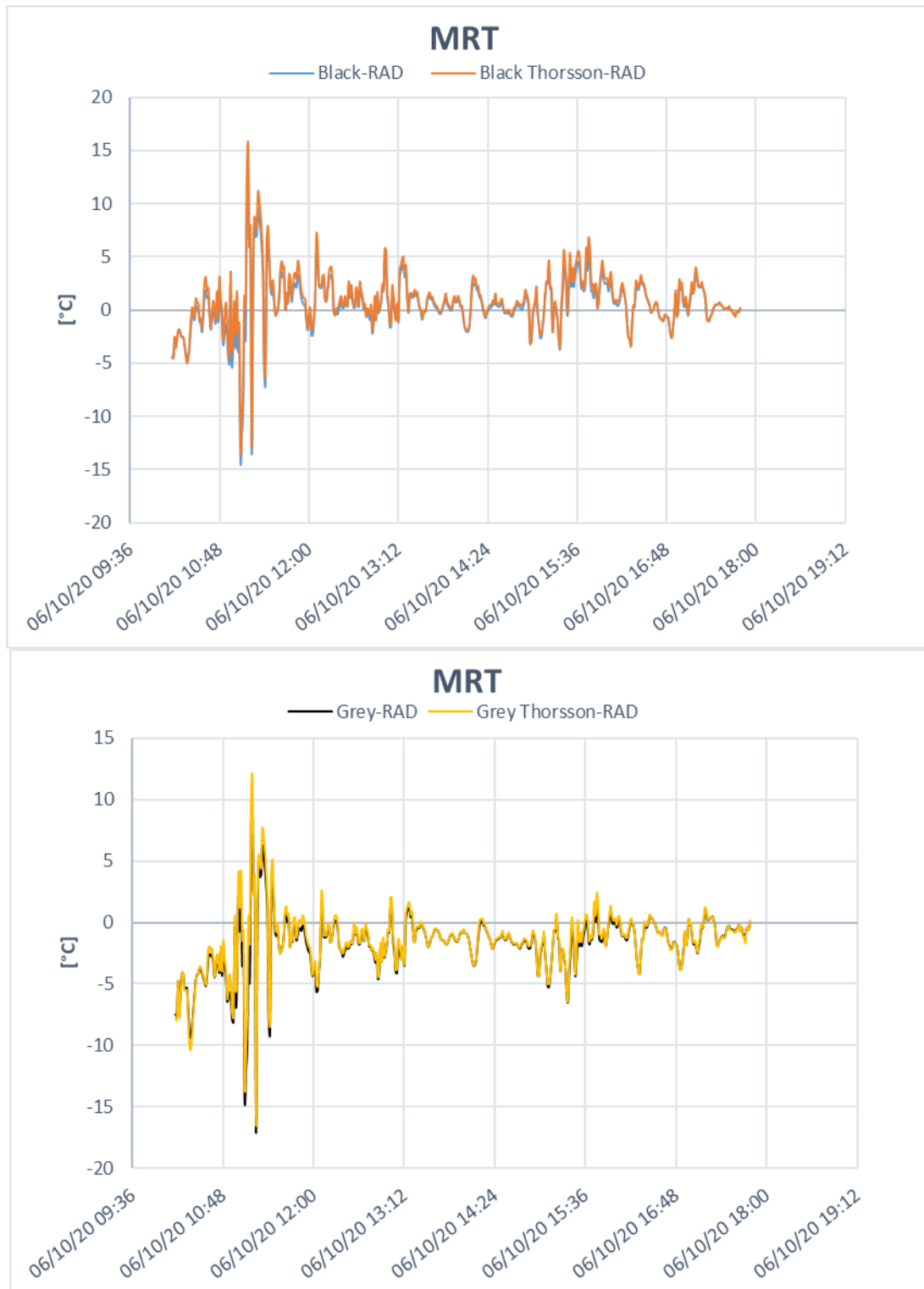


Figure 4. 23. Difference between Kuhen et al.'s and Thorsson et al.'s convective heat transfer coefficients for globe thermometers MRT measurements; 06/10/2020.

All the graphs in Section 4.4 Influence of convective heat exchange coefficient in the evaluation of MRT by using the globe thermometers show that, regardless of the solar height, whether the instrumentation is in shadow or not (excluding night measurements), the correction proposed by Thorsson et al. faces higher MRT values, both when applied to the black globe and the grey globe.

Therefore, we can state that, when the difference in MRT between globe thermometers and net radiometers is positive ($MRT_{Globe} > MRT_{Rad1+2+3}$), the correction increases the term $MRT_{Globe} - MRT_{Rad1+2+3}$; in case of $MRT_{Globe} < MRT_{Rad1+2+3}$, instead, the correction brings the MRT values obtained with the globe thermometers closer to the desired values obtained by using net radiometers.

Generally, when the Thorsson et al.'s correction is applied to the black globe (having $MRT_{Black} > MRT_{Rad1+2+3}$), we face an undesired effect, increasing the difference $MRT_{Globe} - MRT_{Rad1+2+3}$. On the contrary, for the grey globe, the difference $MRT_{Grey} - MRT_{Rad1+2+3}$ is negative for most of the day, as could already be observed in the analysis of *Section 3.1 Mean Radiant Temperature and UTCI assessment*. With this in mind, the correction seems better suited to the grey globe, allowing to approach the values obtained by the three net radiometers solution.

However, this is not reflected in night measurements: in these conditions, in fact, the difference $MRT_{Grey} - MRT_{Rad1+2+3}$ is negative but small in magnitude and almost equal to zero; Thorsson et al.'s correction, by increasing the MRT_{Grey} values, will increase the difference accordingly, making it positive and higher in magnitude.

The results of this analysis are easily deductible from *Table 4. 3*, which shows the MRT mean values for both the black globe and the grey globe, obtained before and after the correction proposed, as well as their difference with respect to $MRT_{Rad1+2+3}$. From the values reported in it, we can see that, for daytime measurements, the new convective heat transfer coefficient always increases the MRT of the black globe, up to a maximum of 9.03 °C for measurements carried out in open field, at the park in the Cascina Merlata district. Also for the measurements carried out using a grey globe, the proposed correction leads to an increase in MRT, albeit more reduced: the greatest increase is still found in open field, on the green rooftop, and is equal to 4.46 °C.

As we noticed from *Figure 4. 17*, for the measurements made during the night hours, the correction by Thorsson et al. always finds an undesirable effect, both if applied to the black globe (increasing the MRT by 0.42 °C), and to the grey globe (increasing the $MRT_{Grey} - MRT_{Rad1+2+3}$ difference by 0.58 °C).

Table 4. 3. Mean values of MRT obtained by means of net radiometers and globe thermometers by adopting different convective heat exchange coefficients.

Building Envelope/ Environment	Measurement date and hour	Instrumentation directly exposed to the solar radiation	MRT (mean values) [°C]				ΔMRT (mean values) [°C]				
			RAD 1+2+3	Black globe Thorsson	Black globe Thorsson	Grey globe Thorsson	Black -RAD	Black Th. - RAD	Grey - RAD	Grey Th. - RAD	
Flat rooftop with a waterproofing membrane	20/07/2020 12:00-19:30	yes	60,22	74,62	83,17		14,40	22,95			
	21/07/2020 9:00-15:40	yes	58,63	66,55	73,49		7,92	14,86			
Light plaster wall	23/07/2020 13:00-16:30	yes, until 16:00	65,41	79,00	86,98		13,59	21,56			
	27/07/2020 12:00-16:30	yes	64,16	70,19	74,88		6,03	10,73			
Porcelain stoneware Facade Cladding	18/09/2020 11:10-17:15	yes	63,38	65,86	69,94	60,05	2,48	6,56		-7,00	-3,33
	28/07/2020 11:50-16:30	yes	60,61	76,17	85,19		15,55	24,58			
Park	26/08/2020 day 15:20-21:00	yes, until sunset (~ 18:00)	41,65	40,74	42,37		-0,91	0,72			
	26-27/08/2020 night 21:00-8:00	no	21,66	20,77	20,34	19,68	-0,89	-1,31		-1,39	-1,97
Green rooftop	27/08/2020 day 8:00-17:15	yes	54,96	62,67	67,81	57,82	7,71	12,85		-1,60	2,86
	01/09/2020 11:30-17:10	yes	54,53	58,98	62,88	48,71	4,45	8,35		-5,82	-2,60
Blue plaster wall	09/09/2020 10:40-17:15	no, until 16:30	33,80	35,56	37,27	31,56	1,76	3,46		-2,24	-1,16
	17/09/2020 11:10-17:15	yes	38,99	40,85	41,98	36,67	1,86	2,99		-2,32	-1,48
Street Canyon	06/10/2020 10:10-17:45	no	21,20	21,77	22,18	19,48	0,57	0,98		-1,72	-1,45

5. Conclusions

Studies related to outdoor thermal comfort are becoming more and more relevant in recent years, especially due to climate change projections, suggesting increasingly severe summer heat waves. In particular, this rising interest is mainly focused on the urban environment, being the most affected by the so-called UHI effect (*Section 1.1 Urban Heat Island effect*).

For urban planners, therefore, the importance of gaining an understanding about thermal stress assessment is growing, in order to make the environment where citizens live as comfortable and healthy as possible. To define the thermal stress perceived by a person in the environment, several thermal indices have been developed, most of which coming from an adaptation for outdoors of already existing indoor indices (Johansson et al. 2014). Among all the indices we can find in literature, the UTCI (*Section 1.2.3.2 Universal Thermal Climate Index (UTCI)*), developed by Jendritzky et al. (G. Jendritzky, A. Maarouf 2001) for outdoor environments, aims to be as universal as possible, covering the whole range of heat exchanges between the human body and the outdoor thermal environment, in different climate and seasons.

For this purpose, UTCI is calculated on the basis of the MRT (*Section 1.2.2 Mean Radiant Temperature assessment*), a parameter introduced to deal with all the radiative fluxes reaching a human body: the incoming and reflected radiation, the direct and diffuse short-wave radiation and the long-wave radiation coming from surrounding surfaces, ground and sky. However, while there are consolidated international standards defining instruments and techniques for carrying out measurements of thermal comfort parameters for indoor environments, there is a strong lack regarding outdoor assessments. Several researchers in this field have therefore used different measurement techniques in their studies, making difficult to compare the results.

This thesis takes into consideration different measurement techniques, involving different instruments, commonly adopted in literature, including integral radiation measurements by means of net radiometers (considered the most accurate method to evaluate MRT) and globe thermometers with different size and colours to assess outdoor thermal comfort in terms of MRT and UTCI. This choice is due to the high cost of net radiometers compared to globe thermometers, a factor that has prompted most researchers to adopt cheaper measurement techniques. The results highlight the main differences, in the calculation of the outdoor comfort indices, between the adopted measurement techniques, under different meteorological conditions and in different environments.

Several experimental campaigns were carried out, showing that the black globe always tends to overestimate the MRT, compared to the solution provided by the combination of the three net radiometers. The difference $MRT_{Black} - MRT_{Rad1+2+3}$ is reduced to values below 2 °C when the instrumentation is partially shaded, and it becomes negligible (and sometimes negative) when the instrumentation is completely in shade; it reaches instead values higher than 15 °C (considering the average difference over a single measurement campaign duration) in open field measurements, where the instrumentation is entirely exposed to the direct solar radiation. Moreover, if we consider the MRT results calculated per minute instead of the average difference, $MRT_{Black} - MRT_{Rad1+2+3}$ reaches values even higher than 30 °C. On the other hand, the grey globe tends to slightly underestimate the MRT compared to the net radiometers, presenting an average deviation lower than 2 °C when the instrumentation is in shade and lower than 8 °C in case of instruments exposed to the direct solar radiation. As for the black globe, if the comparison is instead performed between the results obtained per minute, the difference $MRT_{Rad1+2+3} - MRT_{Grey}$ also exceeds 20 °C.

During the measurements, a further approach was adopted, using as instrument a single radiometer measuring the upward/downward direction. The results provided by this method were found to be similar to those recorded by the black globe thermometer, overestimating up to 20 °C the $MRT_{Rad1+2+3}$. As the sun went down, the difference $MRT_{Rad1} - MRT_{Rad1+2+3}$ decreased, until it became negative in night time measurements.

However, during the analyses it was found that the black globe thermometer generally approximated the $MRT_{Rad1+2+3}$ better than the single radiometer, except for measurements in open field, where the $MRT_{Rad1} - MRT_{Rad1+2+3}$ difference was lower than $MRT_{Black} - MRT_{Rad1+2+3}$. This consequently leads us

to think about the relevance of vertical radiative fluxes in open field measurements, not correctly described by the view factors adopted in the MRT calculation using the three net radiometers. An analysis performed by Thorsson et al. (Thorsson et al. 2007) pointed out that the view factors commonly adopted in literature, which assimilate a standing person to a square-based parallelepiped with a ratio $H/L = 3.5$, were not so accurate for open spaces, where vertical radiative fluxes have a greater relevance than they would have in measurements carried out in street canyons or environments having “barriers” to the direct solar radiation. As suggested by Thorsson et al., we then tried to adopt, for open field measurements, spherical view factors which attribute the same weight to both vertical and horizontal fluxes: as result, a smaller difference was found between the MRT values provided by net radiometers and the ones obtained with globe thermometers, becoming more similar to the difference faced in the other measurement environments. As evidenced in the analyses, the variation of solar height during the day and in different months strongly affects the MRT difference experienced between one instrument and another. This can be explained, among other reasons, with the weight each single instrument attributes to the radiative fluxes coming from different directions. In particular, the globe thermometers, given their spherical shape, attribute an equal weight to the flows coming from any direction, while the calculation of MRT using net radiometers is based on specific view factors defining different weights for the six directions measured. This seems becoming particularly evident in open field measurements, without obstacles to the direct solar radiation, where we faced the greatest difference $MRT_{Globe} - MRT_{Rad1+2+3}$.

As discussed for net radiometers, there is not a unique and standardized method for assessing MRT in the outdoor environments with globe thermometers. Consequently, different researchers adopted different approaches in the calculation of convective heat exchanges between the globe thermometers and the surrounding environment. In particular, the different convective heat transfer coefficients adopted can greatly vary the results obtained, making it difficult to compare different studies. Our analyses have shown how, for the grey globe thermometer, a good solution is to adopt a corrective factor introduced by Thorsson et al. in 2007 (Thorsson et al. 2007), with the aim of better simulating the convective heat exchange between the globe and the surrounding outdoor environment. However, it was found that this correction, if applied to the black globe, would lead to an undesirable result, moving the MRT values obtained with the globe away from those provided by the three net radiometers, taken as a reference.

The MRT is only one, albeit the most important, of the parameters affecting the determination of UTCI, the thermal index chosen to define the stress categories in the measurements carried out. The analyses evidenced a strong and positive correlation between UTCI and T_{air} , while the correlation turned out to be weaker between UTCI and other meteorological parameters such as V_{air} and RH.

The radiative properties of the different measurement environments have also been shown to have a strong influence on perceived thermal comfort. In particular, the greater the reflectivity of the surrounding surfaces and, in particular, of the ground, the greater the UTCI value measured in this environment (except for measurements carried out in open field).

In conclusion, this thesis work tried to provide information about the accuracy of the individual instruments commonly used in literature for the evaluation of outdoor thermal comfort parameters, investigating the criticalities of measurement methods, such as the one based on globe thermometers, cheaper than the integral radiation measurements and so more used in past studies. An attempt was then made to define applicability criteria of corrections which could improve the accuracy of these cheaper methods, in order to approach the reference results.

Future researches may be addressed at analysing critical issues highlighted in this thesis work which do not have yet a universally recognized solution, such as which view factors are more suitable to describe the actual radiative fluxes in open field for the calculation of MRT by net radiometers or which convective coefficient better represents the heat exchange between globe thermometer and the surrounding environment, starting from the considerations this thesis offers.

Nomenclature

Acronyms

1D	One-dimensional
3D	Three-dimensional
ET	Effective Temperature
FIR	Far-infra-red
GIS	Geographic Information System
IR	Infra-red
MRT	Mean Radiant Temperature
PET	Physiologically Equivalent Temperature
PMV	Predicted Mean Vote
PT	Perceived Temperature
SET	Standard Effective Temperature
SVF	Sky View Factor
UHI	Urban Heat Island
UTCI	Universal Thermal Comfort Index

Symbols

α	[-]	Absorptivity of a surface
α_g	[-]	Solar absorption coefficient of globe thermometers
α_k	[-]	Absorption coefficient for short-wave radiant fluxes of net radiometers
ε_g	[-]	Emissivity of globe thermometers
ε_p	[-]	Emissivity of the human body
ρ	[-]	Reflectivity of a surface
σ	[Wm ⁻² K ⁻⁴]	Stefan-Boltzmann constant
D	[m]	Diameter of globe thermometers
D (z)	[Wm ⁻² K ⁻³]	Total diffuse short-wave radiation flux absorbed by a body at height z
E (z)	[Wm ⁻² K ⁻³]	Long-wave radiation flux absorbed by a body at height z
F_i	[-]	View factor for the i-th direction between a human body and the surrounding surfaces
G_g	[W/m ²]	Solar irradiance incident on a globe thermometer
h_{conv}	[W/(m ² K)]	Coefficient of convective heat exchange between air and globe
h_{CG}	[W/(m ² K)]	Coefficient of heat transfer in forced convection at the level of a globe thermometer
h_{RG}	[W/(m ² K)]	Coefficient of heat transfer by radiation at the level of a globe thermometer

$I(z)$	$[\text{Wm}^{-2}\text{K}^{-3}]$	Direct short-wave radiation flux absorbed by a body at height z
K_i	$[\text{W}/\text{m}^2]$	Short-wave radiant fluxes from the i -th direction
L_i	$[\text{W}/\text{m}^2]$	Long-wave radiant fluxes from the i -th direction
$LW_{UP,i}$	$[\text{W}/\text{m}^2]$	Long-wave radiant fluxes recorded by the i -th radiometer, measured by the correspondent up-facing pyrgeometer
$LW_{DOWN,i}$	$[\text{W}/\text{m}^2]$	Long-wave radiant fluxes recorded by the i -th radiometer, measured by the correspondent down-facing pyrgeometer
M	$[\text{W}/\text{m}^2]$	Metabolic rate of the human body
MRT	$[^\circ\text{C}]$	Mean Radiant Temperature
$MRT_{Rad1+2+3}$	$[^\circ\text{C}]$	Mean Radiant Temperature calculated by using three net radiometers
$MRT_{Rad1+2+3,standing\ man}$	$[^\circ\text{C}]$	Mean Radiant Temperature calculated by using three net radiometers with "standing man" view factors
$MRT_{Rad1+2+3,sphere}$	$[^\circ\text{C}]$	Mean Radiant Temperature calculated by using three net radiometers with "sphere" view factors
MRT_{Rad1}	$[^\circ\text{C}]$	Mean Radiant Temperature calculated by using one net radiometer measuring upward and downward direction
MRT_{Black}	$[^\circ\text{C}]$	Mean Radiant Temperature calculated by using black globe thermometer
$MRT_{Black.Th.}$	$[^\circ\text{C}]$	Mean Radiant Temperature calculated by using black globe thermometer with the convective heat transfer coefficient used by Thorsson et al.
MRT_{Grey}	$[^\circ\text{C}]$	Mean Radiant Temperature calculated by using grey globe thermometer
$MRT_{Grey.Th.}$	$[^\circ\text{C}]$	Mean Radiant Temperature calculated by using grey globe thermometer with the convective heat transfer coefficient used by Thorsson et al.
\dot{Q}_C	$[\text{W}/\text{m}^2]$	Convective flux

\dot{Q}_K	[W/m ²]	Conductive flux
\dot{Q}_R	[W/m ²]	Radiative flux
\dot{Q}_{Re}	[W/m ²]	Heat flux due to the respiration (latent and sensible)
\dot{Q}_{SW}	[W/m ²]	Flux of latent heat due to the perspiration
RH	[%]	Relative humidity
S	[m ²]	Surface area of an element
S _s	[Vm ² /W]	Sensitivity of the net radiometer sensor
$SW_{UP,i}$	[W/m ²]	Short-wave radiant fluxes recorded by the i-th radiometer, measured by the correspondent up-facing pyranometer
$SW_{DOWN,i}$	[W/m ²]	Short-wave radiant fluxes recorded by the i-th radiometer, measured by the correspondent down-facing pyranometer
S_{STR}	[W/m ²]	Mean radiant flux density
T_{air}	[K]	Air temperature
T_g	[K]	Temperature of globe thermometers
T_{op}	[K]	Operative temperature
T_{rad}	[K]	Radiant temperature
T_s	[K]	Temperature of the net radiometer sensor
T_{sky}	[K]	Sky temperature

$T_{surface}$	[K]	Temperature of a surface
U	[V]	Output of the net radiometer sensor
UTCI	[°C]	Universal Thermal Climate Index
$UTCI_{Rad1+2+3}$	[°C]	Universal Thermal Climate Index calculated by using three net radiometers
$UTCI_{Black}$	[°C]	Universal Thermal Climate Index calculated by using black globe thermometer
$UTCI_{Grey}$	[°C]	Universal Thermal Climate Index calculated by using grey globe thermometer
V	[m ³]	Volume of an element
V_{air}	[m/s]	Air velocity
\dot{W}	[W/m ²]	Rate of work density of a human body

Bibliography

- Acero, Juan A., and Jon Arrizabalaga. 2018. "Evaluating the Performance of ENVI-Met Model in Diurnal Cycles for Different Meteorological Conditions." *Theoretical and Applied Climatology*. <https://doi.org/10.1007/s00704-016-1971-y>.
- Acero, Juan A., and Karmele Herranz-Pascual. 2015. "A Comparison of Thermal Comfort Conditions in Four Urban Spaces by Means of Measurements and Modelling Techniques." *Building and Environment*. <https://doi.org/10.1016/j.buildenv.2015.06.028>.
- Ali-Toudert, Fazia, and Helmut Mayer. 2006. "Numerical Study on the Effects of Aspect Ratio and Orientation of an Urban Street Canyon on Outdoor Thermal Comfort in Hot and Dry Climate." *Building and Environment*. <https://doi.org/10.1016/j.buildenv.2005.01.013>.
- Andrade, Henrique, Maria João Alcoforado, and Sandra Oliveira. 2011. "Perception of Temperature and Wind by Users of Public Outdoor Spaces: Relationships with Weather Parameters and Personal Characteristics." *International Journal of Biometeorology*. <https://doi.org/10.1007/s00484-010-0379-0>.
- ASHRAE 55 - 2013. "Thermal Environmental Conditions for Human Occupancy".
- ASHRAE 55 - 2017. "ANSI/ASHRAE Standard 55-2017 : Thermal Environmental Conditions for Human Occupancy."
- ASHRAE Standard 2001. "ASHRAE Handbook of Fundamentals 2001".
- Becker, Stefan, Oded Potchter, and Yaron Yaakov. 2003. "Calculated and Observed Human Thermal Sensation in an Extremely Hot and Dry Climate." *Energy and Buildings*. [https://doi.org/10.1016/S0378-7788\(02\)00228-1](https://doi.org/10.1016/S0378-7788(02)00228-1).
- Blazejczyk, Krzysztof, Yoram Epstein, Gerd Jendritzky, Henning Staiger, and Birger Tinz. 2012. "Comparison of UTCI to Selected Thermal Indices." *International Journal of Biometeorology*. <https://doi.org/10.1007/s00484-011-0453-2>.
- Blocken, Bert. 2015. "Computational Fluid Dynamics for Urban Physics: Importance, Scales, Possibilities, Limitations and Ten Tips and Tricks towards Accurate and Reliable Simulations." *Building and Environment*. <https://doi.org/10.1016/j.buildenv.2015.02.015>.
- Bröde, Peter, Eduardo L. Krüger, Francine A. Rossi, and Dusan Fiala. 2012. "Predicting Urban Outdoor Thermal Comfort by the Universal Thermal Climate Index UTCI-a Case Study in Southern Brazil." *International Journal of Biometeorology*. <https://doi.org/10.1007/s00484-011-0452-3>.
- Bruse, Michael, and Heribert Fleer. 1998. "Simulating Surface-Plant-Air Interactions inside Urban Environments with a Three Dimensional Numerical Model." *Environmental Modelling and Software*. [https://doi.org/10.1016/S1364-8152\(98\)00042-5](https://doi.org/10.1016/S1364-8152(98)00042-5).
- Cheng, Vicky, Edward Ng, Cecilia Chan, and Baruch Givoni. 2012. "Outdoor Thermal Comfort Study in a Sub-Tropical Climate: A Longitudinal Study Based in Hong Kong." *International Journal of Biometeorology*. <https://doi.org/10.1007/s00484-010-0396-z>.
- Clever cities. n.d. "European Project CLEVER Cities." <https://clevercities.eu>.
- D.A. McIntyre. 1980. "Indoor Climate. Applied Science Publishers, London."
- Eliasson, Ingegård. 2000. "The Use of Climate Knowledge in Urban Planning." *Landscape and Urban*

Planning. [https://doi.org/10.1016/S0169-2046\(00\)00034-7](https://doi.org/10.1016/S0169-2046(00)00034-7).

- Eliasson, Ingegård, Igor Knez, Ulla Westerberg, Sofia Thorsson, and Fredrik Lindberg. 2007. "Climate and Behaviour in a Nordic City." *Landscape and Urban Planning*. <https://doi.org/10.1016/j.landurbplan.2007.01.020>.
- Erell, Evyatar, David Pearlmutter, Daniel Boneh, and Pua Bar Kutiel. 2014. "Effect of High-Albedo Materials on Pedestrian Heat Stress in Urban Street Canyons." *Urban Climate*. <https://doi.org/10.1016/j.uclim.2013.10.005>.
- Fang, Zhaosong, Zhang Lin, Cheuk Ming Mak, Jianlei Niu, and Kam Tim Tse. 2018. "Investigation into Sensitivities of Factors in Outdoor Thermal Comfort Indices." *Building and Environment*. <https://doi.org/10.1016/j.buildenv.2017.11.028>.
- Fiala, Dusan, George Havenith, Peter Bröde, Bernhard Kampmann, and Gerd Jendritzky. 2012. "UTCI-Fiala Multi-Node Model of Human Heat Transfer and Temperature Regulation." *International Journal of Biometeorology*. <https://doi.org/10.1007/s00484-011-0424-7>.
- Fischer, E. M., and C. Schär. 2010. "Consistent Geographical Patterns of Changes in High-Impact European Heatwaves." *Nature Geoscience*. <https://doi.org/10.1038/ngeo866>.
- Forouzandeh, Aysan. 2018. "Numerical Modeling Validation for the Microclimate Thermal Condition of Semi-Closed Courtyard Spaces between Buildings." *Sustainable Cities and Society*. <https://doi.org/10.1016/j.scs.2017.07.025>.
- G. Jendritzky, A. Maarouf, H. Staiger. 2001. *Looking for a Universal Thermal Climate Index UTCI for Outdoor Applications, Wind. Conf. Therm. Conf.*
- Georgatou, Christine, and Denia Kolokotsa. 2016. "Urban Climate Models." In *Urban Climate Mitigation Techniques*. <https://doi.org/10.4324/9781315765839>.
- Givoni, Baruch, Mikiko Noguchi, Hadas Saaroni, Oded Pochter, Yaron Yaakov, Noa Feller, and Stefan Becker. 2003. "Outdoor Comfort Research Issues." In *Energy and Buildings*. [https://doi.org/10.1016/S0378-7788\(02\)00082-8](https://doi.org/10.1016/S0378-7788(02)00082-8).
- Gulyás, Ágnes, János Unger, and Andreas Matzarakis. 2006. "Assessment of the Microclimatic and Human Comfort Conditions in a Complex Urban Environment: Modelling and Measurements." *Building and Environment*. <https://doi.org/10.1016/j.buildenv.2005.07.001>.
- Havenith, George, Dusan Fiala, Krzysztof Błazejczyk, Mark Richards, Peter Bröde, Ingvar Holmér, Hannu Rintamaki, Yael Benshabat, and Gerd Jendritzky. 2012. "The UTCI-Clothing Model." *International Journal of Biometeorology*. <https://doi.org/10.1007/s00484-011-0451-4>.
- Höppe, P. 1992. "A New Procedure to Determine the Mean Radiant Temperature Outdoors." *Wetter Und Leben*.
- Höppe, Peter. 1999. "The Physiological Equivalent Temperature - A Universal Index for the Biometeorological Assessment of the Thermal Environment." *International Journal of Biometeorology*. <https://doi.org/10.1007/s004840050118>.
- Hove, L. W.A. van, C. M.J. Jacobs, B. G. Heusinkveld, J. A. Elbers, B. L. Van Driel, and A. A.M. Holtslag. 2015. "Temporal and Spatial Variability of Urban Heat Island and Thermal Comfort within the Rotterdam Agglomeration." *Building and Environment*. <https://doi.org/10.1016/j.buildenv.2014.08.029>.
- Hukseflux. 2016. "Hukseflux Thermal Sensors User Manual HFP01," 1–43. https://www.hukseflux.com/sites/default/files/product_manual/HFP01_HFP03_manual_v1721.pdf

- Huttner, Sebastian. 2012. "Further Development and Application of the 3D Microclimate Simulation ENVI-Met." *Mainz: Johannes Gutenberg-Universität in Mainz*.
- ISO 9060 1990. "ISO 9060: Solar Energy - Specification and Classification of Instruments for Measuring Hemispherical Solar and Direct Solar Radiation." *International Organization for Standardization*.
- ISO 17713-1 2007a. "ISO 17713-1: Meteorology — Wind Measurements — Part 1: Wind Tunnel Test Methods for Rotating Anemometer Performance".
- ISO 17714 2007b. "ISO 17714:2007 Meteorology - Air Temperature Measurements - Test Methods for Comparing the Performance of Thermometer Shields/Screens and Defining Important Characteristics".
- ISO 28902 2012. "ISO 28902-1: Air Quality - Environmental Meteorology Part 1: Ground-Based Remote Sensing of Visual Range by Lidar".
- ISO 19289 2015. "ISO 19289: Air Quality - Meteorology - Siting Classifications for Surface Observing Stations on Land".
- ISO 28902 2017. "ISO 28902-2: Air Quality — Environmental Meteorology Part 2: Ground-Based Remote Sensing of Wind by Heterodyne Pulsed Doppler Lidar".
- ISO 28902 2018. "ISO 28902-3: Air Quality — Environmental Meteorology Part 3: Ground-Based Remote Sensing of Wind by Continuous-Wave Doppler Lidar".
- ISO 7730 2005. "ISO 7730: Ergonomics of the Thermal Environment Analytical Determination and Interpretation of Thermal Comfort Using Calculation of the PMV and PPD Indices and Local Thermal Comfort Criteria."
- ISO 19926 2015. "ISO 19926: The First Series of International Consensus Standards on Weather Radar."
- Jamei, Elmira, Priyadarsini Rajagopalan, Mohammadmehdi Seyedmahmoudian, and Yashar Jamei. 2016. "Review on the Impact of Urban Geometry and Pedestrian Level Greening on Outdoor Thermal Comfort." *Renewable and Sustainable Energy Reviews*. <https://doi.org/10.1016/j.rser.2015.10.104>.
- Johansson, Erik, and Rohinton Emmanuel. 2006. "The Influence of Urban Design on Outdoor Thermal Comfort in the Hot, Humid City of Colombo, Sri Lanka." *International Journal of Biometeorology*. <https://doi.org/10.1007/s00484-006-0047-6>.
- Johansson, Erik, Sofia Thorsson, Rohinton Emmanuel, and Eduardo Krüger. 2014. "Instruments and Methods in Outdoor Thermal Comfort Studies - The Need for Standardization." *Urban Climate*. <https://doi.org/10.1016/j.uclim.2013.12.002>.
- Kántor, Noémi, Attila Kovács, and Tzu Ping Lin. 2015. "Looking for Simple Correction Functions between the Mean Radiant Temperature from the 'Standard Black Globe' and the 'Six-Directional' Techniques in Taiwan." *Theoretical and Applied Climatology*. <https://doi.org/10.1007/s00704-014-1211-2>.
- Kántor, Noémi, Tzu Ping Lin, and Andreas Matzarakis. 2014. "Daytime Relapse of the Mean Radiant Temperature Based on the Six-Directional Method under Unobstructed Solar Radiation." *International Journal of Biometeorology*. <https://doi.org/10.1007/s00484-013-0765-5>.
- Kántor, Noémi, and János Unger. 2010. "Benefits and Opportunities of Adopting GIS in Thermal Comfort Studies in Resting Places: An Urban Park as an Example." *Landscape and Urban Planning*. <https://doi.org/10.1016/j.landurbplan.2010.07.008>.
- Kántor, Noémi, János Unger, and Ágnes Gulyás. 2012. "Subjective Estimations of Thermal Environment in Recreational Urban Spaces-Part 2: International Comparison." *International Journal of*

Biometeorology. <https://doi.org/10.1007/s00484-012-0564-4>.

- Kleerekoper, Laura, Marjolein Van Esch, and Tadeo Baldiri Salcedo. 2012. "How to Make a City Climate-Proof, Addressing the Urban Heat Island Effect." *Resources, Conservation and Recycling*. <https://doi.org/10.1016/j.resconrec.2011.06.004>.
- Kleerekoper, Laura, Mohammad Taleghani, Andy van den Dobbelsteen, and Truus Hordijk. 2017. "Urban Measures for Hot Weather Conditions in a Temperate Climate Condition: A Review Study." *Renewable and Sustainable Energy Reviews*. <https://doi.org/10.1016/j.rser.2016.11.019>.
- Krüger, E. L., F. O. Minella, and A. Matzarakis. 2014. "Comparison of Different Methods of Estimating the Mean Radiant Temperature in Outdoor Thermal Comfort Studies." *International Journal of Biometeorology*. <https://doi.org/10.1007/s00484-013-0777-1>.
- Krüger, E. L., F. O. Minella, and F. Rasia. 2011. "Impact of Urban Geometry on Outdoor Thermal Comfort and Air Quality from Field Measurements in Curitiba, Brazil." *Building and Environment*. <https://doi.org/10.1016/j.buildenv.2010.09.006>.
- Krüger, Eduardo, Patricia Drach, Rohinton Emmanuel, and Oscar Corbella. 2013. "Urban Heat Island and Differences in Outdoor Comfort Levels in Glasgow, UK." *Theoretical and Applied Climatology*. <https://doi.org/10.1007/s00704-012-0724-9>.
- Krüger, Eduardo L., and Francine A. Rossi. 2011. "Effect of Personal and Microclimatic Variables on Observed Thermal Sensation from a Field Study in Southern Brazil." *Building and Environment*. <https://doi.org/10.1016/j.buildenv.2010.09.013>.
- Kuehn, L. A., R. A. Stubbs, and R. S. Weaver. 1970. "Theory of the Globe Thermometer." *Journal of Applied Physiology*. <https://doi.org/10.1152/jappl.1970.29.5.750>.
- Lai, Alan, Minjung Maing, and Edward Ng. 2017. "Observational Studies of Mean Radiant Temperature across Different Outdoor Spaces under Shaded Conditions in Densely Built Environment." *Building and Environment*. <https://doi.org/10.1016/j.buildenv.2016.12.034>.
- Lee, Hyunjung, Helmut Mayer, and Liang Chen. 2016. "Contribution of Trees and Grasslands to the Mitigation of Human Heat Stress in a Residential District of Freiburg, Southwest Germany." *Landscape and Urban Planning*. <https://doi.org/10.1016/j.landurbplan.2015.12.004>.
- Lee, Hyunjung, Helmut Mayer, and Dirk Schindler. 2014. "Importance of 3-D Radiant Flux Densities for Outdoor Human Thermal Comfort on Clear-Sky Summer Days in Freiburg, Southwest Germany." In *Meteorologische Zeitschrift*. <https://doi.org/10.1127/0941-2948/2014/0536>.
- Lin, Tzu Ping. 2009. "Thermal Perception, Adaptation and Attendance in a Public Square in Hot and Humid Regions." *Building and Environment*. <https://doi.org/10.1016/j.buildenv.2009.02.004>.
- Lin, Tzu Ping, Richard De Dear, and Ruey Lung Hwang. 2011. "Effect of Thermal Adaptation on Seasonal Outdoor Thermal Comfort." *International Journal of Climatology*. <https://doi.org/10.1002/joc.2120>.
- Lin, Tzu Ping, Andreas Matzarakis, and Ruey Lung Hwang. 2010. "Shading Effect on Long-Term Outdoor Thermal Comfort." *Building and Environment*. <https://doi.org/10.1016/j.buildenv.2009.06.002>.
- Lin, Tzu Ping, Kang Ting Tsai, Ruey Lung Hwang, and Andreas Matzarakis. 2012. "Quantification of the Effect of Thermal Indices and Sky View Factor on Park Attendance." *Landscape and Urban Planning*. <https://doi.org/10.1016/j.landurbplan.2012.05.011>.
- Maggiotto, Giuseppe, Riccardo Buccolieri, Marco Antonio Santo, Laura Sandra Leo, and Silvana Di Sabatino. 2014. "Validation of Temperature-Perturbation and CFD-Based Modelling for the Prediction of the

- Thermal Urban Environment: The Lecce (IT) Case Study." *Environmental Modelling and Software*.
<https://doi.org/10.1016/j.envsoft.2014.06.001>.
- Mahmoud, Ayman Hassaan Ahmed. 2011. "Analysis of the Microclimatic and Human Comfort Conditions in an Urban Park in Hot and Arid Regions." *Building and Environment*.
<https://doi.org/10.1016/j.buildenv.2011.06.025>.
- Mairie de Paris. 2014. "Végétalisation Des Murs et Des Toits." *Habiter Durable* 1: 1–11.
- Makaremi, Nastaran, Elias Salleh, Mohammad Zaky Jaafar, and Amir Hosein GhaffarianHoseini. 2012. "Thermal Comfort Conditions of Shaded Outdoor Spaces in Hot and Humid Climate of Malaysia." *Building and Environment*. <https://doi.org/10.1016/j.buildenv.2011.07.024>.
- Martilli, Alberto. 2014. "An Idealized Study of City Structure, Urban Climate, Energy Consumption, and Air Quality." *Urban Climate*. <https://doi.org/10.1016/j.uclim.2014.03.003>.
- Matzarakis, Andreas, and Christina Endler. 2010. "Climate Change and Thermal Bioclimate in Cities: Impacts and Options for Adaptation in Freiburg, Germany." *International Journal of Biometeorology*.
<https://doi.org/10.1007/s00484-009-0296-2>.
- Matzarakis, Andreas, Frank Rutz, and Helmut Mayer. 2007. "Modelling Radiation Fluxes in Simple and Complex Environments - Application of the RayMan Model." *International Journal of Biometeorology*.
<https://doi.org/10.1007/s00484-006-0061-8>.
- Mayer, H., and P. Höppe. 1987. "Thermal Comfort of Man in Different Urban Environments." *Theoretical and Applied Climatology*. <https://doi.org/10.1007/BF00866252>.
- Metje, N., M. Sterling, and C. J. Baker. 2008. "Pedestrian Comfort Using Clothing Values and Body Temperatures." *Journal of Wind Engineering and Industrial Aerodynamics*.
<https://doi.org/10.1016/j.jweia.2008.01.003>.
- Mirzaei, Parham A., and Fariborz Haghighat. 2010. "Approaches to Study Urban Heat Island - Abilities and Limitations." *Building and Environment*. <https://doi.org/10.1016/j.buildenv.2010.04.001>.
- Morakinyo, Tobi Eniolu, Ling Kong, Kevin Ka Lun Lau, Chao Yuan, and Edward Ng. 2017. "A Study on the Impact of Shadow-Cast and Tree Species on in-Canyon and Neighborhood's Thermal Comfort." *Building and Environment*. <https://doi.org/10.1016/j.buildenv.2017.01.005>.
- Ng, Edward, and Vicky Cheng. 2012. "Urban Human Thermal Comfort in Hot and Humid Hong Kong." In *Energy and Buildings*. <https://doi.org/10.1016/j.enbuild.2011.09.025>.
- Nikolopoulou, M., N. Baker, and K. Steemers. 1999. "Improvements to the Globe Thermometer for Outdoor Use." *Architectural Science Review*. <https://doi.org/10.1080/00038628.1999.9696845>.
- Nikolopoulou, Marialena, Nick Baker, and Koen Steemers. 2001. "Thermal Comfort in Outdoor Urban Spaces: Understanding the Human Parameter." *Solar Energy*. [https://doi.org/10.1016/S0038-092X\(00\)00093-1](https://doi.org/10.1016/S0038-092X(00)00093-1).
- Nikolopoulou, Marialena, and Spyros Lykoudis. 2006. "Thermal Comfort in Outdoor Urban Spaces: Analysis across Different European Countries." *Building and Environment*.
<https://doi.org/10.1016/j.buildenv.2005.05.031>.
- Oke, T. R., and H. A. Cleugh. 1987. "Urban Heat Storage Derived as Energy Balance Residuals." *Boundary-Layer Meteorology*. <https://doi.org/10.1007/BF00116120>.
- Ole Fanger, P. 1970. "Thermal Comfort. Analysis and Applications in Environmental Engineering."

Copenhagen: Danish Technical Press.

- Oliveira, Sandra, and Henrique Andrade. 2007. "An Initial Assessment of the Bioclimatic Comfort in an Outdoor Public Space in Lisbon." *International Journal of Biometeorology*. <https://doi.org/10.1007/s00484-007-0100-0>.
- Pearlmutter, D., A. Bitan, and P. Berliner. 1999. "Microclimatic Analysis of 'compact' Urban Canyons in an Arid Zone." In *Atmospheric Environment*. [https://doi.org/10.1016/S1352-2310\(99\)00156-9](https://doi.org/10.1016/S1352-2310(99)00156-9).
- Pearlmutter, David, P. Berliner, and E. Shaviv. 2006. "Physical Modeling of Pedestrian Energy Exchange within the Urban Canopy." *Building and Environment*. <https://doi.org/10.1016/j.buildenv.2005.03.017>.
- Pioppi, Benedetta, Ilaria Pigliautile, Cristina Piselli, and Anna Laura Pisello. 2020. "Cultural Heritage Microclimate Change: Human-Centric Approach to Experimentally Investigate Intra-Urban Overheating and Numerically Assess Foreseen Future Scenarios Impact." *Science of the Total Environment*. <https://doi.org/10.1016/j.scitotenv.2019.134448>.
- Roth, Matthias, and Vanessa Huimin Lim. 2017. "Evaluation of Canopy-Layer Air and Mean Radiant Temperature Simulations by a Microclimate Model over a Tropical Residential Neighbourhood." *Building and Environment*. <https://doi.org/10.1016/j.buildenv.2016.11.026>.
- Salata, Ferdinando, Iacopo Golasi, Roberto de Lieto Vollaro, and Andrea de Lieto Vollaro. 2016. "Urban Microclimate and Outdoor Thermal Comfort. A Proper Procedure to Fit ENVI-Met Simulation Outputs to Experimental Data." *Sustainable Cities and Society*. <https://doi.org/10.1016/j.scs.2016.07.005>.
- Salata, Ferdinando, Iacopo Golasi, Davide Petitti, Emanuele de Lieto Vollaro, Massimo Coppi, and Andrea de Lieto Vollaro. 2017. "Relating Microclimate, Human Thermal Comfort and Health during Heat Waves: An Analysis of Heat Island Mitigation Strategies through a Case Study in an Urban Outdoor Environment." *Sustainable Cities and Society*. <https://doi.org/10.1016/j.scs.2017.01.006>.
- Sangiorgio, Valentino, Francesco Fiorito, and Mattheos Santamouris. 2020. "Development of a Holistic Urban Heat Island Evaluation Methodology." *Scientific Reports*. <https://doi.org/10.1038/s41598-020-75018-4>.
- Santamouris, M., N. Papanikolaou, I. Livada, I. Koronakis, C. Georgakis, A. Argiriou, and D. N. Assimakopoulos. 2001. "On the Impact of Urban Climate on the Energy Consumption of Building." *Solar Energy*. [https://doi.org/10.1016/S0038-092X\(00\)00095-5](https://doi.org/10.1016/S0038-092X(00)00095-5).
- Savio, Peter, Cynthia Rosenzweig, William D Solecki, and Ronald B Slosberg. 2006. "Mitigating New York City's Heat Island with Urban Forestry, Living Roofs and Light Surfaces. New York City Regional Heat Island Initiative. Final Report." *New York*.
- Sharmin, Tania, Koen Steemers, and Andreas Matzarakis. 2017. "Microclimatic Modelling in Assessing the Impact of Urban Geometry on Urban Thermal Environment." *Sustainable Cities and Society*. <https://doi.org/10.1016/j.scs.2017.07.006>.
- Spagnolo, Jennifer, and Richard de Dear. 2003. "A Field Study of Thermal Comfort in Outdoor and Semi-Outdoor Environments in Subtropical Sydney Australia." *Building and Environment*. [https://doi.org/10.1016/S0360-1323\(02\)00209-3](https://doi.org/10.1016/S0360-1323(02)00209-3).
- Standard, International. ISO 7726 1998. "ISO 7726 Ergonomics of the Thermal Environment — Instruments for Measuring Physical Quantities."
- Stathopoulos, Theodore, Hanqing Wu, and John Zacharias. 2004. "Outdoor Human Comfort in an Urban Climate." *Building and Environment*. <https://doi.org/10.1016/j.buildenv.2003.09.001>.

- Svensson, Marie K., and Ingegärd Eliasson. 2002. "Diurnal Air Temperatures in Built-up Areas in Relation to Urban Planning." *Landscape and Urban Planning*. [https://doi.org/10.1016/S0169-2046\(02\)00076-2](https://doi.org/10.1016/S0169-2046(02)00076-2).
- Taha, Haider. 1997. "Urban Climates and Heat Islands: Albedo, Evapotranspiration, and Anthropogenic Heat." *Energy and Buildings*. [https://doi.org/10.1016/s0378-7788\(96\)00999-1](https://doi.org/10.1016/s0378-7788(96)00999-1).
- Tan, Chun Liang, Nyuk Hien Wong, and Steve Kardinal Jusuf. 2013. "Outdoor Mean Radiant Temperature Estimation in the Tropical Urban Environment." *Building and Environment*. <https://doi.org/10.1016/j.buildenv.2013.03.012>.
- Thorsson, Sofia, Fredrik Lindberg, Ingegärd Eliasson, and Björn Holmer. 2007. "Different Methods for Estimating the Mean Radiant Temperature in an Outdoor Urban Setting." In *International Journal of Climatology*. <https://doi.org/10.1002/joc.1537>.
- Thorsson, Sofia, Maria Lindqvist, and Sven Lindqvist. 2004. "Thermal Bioclimatic Conditions and Patterns of Behaviour in an Urban Park in Göteborg, Sweden." *International Journal of Biometeorology*. <https://doi.org/10.1007/s00484-003-0189-8>.
- Toparlar, Y., B. Blocken, B. Maiheu, and G. J.F. van Heijst. 2017. "A Review on the CFD Analysis of Urban Microclimate." *Renewable and Sustainable Energy Reviews*. <https://doi.org/10.1016/j.rser.2017.05.248>.
- Tseliou, Areti, Ioannis X. Tsiros, Marialena Nikolopoulou, and Georgios Papadopoulos. 2016. "Outdoor Thermal Sensation in a Mediterranean Climate (Athens): The Effect of Selected Microclimatic Parameters." *Architectural Science Review*. <https://doi.org/10.1080/00038628.2015.1028022>.
- Tsoka, S., A. Tsikaloudaki, and T. Theodosiou. 2018. "Analyzing the ENVI-Met Microclimate Model's Performance and Assessing Cool Materials and Urban Vegetation Applications—A Review." *Sustainable Cities and Society*. <https://doi.org/10.1016/j.scs.2018.08.009>.
- VDI. 1998. "VDI 3787 Part I: Environmental Meteorology, Methods for the Human-Biometeorological Evaluation of Climate and Air Quality for the Urban and Regional Planning at Regional Level. Part I: Climate." *VDI/DIN-Handbuch Reinhaltung Der Luf*.
- VDI. 2008. "VEREIN DEUTSCHER INGENIEURE Umweltmeteorologie Methoden Zur Human-Biometeorologischen Bewertung von Klima Und Lufthygiene Für Die Stadt-Und Regionalplanung Teil I: Klima Environmental Meteorology Methods for the Human Biometeorological Evaluation of Clima." www.vdi-richtlinien.de.
- WMO. 2008. *WMO-No.8*.
- Xi, Tianyu, Qiong Li, Akashi Mochida, and Qinglin Meng. 2012. "Study on the Outdoor Thermal Environment and Thermal Comfort around Campus Clusters in Subtropical Urban Areas." *Building and Environment*. <https://doi.org/10.1016/j.buildenv.2011.11.006>.
- Yahia, Moohammed Wasim, and Erik Johansson. 2013a. "Evaluating the Behaviour of Different Thermal Indices by Investigating Various Outdoor Urban Environments in the Hot Dry City of Damascus, Syria." *International Journal of Biometeorology*. <https://doi.org/10.1007/s00484-012-0589-8>.
- Yang, Feng, Stephen S.Y. Lau, and Feng Qian. 2011. "Urban Design to Lower Summertime Outdoor Temperatures: An Empirical Study on High-Rise Housing in Shanghai." *Building and Environment*. <https://doi.org/10.1016/j.buildenv.2010.10.010>.
- Yang, Shing Ru, and Tzu Ping Lin. 2016. "An Integrated Outdoor Spaces Design Procedure to Relieve Heat Stress in Hot and Humid Regions." *Building and Environment*. <https://doi.org/10.1016/j.buildenv.2016.01.001>.

- Yang, Wei, Nyuk Hien Wong, and Steve Kardinal Jusuf. 2013. "Thermal Comfort in Outdoor Urban Spaces in Singapore." *Building and Environment*. <https://doi.org/10.1016/j.buildenv.2012.09.008>.
- Yin, Ji Fu, You Fei Zheng, Rong Jun Wu, Jian Guo Tan, Dian Xiu Ye, and Wei Wang. 2012. "An Analysis of Influential Factors on Outdoor Thermal Comfort in Summer." *International Journal of Biometeorology*. <https://doi.org/10.1007/s00484-011-0503-9>.
- Zhao, T. F., and K. F. Fong. 2017. "Characterization of Different Heat Mitigation Strategies in Landscape to Fight against Heat Island and Improve Thermal Comfort in Hot-Humid Climate (Part II): Evaluation and Characterization." *Sustainable Cities and Society*. <https://doi.org/10.1016/j.scs.2017.05.006>.